MODEL-BASED CARDIOVASCULAR MONITORING IN CRITICAL CARE FOR IMPROVED DIAGNOSIS OF CARDIAC DYSFUNCTION

James Alexander Michael Revie

A thesis submitted for the degree of

Doctor of Philosophy in Mechanical Engineering

at the

University of Canterbury,

Christchurch, New Zealand

October 2012

ACKNOWLEDGEMENTS

There are many people I would like to acknowledge for helping me with my research. First I would like to thank my supervisors Geoff Chase, Thomas Desaive, and Geoff Shaw for their guidance. I am very fortunate to have such supportive and knowledgeable supervisory team. Their direction significantly helped mould my PhD and ensured I did not stray too far from the true path!

I would especially like to thank my main supervisor Geoff Chase for granting the opportunity to do cardiovascular research at Canterbury. Geoff always made time to answer my questions and spent a lot of time editing my writing. I really appreciate your guidance and contributions to this work. Without your support this thesis would not have been possible.

In addition, I would like to acknowledge the following people:

Thomas Desaive, my co-supervisor from Belgium. Who looked after me when I did an internship at the University of Liege, provided useful improvements for my papers, and introduced me to the experimental side of cardiovascular research.

Geoff Shaw, my contact in the Christchurch Hospital. Whose clinical experience and knowledge was invaluable to me understanding the physiological side of my work. Thank you for setting up and coordinating the clinical studies in the ICU.

Chris Hann, a specialist in physiological modelling. His initial support, enthusiasm, and guidance on cardiovascular modelling and parameter identification methods helped set the foundation for this research.

Colleagues who provided useful contributions including: David Stevenson, for providing the patient-specific driver functions for the models; Antoine Pironet, for suggestions on improving the parameter identification method; Chris Pretty, for contributions to analysing the septic shock results; and Paul Docherty for insights into structural identifiability.

Mike Forrester and Rodney Elliot, for their technical assistance in acquiring data from the ICU medical devices.

Students, Stefan Heldmann for his initial assistance on adapting the parameter identification to clinical measurements; Abhishek Vadnerkar on quantifying the effect of the deadspace volume on the driver function; Gregoire Coat for testing a simplified cardiopulmonary model; and Dougie Squire, for his work into analysing the aortic pressure waveform.

Finally, I would like to thank my lovely soon to be wife Lauren, along with my parents, sister, and friends for your friendship and support.

TABLE OF CONTENTS

Abstract ..... **xxiii**

Chapter 1: Introduction and Motivation **1**

1.1 Hemodynamic Monitoring in the ICU 2

1.1.1 Data Rich, but Information Poor 3

1.1.2 One Size Fits All 4

1.1.3 Model-Based Approaches 5

1.2 Goals of this Research 6

1.3 Application of Research 7

Chapter 2: Cardiovascular Physiology **8**

2.1 Cardiovasular System Overview 8

2.2 The Circulation 9

2.2.1 Arterial System 10

2.2.2 The Capillaries 10

2.2.3 Venous System 11

2.3 The Heart 11

2.3.1 Anatomy 11

2.3.2 Electrical Activation 12

2.3.3 The Cardiac Cycle 15

2.4 Basic Concepts 16

2.4.1 Preload 18

2.4.2 Afterload 19

2.4.3 Contractility 20

2.4.4 Heart Rate 22

2.4.5 Cardiac output 22

2.4.6 Blood pressure 22

2.4.7 Summary of Concepts 23

2.5 Interdependence of Preload, Afterload and Contractility 24

2.5.1 Preload → Afterload 24

2.5.2 Afterload → Preload 24

2.5.3 Contractility → Preload 25

2.5.4 Summary of Preload, Afterload and Contractility Interdependence 25

2.6 Homeostasis Mechanisms 25
2.6.1 Neural Regulation 26
2.6.2 Auto Regulatory Mechanisms 26
2.6.3 Humoral Regulation 27
2.7 Ventricular Interaction 28
2.7.1 Inter-Ventricular Septum 28
2.7.2 Pericardium 29
2.8 Cardiopulmonary Interaction 30
2.8.1 Intrathoracic Pressure 31
2.8.2 Lung Volume 31
2.9 Ventricular Arterial Coupling 33
2.10 Summary 33
Chapter 3: Cardiovascular System Model 34
3.1 Introduction 34
3.2 Model Assumptions 37
3.3 Model Development 37
3.3.1 Passive Chamber 37
3.3.2 Inter Chamber Flow (Non-Valvular) 38
3.3.3 Heart Valve Flow 39
3.3.4 Ventricular Chambers 40
3.3.5 Ventricular Interaction 43
3.4 Model Equations 46
3.5 Simulation 51
3.6 Discussion 53
3.6.1 Validity of Assumptions and Modelling Concepts 53
3.6.2 Simulation 56
3.6.3 Limitations 56
3.7 Summary 56
Chapter 4: CVS Model Parameter Identification 58
4.1 Introduction 58
4.2 Parameter Identification Assumptions and Measurements 59
4.2.1 Assumptions 59
4.2.2 Available and Inferable ICU Measurements 60
4.3 Structural Identifiability 61

4.4 Parameter Identification Concepts 64
4.4.1 Simplified Models 64
4.4.2 Proportional Gain Control 66
4.5 Specifics of Parameter Identification 69
4.5.1 Systemic Model Identification 69
4.5.2 Pulmonary Model Identification 71
4.5.3 Identify Ventricular Chambers 73
4.5.4 Identification of Venous Chambers 75
4.5.5 Averaging Valve Resistances 75
4.5.6 Summary 76
4.6 Discussion 79
4.6.1 Validity and Justication of Assumptions 79
4.6.2 Simplified Models 81
4.6.3 Parameter Identification Limitations 81
4.7 Summary 83
Chapter 5: Parameter Identification Validation 84
5.1 Introduction 84
5.2 Methods 85
5.2.1 Porcine Measurements 85
5.2.2 Model Identification Analyses 85
5.2.3 Data Analysis 86
5.3 Results 86
5.3.1 Convergence 86
5.3.2 Sensitivity Analysis 87
5.3.3 Repeatability of Model Identification Analysis 88
5.3.4 Validation Against Independent Measurements 92
5.4 Discussion 98
5.4.1 Convergence 98
5.4.2 Parameter Sensitivity 99
5.4.3 Inter-Beat Repeatability 100
5.4.4 Validation Against Independent Metrics 101
5.5 Summary 102
Chapter 6: Model-Based Monitoring of Pulmonary Embolism 103
6.1 Introduction 103

6.1.1 Patho-Physiology and Treatment of Pulmonary Embolism 104
6.2 Methods 106
6.2.1 Porcine Experiments and Data 106
6.2.2 Model Identification 106
6.2.3 Data and Statistical Analysis 107
6.3 Results 107
6.3.1 Comparison to Experimentally Derived Metrics 109
6.3.2 Pulmonary Embolism Trends 111
6.3.3 Subject-Specific Response 114
6.4 Discussion 117
6.4.1 Comparison With Clinically Derived Metrics 117
6.4.2 Detecting Acute Pulmonary Embolism 118
6.4.3 Subject-Specific Modelling 118
6.4.4 Limitations 119
6.5 Summary 119
Chapter 7: Model-Based Monitoring of Septic Shock 121
7.1 Introduction 121
7.1.1 Patho-Physiology and Treatment of Septic Shock 122
7.2 Methods 124
7.2.1 Porcine Experiments and Data 124
7.2.2 Model Identification 125
7.2.3 Data and Statistical Analysis 125
7.3 Results 126
7.3.1 Comparison to Experimentally Derived Metrics 127
7.3.2 Septic Shock Trends 130
7.3.3 Subject-Specific Response 132
7.4 Discussion 136
7.4.1 Detecting Septic Shock 136
7.4.2 Comparison to Experimentally Derived Metrics 136
7.4.3 Hemodynamic Effects of Large Pore Hemofiltration 137
7.4.4 Subject-Specific Modelling 137
7.4.5 Limitations 138
7.5 Summary 138
Chapter 8: Model-Based Monitoring of Recovery Post Mitral Valve Surgery 140

8.1 Introduction 140
8.1.1 Mitral Regurgitation, Repair, Replacement, and Recovery 141
8.2 Methods 144
8.2.1 Clinical Study 144
8.2.2 Patients 144
8.2.3 Measured Data 145
8.2.4 Inferred Data 145
8.2.5 Parameter Identification 146
8.3 Results 147
8.3.1 Recorded Data 147
8.3.2 Patient-Specific Models 149
8.4 Discussion 152
8.4.1 Model-Based Approach 152
8.4.2 Patient-Specific Modelling of Hemodynamic Recovery 152
8.4.3 Limitations 153
8.5 Summary 153
Chapter 9: Aorta Model 155
9.1 Introduction 155
9.2 Model Assumptions 157
9.3 Model Development 158
9.4 Simulation 160
9.5 Discussion 162
9.5.1 Validity of Assumptions and Modelling Concepts 162
9.5.2 Model Simulation 162
9.5.3 Limitations 163
9.6 Summary 163
Chapter 10: Aorta Model Energetics in Septic Shock 164
10.1 Introduction 164
10.2 Methods 165
10.2.1 Porcine Trials and Measurements 165
10.2.2 Model Identification 165
10.2.3 Data and Statisitical Analysis 166
10.3 Results 167
10.3.1 Comparison of Ventricular and Arterial Work 169

10.3.2 Effects of Septic Shock on Aortic Energetics and Volume 169
10.3.3 Estimation of Ventricular Arterial Coupling 172
10.4 Discussion 173
10.4.1 Model Energetics 173
10.4.2 Septic Shock Trends 174
10.4.3 Ventricular Arterial Coupling 176
10.4.4 Limitations 176
10.5 Summary 176
Chapter 11: Conclusions 177
11.1 Patient-Specific Cardiovascular System Models 177
11.2 Pulse Wave Analysis of Aortic Flow and Energetics 180
Chapter 12: Future Work 181
12.1 Integrate Model With Clinical Therapies and Treatment Protocols 181
12.2 Testing on Other Diseases States 181
12.3 Relationship of Left and Right Ventricle End Systolic Elastance 182
12.4 Computational Speed 182
12.5 Pulse Contour Calculation of CO 183
12.6 Cardiopulmonary Gas Exchange Model 183
Appendix A: Structural Identifiability Test 185
12.7 Input File of Six-Chamber CVS Model 185
12.8 Output File of Six-Chamber CVS Model 186
Appendix B: Mitral Valve Replacement Patient Treatment Data 195
References 195

LIST OF FIGURES

Figure 2.1: Overview of the anatomy of the cardiovascular system (McKinlay and O'Loughlin, 2007) showing the heart, systemic circuit, and pulmonary circuit. 9
Figure 2.2: Example of capillaries connecting the venous and arterials systems via an arteriole and a venule (Starfinger, 2008). 11
Figure 2.3: Anatomical features of the heart not including the pericardium. 12
Figure 2.4: Electrical conduction system of the heart. Picture modified from the work of (Lynch and Jaffe, 2006). 13
Figure 2.5: Electrocardiogram showing the P-wave, QRS complex, and T wave. 14
Figure 2.6: Example of the cardiac events which occur during the cardiac cycle. Two complete cardiac cycles are illustrated showing the pressures in the left atrium, left ventricle, and aorta; volume in the left ventricle; and electrocardiogram. 16
Figure 2.7: Pressure-volume loop showing the four phases of the cardiac cycle. The pressure volume loop is confined below the end systolic pressure-volume relationship (ESPVR) and above end diastolic pressure-volume relationship (EDPVR). The arterial elastance (E_a) reflects the arterial load imposed on the ventricle. The stroke volume of the ventricle is the difference between the end diastolic volume (EDV) and end systolic volume (ESV). Q_{av} and Q_{mt} represent flow through the aortic and mitral valves. 17
Figure 2.8: Effect of changing preload (end diastolic volume) on the ventricular pressure volume loop. The control pressure-volume loop is plotted in black. 18
Figure 2.9: Effect of changing afterload (arterial elastance, E_a) on the ventricular pressure volume loop. The control pressure-volume loop is plotted in black. 20
Figure 2.10: Effect of changing contractility (slope of ESPVR, E_{es}) on the ventricular pressure volume loop. The control pressure-volume loop is plotted in black. 21
Figure 2.11: Cross-sectional schematic of heart showing normal position of inter-ventricular septum (S) with respect to the left ventricle (LV) and right ventricle (RV), from (Starfinger, 2008). 29
Figure 2.12: Illustration of the pericardium (Starfinger, 2008). 30
Figure 2.13: Effect of lung volume on pulmonary vascular resistance (PVR). PVR is lowest near function residual capacity (FRC) and increases as lung volume decreases towards residual volume (RV) or increases to total lung capacity (TLC) (Shekerdemian and Bohn, 1999). 32

Figure 3.1: Schematic of the cardiovascular system model with elastances (E), resistances (R), and inertance (L). The circles represent pressure-volume (P, V) chambers. The subscripts represent: mt, mitral; es, end systolic; lvf, left ventricle free wall; av, aortic valve; sys, systemic; tc, tricuspid; pv, pulmonary valve; rvf, right ventricle free wall; pul, pulmonary; pu, pulmonary vein. 35
Figure 3.2: Single passively elastic chamber. 37
Figure 3.3: Schematic of inter chamber flow 38
Figure 3.4: Illustration of flow across a heart valve. 39
Figure 3.5: A standard pressure volume loop showing the four stages of the cardiac cycle and the end systolic (es) and end diastolic (ed) pressure volume relationships (ESPVR and EDPVR). Q_{av} and Q_{mt} are the flows in and out of the ventricle. Stroke volume (SV) is the difference between the end diastolic and end systolic volumes (EDV – ESV). Afterload is represented by E_a in the diagram. 41
Figure 3.6: Example of a normalised left ventricular driver function ($e_{lv}(t)$) for a healthy pig. 42
Figure 3.7: Schematic of a dynamically elastic chamber, where $P_2(t)$ represents the ventricular pressure. 42
Figure 3.8: Adding ventricular interaction, via septum and pericardium dynamics (V_{spt}, P_{pcd}), to the left and right ventricular chambers (lv, rv). 43
Figure 3.9: Cross-section of the left and right ventricles showing the volume definitions used to calculate the septum volume (V_{spt}) and pericardium pressure (P_{pcd}) (Smith, 2004). 44
Figure 3.10: Cross-section of the ventricles and pericardium showing the definitions of all the cardiac pressures (Smith, 2004). 45
Figure 3.11: Example of some of the simulated CVS model outputs for healthy human parameters and analytically derived driver functions (e_{lv} and e_{rv}). These outputs include left ventricular pressure (P_{lv}), aortic pressure (P_{ao}), left ventricular volume (V_{lv}), right ventricular pressure (P_{rv}), pulmonary artery pressure (P_{pa}), and right ventricular volume (V_{rv}). 53
Figure 4.1: Decoupled simplified models of (a) the systemic and (b) pulmonary circulations with inertia and ventricular interaction removed. Note for comparison the orientation of the pulmonary circulation has been reversed with respect to Figure 3.1. 65
Figure 4.2: General outline of the parameter identification process. C and NC stand for if converged and if not converged. 66

Figure 4.3: Example of the proportional gain control process iteratively fitting the mean and amplitude of the aortic pressure ($P_{ao,mean}$, PP_{ao}). The grey line in the plots represent the measured aortic pressure and the black line represents the modelled aortic pressure. Superscripts stand for iteration number. The top panel shows aortic pressure simulated from the aortic model using initial guesses for aortic elastance (E_{ao}) and systemic resistance (R_{sys}). The second and third panels show the re-simulated aortic pressure after the first and second iterations of the proportional gain control process. 68
Figure 4.4: Relationship used to separate the end systolic left ventricular elastance ($E_{es,lvf}$) from the sum of the ventricular elastances ($E_{es,sum}$). The coefficient C_E is calculated from the mean aortic, mean pulmonary artery, and vena cava pressures using Equation (4.25). 80
Figure 5.1: Regression (top) and Bland-Altman analysis showing 2 standard deviation limits (bottom) of the modelled and measured left ventricular end diastolic volume (LVEDV) in the pulmonary embolism study..... 93
Figure 5.2: Regression (top) and Bland-Altman analysis showing 2 standard deviation limits (bottom) of the modelled and measured right ventricular end diastolic volume (RVEDV) in the pulmonary embolism study. 94
Figure 5.3: Regression (top) and Bland-Altman analysis showing 2 standard deviation limits (bottom) of the modelled and measured left ventricular end diastolic volume (LVEDV) in the septic shock study. 96
Figure 5.4: Regression (top) and Bland-Altman analysis showing 2 standard deviation limits (bottom) of the modelled and measured right ventricular end diastolic volume (RVEDV) in the septic shock study. 97
Figure 6.1: Evolution of the averaged hemodynamic measurements recorded during the trials. * indicates P<0.05 for indicating a significant temporal change over T0-T60, T120-T150, or T240-T265 after the insertion of emboli. The data is presented as mean +/- SD. 108
Figure 6.2: Comparison of the experimentally derived (Ghuysen et al., 2008) and modelled pulmonary afterload. The data is presented as mean +/- SD. 110
Figure 6.3: Comparison of the experimentally derived (Ghuysen et al., 2008) and modelled right ventricular end systolic elastance ($E_{es,rvf}$). The data is presented as mean +/- SD..... 110

Figure 6.4: Comparison of the experimentally derived (Ghuysen et al., 2008) and modelled right ventricular-vascular coupling (RVVC or E_{es}/E_a). The data is presented as mean +/- SD. 111
Figure 6.5: Modelled left and right ventricular afterload. The data is presented as mean +/- SD. 112
Figure 6.6: Modelled left and right ventricular end diastolic volume (LVEDV, RVEDV). The data is presented as mean +/- SS. 113
Figure 6.7: Modelled left and right ventricular end systolic elastance ($E_{es,lvf}$, $E_{es,rvf}$). The data is presented as mean +/- SD. 114
Figure 6.8: Temporal evolution of the subject-specific hemodynamic measurement recorded during the porcine trials and used to identify the subject-specific CVS models. 115
Figure 6.9: Identified subject-specific metrics of preload (LEVDV, RVEDV), afterload (R_{sys}, R_{pul}), contractility ($E_{es,lvf}$, $E_{es,rvf}$), and right ventricular vascular index (RVEDV/LVEDV). 116
Figure 7.1: Illustration of the effects of septic shock before and after fluid resuscitation, from Dellinger (Dellinger, 2003). VR, venous return; VC, venous capacitance; AO, aorta; AR, arteriolar resistance; RA, right atrium; LA, left atrium; RV, right ventricle; LV, left ventricle; PA, pulmonary artery. 123
Figure 7.2: Evolution of the averaged hemodynamic measurements recorded during the trials. * indicates P<0.05 for expected temporal changes over T0-T60 due to the induction of septic shock. The data is presented as mean +/- SD. 127
Figure 7.3: Comparison of the experimentally derived (Lambermont et al., 2006) and modelled pulmonary afterload. The data is presented as mean +/- SD. 128
Figure 7.4: Comparison of the experimentally derived (Lambermont et al., 2006) and modelled right ventricular end systolic elastance ($E_{es,rvf}$). The data is presented as mean +/- SD. 129
Figure 7.5: Comparison of the experimentally derived (Lambermont et al., 2006) and modelled right ventricular-vascular coupling (RVVC). The data is presented as mean +/- SD. 129
Figure 7.6: Modelled left and right ventricular end diastolic volume (LVEDV, RVEDV). The data is presented as mean +/- SD. 130
Figure 7.7: Modelled left and right ventricular afterload. The data is presented as mean +/- SD. 131
Figure 7.8: Modelled left and right ventricular end systolic elastance ($E_{es,lvf}$, $E_{es,rvf}$). The data is presented as mean +/- SD. 132

Figure 7.9: Temporal evolution of the subject-specific hemodynamic measurement recorded during the porcine trials and used to identify the subject-specific CVS models. 134
Figure 7.10: Identified subject-specific metrics of preload (LEVDV, RVEDV), afterload (R_{sys}, R_{pul}), and contractility ($E_{es,lvf}$, $E_{es,rvf}$). 135
Figure 8.1: Illustration of a normal and prolapsed mitral valve leaflet (yalemedicalgroup.org, 2012). 141
Figure 8.2: Evolution of the patient-specific hemodynamic vital signs recorded during the first 12 hours post mitral valve surgery. 148
Figure 8.3: Evolution of the patient-specific metrics of preload (left and right end diastolic volumes), afterload (systemic and pulmonary vascular resistance), contractility (left and right ventricular end diastolic elastances), and ventricular filling pressures (pulmonary vein pressure) identified from the CVS model. 151
Figure 9.1: Schematic of the modified aortic model used in this research showing the flows in and out of the arterial system (Q_{in}, Q_{out}), the aortic pressure (P_{ao}), reservoir pressure (P_{wk}). The parameters of the system are: R_{prox}, proximal resistance of the aorta; C, compliance of the arterial system; R, peripheral systemic resistance; and P_{∞} the downstream pressure of the arterial system. 156
Figure 9.2: Aortic pressure separated into reservoir (P_{wk}) and excess pressure (P_{ex}) components. 157
Figure 9.3: Example of the inputs and outputs of the model used to simulate healthy aortic hemodynamics in a pig. The flow into the aorta (Q_{in}) acts as the input for the model and flow out of the arterial system (Q_{out}), aortic pressure (P_{ao}), and reservoir pressures (P_{wk}) represent the outputs of the model. 161
Figure 10.1: Left ventricular pressure volume loop analysis used to calculate end systolic elastance (E_{es}) and afterload (E_a) during a vena cava occlusion manoeuvre. 167
Figure 10.2: Evolution of mean arterial pressure (MAP), left ventricular end diastolic volume (LVEDV), stroke volume (SV), heart rate (HR), and maximum left ventricular pressure ($P_{lv,max}$) measurements during the trials. * indicates $P<0.05$ for expected temporal changes over T0-T30, T30-T60, or T0-T60 due to the induction of septic shock. Data presented as mean +/- SD. 168
Figure 10.3: Regression (top) and Bland-Altman (bottom) analysis comparing work derived from the aorta model (W_{ao}) with work calculated from the area enclosed left ventricular pressure-volume loops (W_{lv}). 170

Figure 10.4: Temporal change in the total hydraulic work of aortic flow (W_{ao}) and its components, reservoir work (W_{wk}) and excess work (W_{ex}), across the duration of the pig study. Each bar represents the averaged value across the four pigs..... 171
Figure 10.5: Change in volume stored in the arterial reservoir (dV_{wk}) as a percentage of stroke volume (SV). Data is presented as mean +/- SEM. 171
Figure 10.6: Comparison ventricular arterial coupling (E_{lv}/E_a), derived pressure volume loop analysis, with the ratio of excess to reservoir work (W_{ex}/W_{wk}), derived from the fitted aorta models. 172
Figure 10.7: Comparison of the inverse of afterload (1/Ea) calculated from pressure-volume loop analysis with excess work (W_{ex}) derived from the aorta model. 173
Figure 10.8: Temporal profile of systemic peripheral resistance, R (top), aortic compliance, C (middle), and ratio of the decay constant to heartbeat period, τ / T (bottom), during the pig study. Data is presented as mean +/- SD. 175
Figure 10.9: Example of the aortic pressure separated into reservoir and pressure (P_{wk}) and excess pressure (P_{ex}) components before the endotoxin infusion (T0) and 180 minutes (T210) after endotoxin infusion. 175

LIST OF TABLES

Table 2.1: The effect on stroke volume (SV), cardiac output (CO), and blood pressure (BP) when one of preload, afterload, contractility, or heart rate are changed independent of the other factors. 24

Table 2.2: Summary of the interdependence between preload, afterload, and contractility. Please note that the magnitudes of the secondary and tertiary effects are smaller than the magnitude of the primary intervention. SV, stroke volume; BP, blood pressure; ESV, end systolic volume; EDV, end diastolic volume. 25

Table 3.1: List of CVS model outputs (* denotes output is a state variable). 49

Table 3.2: List of CVS model parameters and their corresponding value for a healthy human. 50

Table 4.1: Typically available hemodynamic measurements in the ICU and their corresponding equivalent in the CVS model. t_{mt}, mitral valve closure time; P_{ao}, aortic pressure; P_{pa}, pulmonary artery pressure; P_{vc}, vena cava pressure; Q_{sys}, systemic flow; V_{lv}, left ventricular volume; V_{rv}, right ventricular volume. 60

Table 4.2: Initial systemic model parameter inputs. 69

Table 4.3: Initial pulmonary model parameter inputs. 72

Table 4.4: Parameter bounds used in the parameter identification method 76

Table 4.5: Step-wise parameter identification process of the six-chamber cardiovascular system model. 78

Table 5.1: Convergence analysis of the parameters of the systemic and pulmonary sub-models and six-chamber model for the PE case. Data presented for 51 subject-specific CVS models compares the model output to measured data to a bias +/- 2SD. 87

Table 5.2: Parameter sensitivity analysis of Pig 1 at T0 showing identified parameters for +/-10% (or -/+ 0.005s for t_{mt} and t_{tc}) change in the measured input value used in the identification method. 'ID value' indicates the parameter value identified when the inputs of the identification process were not altered. 89

Table 5.3: Parameter sensitivity analysis of Pig 1 at T150 showing identified parameters for +/-10% (or -/+ 0.005s for t_{mt} and t_{tc}) change in the measured input value used in the identification method. 'ID value' indicates the parameter value identified when the inputs of the identification process were not altered. 90

Table 5.4: Identified parameters of the CVS model from measurements obtained from three adjacent beats. The table shows the parameter values and the percentage

change in brackets for beats 2 and 3 in the parameter value in comparison to beat 1. 91
Table 5.5: Mean, bias and precision metrics, median absolute percentage errors with 5th and 95th percentile bounds, and correlation coefficients of the measurements used for validation of the model identification process in the pulmonary embolism pig study. 92
Table 5.6: Mean, bias and precision metrics, median absolute percentage errors with 5th and 95th percentile bounds, and correlation coefficients of the measurements used for validation of the model identification process in the septic shock pig study....95
Table 6.1: Bias, precision, and correlation metrics comparing the modelled to experimentally derived indices of afterload, contractility, and right ventricular vascular coupling (RVVC). 109
Table 7.1: Bias, precision, and correlation metrics comparing the modelled to experimentally derived indices of afterload, contractility, and right ventricular vascular coupling (RVVC). 128
Table 8.1: Demographics of patients who underwent mitral valve (MV) surgery. CABG, coronary artery bypass surgery; AV, aortic valve; CAD, coronary artery disease; IHD, ischemic heart disease; AF, atrial fibrillation. Note CABGx2 or x4 refers to double or quadruple coronary artery bypass graft....144
Table 9.1: Inputs, outputs, and parameters of the aorta model. 160
Table 9.2: Parameters used to simulate healthy swine hemodynamics. 160
Table B.1: Treatment received by patient 1 (Weight = 96Kg) in the first 12 hours post mitral valve surgery 195
Table B.2: Treatment received by patient 2 (Weight = 56.5Kg) in the first 12 hours post mitral valve surgery 196
Table B.3: Treatment received by patient 3 (Weight = 65Kg) in the first 12 hours post mitral valve surgery 196
Table B.4: Treatment received by patient 4 (Weight = 69Kg) in the first 12 hours post mitral valve surgery 197

NOMENCLATURE

Roman Symbols

C	Compliance
D	Observable model output
e	normalised time varying elastance
E	Elastance
H	Heaviside function
L	Inertance
P	Pressure
P	unknown parameter set
Q	Flow
R	Resistance
S	Septum
t	Time
T	Time
T	period
V	Volume
W	Work
Z	Impedence

Greek Symbols

λ	Parameter of end diastolic pressure volume relationship
τ	Decay constant

Subscripts

6	Six chamber
a	Arterial
ao	Aorta
approx	Approximate
av	Aortic valve
d	Unstressed/deadspace volume

dia	Diastolic
es	end systolic
ed	end diastolic
ex	excess
lv	Left ventricle
lvf	Left ventricle free wall
max	Maximum
meas	Measured
min	Minimum
mt	Mitral
0	Value at zero pressure
pa	Pulmonary artery
pcd	Pericardium (plus thoracic component)
peri	Pericardium
prox	Proximal
pu	Pulmonary vein
pul	Pulmonary
pv	Pulmonary valve
rv	Right ventricle
rvf	Right ventricle free wall
spt	Septum
sys	Systemic
sys	Systolic
tc	Tricuspid
th	Intrathoracic
v	venous
vc	Vena cava
wk	Windkessel or reservoir

Acronyms

AF	Atrial Fibrillation
AP	Arterial pressure
APE	Acute pulmonary embolism
CABG	Coronary artery bypass graft

CAD	Coronary artery disease
CO	Cardiac Output
CT	Computed tomography
CVD	Cardiovascular disease
CVP	Central venous pressure
CVS	Cardiovascular system
DE	Differential Equation
DIC	Disseminated intravascular coagulation
DVT	Deep vein thrombosis
ECG	Electrocardiogram
EDV	End diastolic volume
EDPVR	End diastolic pressure volume relationship
ESP	End systolic pressure
ESV	End systolic volume
ESPVR	End systolic pressure volume relationship
GEDV	Global end diastolic volume
HR	Heart rate
ICU	Intensive care unit
IHD	Ischemic heart disease
LPHF	Large pore hemofiltration
MAP	Mean arterial pressure
MV	Mitral valve
MVR	Mitral valve replacement or repair
PAC	Pulmonary artery catheter
PAP	Pulmonary artery pressure
PE	Pulmonary embolism
PEEP	Peak end expiratory pressure
PI	Identified pulmonary model parameters
PIP	Peak inspiratory pressure
PO	Pulmonary model outputs
PM	Pulmonary measurement set
PP	Pulse pressure
PVR	Pulmonary vascular resistance
RVEI	Right ventricle expansion index

RVVC	Right ventricle vascular coupling
SD	Standard deviation
SI	Identified systemic model parameters
SO	Systemic model outputs
SM	Systemic model measurement set
SS	Septic shock
SV	Stroke volume
SVR	Systemic vascular resistance
TBV	Total blood volume
TPR	Total peripheral resistance
VAC	Ventricular arterial coupling

Other symbols

C_E	Ratio of left and right ventricle end systolic elastances
CO_2	Carbon dioxide
FiO_2	Fraction of inspired oxygen
O_2	Oxygen
PCO_2	Partial pressure of carbon dioxide
SpO_2	Pulse oximeter oxygen saturation

ABSTRACT

Cardiovascular disease is highly prevalent in modern society due to a mixture of aging demography and sedentary lifestyles. In western countries, it is the leading cause of mortality, and a major, growing economic cost. As a result, it is also a major problem in the intensive care unit (ICU).

In critical care, intensive monitoring is required to help diagnose cardiac and circulatory dysfunction, and to provide targets to drive therapy. However, complex interactions between a patient's disease and internal compensatory mechanisms can hide the underlying disorder. Hence, two different disease states may look the same in the data available from the range of typical monitoring devices. In such cases, correct diagnosis is difficult. Clinical staff must rely on their skill and experience to choose therapy, increasing the chance of clinical errors, as well as, increasing variability in care and patient outcome.

To simplify this clinical scenario, a method has been developed to identify patient-specific six-chamber models of the cardiovascular system (CVS) from typically available ICU measurements. The approach utilises a proportional gain parameter identification approach to aggregate available hemodynamic measurements into an easy to understand framework of cardiac and circulatory physiology. The personalised lumped parameter CVS models provide a unique physiologically and clinically relevant expression of a patient's global cardiovascular state. Therefore, they can be used to provide useful information to assist clinical staff with diagnosis and treatment decisions.

This parameter identification approach was validated in two pig studies on septic shock and acute pulmonary embolism. The outputs of the subject-specific CVS models were shown to accurately converge to the observed measurements. The modelled maximum left and right ventricular pressures and volumes were nearly always predicted within median percentage errors of less than 20% of measured values, which is acceptable for this type of physiological monitoring. These measurements were not used during the identification process. Thus, this result is a true independent validation of the parameter identification process.

The identified CVS models were also able to track known disease-dependent trends in the pigs during these studies. In acute pulmonary embolism, as blood clots were inserted into the pigs, an increase in the modelled pulmonary vascular resistance was observed, as expected. A large increase in the ratio of the right to left ventricular end diastolic volumes was seen in the models of the pigs near death. This result shows the pigs could no longer compensate for the effects of the pulmonary

emboli, and thus, indicate that the subject-specific models can be used to monitor the severity of pulmonary embolism.

In septic shock, a decrease in systemic vascular resistance was identified in all the pigs after endotoxin infusion. Systemic vascular resistance recovered in two of the pigs after hemofiltration therapy was initiated. However, this parameter remained decreased in the other two pigs in the study, indicating they were not responding positively to therapy. This study and its results show how subject-specific CVS models could be used to monitor the effectiveness of therapy and its ability to differentiate between (similar) subjects. It also validates the models and methods for a further common CVS dysfunction.

Patient-specific CVS models were also identified from human measurements in patients who were recovering from mitral valve surgery in the Christchurch Hospital ICU (New Zealand). This research represents the first real clinical test of the approach on humans in an uncontrolled clinical environment. In this study, the CVS models noticed decreased pulmonary vascular resistance, and reduced pulmonary vein pressures, were responsible for a drop in pulmonary artery pressures in the patients. A decrease in left ventricular contractility was seen in one patient indicating cardiac decompensation post-surgery. However, the other patients seemed to recover well with improved left ventricular function and decreased pulmonary artery pressures. These results indicate how the model-based method can help track the path of cardiac recovery post mitral valve surgery, in the first human clinical test of the approach.

A second component of this thesis involved the development of a model-based method for examining morphological changes that occur in the aortic pressure waveform (P_{ao}) due to the effects of septic shock. In this model, P_{ao} is separated into two components representing viscous effects of flow, called the excess pressure (P_{ex}), and the elastic recoil of the arterial walls to the change in volume in the arterial system, called the reservoir pressure (P_{wk}). Subject-specific aortic models, identified from measurements from a porcine study on septic shock, were used to calculate the hydraulic work associated with the excess and reservoir pressures (W_{ex}, W_{wk}). Changes in these energetics were compared to metrics derived from left ventricular pressure-volume analysis. Total aortic work (W_{ao}=W_{ex}+W_{wk}) compared well to clinically assessed left ventricular work (R^2=0.88). Another strong relationship (R^2 = 0.76) was found between the inverse of afterload (1/Ea) and W_{ex}. As septic shock progressed, a drop in W_{wk} was seen, indicating the arterial system loses its ability to store the stroke volume (SV) from the ventricle for release during diastole, resulting in a flattening of the diastolic pressure. These results indicate that one of the main reasons left ventricular afterload

decreases during septic shock is because the arterial system loses its ability to act as a storage reservoir.

Overall, this work developed and presented two model-based methods for analysing, diagnosing, and monitoring a variety of common cardiovascular diseases. Parameter identification methods were used to combine typically available hemodynamic measurements into a clear physiological picture of a patient's cardiac and circulatory physiology. The resultant patient-specific CVS models were shown to track known disease and treatment dependent hemodynamic changes and identified key determinants of cardiac function, such as preload, afterload, and contractility. They were able to clearly differentiate between subjects and their response to therapy, which is clinically very important. Hence, the main accomplishment of this thesis was identifying physiologically accurate subject-specific CVS models, from available ICU measurements, for simplifying the monitoring of cardiovascular status. These methods provide a feasible and potentially practical means of improving care and reducing the economic cost of CVS dysfunction in the ICU.

CHAPTER 1: INTRODUCTION AND MOTIVATION

The intensive care unit (ICU) treats some of the sickest and most critically ill patients in the hospital. The majority of these patients would die without therapeutic intervention. Generally, they suffer from a severe patho-physiological disorder and require support for failing organs. Intensive monitoring is needed to ensure accurate diagnoses, that the correct therapy is applied, and to track the effectiveness of the treatment. However, the overflow of monitored information in the ICU can overwhelm human cognitive limits. On the other hand, abstract, indirect, or limited data can make the clinical picture unclear. Therefore, patient monitoring in the ICU is a balancing act between information levels and clarity in an attempt to optimise decision making.

Patients with severe cardiovascular disease (CVD) generally require intensive monitoring and support (Boldt, 2002, Pinsky, 2007, Tibby and Murdoch, 2003). Cardiovascular dysfunction can occur in many areas of the cardiovascular system (CVS) as a result of a wide range of causes, including age, congenital defects, and/or illness. Compounding the problem is the fact that cardiac and circulatory diseases are extremely common in society and are the largest cause of death in the western world, accounting for 37% of deaths in New Zealand (World Health Organisation, noncommunicable diseases New Zealand profile) and 48% of deaths in Europe (Allender et al., 2008) in 2008. Moreover, it has been estimated that more than 50% of postoperative deaths are caused by cardiac events (Mangano, 1994, Ramsay, 1999).

Because of its high prevalence in society, CVD is a major cause of ICU admission and mortality (Ramsay, 1999, Dellinger, 2003, Dellinger et al., 2004, Bahloul et al., 2010). Many admissions to the ICU are for cardiac and circulatory monitoring or dysfunction (Walsh et al., 2005, Seferian and Afessa, 2006, Dellinger et al., 2004), with many further admissions resulting from cardiovascular complications that occur intraoperatively (Tuman et al., 1992, Mangano, 1994, Ramsay, 1999). Even in non-cardiac surgery patients, one third have coronary artery disease (CAD), or two or more risk factors of CAD, or are older than 65 years (Mangano, 1994). In the United States, the cost of cardiovascular complications following an operation is estimated to be 33 billion USD (Mangano, 1994), which is only a fraction of the overall cost of CVD. This total direct medical cost of CVD is approximately $273 billion in the United States (Heidenreich et al., 2011) and is expected triple to $818 billion by 2030 (Heidenreich et al., 2011), due to increasing obesity, sedentary lifestyles, and an aging population. Hence, the treatment and flow-on effects of cardiovascular disorders will continue to be a major clinical and cost burden in the ICU for the foreseeable future.

Traditional hemodynamic monitoring in critical care is often constrained by the ease and frequency at which measurements can be made and taken. The use, number, and positioning of catheter containing sensors is determined by the perceived risk to benefit ratio of inserting the device(s). Hence, catheters cannot always be placed in the most ideal position for monitoring a certain pathological state. Other factors, including expense and obstruction to clinical work flow, limit the regularity at which other measurements are taken, such as with the use of computer tomography and echocardiography. Due to these constraints clinicians often do not receive a full picture of a patient's hemodynamic state, which can result in misdiagnosis and incorrect treatment, leading to inefficient use of hospital resources, increased length of stay, and death (Angus et al., 2001, Brun-Buisson, 2000, Franklin and Mathew, 1994, Perkins et al., 2003, Smith et al., 2002).

Hence, there is a need for improved cardiovascular monitoring in intensive care. Integration of all available measurements in a mathematical framework of cardiovascular physiology could be employed to continuously predict cardiac and circulatory status in regions that cannot be directly measured. Such a method would provide one means to untangle the complex, often confusing interactions that occur between different measurements to better reveal a patient's underlying disease state, and therefore, maximise the useful information gained from the available ICU data.

1.1 HEMODYNAMIC MONITORING IN THE ICU

Hemodynamic monitoring is the first port of call when evaluating the state of critically ill patients in the ICU. These patients are monitored to diagnose and identify the severity of cardiovascular insufficiency, as well as the response to therapy. The rationale behind cardiovascular monitoring is that (Pinsky, 2007):

- Hemodynamic monitoring can help identify disease even though the link between the monitored variable and dysfunction is unknown.
- Hemodynamic parameters define cardiovascular state, and restoration of these parameters to normal values will improve tissue perfusion and patient outcomes.
- Monitored variables can drive goal-directed therapy in a manner that cannot be otherwise predicted.

However, very simply, when monitored hemodynamic variables do not influence therapy, they cannot improve outcome. Hemodynamic monitoring can only provide benefit to the patient when coupled with treatment. Hence, the insertion of a catheter in the absence of a defined and effective

treatment protocol requiring the information it delivers is unlikely to result in improved cardiovascular status (Connors et al., 1996, Pinsky, 2007, Sandham et al., 2003, Yu et al., 2003). This fact may be the reason why historically many randomised control trials evaluating a given intervention fail to produce significant reduction in mortality (Ospina-Tascon et al., 2008). Thus, in recent times, many therapies have been developed that couple monitored variables with treatment.

Even with advances in clinical practice and available technology, there still exist many limitations in current day-to-day, clinical hemodynamic management. Variation in clinical management between centres (Kennedy et al., 2010, Wennberg, 2002) means that not all patients are receiving the same optimal treatment, which can lead to increased cost and length of stay in these patients (Kennedy et al., 2010). Even when therapy is standardised, it is optimised to improve population outcomes and may neglect the patient-specific needs of the individual. In more general terms, the information gained from available measurements is not always maximised to give the greatest benefit to the patient.

To solve these issues, a model-based system could be used to aggregate available ICU measurements in a mathematical framework of cardiovascular physiology. This methodology could help provide improved patient-specific targets for goal directed therapies and a means to maximise the utilisation of available measurements. Hence, such a method enables a way of standardising therapy while still accounting for inter-patient variability.

1.1.1 DATA RICH, BUT INFORMATION POOR

Many measurements can be taken from the typical ICU patient. However, the information gained from these measurements is not always maximised (Pinsky, 2003). For example, it is commonplace for the whole arterial pressure waveform to be measured. However, treatment is only based on discrete measures derived from the arterial pressure waveform including systolic and diastolic pressure. All the clinically useful information stored in the shape of the arterial pressure waveform (Thiele and Durieux, 2011) is ignored. This outcome indicates that the measurement of arterial pressure is not being optimised in critical care.

Similarly, monitoring stroke volume (SV) and cardiac output (CO), has in recent times been shown to have little effect on patient outcomes (Mutoh et al., 2007, Pinsky, 2007). These particular findings are strange, as it is obvious that CO is an important measure of cardiovascular health. Thus, the results of these studies indicate that both SV and the arterial pressure waveform, to name two examples, are being underutilised in the ICU.

A majority of hemodynamic pressure measurements in the ICU are taken continuously by catheters attached to digital data acquisition systems. However, most of this data is lost, because, in most ICUs, only a discrete manual record of these measurements is kept for each patient on their patient data sheet. On this record, measurements of pressure and other vital signs are typically recorded at hourly intervals, reflecting a very crude temporal depiction of the patient's recent history. A patient's state can change markedly within a couple of minutes. Thus, measurements recorded hourly are insufficient to describe the continuously changing nature of a patient's clinically relevant hemodynamics. Hence, extreme caution must be used when trying to devise any useful trends from the data stored on the patient sheet.

These brief and simple examples illustrate how the ICU is data rich, but in some respects, information poor. The information gained from the measurements in ICU is limited by the manual nature in which the measurements are initially processed and recorded on patient data sheets. If this process could be automated, which is easily achievable in a modern hospital, complete continuous real-time data can be recorded electronically. Automation of the data recording would reduce the clinical workload, enable the ability to track hemodynamic trends minute-to-minute or beat-to-beat, and allow more advanced processing of the available measurements to obtain further insight. Thus, automating the information flow, and maximising the information gathered from measurements already taken in the typical ICU, would provide many benefits at little extra cost.

1.1.2 ONE SIZE FITS ALL

Most new clinical practices are based on empirical findings from large multi-centre randomised controlled trials (Vincent, 2004). These evidence-based studies statistically analyse treatments that influence average outcomes in the study population (Feinstein and Horwitz, 1997, Tonelli, 1998). Hence, most treatments in the ICU have been optimised for the 'average patient' in a one size fits all approach, overlooking the needs of the individual patient (Charlton, 1997, Sleigh, 1997, Feinstein and Horwitz, 1997, Tonelli, 1998).

However, every patient in the ICU is different. Each patient has a unique expression for a given disease or disorder, and a distinct response to the corresponding therapy. Therefore, hemodynamic management must be personalised to each patient and not just the 'average patient' to improve current practice.

One way to personalise hemodynamic management is to track and monitor patient-specific hemodynamic parameters for goal directed therapies. To do this, cardiovascular monitoring must be

individualised for each patient to help calculate personalised targets for their treatments. This approach would enable therapy to be personalised for each patient, while still utilising current treatments. Therefore, treatment can be tailored for the individual rather than for the ICU population. Such approaches could be implemented at little extra expense, as current therapy techniques would only require a slight protocol adaption to modify or optimise current treatment using existing sensors for each patient. Moreover, the approach also has the potential to benefit a wider portion of the ICU population as it can be tailored to every patient, including those who do not fit the 'average patient' profile.

1.1.3 MODEL-BASED APPROACHES

It has been proposed, and proven, with glycaemia control (Le Compte et al., 2009, Lonergan et al., 2006, Wong et al., 2008, Chase et al., 2008, Evans et al., 2011) and in other fields (Chase et al., 2011, Chiari et al., 1998, Pasterkamp et al., 2005, Uckun et al., 1993), that computer-based models can be used to assist medical staff with therapy-based decisions. For a model-based method to be clinically viable for hemodynamic monitoring in clinical practice it should:

- accurately predict static markers of the cardiovascular health,
- track pathologically important hemodynamic trends,
- track the effectiveness of treatment,
- be inexpensive and easy to implement,
- provide continuous real-time feedback,
- be an improvement on current hemodynamic monitoring methods.

If these points can be achieved, a better understanding of the patient's disease state can be obtained at little extra cost and without the need for additional invasive measurements. Furthermore, the effectiveness of treatment can be monitored with greater accuracy, ultimately leading to improved outcome.

The benefits of using a model-based method is that it provides a means of personalising hemodynamic monitoring. Patient-specific models of the CVS could be identified using commonly available ICU data. Identified information gained from the patient-specific models can be used to predict the response of hemodynamically unstable patients in the ICU to common clinical treatments, to answer critical, "holy grail" questions, such as (Pinsky, 2007):

- Will fluid resuscitation increase cardiac output?

- During hypotension is vascular tone increased, decreased, or normal?
- Is the heart capable of maintaining cardiac output once arterial pressure is restored or will it go into failure?

Where, at present, it is difficult to answer these questions using the currently available information in the ICU (Pinsky, 2007).

Cardiac and circulatory physiology embedded in these patient-specific models can help extrapolate and interpolate between measurements, to approximate hemodynamics in unmeasureable regions of the CVS. The method could also provide a way of standardising hemodynamic management while still allowing patient-specific treatment. Furthermore, the approach could be applied in real-time, and at little extra cost, as it would only require measurements that are already commonly recorded in the ICU. Hence, model-based monitoring has many advantages and few disadvantages.

1.2 GOALS OF THIS RESEARCH

The aim of this thesis is to use patient-specific computer models of the CVS to simplify and improve hemodynamic monitoring in critical care. CVS models can be personalised to each patient using common ICU measurements to track an individual's cardiovascular response to a disease or treatment. Identified parameters and outputs of these models can provide improved indices of cardiovascular health and help better track disease and treatment dependent hemodynamic changes.

This research utilises the physiologically validated CVS model developed by Smith (Smith, 2004, Smith et al., 2004) to help identify the cardiovascular phenomena. Smith's lumped parameter model is capable of representing many hemodynamic situations commonly seen in the ICU (Smith et al., 2007, Starfinger et al., 2008a, Starfinger et al., 2008b, Starfinger et al., 2007) using only a minimal number of physiological parameters. Thus, the CVS model provides a good initial platform for identifying clinically relevant cardiovascular dynamics.

Starfinger proposed and developed a method for identifying parameters from Smith's CVS model (Starfinger, 2008, Starfinger et al., 2008a, Starfinger et al., 2008b, Starfinger et al., 2007). However, Starfinger's method could not uniquely identify all the parameters of the CVS model from the minimal measurement set available in the ICU. Hence, this research builds on the prior work of Starfinger et al (Starfinger, 2008, Starfinger et al., 2008a, Starfinger et al., 2008b, Starfinger et al.,

2007) in an attempt to try and fully identify patient-specific CVS models from the measurements available in intensive care.

1.3 APPLICATION OF RESEARCH

In this research, subject-specific models of cardiovascular dynamics were retrospectively fitted to porcine measurements to analyse the viability of this approach. Measurements were obtained from two pig studies on pulmonary embolism and septic shock. Subject-specific models were retrospectively fitted to these measurements to track the progression of disease and internal reflex response of the animals. More specifically, the effects of these diseases on identified metrics of ventricular preload, contractility, and afterload were analysed.

The method was also tested retrospectively on human measurements. Patient-specific models were fitted to patients recovering from mitral valve surgery. The parameters and outputs of the model were analysed to monitor the recovery, response to therapy, and compensation of the left ventricle to a new or repaired mitral valve, in these patients. The results of this research provide the first human validation of the model identification method.

Finally, a second model-based method was used to model aortic energetics. The new model was identified from porcine measurements to analyse the effects of septic shock on ventricular-vascular coupling. This method provides an alternative approach which can be used to model important hemodynamic variables when the pulmonary artery pressure is unknown.

CHAPTER 2: CARDIOVASCULAR PHYSIOLOGY

This chapter gives a brief overview of the important aspects of cardiovascular physiology. It is designed to provide the essential foundation information required to understand the research, models, results, and discussions in the following chapters.

2.1 CARDIOVASULAR SYSTEM OVERVIEW

The CVS consists of 3 main components including the heart, blood, and blood vessels. These components are responsible for passing nutrients, gases, hormones, blood cells, etc. to and from the cells in the body to help maintain homeostasis. The heart acts as the pump for this hydraulic system providing the driving force for the flow through the blood vessels by means of repeated rhythmic contractions. The blood vessels make up the two major circuits within the CVS, the systemic circulation and the pulmonary circulation, which are connected in series by the heart.

In the pulmonary circulation, blood is pumped through the right atrium and ventricle into the pulmonary artery and through the lungs, where carbon dioxide is exchanged with oxygen. The oxygenated blood returns to the heart via the pulmonary vein, where it is pumped through the left atrium and ventricle into the systemic circulation, beginning with the aorta. The aorta and arterial network deliver blood from the left ventricle to the systemic capillaries providing nourishment to body's tissues. The systemic veins complete the closed circuit system, returning blood from the capillaries to the right atrium, to be re-pumped through the pulmonary circulation.

Figure 2.1 shows an overview of the CVS, and these two primary circuits. Oxygenated blood in the pulmonary veins, left heart, and systemic arteries is shown in red. Deoxygenated blood in the systemic veins, right heart, and pulmonary arteries is shown in blue.

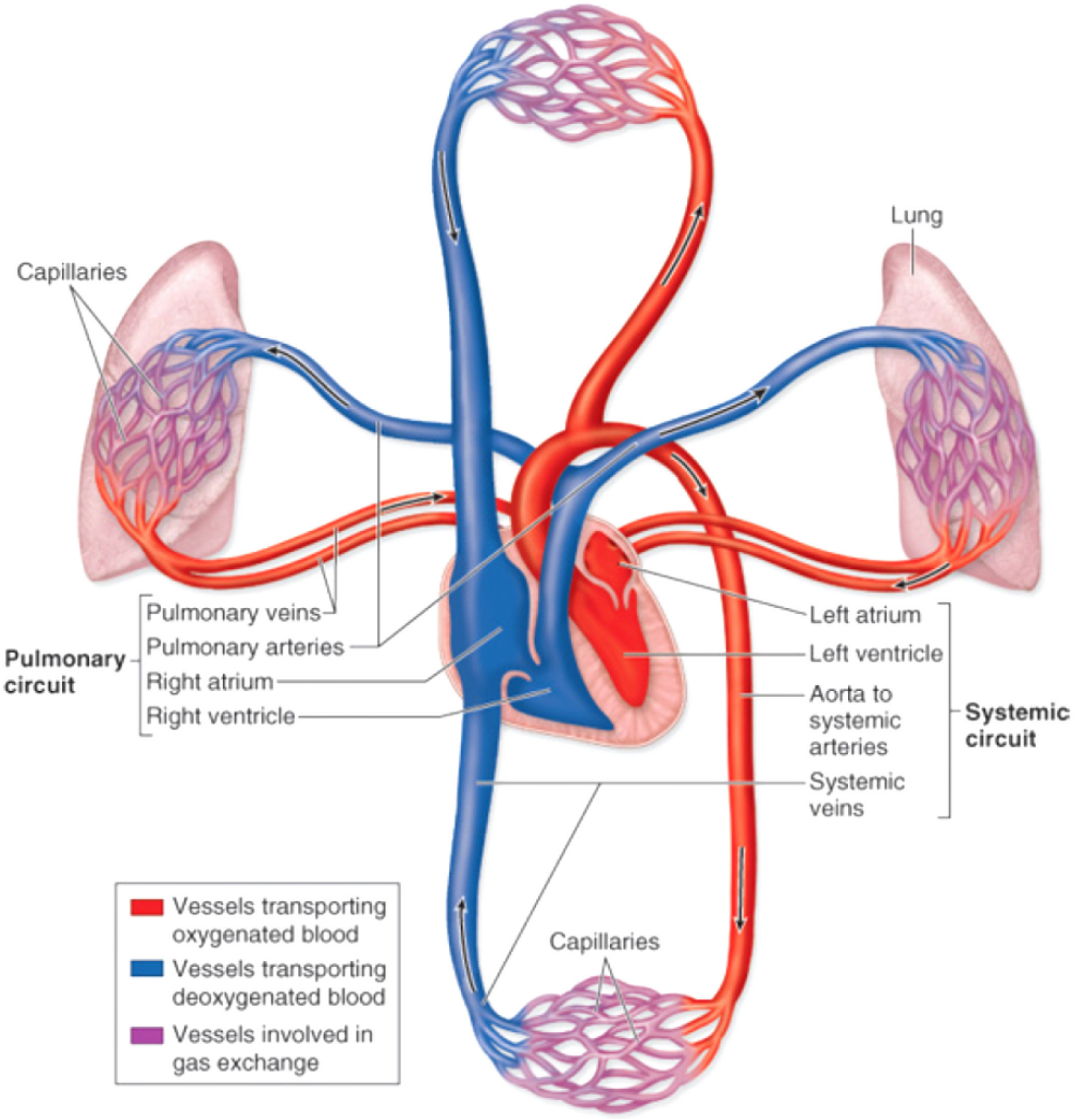

Figure 2.1: Overview of the anatomy of the cardiovascular system (McKinlay and O'Loughlin, 2007) showing the heart, systemic circuit, and pulmonary circuit.

2.2 THE CIRCULATION

The circulation is split up into two circuits: the systemic circuit and the pulmonary circuit. Both circuits are made of three parts: an arterial system, a capillary network, and a venous system. These three components are discussed in further detail in the following.

2.2.1 ARTERIAL SYSTEM

The arterial system transports blood from the heart to capillaries. The aorta is the root of the arterial system, which receives the blood ejected from the left ventricle via the aortic valve. As the aorta branches, and these arteries branch further, they become successively smaller in diameter. The smallest are the arterioles which supply the capillaries.

These arteries can be divided into two types, elastic and muscular, depending on their structure. In general, the larger arteries are elastic and the smaller arteries are muscular. The function of the elastic arteries is to diffuse the flow pulse ejected from the ventricle, and thus smooth the pressure and flow profile of the blood before it reaches the capillaries. Blood flows with almost no resistance in these larger arteries.

In contrast, the resistance to flow is considerable in the much smaller arterioles. These vessels control local blood flow and collectively have the greatest influence on systemic blood pressure. The arterioles make up the greatest component of, and act to regulate, the resistance of the systemic circulation. Hence, they are the principal determinant of flow through the CVS.

The combination of the elastic arteries and resistance regulating arterioles provide a means for the arterial network to distribute a constant flow of blood from the ventricle to capillary beds. This blood carries oxygen and nutrient to the tissues. The constant flow through the capillaries ensures a consistence and smooth supply of nutrients to the organs across a heartbeat.

2.2.2 THE CAPILLARIES

The capillaries bridge the arterial and venous systems via a parallel network. The capillaries are where all the important exchanges occur in the circulatory system. These exchanges include the diffusion and transfer of gases, sugars, hormones, waste products, and other nutrients to surrounding tissue. Equally, these surrounding tissues surrender waste products, such as carbon dioxide, to be returned via the venous system. Figure 2.2 shows an example of a network of capillaries connecting an arteriole and venule.

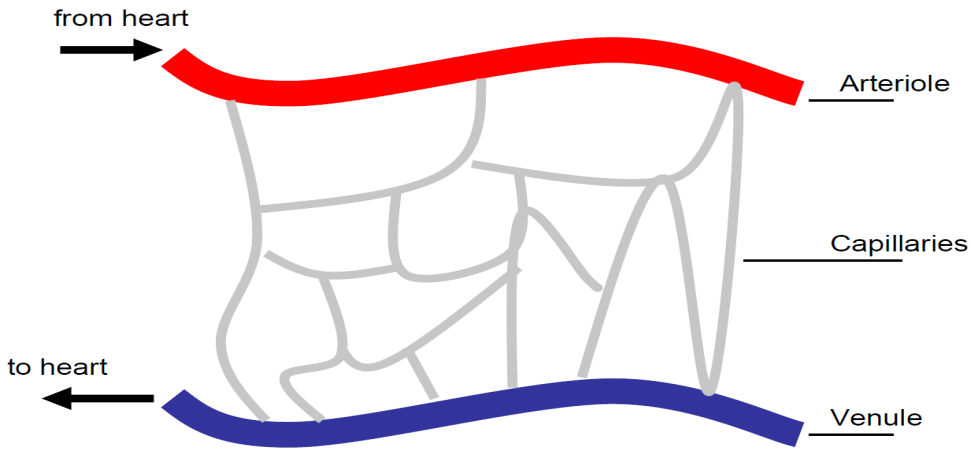

Figure 2.2: Example of capillaries connecting the venous and arterials systems via an arteriole and a venule (Starfinger, 2008).

2.2.3 VENOUS SYSTEM

The venous system returns blood from the capillaries to the heart. Flow enters the venous system via transfer between the capillaries and the venules. The venous system transports blood from the venules to the heart, via a converging network of veins, which increase in diameter as they approach the heart. The walls of these veins are thin and very compliant and can expand to store blood, if required. They are thus complimentary to the arterial system controlling the venous return of blood to the heart.

2.3 THE HEART

2.3.1 ANATOMY

The heart is the main pump of the CVS. It consists of two sides and four distinct chambers. The left side, including the left atrium and left ventricle chambers, pumps oxygenated flow from the pulmonary veins into the aorta. The right side, consisting of the right atrium and right ventricle chambers, pumps deoxygenated flow from the vena cava into the pulmonary artery. The sides of the heart are separated via two septal walls one situated between the atria and the other between the ventricles.

Four heart valves control flow between these chambers. The mitral (or left atrioventricular) and aortic (aortic semilunar) valves regulate the flow in and out of the left ventricle, and the tricuspid

(right atrioventricular) and pulmonary artery (pulmonary semilunar) valves regulate flow in the right ventricle. These valves ensure one way flow through heart, avoiding regurgitation, allowing pressure to build in the ventricles during myocardium contraction.

All the chambers of the heart are encapsulated inside a fibrous sac called the pericardium. The pericardium provides a reactor wall against which the heart can push as it pumps blood. The structure of the heart is illustrated on Figure 2.3. Please note the pericardium is not included in Figure 2.3 but can be seen in Figure 2.12.

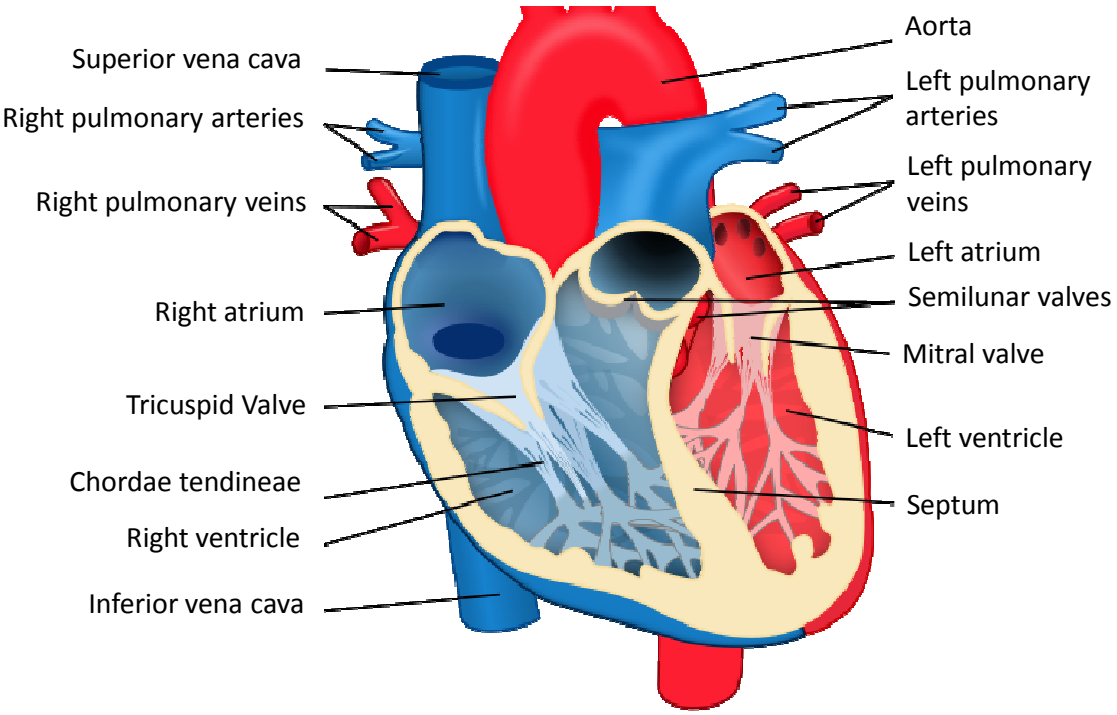

Figure 2.3: Anatomical features of the heart not including the pericardium.

2.3.2 ELECTRICAL ACTIVATION

Each contraction of the heart is initiated by an electrical stimulus. A region of the heart called the sinoatrial node acts as the pacemaker for these contractions controlling the rate at which cardiac muscle cells contract. At the start of a heartbeat, electrical impulses produced in the sinoatrial node cause contraction in the atria. At the same time, action potentials travel to the atrioventricular node via intermodal pathways. Here, the electrical impulses are delayed by approximately 0.1s, before being conducted through the bundle of His to the bundle branches. The stimulus travels through these branches, via the purkinje fibres, exciting the endocardium at the apex of the heart, and finally

the ventricular myocardium, into contraction. The total travel time of the electrical impulses from the sinoatrial node to the ventricular myocardium, is approximately 0.19s in normal individuals. The total cycle between electrical pulses is approximately 0.8s, equivalent to a single heartbeat. An illustration of the electrical conduction pathway in the heart is shown in Figure 2.4.

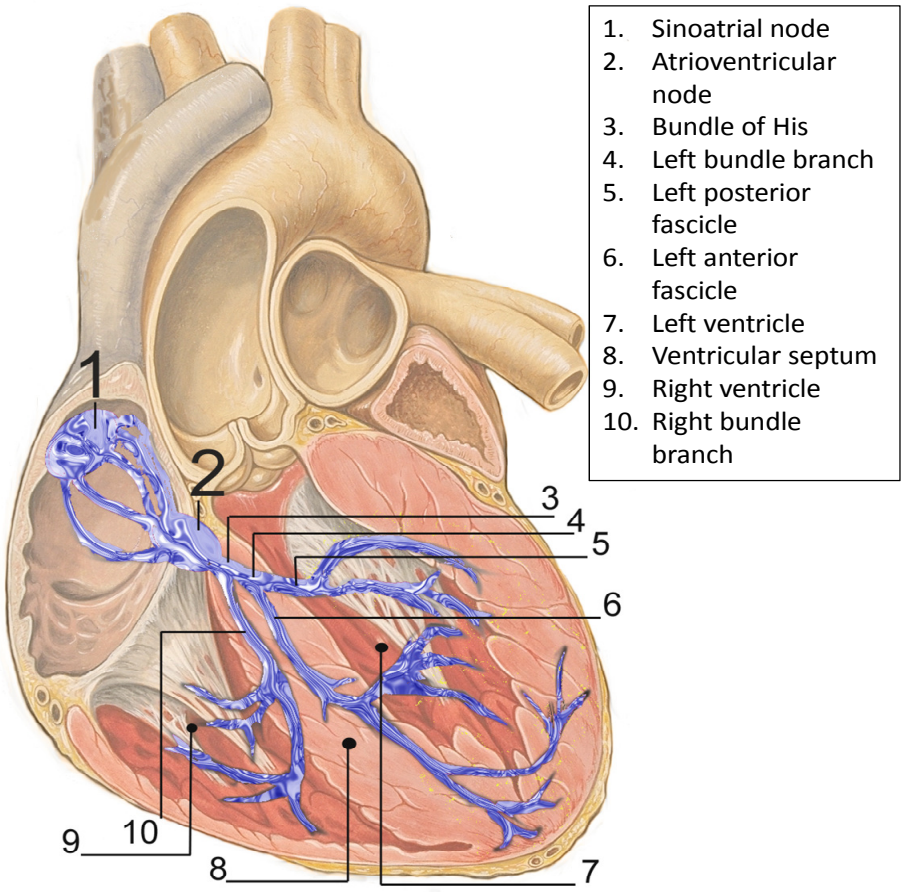

Figure 2.4: Electrical conduction system of the heart. Picture modified from the work of (Lynch and Jaffe, 2006).

The electrical impulses produced during the heart cycle conduct throughout the body. On the skin these impulses can be detected using an electrode and recorded as an electrocardiogram (ECG). An example of an ECG is shown in Figure 2.5. On the ECG, the P-wave represents the conduction of electrical impulses through the atria, the QRS-complex depicts the spread of electrical activity throughout the ventricular myocardium, and the T-wave portrays the repolarisation of the ventricles, the last event of the electrical cycle.

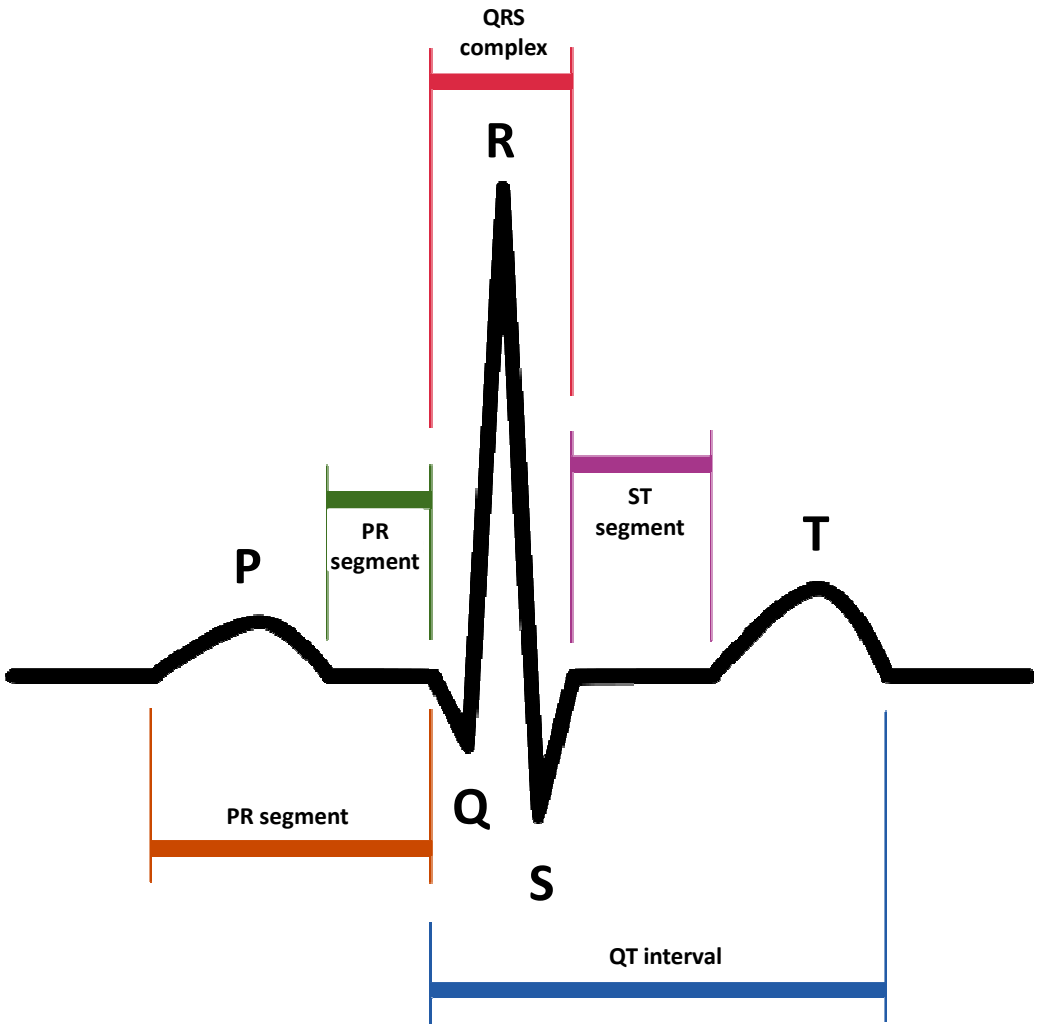

Figure 2.5: Electrocardiogram showing the P-wave, QRS complex, and T wave.

An electrochemical mechanism turns the electrical impulses in the heart into muscle contraction. When myocardial cells are stimulated above a certain threshold voltage-gated calcium channels open allowing positively charged Ca^{2+} to enter the cell. These ions cause depolarisation in the cell resulting in muscle contraction. After a delay, potassium channels open resulting in a flow of K^{+} out of the cell causing repolarisation and relaxation of the myocardial cell. Hence, the cell returns to its resting state, until it is re-stimulated.

The electrical activation of the heart controls the sequence of the events that occur within the cardiac cycle. The electrical impulses, initiated by the sinoatrial node, set the heart rate and instigate heart muscle contraction. Furthermore, the pathway of electrical conductance ensures the atria contract prior to the ventricles to keep the heart running efficiently. Hence, the sinoatrial node and

electrical conductance pathway play an important role in ordering the mechanical events of the cardiac cycle.

2.3.3 THE CARDIAC CYCLE

The electrochemical reaction in the heart causes the myocardium to repeatedly contract and relax. This contraction and relaxation of the heart can be broken up into four segments representing one full cardiac cycle. The contractile phase in the cardiac cycle is called systole, representing an isovolumetric contraction period followed by ventricular ejection. The relaxation phase is called diastole which consists of a short isovolumetric relaxation segment followed by filling. Figure 2.6 shows the relationship between the electrical activation of the heart and left ventricular dynamics during the **filling**, **contraction**, **ejection**, and **relaxation** phases of the cardiac cycle.

These four stages of the cardiac cycle can be described with reference to the pressure and volume in the ventricle, flows in and out of the mitral and aortic valves, and pressures in the left atrium and aorta, as shown on Figure 2.6. During ventricular **filling** left atrial pressure is higher than left ventricular pressure. Hence, the mitral valve opens and blood flows into the left ventricle. This **filling** phase ends at the beginning of **contraction**, when the myocardium begins to contract, causing left ventricular pressure to increase, resulting in closure of the mitral valve. Isovolumetric **contraction** follows, where pressure increases sharply with little change in volume. When ventricular pressure increases above aortic pressure, the aortic valve opens, indicating the beginning of the **ejection** phase and causing blood to be ejected into the aorta. Ventricular **ejection** continues until the myocardium starts to relax and ventricular pressure decreases, causing the aortic valve to close. A short isovolumetric **relaxation** period follows, where pressure decreases quickly with little change in volume. The mitral valve opens once ventricular pressure drops below the left atrial pressure, and the whole cycle starts again.

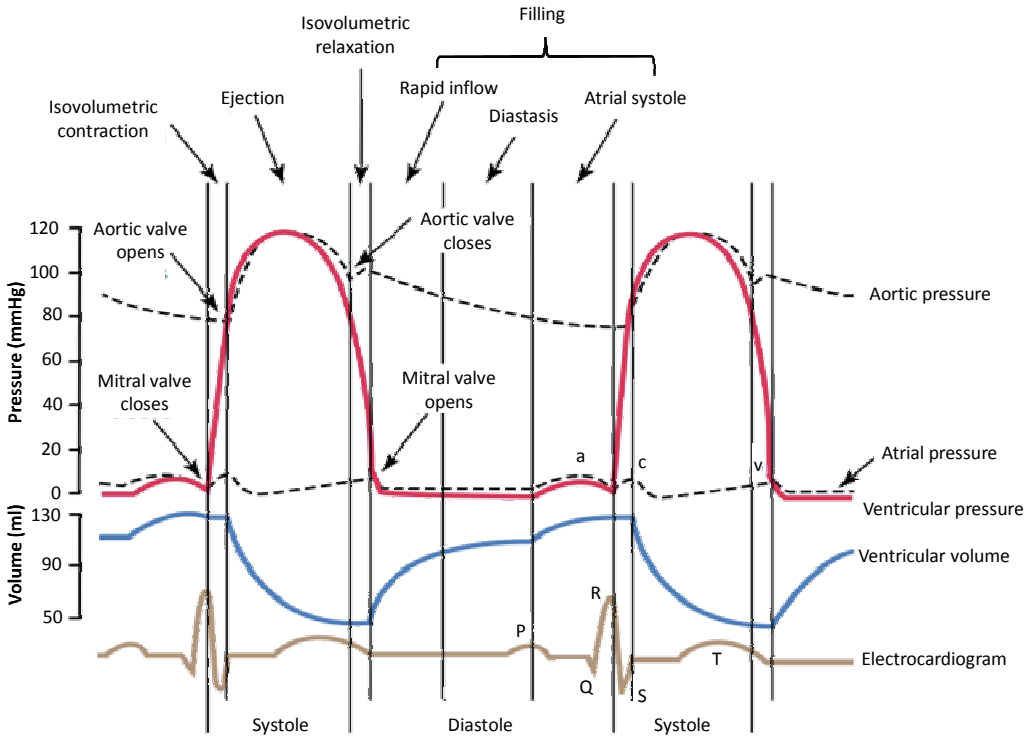

Figure 2.6: Example of the cardiac events which occur during the cardiac cycle. Two complete cardiac cycles are illustrated showing the pressures in the left atrium, left ventricle, and aorta; volume in the left ventricle; and electrocardiogram.

2.4 BASIC CONCEPTS

The cardiac cycle can also be analysed via ventricular pressure-volume (P-V) loops. Figure 2.7 shows an example of a ventricular P-V loop. A given P-V loop is confined between the end diastolic pressure volume relationship (EDPVR) and the end systolic pressure volume relationship (ESPVR). The difference between the end diastolic volume (EDV, maximum ventricular volume) and the end systolic volume (ESV, minimum ventricular volume) represents the stroke volume of the ventricle.

$$SV = EDV - ESV \tag{2.1}$$

The arterial load on the ventricle (E_a) can be inferred from the relation between end systolic pressure (ESP) and SV on the P-V loop (Kelly et al., 1992), as shown on Figure 2.7.

$$E_a = \frac{ESP}{SV} \tag{2.2}$$

Moreover, the area enclosed by the P-V loop represents the hydraulic work done by the ventricle over one heartbeat.

Changes in the shape of the P-V loop reflect alterations in cardiac state, including changes in **preload**, **afterload**, and **contractility** of the ventricle, which are defined in Sections 2.4.1, 2.4.2, and 2.4.3 respectively. However, P-V loops do not reveal temporal factors, such as changes in **heart rate**, which is another important determinant of cardiac function. The combination of these four factors:

- Preload
- Afterload
- Contractility
- Heart rate

determine the amount of forward flow, **cardiac output**, and the **blood pressure** in the cardiovascular system.

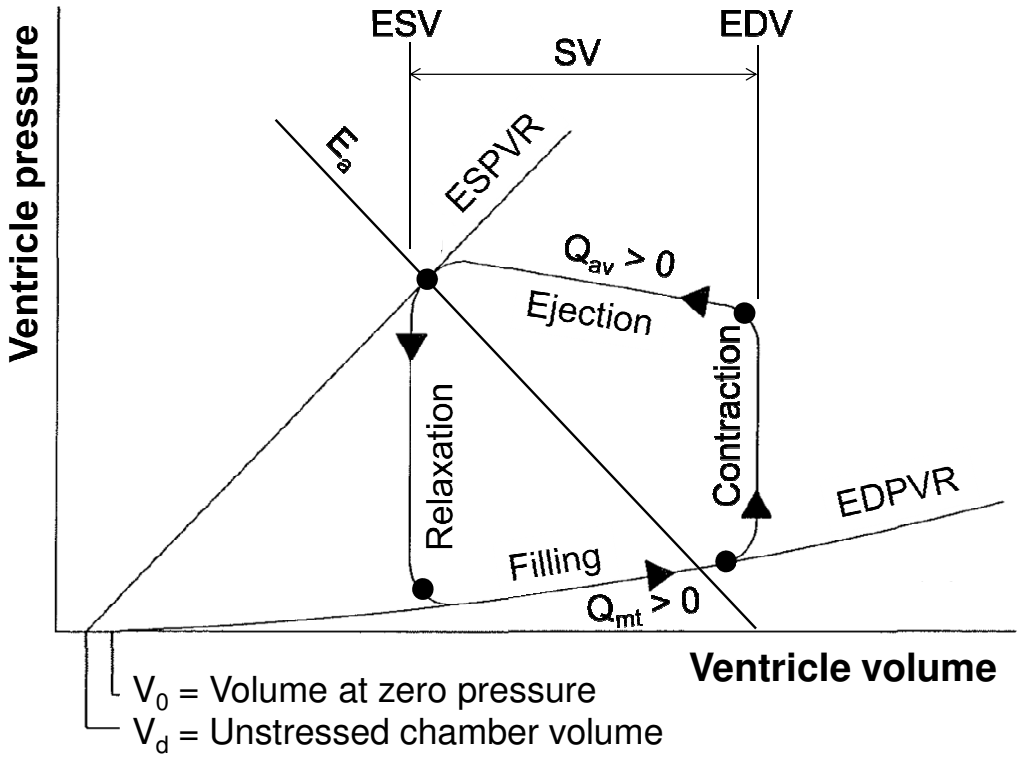

Figure 2.7: Pressure-volume loop showing the four phases of the cardiac cycle. The pressure volume loop is confined below the end systolic pressure-volume relationship (ESPVR) and above end diastolic pressure-volume relationship (EDPVR). The arterial elastance (E_a) reflects the arterial load imposed on the ventricle. The stroke volume of the ventricle is the difference between the end diastolic volume (EDV) and end systolic volume (ESV). Q_{av} and Q_{mt} represent flow through the aortic and mitral valves.

2.4.1 PRELOAD

Preload is the end volumetric pressure that stretches the ventricle to it greatest geometrical dimension during a heartbeat. Strictly speaking, it is defined as the initial stretch of a single cardiac cell prior to contraction. However, it is not feasible to measure the stretch of a cardiac cell *in vivo*. Hence, in practice, the more clinically available measurement of EDV is often used to represent preload.

Physiologically, preload plays an important role in determining stroke volume, and consequentially cardiac output. Increased ventricular filling, or preload, augments the stroke volume, whereas decreased ventricular filling drops stroke volume. In other words, the ventricular muscles contract with more force when they are preloaded or stretched prior to contraction (Frank, 1895, Starling and Visscher, 1927). This mechanism is commonly known as the Frank-Starling mechanism (see Section 2.6.2).

Figure 2.8 shows the effects of changing preload on the ventricular P-V loops. In this example, preload is considered to be the EDV of the ventricle, and ventricular contractility and afterload are kept constant. It is seen that an increase in preload causes an increase in SV and systolic pressure in the ventricle. SV increases because EDV increases more than end diastolic volume. The opposite effects are seen when the preload is decreased.

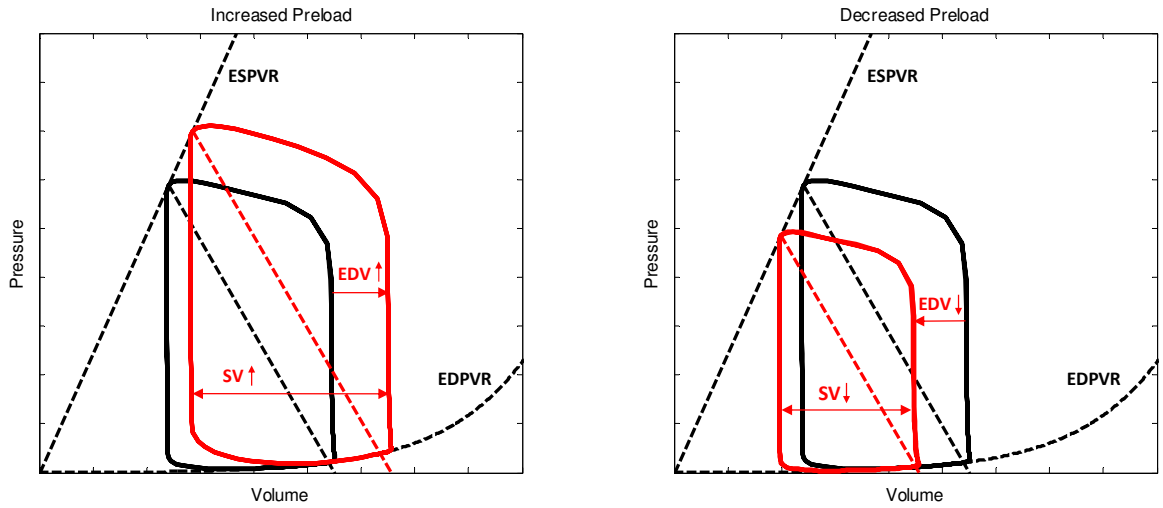

Figure 2.8: Effect of changing preload (end diastolic volume) on the ventricular pressure volume loop. The control pressure-volume loop is plotted in black.

Many factors influence the preload on the ventricle (Klabunde, 2004) including but not limited to:

- Venous return and pressure
    - Venous tone
    - Total blood volume
    - Respiration
- Outflow resistance and afterload
- Ventricular compliance
- Atrial contractility

Clinically, preload can be improved through fluid resuscitation, which increases total blood volume, augmenting venous return and venous pressure, increasing the volume in the ventricle (O'Neill and Perrin, 2002). However, positive pressure ventilation increases intrathoracic pressure (P_{th}), which augments atrial pressure, decreasing the pressure gradient driving flow back to the heart (Pinsky, 2005, Shekerdemian and Bohn, 1999, Soni and Williams, 2008). Hence, venous return drops, diminishing both preload and SV. These two examples indicate how common therapies can be used to influence preload. However, other factors, such as disease and auto regulatory responses, can also significantly alter ventricular blood volume. Therefore, it can be difficult to determine the main reasons for changes in preload in clinical setting.

2.4.2 AFTERLOAD

Afterload is the load against which the heart must contract to eject blood. It is technically defined as the tension or stress developed in the wall of the ventricle during ejection. Under normal healthy conditions, afterload is imposed on the heart by the arterial system. However, during cardiovascular disease, afterload can be augmented by factors other than the properties of the arterial system, such as aortic stenosis. There are several measurements or surrogates that reflect afterload, including:

- Aortic or arterial pressure (P_{ao})
- Systemic resistance (R_{sys})
- Arterial impedance (Z_a)
- Arterial elastance (E_a)

Arterial elastance (E_a) is the gold standard clinical measure of afterload (Kelly et al., 1992). Changes in E_a are used to analyse the effects of afterload on the ventricular P-V loops, as illustrated in Figure 2.9. An increase in afterload, independent of changes in contractility and preload, causes an increase in systolic pressure and a decrease in SV. However, a decrease in E_a causes increased SV and decreased systolic pressure.

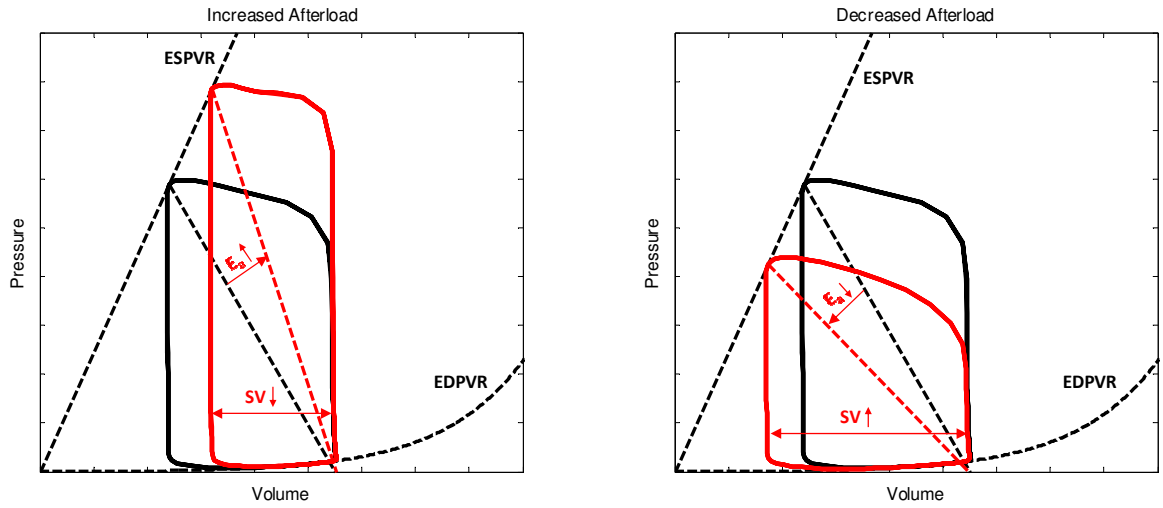

Figure 2.9: Effect of changing afterload (arterial elastance, E_a) on the ventricular pressure volume loop. The control pressure-volume loop is plotted in black.

In the ICU, afterload can be altered through the administration of vasoactive drugs. Drugs that cause vasodilation decrease afterload by decreasing vascular tone, increasing vascular diameter and decreasing resistance to flow. Whereas, vasoconstriction results in a narrowing of blood vessels, and, as a consequence, increases resistance to flow and afterload. In a setting where blood pressure is measured, such as in the ICU, vasoconstrictor and vasodilator agents can be titrated to alter afterload and achieve a desired blood pressure.

2.4.3 CONTRACTILITY

Ventricular contractility represents the ability of the myocardium to contract independent of changes in preload and afterload. The gold standard measure of contractility is end systolic elastance (E_{es}) (Grossman et al., 1977, Sagawa, 1981, Suga et al., 1973) represented by the slope of the ESPVR on Figure 2.7 . This relationship defines the maximum pressure that can be produced by the ventricle for a given unit of volume, for any one heartbeat. E_{es} is often considered to be relatively constant

over a normal range of loading conditions for a given inotropic state (Kass et al., 1987), and thus, it can be represented by the following relationship:

$$E_{es} = \frac{P_{es}}{V_{es} - V_d} \tag{2.3}$$

where P_{es} and V_{es} are the end systolic pressure and volume in the ventricle and V_d is the unstressed volume.

The effects of E_{es} on the ventricle P-V loops are shown in Figure 2.10. Increased contractility leads to a rise in systolic pressure and SV. Conversely, decreased contractility results in a drop in systolic pressure and SV.

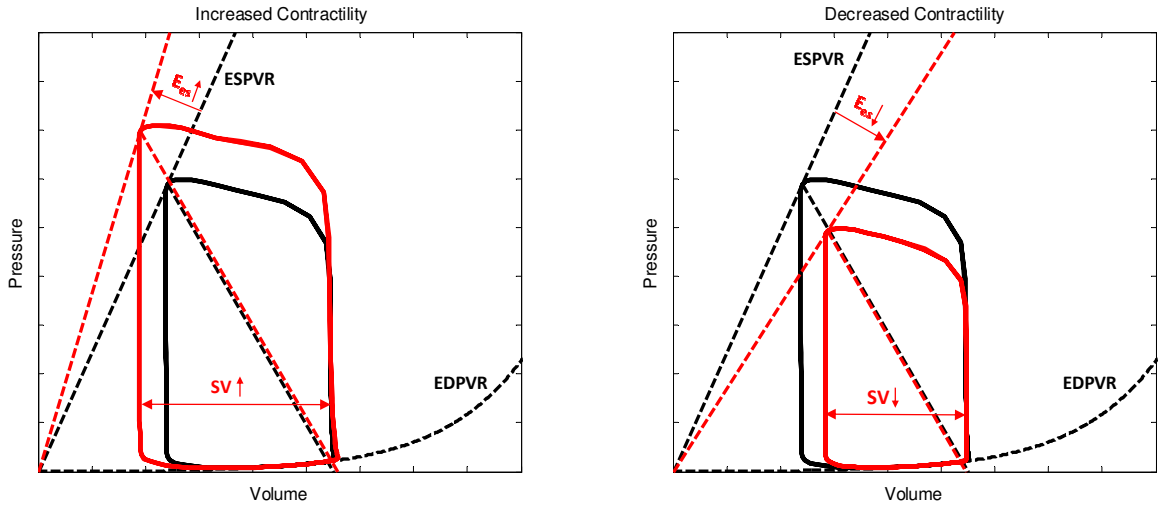

Figure 2.10: Effect of changing contractility (slope of ESPVR, E_{es}) on the ventricular pressure volume loop. The control pressure-volume loop is plotted in black.

In the ICU patient, contractility can be altered through the use of inotropes (Paolocci et al., 2003, Sagawa, 1981, Suga et al., 1983). Positive inotropic agents increase myocardial contractility, and hence, augment SV. While, negative inotropic agents decrease myocardial contractility, and can be used to decrease cardiac workload.

2.4.4 HEART RATE

Heart rate (HR) is the number of heartbeats which occur within a minute. As mentioned in Section 2.3.2, HR is determined by the rhythm produced by the sinoatrial node. It is the inverse of the interval between adjacent R-waves as seen on the ECG (Figure 2.5).

During treatment, chronotropic drugs can be use to change HR by affecting the rhythm produced by the sinoatrial node. Positive chronotropes increase HR, whereas negative chronotropes decrease HR.

2.4.5 CARDIAC OUTPUT

Cardiac output (CO) is the volume of blood pumped by the heart over one minute. It is defined as:

$$CO = HR \cdot SV \tag{2.4}$$

Where HR is the heart rate (beats per minute) and SV is the stroke volume (in litres). Hence, CO (litres/minute) is a product of HR and also preload, afterload, and contractility, which effect SV.

In a healthy person, CO adjusts to meet the metabolic demands, ensuring sufficient oxygen and nutrient supply to the cells of the body. However, detrimental changes in CO can be caused by cardiovascular disorders, especially in hypotension and heart failure, creating an imbalance between nutrient supply and metabolic demand. Cardiovascular disorders can be associated with an increase in CO, as occurs during septic shock (MacLean et al., 1967), or a decrease in CO, as for example in cardiogenic shock (Hollenberg et al., 1999, Hochman and Ohman, 2009) and hypovolemia (Kreimeier, 2000). These diseases and disorders are common problems in the ICU (Martin et al., 2003, Hochman and Ohman, 2009, Antonelli et al., 2007). Hence, the ability to monitor, and accurately interpret the reasons for changes in, CO in critical care is of great importance.

In the ICU, CO can be continuously estimated using a number of pulse pressure analysis methods (Cottis et al., 2003, Linton et al., 1993, Opdam et al., 2007). These methods are normally calibrated against a dilution technique (Cottis et al., 2003, Opdam et al., 2007). In general they are well accepted measures.

2.4.6 BLOOD PRESSURE

Blood pressure is one of the principal vital signs used to guide therapy in critical care. It represents the pressure exerted on the vascular walls in the CVS. The term ‘blood pressure’ when used without

specification, normally refers to arterial pressure of the systemic circulation. During each heartbeat blood pressure varies between a maximum systolic pressure (P_{sys}) and a minimum diastolic pressure (P_{dia}). This pressure is principally produced by the pumping action of the heart. The flow ejected from the heart is converted to pressure by the resistance of the vasculature. Differences in blood pressure cause blood to flow through the CVS. Mean blood pressure decreases as flow moves away from the heart, through the arteries, capillaries and veins, due to the effects of viscosity.

Mean arterial pressure (MAP) is the average of arterial pressure over one heartbeat. It can be represented by the product of CO and total peripheral resistance (TPR) plus central venous pressure (CVP) (Stouffer, 2008).

$$MAP = CO \times TPR + CVP \tag{2.5}$$

In a healthy person normal autonomic reflex responses regulate vascular resistance and the output of the heart to ensure a suitable blood pressure. However, cardiovascular disorders can cause abnormal changes in the heart's output and resistance of the blood vessels, which overwhelm reflex responses, and, as a result, alter blood pressure. Hence, monitoring blood pressure can help assess pathological induced changes in cardiac function and vascular tone.

In the ICU, blood pressure is often monitored using invasive, fluid filled catheters, which are inserted into the radial or femoral artery. These catheters provide a continuous measurement of the arterial pressure waveform. From the waveform, MAP is often estimated from P_{sys} and P_{dia}, while there is a normal resting heart rate (Stouffer, 2008).

$$MAP \approx P_{dia} + \frac{1}{3}\left(P_{sys} - P_{dia}\right) \tag{2.6}$$

2.4.7 SUMMARY OF CONCEPTS

Preload, afterload, contractility, and heart rate are the four main independent determinants of cardiovascular performance. The product of these factors contributes to the blood pressure and cardiac output observed in the circulation. For example, in this fundamental model of cardiovascular performance, if CO increases while preload, afterload, and heart rate are held constant, then the change in CO must be due to the change in contractility. The same principles apply if preload, afterload, or heart rate were changed independently of the other metrics, as summarised in Table

2.1. Hence, analysis of these factors can be used to help interpret patho-physiological and treatment dependent changes that occur in the CVS.

Table 2.1: The effect on stroke volume (SV), cardiac output (CO), and blood pressure (BP) when one of preload, afterload, contractility, or heart rate are changed independent of the other factors.

Intervention	Effect		
	SV	CO	BP
↑ Preload	↑	↑	↑
↑ Afterload	↓	↓	↑
↑ Contractility	↑	↑	↑
↑ Heart Rate	-	↑	↑

2.5 INTERDEPENDENCE OF PRELOAD, AFTERLOAD AND CONTRACTILITY

The previous section presented the independent effects of preload, afterload, and contractility. In reality, these factors are interdependent. Hence, the interaction between these factors also plays an important part in determining cardiovascular performance.

2.5.1 PRELOAD → AFTERLOAD

Increased preload augments the SV of the ventricle. This change leads to increased CO and arterial blood pressure, causing the afterload on the ventricle to increase, partially offsetting the increased SV by increasing ESV (Klabunde, 2004). Conversely, a decrease in preload reduces SV, which is partially offset by a decrease in afterload. Hence, there is a proportional dependency between preload and afterload.

2.5.2 AFTERLOAD → PRELOAD

Increased afterload causes the heart to eject a smaller SV, predominantly due to an increased ESV. With more volume remaining at the end of systole, the ventricle fills to a greater EDV after diastole. This increase in EDV is smaller than ESV, so SV is still decreased. However, as a secondary effect, preload is partially increased (Klabunde, 2004). Hence, there exists a proportional relationship between afterload and preload.

2.5.3 CONTRACTILITY → PRELOAD

Increased contractility causes the heart to eject a larger SV, mostly due to decreased ESV. With less blood volume remaining in the ventricle after ejection, the ventricle fills to a smaller EDV during diastole (Klabunde, 2004). This secondary effect results in a decrease in preload on the ventricle, although the drop in EDV is smaller than ESV, so SV is still increased. The opposite effect is seen if contractility is decreased. Therefore, changes in contractility have an inverse effect on preload.

2.5.4 SUMMARY OF PRELOAD, AFTERLOAD AND CONTRACTILITY INTERDEPENDENCE

In the CVS, preload, afterload, and contractility interact with each other. This interdependence generally acts like a negative feedback mechanism, partially offsetting large changes in SV and BP. A summary of the main interactions between preload, afterload and contraction is shown in Table 2.2.

Table 2.2: Summary of the interdependence between preload, afterload, and contractility. Please note that the magnitudes of the secondary and tertiary effects are smaller than the magnitude of the primary intervention. SV, stroke volume; BP, blood pressure; ESV, end systolic volume; EDV, end diastolic volume.

Primary Intervention		**Secondary Effect**	
Result	**Effect**	**Result**	**Effect**
↑ Preload	SV↑ & BP↑	↑ Afterload	ESV↑ & SV↓
↑ Afterload	SV↓ & BP↑	↑ Preload	EDV↑ & SV↑
↑ Contractility	SV↑ & BP↑	↓ Preload	EDV↓ & SV↓

2.6 HOMEOSTASIS MECHANISMS

There exist many homeostasis mechanisms within the cardiovascular system. These reflex actions help maintain the balance of metabolic demand and nutrient supply in the body. In the CVS, **neural regulation**, **auto regulatory mechanisms**, and **humoral regulation** make up the three main types of homeostasis mechanisms.

2.6.1 NEURAL REGULATION

Neural regulation represents the homeostasis mechanisms that act via the autonomous nervous system. These control mechanisms act through two main pathways: 1) the parasympathetic nervous system; and 2) the sympathetic nervous system. The sympathetic nervous system promotes the 'fight or flight' response in the body by increasing heart rate and contractility, and diverting blood flow to skeletal muscle and the lungs. In contrast, activation of the parasympathetic nervous system causes a 'rest and digest' response decreasing heart rate and contraction, and diverting blood to the gastro-intestinal tract to improve digestion. An example of neural regulation is the baroreflex (Klabunde, 2004).

The baroreflex is one of the body's mechanisms for maintaining blood pressure. It provides a negative feedback loop, in which an elevated blood pressure causes heart rate to decrease, and, in consequence, a decrease in blood pressure. Similarly, decreased blood pressure activates the baroreflex, causing heart rate and blood pressure to increase. The baroreflex is activated via baroreceptors, which make up a system of pressure sensors around the CVS that communicate with the sympathetic and parasympathetic nervous systems. Elevated blood pressure causes sympathetic inhibition and parasympathetic activation, leading to decreased heart rate. Conversely, lowered blood pressure results in sympathetic activation and parasympathetic inhibition. These factors cause vasoconstriction, and increased heart rate and contractility, and thus, an increase in blood pressure. Hence, the baroreflex helps to lessen the effects of acute changes in arterial pressure.

2.6.2 AUTO REGULATORY MECHANISMS

In this thesis, auto regulatory mechanisms refer to local mechanisms that help maintain homeostasis, independent of neural factors. Some of the main auto regulatory mechanisms in the CVS include: 1) circulatory auto regulation; 2) the Frank-Starling mechanism; 3) the Anrep effect; and 4) the Bowditch effect.

Circulatory auto regulation refers to local blood flow regulation. It is defined as the intrinsic ability of an organ to maintain a constant blood flow despite changes in perfusion pressure (Klabunde, 2004). Most organs of the body show some degree of auto regulation. However, it is most noticeable in the vital organs, including the brain, heart and the kidney (Klabunde, 2004). When perfusion pressure, defined as arterial minus venous pressure ($P_a - P_v$), across these organs falls, blood flow (Q) decreases as described by the following relationship:

$$Q = \frac{P_a - P_v}{R} \quad \textbf{(2.7)}$$

To increase flow, the small arteries and arterioles dilate causing arterial resistance (R) to drop. As a result, blood flow increases in response to the decreased resistance (Klabunde, 2004). Thus, circulatory auto regulation ensures the blood flow, and thus oxygen, is diverted to the parts of the body where it is most needed.

The Frank-Starling mechanism (or law) states that the SV of a ventricle increases in response to increased volume of blood filling that ventricle (EDV). The increased volume stretches the ventricular wall, causing the myocardium to contract more forcefully, and produce a larger SV (Frank, 1898, Frank, 1895, Guyton and Hall, 2000, Starling and Visscher, 1927). This mechanism allows the heart to act like a 'demand pump' in that it ejects whatever blood it receives from the venous return. This functionality ensures intrinsic synchronisation between the cardiac output and the venous return, without the need for external regulation.

The Anrep effect represents the intrinsic ability of the heart to increase contractility in response to increased afterload (Anrep, 1912). The significance of this effect is that the increase in contractility partially compensates for the decreased SV during increased afterload. Without this function, increased afterload would cause greater reduction in SV than normally observed.

The Bowditch effect (or Treppe phenomena) represents a frequency-force relationship of myocardial contractility (Bowditch, 1871, Klabunde, 2004). When HR is increased, CO is elevated through an increased number of heart beats per minute. In a healthy heart, increased frequency also leads to a rise in contractility (Bowditch, 1871, Klabunde, 2004) known as the Bowditch effect. However, in a failing myocardium, the relationship between heart rate and contractility may be inversed.

2.6.3 HUMORAL REGULATION

Humoral regulation refers to the control of circulatory dynamics through the release and absorption of hormones and ions into the body's fluids. Some of these substances are produced in special glands and are transported in bloodstream throughout the body. In contrast, other substances are formed in localised areas of the CVS and only cause localised circulatory effects. These substances can cause vasoconstriction and vasodilation within the CVS, and hence, provide a means of controlling the relationship between pressure and flow. One example of the humoral regulation is the renin-angiotensin system (Klabunde, 2004).

The rennin-angiotensin system is a hormone system that regulates pressure and volume in the CVS. When blood volume is low the kidney releases renin into the blood stream. Renin initiates a chemical process leading to production of angiotensin II, a potent vasoconstrictor. The resulting vasoconstriction of the vessels causes blood pressure to increase (Klabunde, 2004). Angiotensin II also stimulates the secretion of aldosterone which increases the volume of fluid in the body (Klabunde, 2004) and, as a result, also increases blood pressure.

2.7 VENTRICULAR INTERACTION

Inter-ventricular communication plays a significant part in defining ventricular dynamics. The main physical conduits for this parallel interaction between the ventricles are the **inter-ventricular septum** and the **pericardium** (Williams and Frenneaux, 2006).

2.7.1 INTER-VENTRICULAR SEPTUM

The inter-ventricular septum is an active muscular membrane separating the left and right ventricular chambers. It is normally convex towards the right ventricle, as seen in Figure 2.11. Changes in the pressure difference between the ventricles can cause the septum to shift, altering the ratio of volume between the chambers. Hence, the septum acts to balance the pressure and volume between the left and right ventricles.

During right ventricular distension and pulmonary hypertension, the septum is pushed towards the left ventricle (Atherton et al., 1997). This left-ward shift decreases left ventricular preload, compromising left ventricular function (Atherton et al., 1998). Therefore, analysis of the septum motion can be diagnostic of specific cardiac dysfunction.

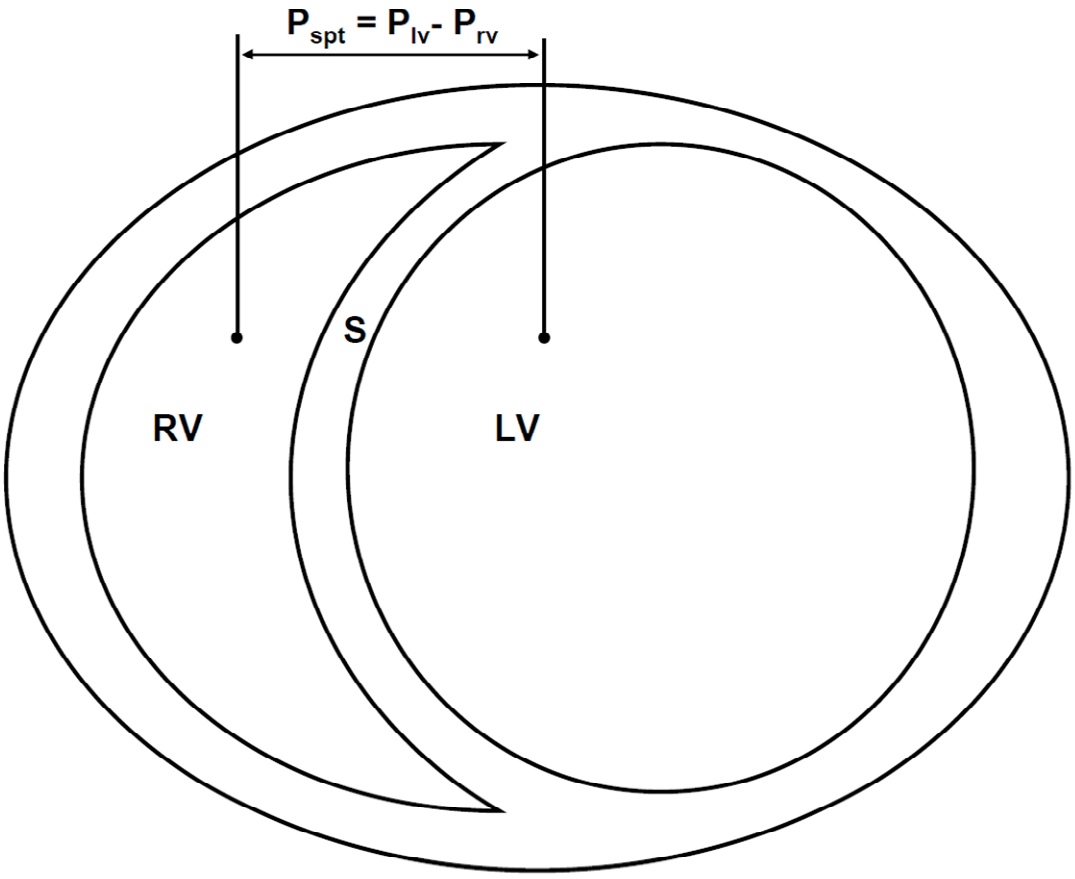

Figure 2.11: Cross-sectional schematic of heart showing normal position of inter-ventricular septum (S) with respect to the left ventricle (LV) and right ventricle (RV), from (Starfinger, 2008).

2.7.2 PERICARDIUM

The pericardium is a passive fibrous sac that encapsulates the entire heart, as seen in Figure 2.12. When the total volume of the heart increases, the pericardial sac stretches, exerting an added pressure on the heart chambers. Therefore, the pericardium acts to stop the heart overfilling by acting as a reaction wall against which the heart exerts pumping pressure (Elzinga et al., 1974, Little and Freeman, 2006). Moreover, the pericardium appears to play an important bi-ventricular role in compensating for sudden changes in the atrial volumes (Kroeker et al., 2003). However, pericardium disorders can thus significantly affect the heart's ability to pump blood, as in pericarditis (Little and Freeman, 2006).

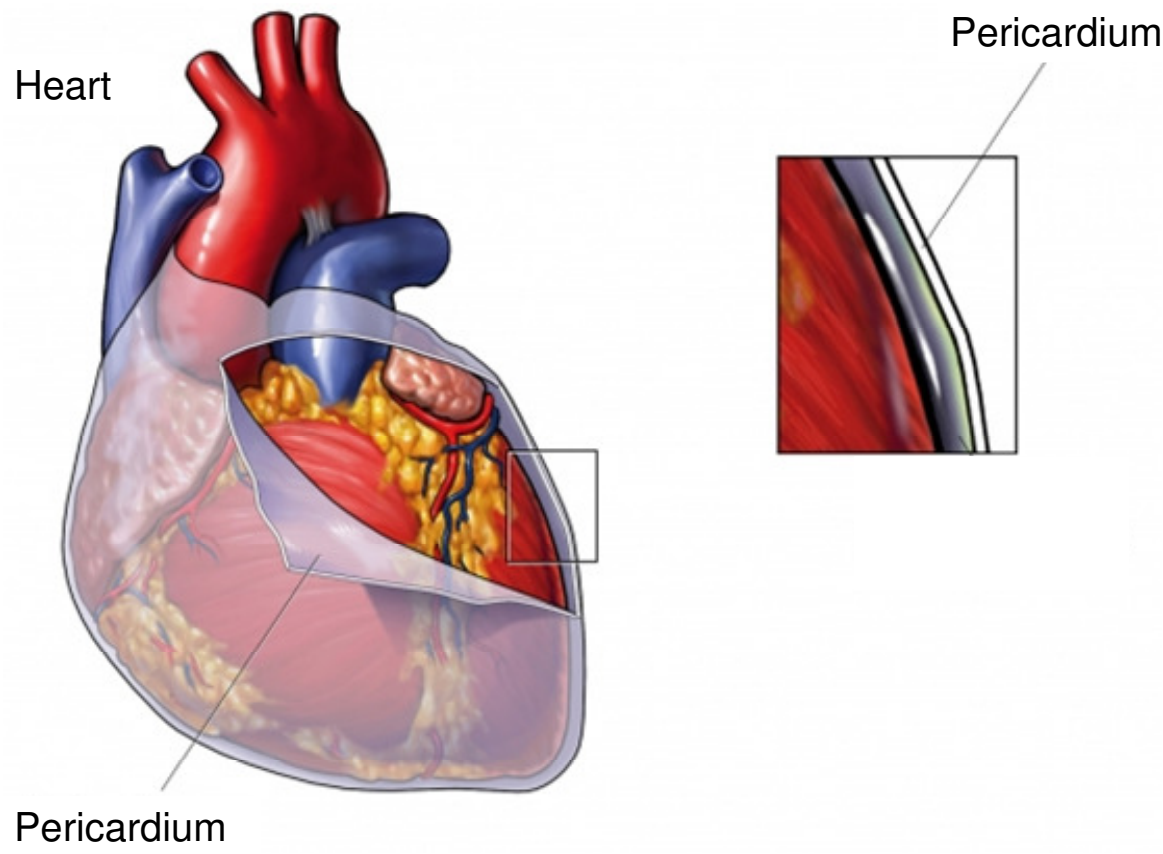

Figure 2.12: Illustration of the pericardium (Starfinger, 2008).

2.8 CARDIOPULMONARY INTERACTION

The cardiovascular and pulmonary systems are highly integrated to ensure end organ perfusion and oxygenation. Due to this high integration, and the close proximity of the heart and lungs, there exists strong mechanical cardiopulmonary coupling. Hence, the pressures and volumes in the lungs affect cardiovascular dynamics.

Changes in respiratory dynamics influence hemodynamics via the alteration of intrathoracic pressure and pulmonary vascular resistance (Pinsky, 2005, Shekerdemian and Bohn, 1999, Soni and Williams, 2008). The effects of cardiopulmonary interaction are normally well tolerated in healthy individuals. However, they can be detrimental to the hemodynamics of critically ill patients in the presence of cardiac or pulmonary pathologies. Moreover, the use of positive pressure ventilation can amplify these effects, negatively or positively modifying cardiovascular pressures, volumes, and flows. Hence, it is important to understand cardiopulmonary interaction when trying to analyse cardiac and

circulatory function. In this section, respiratory induced changes in cardiovascular dynamics are discussed through analysis of **intrathoracic pressure** and **lung volume**.

2.8.1 INTRATHORACIC PRESSURE

Intrathoracic pressure (P_{th}), also known as intrapleural pressure, represents the pressure in the thoracic cavity. The heart and pulmonary vessels reside inside the thoracic chamber. Therefore, changes in P_{th} influence the pressures within the heart chambers, and affect the pressure gradients of both the venous return to the right ventricle and outflow to the left ventricle. A rise in P_{th}, increases right atrial pressure, and decreases transmural left ventricular systolic pressure (Pinsky, 2005, Shekerdemian and Bohn, 1999, Soni and Williams, 2008). Both these factors reduce the pressure gradients of venous return and left ventricle ejection, leading to decreases in intrathoracic volume (Pinsky, 2005). The opposite occurs when P_{th} decreases, resulting in increased intrathoracic volume.

During spontaneous, unassisted breathing P_{th} is normally negative, augmenting venous return at the cost of added left ventricle afterload (increased left ventricle transmural pressure), which is easily compensated for in a healthy subject. On the other hand, positive pressure ventilation increases P_{th} and right atrial pressure, decreasing venous return and preload, resulting in diminished stroke volume and cardiac output (Pinsky, 2005, Shekerdemian and Bohn, 1999, Soni and Williams, 2008). Therefore, positive pressure ventilation generally has a negative effect on left ventricle filling. However, higher P_{th} reduces left ventricle afterload, which may outweigh the cost of decreased venous return in patients with compromised cardiac function (Pinsky, 2005).

2.8.2 LUNG VOLUME

Pulmonary vascular resistance (PVR) represents the resistance of blood flow through the lungs. During spontaneous inspiration lung volume increases causing the alveoli capillaries to stretch, increasing PVR, through decreasing the cross sectional area of these vessels. During forced expiration P_{th} becomes positive causing the lung volume to decrease. The positive P_{th} compresses the extra-alveolar vessels (larger pulmonary arteries and veins) causing the resistance in these vessels to increase. Hence, at low lung volumes the resistance of the extra-alveolar vessels is largest, whereas, at high volumes the resistance of the alveolar capillaries dominate. The combination of both these components that contribute to PVR means there is optimal volume range, around functional residual capacity (FRC), where PVR is minimal (Levitzky, 2007), as shown by Figure 2.13.

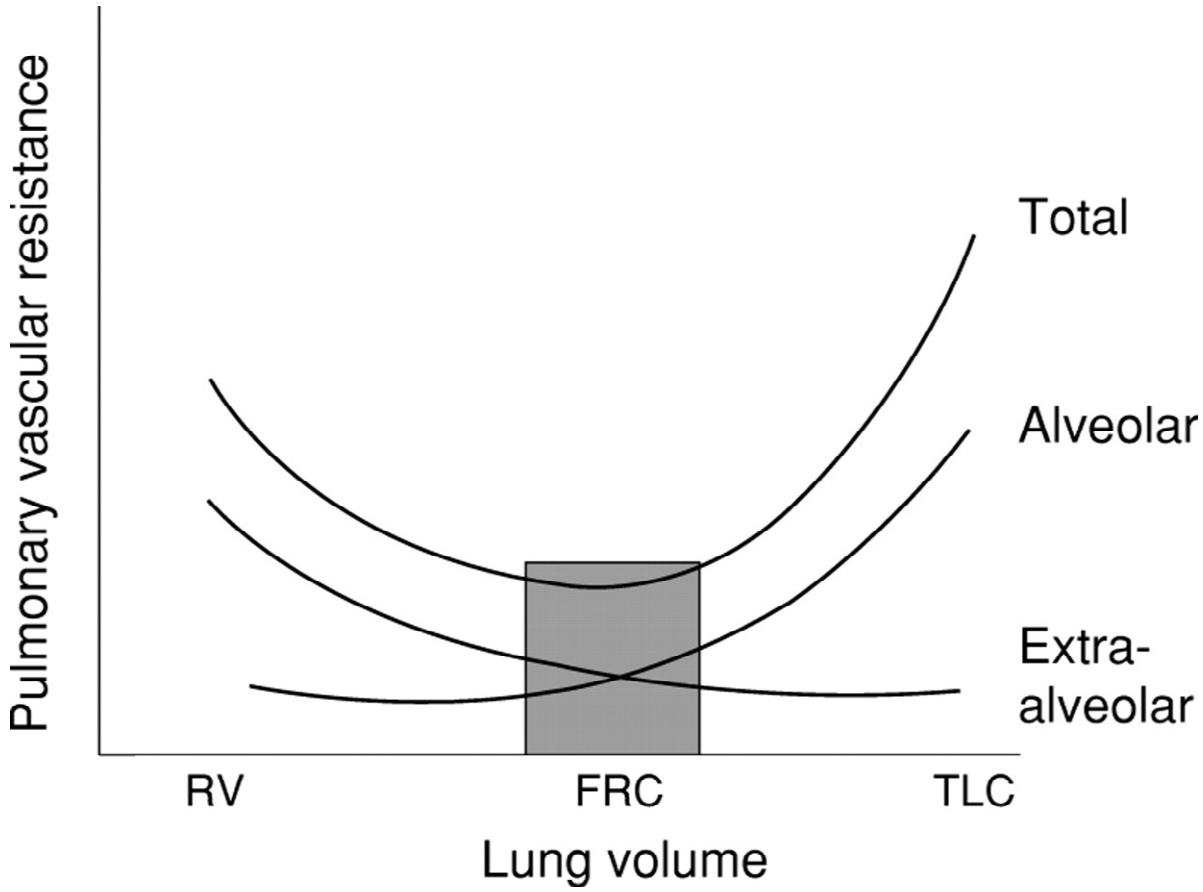

Figure 2.13: Effect of lung volume on pulmonary vascular resistance (PVR). PVR is lowest near function residual capacity (FRC) and increases as lung volume decreases towards residual volume (RV) or increases to total lung capacity (TLC) (Shekerdemian and Bohn, 1999).

The oscillatory changes in pulmonary vascular resistance during spontaneous breathing result in transient increases in right ventricle preload. These increases cause the inter-ventricular septum to shift leftward, decreasing left ventricle preload. These respiratory induced changes in ventricular interaction, result in transient decreases in left ventricle SV, and, as a consequence, inspiratory-associated decreases in arterial pulse pressure, known as pulsus paradoxus (Pinsky, 2005).

During positive pressure ventilation, the inflated lungs result in increased PVR and may lead to pulmonary hypertension. However, the increased pressure and lung volume also help reduce the effects of hypoxic pulmonary vasoconstriction, symptomatic of acute hypoxemic respiratory failure, which causes alveolar collapse and a decrease in PVR (Pinsky, 2005). Hence, increased lung volume and pressure may decrease PVR if it reverses hypoxic vasoconstriction (Pinsky, 2005). Otherwise, lung inflation will increase PVR, increasing pulmonary pressures and may precipitate acute right ventricle failure.

During hyperinflation the lungs compress against the heart. This added external force on the heart causes ventricular preload to decrease, leading to decreased cardiac output. However, with sufficient fluid resuscitation, preload and CO can be returned to their original levels (Pinsky, 2005).

2.9 VENTRICULAR ARTERIAL COUPLING

Ventricular arterial coupling (VAC) reflects the interaction between the ventricle and the arterial system. It describes the relationship between ventricular contractility and afterload and is normally represented as the ratio of the end systolic ventricular elastance over the arterial elastance (E_{es}/E_a) (Sunagawa et al., 1983). This ratio defines the efficiency of which the myocardium is pumping blood through the arteries. Theoretically, optimal transmission from the ventricles to arteries occurs when E_{es}/E_a is between 1 and 2 (Starling, 1993). A low E_{es}/E_a is reflective of myocardial dysfunction (Asanoi et al., 1989) or hypertension (Osranek et al., 2008), where the contractility of the heart can no longer maintain optimal efficiency. A high VAC can be seen during hypotension, such as in sepsis (Lambermont et al., 2004), where a drop in vascular tone leads to a decrease in afterload. The compromised afterload causes arterial pressure to drop, in the presence of adequate cardiac output, indicating inefficient energy transfer between the ventricle and arterial system.

VAC is an important measure of pumping efficiency. However, it is not used clinically as it is difficult to measure. E_a can be estimated from the arterial pressure waveform. However, determination of E_{es} requires invasive measures of the left ventricular pressure volume loop. Hence, a non-invasive method for accurately estimating VAC, to optimise the ratio of contractility and afterload in the CVS, would be of significant benefit when trying to optimise treatments in the ICU.

2.10 SUMMARY

This chapter outlined an overview of cardiac and circulatory anatomy and basic hemodynamic concepts. The idea of preload, afterload, and contractility were introduced along with principles of ventricular interaction and cardiopulmonary integration. These fundamental concepts are used as the physiological foundation for the development of the mathematical CVS model presented in the next chapter.

CHAPTER 3: CARDIOVASCULAR SYSTEM MODEL

A cardiovascular system (CVS) model is used to describe cardiac and circulatory dynamics. This lumped parameter model is used to represent and simulate the essential dynamics and features of the CVS, while only requiring a minimal number of parameters. The CVS model presented in this chapter has been previously published by Smith et al (Smith, 2004, Smith et al., 2004, Smith et al., 2005, Smith et al., 2006) and Starfinger (Starfinger, 2008). This model provides a framework of cardiovascular physiology for which patient-specific cardiac and circulatory metrics can be identified to help monitor cardiovascular disorders and treatments (please see Chapters 4, 5, 6, 7, and 8).

3.1 INTRODUCTION

The model presented simulates the main hemodynamics of the cardiovascular system. The aim is to accurately represent all the important hemodynamics using a minimal number of parameters. The goal of this approach is to optimise the balance between accuracy and complexity. To optimise this ratio a six-chamber lumped parameter model was developed, representing a closed loop system of the left and right ventricles and the systemic and pulmonary circulations. Such a model can be used to represent the cardiac and circulatory state of the CVS in a variety of pathological, physiological, and clinical conditions (Revie et al., 2011a, Smith et al., 2007, Smith et al., 2006, Starfinger et al., 2008a, Starfinger et al., 2008b).

Figure 3.1 shows a schematic of the CVS model made of six elastic chambers connected in series by resistances, inductors, and diodes. The diodes represent heart valves and the inductors describe the inertial effects of blood flowing into and out of the ventricular chambers. The resistances capture the pressure drop between chambers as blood flows through the circulation. The six elastic chambers simulate the pressure volume relationship in the:

- Left ventricle (lv)
- Aorta (ao)
- Vena cava (vc)
- Right ventricle (rv)
- Pulmonary artery (pa)
- Pulmonary veins (pu)

Due to the lumped parameter nature of the model, each chamber actually represents an average or sum of a number of smaller physiological chambers. The aortic chamber describes the summed elastance of all the large arteries and not solely the dynamics of the aorta. Similarly, the pulmonary artery chamber simulates the elastance of the main arteries feeding the lungs. The vena cava and pulmonary vein chambers represent the main veins of their respective circulations and they also incorporate the elastances of their adjacent atriums. Hence, the model of Figure 3.1 divides the CVS into six lumped blood reservoirs representing the main hemodynamic components of the circulation.

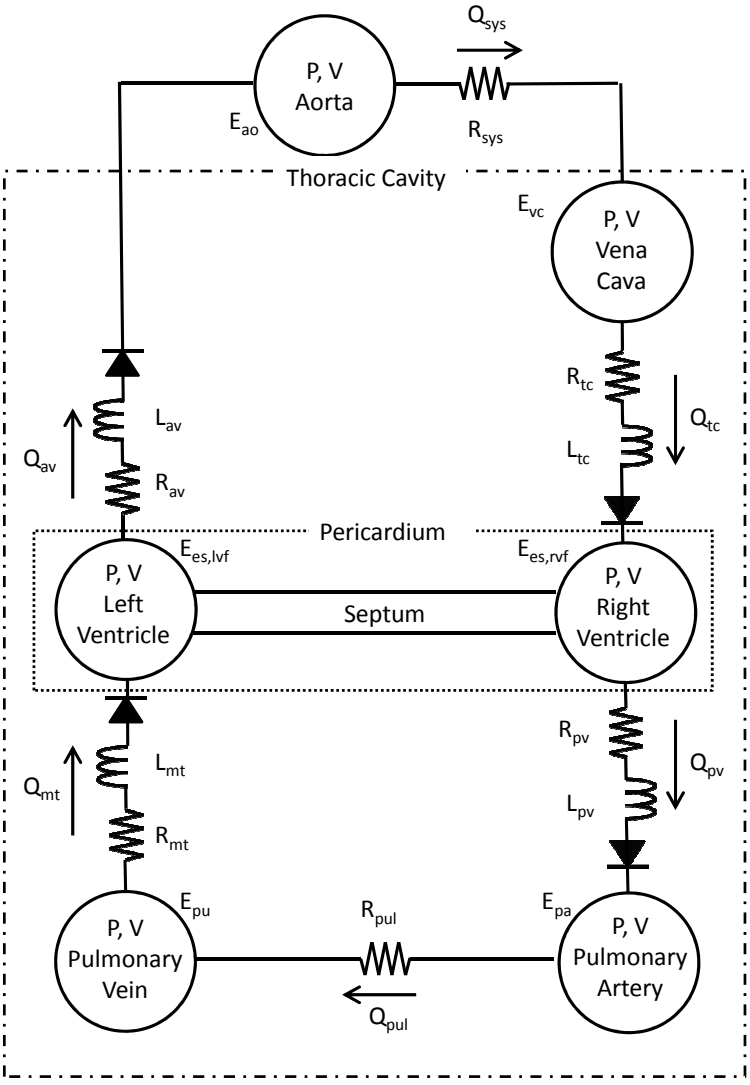

Figure 3.1: Schematic of the cardiovascular system model with elastances (E), resistances (R), and inertance (L). The circles represent pressure-volume (P, V) chambers. The subscripts represent: mt, mitral; es, end systolic; lvf, left ventricle free wall; av, aortic valve; sys, systemic; tc, tricuspid; pv, pulmonary valve; rvf, right ventricle free wall; pul, pulmonary; pu, pulmonary vein.

The left and right ventricles act as the pumps for the model and are dynamically elastic. The non-linear relationship between pressure and volume in these chambers is simulated using normalised time-varying elastance, also known as the driver function. The other chambers are passively elastic, and thus, modelled using constant elastance, enforcing a linear relationship between pressure and volume.

The series of resistances (R) and inertances (L) define the flow between the elastic chambers. Each R represents the pressure drop between adjacent chambers and each L defines the pressure gradient required to cause a change in flow-rate. Pressure- and flow-gated valves (Hann et al., 2005, Smith et al., 2004) describe flow through the heart valves (mitral, aortic, tricuspid, and pulmonary), which open when the upstream pressure is higher than the downstream pressure and close when the flow through the valves becomes negative. These heart valves are shown as diodes in Figure 3.1. As with elastance, these resistance and inertance parameters represent the lumped effects of the flow.

Parallel interaction between the systemic and pulmonary circulations is also modelled through left and right ventricular coupling. The effects of the inter-ventricular septum that separates the ventricles, and the pericardium that encapsulates the heart, are simulated to account for inter-ventricular interaction, as seen in Figure 3.1. Furthermore, the effects of respiration, which acts on every chamber excluding the aortic, can be simulated via changes in the thoracic pressure, as shown in Figure 3.1. The difference between the model shown in Figure 3.1 and the model of Smith et al. (Smith et al., 2004) is that the vena cava chamber now sits inside the thoracic cavity, and hence, is influenced by changes in thoracic pressure during breathing. This change more realistically represents the effects on the circulation by decreasing the afterload on the ventricle when intrathoracic pressure is positive (Pinsky, 2005, Shekerdemian and Bohn, 1999, Soni and Williams, 2008).

The following sections of this chapter develop the basic concepts and mathematics of the CVS model previously described in (Smith, 2004, Smith et al., 2005, Smith et al., 2006, Starfinger, 2008). The interaction between pressure, volume, and flow in the CVS is described using elastance, resistance, and inertia. Governing equations will be developed for a one chamber passive model and a one chamber ventricular model, along with equations for heart valve flow and ventricular interaction. The cardiovascular system will then be discretised and specific equations will be defined for each chamber. Finally, the validity of the model assumptions and equations will be discussed in Section 3.6.

3.2 MODEL ASSUMPTIONS

Several assumptions were required to minimise the number of parameters in the CVS model. These assumptions include:

- Conservation of mass
- Poiseuille flow
- Constant elastance (in passive chambers)
- Constant resistance
- Constant inertance
- No backflow through heart valves
- Linear ESPVR
- Exponential EDPVR
- Effects of atria are small

The validity of these assumptions is discussed in Section 3.6.

3.3 MODEL DEVELOPMENT

The following sections develop and introduce the governing equations (shown in grey) and accompanying equations used to describe the CVS model.

3.3.1 PASSIVE CHAMBER

A single elastic chamber is represented by the circle in Figure 3.2. This figure illustrates the pressures, volumes, and flows acting on the chamber.

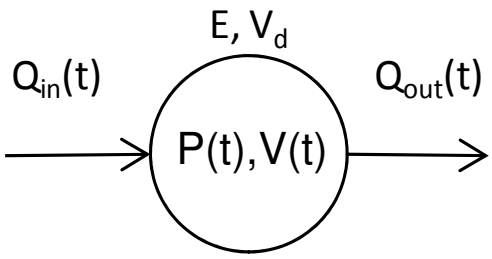

Figure 3.2: Single passively elastic chamber.

Pressure and volume in the chamber can vary with time (P(t), V(t)) and are related to each other through constants representing the elastance and unstressed volume of the chamber (E, V_d). V(t) represents the stressed volume and V_d is the unstressed volume that does not contribute to increases in P(t). Changes in V(t) are dependent on the flow in and out (Q_{in}, Q_{out}) of the chamber. Hence, a differential equation (DE) can be derived by considering a mass balance over the chamber.

$$\dot{V}(t) = Q_{in}(t) - Q_{out}(t) \quad \textbf{(3.1)}$$

$$P(t) = E\left(V(t) - V_d\right) \quad \textbf{(3.2)}$$

These governing equations of the CVS model represent the interaction between pressure, volume and flow in a single passive chamber. These equations are used to represent the pressure-volume relationship in non-cardiac chambers, specifically, the aorta, vena cava, pulmonary artery, and pulmonary vein as shown in Figure 3.1.

3.3.2 INTER CHAMBER FLOW (NON-VALVULAR)

Flow between adjacent chambers is illustrated by Figure 3.3. In this example, the upstream and downstream chambers act as two time varying pressure sources ($P_1(t)$ and $P_2(t)$).

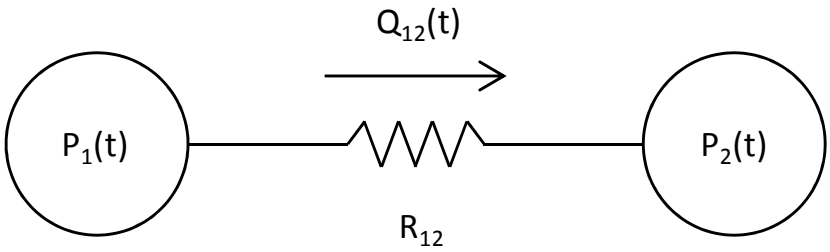

Figure 3.3: Schematic of inter chamber flow

Flow between the chambers (Q_{12}) is dependent on the pressure difference, $P_1(t) - P_2(t)$, and the resistance to flow R_{12}, which is assumed to be constant. Thus, assuming poiseuille flow the following governing equation for non-valvular flow can be derived:

$$Q_{12}(t) = \frac{P_1(t) - P_2(t)}{R_{12}} \tag{3.3}$$

3.3.3 HEART VALVE FLOW

A schematic of flow through a heart valve is shown in Figure 3.4. In this illustration, $P_1(t)$ could be the ventricular pressure and $P_2(t)$ would be the pressure of the downstream artery. However, the same methodology can be used to represent flow into the ventricles, where P_2 becomes the ventricular pressure and P_1 is the upstream venous pressure.

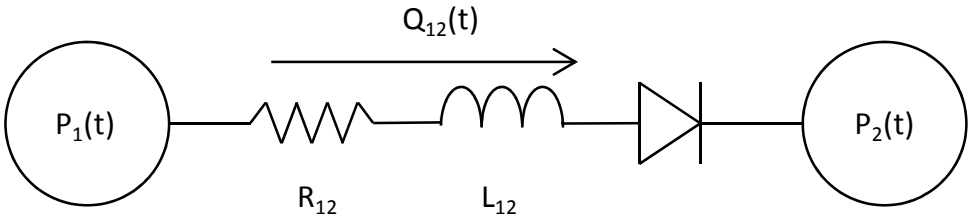

Figure 3.4: Illustration of flow across a heart valve.

The diode in Figure 3.4 represents a heart valve and the inductor (L_{12}) represents the inertance of blood flowing through the valve. It is assumed that there is no backwards flow through the heart valve. A non-linear differential equation (DE) can be used to describe the flow (Q_{12}) across the heart valve:

$$\dot{Q}_{12}(t) = \mathbf{H}\left(\frac{P_1(t) - P_2(t) - R_{12}Q_{12}(t)}{L_{12}}\right)\frac{P_1(t) - P_2(t) - R_{12}Q_{12}(t)}{L_{12}} \tag{3.4}$$

A Heaviside function (**H**(x), where **H**=0 when x<0 and **H**=1 when x >0) is used to enforce forward flow though the heart valve. The valve opens when the pressure difference, P_1-P_2, is greater than zero, as there is initially no flow through the valve during diastole. It closes when the change in flow becomes negative.

3.3.4 VENTRICULAR CHAMBERS

The pressure-volume relationship in a ventricular chamber is more complicated than that in the passive chambers. Due to the effects of myocardial contraction the pressure-volume relationship is non-linear in these chambers. Time varying elastance is the most commonly used method of describing pressure-volume interaction in the ventricle (Beyar et al., 1987, Burkhoff and Tyberg, 1993, Chung et al., 1997, Santamore and Burkhoff, 1991). Maximum and minimum limits for this time-varying elastance are usually defined by the end systolic and end diastolic pressure volume relationships (ESPVR, EDPVR), as shown on Figure 3.5.

ESPVR has been found to be quasi-linear over a physiological range of loading conditions. This relationship describes the maximum pressure that can be produced by the ventricle for a certain volume. Similarly, EDPVR describes the minimum pressure produced by the ventricle for a certain volume. Both these relationships are commonly modelled using a straight line (ESPVR) and exponential curve (EDPVR) (Amoore et al., 1992, Campbell et al., 1990, Suga et al., 1973, Weber et al., 1982). Thus, due to their relative simplicity, the most commonly used equations for modelling ESPVR and EDPVR are defined (Beyar et al., 1987, Chung et al., 1997, Santamore and Burkhoff, 1991):

$$P_{es}(V) = E_{es}\left(V - V_d\right) \quad \textbf{(3.5)}$$

$$P_{ed}(V) = P_0\left(\exp^{\lambda(\mathrm{V}-\mathrm{V}_0)} - 1\right) \quad \textbf{(3.6)}$$

The end systolic pressure (P_{es}) is related to volume (V) using end systolic elastance (E_{es}) and the unstressed chamber volume (V_d), which define a linear relationship. The end diastolic pressure (P_{ed}) is also a function of volume and is characterised by an exponential equation with constants P_0, λ, and V_0, which control the gradient, curvature, and volume at zero pressure. Both the ESPVR and EDPVR are plotted on Figure 3.5. The use of time varying elastance (E(t)) allows the dynamic ventricular chambers to increase (and decrease) pressure even when there is no change in volume, consistent with the contraction (and relaxation) phase of the cardiac cycle. Hence, E(t) provides a means to simulate the pumping action of the heart and acts as the driving function for the CVS model.

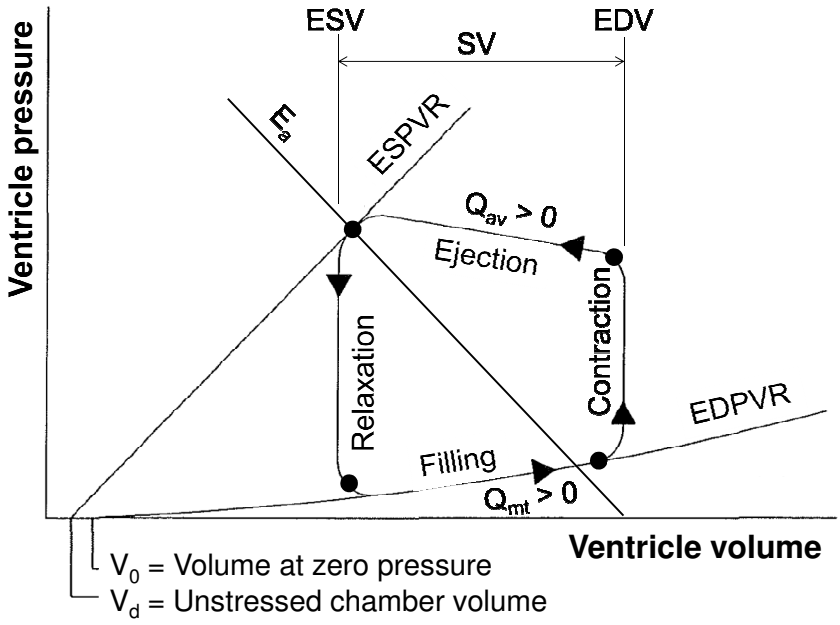

Figure 3.5: A standard pressure volume loop showing the four stages of the cardiac cycle and the end systolic (es) and end diastolic (ed) pressure volume relationships (ESPVR and EDPVR). Q_{av} and Q_{mt} are the flows in and out of the ventricle. Stroke volume (SV) is the difference between the end diastolic and end systolic volumes (EDV –ESV). Afterload is represented by E_a in the diagram.

Segers et al. (Segers et al., 2000b, Segers et al., 2000a) experimentally showed in a canine study that pressure and volume could be linearly related to each other using a non-constant E(t).

$$P(t) = E(t)\left(V(t) - V_d\right) \tag{3.7}$$

where P(t) and V(t) are the pressure and volume in the cardiac chamber. A more useful approach incorporates the ESPVR and EDPVR (Smith, 2004) of Equations (3.5) and (3.6). To apply this method a cardiac driver function (e(t)), normalised between 0 and 1, is used to relate ESPVR and EDPVR. At end systole, e(t) = 1, its maximum value, and at end diastole e(t) = 0, its minimum value. Figure 3.6 shows an example of a driver function (also known as time varying elastance) of a healthy pig that illustrates how e(t) varies between 0 and 1 over one heartbeat. Therefore, the pressure in a dynamically elastic chamber can be related using a weighted sum of Equations (3.5) and (3.6), where the weighting is defined by the value of e(t).

$$P(V,t) = e(t)P_{es}(V) + (1 - e(t))P_{ed}(V) \quad 0 \le e(t) \le 1 \tag{3.8}$$

$$\therefore \quad P(V,t) = e(t)E_{es}(V - V_d) + (1 - e(t))P_0\left(\exp^{\lambda(V-V_0)} - 1\right) \tag{3.9}$$

Equation (3.9) is the governing equation used for relating pressure to volume in dynamically elastic chambers, such as in the ventricular chambers.

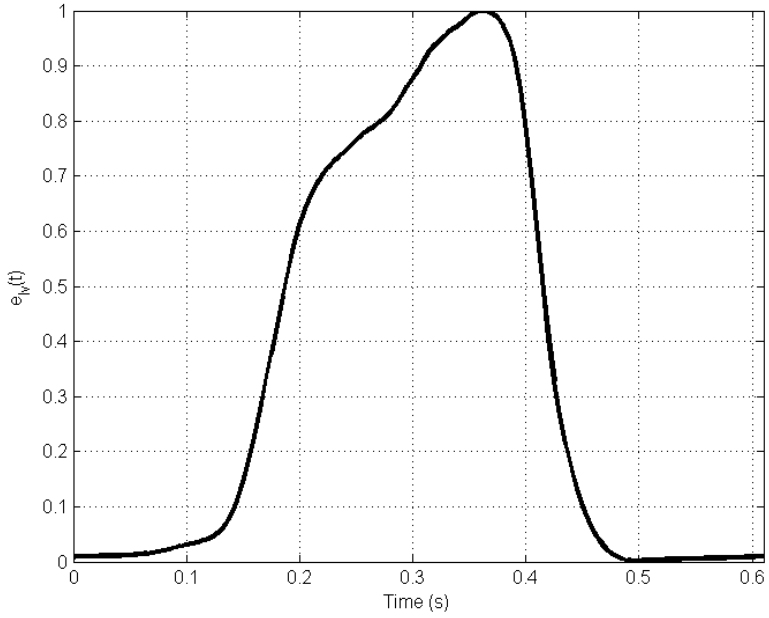

Figure 3.6: Example of a normalised left ventricular driver function ($e_{lv}(t)$) for a healthy pig.

Figure 3.7 shows a schematic of a ventricular chamber with heart valves. $P_2(t)$ and $V_2(t)$ represent the ventricular pressure and volume. $Q_{12}(t)$ and $Q_{23}(t)$ describe the inlet and outlet flow through their corresponding heart valves.

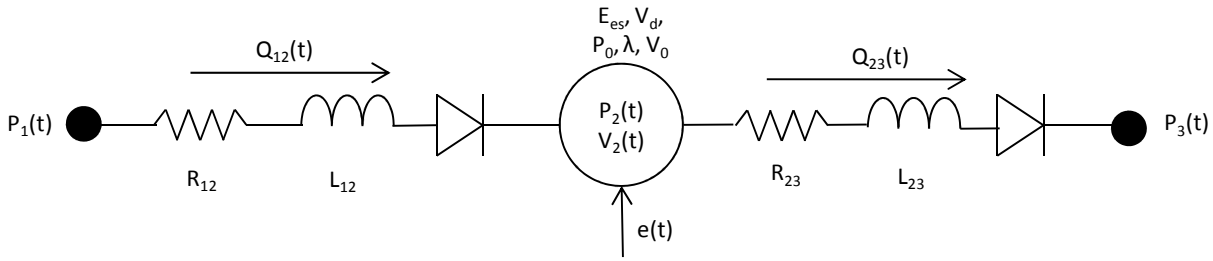

Figure 3.7: Schematic of a dynamically elastic chamber, where $P_2(t)$ represents the ventricular pressure.

3.3.5 VENTRICULAR INTERACTION

Inter-ventricular communication plays a significant part in defining cardiovascular dynamics, where interaction between the two ventricles occurs through the inter-ventricular septum and via the pericardium, as discussed earlier in Section 2.7.2. Hence, it is important to model this interdependence between the ventricles. Figure 3.8 shows schematically how ventricular interaction can be incorporated in a CVS model. The two bold lines connecting the ventricles symbolise the septum and the dash-lined rectangle represents the pericardium. The volume displaced by the septum and the pressure produced by the pericardium are symbolised by the time-varying variables V_{spt} and P_{pcd}. The flows, $Q_{lv,in}$, $Q_{rv,in}$, $Q_{lv,out}$, and $Q_{rv,out}$ represent the time-varying inlet and outlet flows of the ventricles.

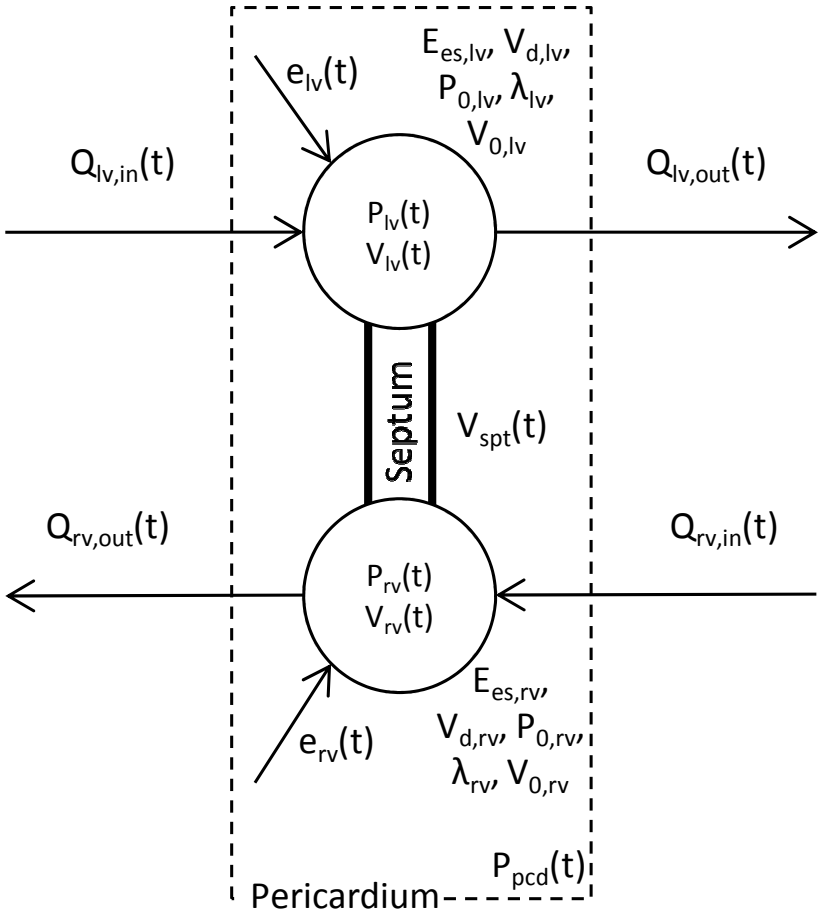

Figure 3.8: Adding ventricular interaction, via septum and pericardium dynamics (V_{spt}, P_{pcd}), to the left and right ventricular chambers (lv, rv).

The equations used to describe septum and pericardium dynamics in this research have been previously described in detail by Smith et al (Smith et al., 2004, Smith, 2004). Hence, in this section,

the development of these equations is only briefly reiterated. The volume definitions required to define the volumes used in the ventricular model are shown in Figure 3.9. The left ventricular, right ventricular, and septal free wall volumes (V_{lvf}, V_{rvf}, V_{spt}) are theoretical volumes (not physical volumes) which represent portions of the overall true ventricular volumes (V_{lv} and V_{rv}). These free walled definitions are used to relate deflection in the cardiac free walls to the actual ventricular volumes.

As seen in Figure 3.9, the left and right ventricular free wall volumes are defined:

$$V_{lvf} = V_{lv} - V_{spt} \quad \textbf{(3.10)}$$

$$V_{rvf} = V_{rv} + V_{spt} \quad \textbf{(3.11)}$$

The septum in a relaxed state normally deflects slightly into the right ventricle. Hence, the sign convention used in the CVS model is that a positive septal volume (V_{spt}) indicates deflection into the right ventricle, as shown in Figure 3.9.

The pericardium volume is defined as the sum of the ventricular volumes:

$$V_{pcd} = V_{lv} + V_{rv} = V_{lvf} + V_{rvf} \quad \textbf{(3.12)}$$

The pericardium volume used in the CVS model excludes the volume of the atria and myocardium, although these details can be easily added if desired.

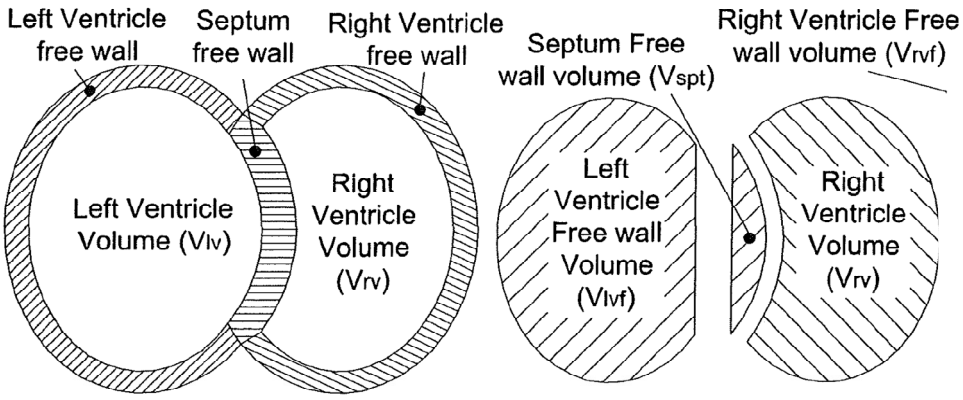

Figure 3.9: Cross-section of the left and right ventricles showing the volume definitions used to calculate the septum volume (V_{spt}) and pericardium pressure (P_{pcd}) (Smith, 2004).

The non-linear pressure-volume relationship defined in Equation (3.8) is used to relate the chamber volumes to pressures. All cardiac related pressures are shown in Figure 3.10. These pressures are defined:

$$P_{lv} = P_{lvf} + P_{peri} \quad \textbf{(3.13)}$$

$$P_{rv} = P_{rvf} + P_{peri} \quad \textbf{(3.14)}$$

$$P_{peri} = P_{pcd} + P_{th} \quad \textbf{(3.15)}$$

where P_{lvf}, P_{rvf}, and P_{pcd} represent the pressure differences across the walls of the left ventricle, right ventricle, and pericardium. P_{th} defines the pressure in the thoracic cavity. Note that, in the CVS model P_{th} is added to the pressure in every chamber except for the aortic, as shown in Figure 3.1.

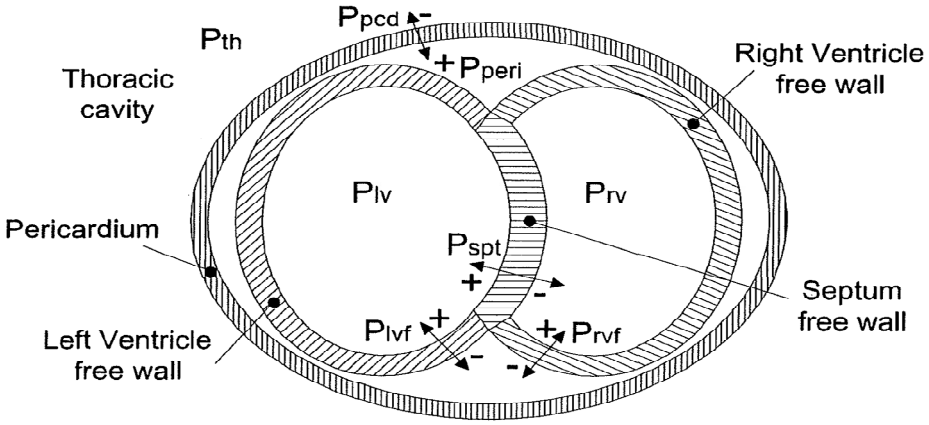

Figure 3.10: Cross-section of the ventricles and pericardium showing the definitions of all the cardiac pressures (Smith, 2004).

Subtracting Equation (3.14) from Equation (3.13) gives the septal pressure (P_{spt}) defined as the pressure difference across the septum.

$$P_{spt} = P_{lv} - P_{rv} = P_{lvf} - P_{rvf} \quad \textbf{(3.16)}$$

These transmural pressures (P_{lvf}, P_{rvf}, P_{spt}, P_{pcd}) represent the force or stretch applied to each free wall. P_{lvf}, P_{rvf}, and P_{spt} are related to their corresponding ESPVR and EDPVR relationships by Equation (3.8), giving:

$$P_{lvf} = e_{lv} P_{es,lvf} + (1 - e_{lv}) P_{ed,lvf} \quad \textbf{(3.17)}$$

$$P_{rvf} = e_{rv} P_{es,rvf} + (1 - e_{rv}) P_{ed,rvf} \quad \textbf{(3.18)}$$

$$P_{spt} = e_{spt} P_{es,spt} + (1 - e_{spt}) P_{ed,spt} \quad \textbf{(3.19)}$$

The pressure across the pericardium (P_{pcd}) passively reacts to changes in volume, whereas the other pressures are actively changing with respect to volume. Hence, a different relationship is used to define P_{pcd}, similar to the EDPVR of Equation (3.6).

$$P_{pcd}(V_{pcd}) = P_{0,pcd}\left(\exp^{\lambda_{pcd}(V_{pcd} - V_{0,pcd})} - 1\right) \quad \textbf{(3.20)}$$

where $P_{0,pcd}$, λ_{pcd}, and $V_{0,pcd}$, define the gradient, curvature, and volume at zero pericardial pressure. Finally, combining Equations (3.9)-(3.11) and (3.16)-(3.19) gives an equation relating V_{spt} to V_{lv} and V_{rv}:

$$\begin{aligned} & e_{spt} E_{es,spt}\left(V_{spt} - V_{d,spt}\right) + \left(1 - e_{spt}\right) P_{0,spt}\left(\exp^{\lambda_{spt}(V_{spt} - V_{0,spt})} - 1\right) \\ & = e_{lv} E_{es,lvf}\left(V_{lv} - V_{spt} - V_{d,lvf}\right) + \left(1 - e_{lv}\right) P_{0,lvf}\left(\exp^{\lambda_{lvf}(V_{lv} - V_{spt} - V_{0,lvf})} - 1\right) \\ & - e_{rv} E_{es,rvf}\left(V_{rv} + V_{spt} - V_{d,rvf}\right) - \left(1 - e_{rv}\right) P_{0,rvf}\left(\exp^{\lambda_{rv}(V_{rv} + V_{spt} - V_{0,rvf})} - 1\right) \end{aligned} \quad \textbf{(3.21)}$$

Through the use of Equations (3.10)-(3.21) the effects of parallel interaction between the ventricles can be quantified. This outcome allows the important effects of ventricular interaction to be captured in the CVS model.

3.4 MODEL EQUATIONS

The governing equations, Equations (3.1), (3.2), (3.3), (3.4), and (3.9), developed in Section 3.3, are used to define the specific equations for the pressures, volumes, and flows in a closed-loop model of the CVS (Starfinger, 2008, Smith et al., 2004, Smith, 2004). A list and description of the model outputs are shown in Table 3.1. Table 3.2 defines the parameters of the CVS model. The discretisation of the governing equations is shown below.

A simple mass balance, described by Equation (3.1), is used to define the change in volume in each of the six CVS chambers.

$$\dot{V}_{lv} = Q_{mt} - Q_{av} \tag{3.22}$$

$$\dot{V}_{ao} = Q_{av} - Q_{sys} \tag{3.23}$$

$$\dot{V}_{vc} = Q_{sys} - Q_{tc} \tag{3.24}$$

$$\dot{V}_{rv} = Q_{tc} - Q_{pv} \tag{3.25}$$

$$\dot{V}_{pa} = Q_{pv} - Q_{pul} \tag{3.26}$$

$$\dot{V}_{pu} = Q_{pul} - Q_{mt} \tag{3.27}$$

Equation (3.3) is used calculate non-valvular flow through the systemic and pulmonary capillary beds.

$$Q_{sys} = \frac{P_{ao} - P_{vc}}{R_{sys}} \tag{3.28}$$

$$Q_{pul} = \frac{P_{pa} - P_{pu}}{R_{pul}} \tag{3.29}$$

Applying Equation (3.4), non-linear DEs can be derived for flow through each of the valves (mitral, aortic, tricuspid, and pulmonary):

$$\dot{Q}_{mt} = \mathbf{H}\left(\frac{P_{pu} - P_{lv} - Q_{mt}R_{mt}}{L_{mt}}\right)\frac{P_{pu} - P_{lv} - Q_{mt}R_{mt}}{L_{mt}} \tag{3.30}$$

$$\dot{Q}_{av} = \mathbf{H}\left(\frac{P_{lv} - P_{ao} - Q_{av}R_{av}}{L_{av}}\right)\frac{P_{lv} - P_{ao} - Q_{av}R_{av}}{L_{av}} \tag{3.31}$$

$$\dot{Q}_{tc} = \mathbf{H}\left(\frac{P_{vc} - P_{rv} - Q_{tc}R_{tc}}{L_{tc}}\right)\frac{P_{vc} - P_{rv} - Q_{tc}R_{tc}}{L_{tc}} \tag{3.32}$$

$$\dot{Q}_{pv} = \mathbf{H}\left(\frac{P_{rv} - P_{pa} - Q_{pv}R_{pv}}{L_{pv}}\right)\frac{P_{rv} - P_{pa} - Q_{pv}R_{pv}}{L_{pv}} \tag{3.33}$$

The pressures volume relationships of the non-cardiac chambers, including the aorta, vena cava, pulmonary artery, and pulmonary vein, are characterised by a linear relationship, defined by Equation (3.2).

$$P_{ao} = E_{ao}\left(V_{ao} - V_{d,ao}\right) \quad \textbf{(3.34)}$$

$$P_{vc} = E_{vc}\left(V_{vc} - V_{d,vc}\right) + P_{th} \quad \textbf{(3.35)}$$

$$P_{pa} = E_{pa}\left(V_{pa} - V_{d,pa}\right) + P_{th} \quad \textbf{(3.36)}$$

$$P_{pu} = E_{pu}\left(V_{pu} - V_{d,pu}\right) + P_{th} \quad \textbf{(3.37)}$$

Note that thoracic pressure is added to the vena cava, pulmonary artery, and pulmonary artery chambers, as these chambers are assumed to reside inside the thoracic cavity.

The pressures in the cardiac chamber are modelled using Equation (3.9).

$$P_{lvf} = e_{lv}E_{es,lvf}\left(V_{lvf} - V_{d,lvf}\right) + \left(1 - e_{lv}\right)P_{0,lvf}\left(\exp^{\lambda_{lvf}\left(V_{lvf} - V_{0,lvf}\right)} - 1\right) \quad \textbf{(3.38)}$$

$$P_{rvf} = e_{rv}E_{es,rvf}\left(V_{rvf} - V_{d,rvf}\right) + \left(1 - e_{rv}\right)P_{0,rvf}\left(\exp^{\lambda_{rvf}\left(V_{rvf} - V_{0,rvf}\right)} - 1\right) \quad \textbf{(3.39)}$$

The free-wall volumes in these equations, V_{lvf} and V_{rvf}, are calculated taking septum interaction into account.

$$V_{lvf} = V_{lv} - V_{spt} \quad \textbf{(3.40)}$$

$$V_{rvf} = V_{rv} + V_{spt} \quad \textbf{(3.41)}$$

The actual left and right ventricular pressures are related to free-wall pressures through consideration of pericardium dynamics:

$$P_{lv} = P_{lvf} + P_{peri} \quad \textbf{(3.42)}$$

$$P_{rv} = P_{rvf} + P_{peri} \quad \textbf{(3.43)}$$

where,

$$P_{peri} = P_{pcd} + P_{th} \quad \textbf{(3.44)}$$

Finally, both septal and pericardial dynamics (as previously described by Equations (3.20) and (3.21)) are calculated using the following equations:

$$\begin{aligned} & e_{spt} E_{es,spt} \left(V_{spt} - V_{d,spt}\right) + \left(1 - e_{spt}\right) P_{0,spt} \left(\exp^{\lambda_{spt}\left(V_{spt} - V_{0,spt}\right)} - 1\right) \\ & = e_{lv} E_{es,lvf} \left(V_{lv} - V_{spt} - V_{d,lvf}\right) + \left(1 - e_{lv}\right) P_{0,lvf} \left(\exp^{\lambda_{lvf}\left(V_{lv} - V_{spt} - V_{0,lvf}\right)} - 1\right) \\ & - e_{rv} E_{es,rvf} \left(V_{rv} + V_{spt} - V_{d,rvf}\right) - \left(1 - e_{rv}\right) P_{0,rvf} \left(\exp^{\lambda_{rvf}\left(V_{rv} + V_{spt} - V_{0,rvf}\right)} - 1\right) \end{aligned} \quad \textbf{(3.45)}$$

$$P_{pcd}\left(V_{pcd}\right) = P_{0,pcd} \left(\exp^{\lambda_{pcd}\left(V_{pcd} - V_{0,pcd}\right)} - 1\right) \quad \textbf{(3.46)}$$

These 25 equations (Equations (3.22)-(3.46)) define a closed loop model of the CVS. The model represents all the major dynamics of the CVS, including one-way heart valves, ventricular interaction, and time varying myocardium activation. Thus, the CVS model can be used to accurately represent important hemodynamics resulting from a healthy or compromised cardiovascular state. Table 3.2 and Table 3.1 define the parameters and outputs of the CVS model. The parameter values listed in Table 3.2 representative of a healthy human.

Table 3.1: List of CVS model outputs (* denotes output is a state variable).

Symbol	Name	Value
P_{lv}	Left ventricular pressure	mmHg
P_{ao}	Aortic pressure	mmHg
P_{vc}	Vena cava pressure	mmHg
P_{rv}	Right ventricular pressure	mmHg
P_{pa}	Pulmonary artery pressure	mmHg
P_{pu}	Pulmonary vein pressure	mmHg
V_{lv}*	Left ventricular volume	ml
V_{ao}*	Aortic volume	ml
V_{vc}*	Vena cava volume	ml
V_{rv}*	Right ventricular volume	ml
V_{pa}*	Pulmonary artery volume	ml
V_{pu}*	Pulmonary vein volume	ml
Q_{mt}*	Mitral valve flow	ml/s
Q_{av}*	Aortic valve flow	ml/s
Q_{sys}	Systemic vascular flow	ml/s
Q_{tc}*	Tricuspid valve flow	ml/s
Q_{pv}*	Pulmonary artery flow	ml/s
Q_{pul}	Pulmonary vascular flow	ml/s
V_{spt}	Septum volume	ml
P_{pcd}	Pericardium pressure	mmHg

Table 3.2: List of CVS model parameters and their corresponding value for a healthy human.

Symbol	Name	Units	Value
$E_{es,lvf}$	Left ventricular end systolic elastance	mmHg/ml	2.8798
E_{ao}	Aortic elastance	mmHg/ml	0.6913
E_{vc}	Vena Cava elastance	mmHg/ml	0.0059
$E_{es,rvf}$	Right ventricular end systolic elastance	mmHg/ml	0.5850
E_{pa}	Pulmonary artery elastance	mmHg/ml	0.369
E_{pu}	Pulmonary vein elastance	mmHg/ml	0.0073
R_{mt}	Mitral valve resistance	mmHg.s/ml	0.0158
R_{av}	Aortic valve resistance	mmHg.s/ml	0.018
R_{sys}	Systemic vascular resistance	mmHg.s/ml	1.0889
R_{tc}	Tricuspid valve resistance	mmHg.s/ml	0.0237
R_{pv}	Pulmonary vein resistance	mmHg.s/ml	0.0055
R_{pul}	Pulmonary vascular resistance	mmHg.s/ml	0.1552
L_{mt}	Mitral valve inertia	$mmHg.s^2/ml$	7.6968e-5
L_{av}	Aortic valve inertia	$mmHg.s^2/ml$	1.2189e-4
L_{tc}	Tricuspid valve inertia	$mmHg.s^2/ml$	8.0093e-5
L_{pv}	Pulmonary valve inertia	$mmHg.s^2/ml$	1.4868e-4
$V_{d,lvf}$	Unstressed left ventricular volume	ml	0
$V_{d,ao}$	Unstressed aortic volume	ml	0
$V_{d,vc}$	Unstressed vena cava volume	ml	0
$V_{d,rvf}$	Unstressed right ventricular volume	ml	0
$V_{d,pa}$	Unstressed pulmonary artery volume	ml	0
$V_{d,pu}$	Unstressed pulmonary vein volume	ml	0
$P_{0,lvf}$	Left ventricular EDPVR gradient parameter	mmHg	0.1203
$P_{0,rvf}$	Right ventricular EDPVR gradient parameter	mmHg	0.2157
λ_{lvf}	Left ventricular EDPVR curvature parameter	1/ml	0.033
λ_{rvf}	Right ventricular EDPVR curvature parameter	1/ml	0.023
$E_{es,spt}$	End systolic septum elastance	mmHg/ml	48.754
$V_{0,lvf}$	Zero-pressure left ventricular volume	ml	0
$V_{0,rvf}$	Zero-pressure right ventricular volume	ml	0
$P_{0,spt}$	Zero-volume septum pressure	mmHg	1.1101
$P_{0,pcd}$	Zero-volume pericardium pressure	mmHg	0.5003
$V_{0,spt}$	Zero-pressure septum volume	ml	2
$V_{0,pcd}$	Zero-pressure pericardium pressure	ml	200
λ_{spt}	Septum lambda	1/ml	0.435
λ_{pcd}	Pericardium lambda	1/ml	0.03
$V_{d,spt}$	Unstressed septum volume	ml	2

3.5 SIMULATION

The CVS model is simulated by solving the system of DEs. The program ODE45 from the software package, Matlab, is used to solve for the state variables. The state vector ($\underline{x}$) is defined:

$$\underline{x} = \left[Q_{mt}, V_{lv}, Q_{av}, V_{ao}, V_{vc}, Q_{tc}, V_{rv}, Q_{pv}, V_{pa}, V_{pu}\right] \quad \textbf{(3.47)}$$

Left and right ventricular time varying elastances (e_{lv} and e_{rv}) act as the driver functions for this system of equations. These functions can be derived on a patient-specific basis using the method of Stevenson et al. (Stevenson et al., 2012a, Stevenson et al., 2012b) or can be calculated directly from measured data. Both these methods produce a discrete signal representation of the driver function. The following equations are used to calculate e_{lv} and e_{rv} from measured data:

$$e_{lv}(t) = \frac{P_{lv,meas}(t)/V_{lv,meas}(t)}{\left\|P_{lv,meas}(t)/V_{lv,meas}(t)\right\|_2} \quad \textbf{(3.48)}$$

$$e_{rv}(t) = \frac{P_{rv,meas}(t)/V_{rv,meas}(t)}{\left\|P_{rv,meas}(t)/V_{rv,meas}(t)\right\|_2} \quad \textbf{(3.49)}$$

These equations are derived from Equation (3.50), where V_d is assumed to be zero and E(t) is normalised to be between 0 and 1, giving $e_{lv}(t)$ for the left ventricle and $e_{rv}(t)$ for the right ventricle. When a personalised driver function cannot be created, a general analytical equation can be used to describe the driver functions of both ventricles (Hann et al., 2005, Hann et al., 2006):

$$e(t) = \exp^{-80(t-T/2)^2} \quad \textbf{(3.51)}$$

where T is the period of a heartbeat. The driver function for the septum is calculated as the average of e_{lv} and e_{rv}:

$$e_{spt}(t) = \frac{e_{lv}(t) + e_{rv}(t)}{2} \quad \textbf{(3.52)}$$

A function can also be used to model the effects of respiration to the CVS model, by making the thoracic pressure (P_{th}) some function of time.

$$P_{th} = f(t) \tag{3.53}$$

Parameter values used to simulate a healthy cardiovascular state are shown in Table 3.2. To run the CVS model a set of initial conditions are required for the state vector ($\underline{x_0}$):

$$\underline{x_0} = [245.5, 94.7, 0, 133.3, 329.8, 190.1, 90.7, 0, 43.0, 808.5] \tag{3.54}$$

These values were used for the initial conditions in this example as they were found to be close to the steady state values for healthy human parameters.

Before simulation of the CVS model the ODE solver options are optimised to ensure accurate and timely convergence. Relative and absolute tolerances are set to $1x10^{-6}$ for ODE45. Two different maximum step size limits are used during the simulations. When Equation (3.51) is used to produce the driver functions a maximum step size of 0.01s is implemented. However, when Equation (3.48) and (3.49) are utilised 0.001s is used for this setting because the ODE solver requires a smaller time step to accurately solve regions of sharp curvature in the solution that are introduced by the measured driver functions. Once these ODE solver options have been set the model is simulated for a time span of 20 heartbeats to ensure steady state conditions are reached. The model is then re-simulated for another three heartbeats, using the outputs of the previous simulation as initial conditions, to enforce a steady state simulation. The remaining outputs, which are not state variables, are calculated post simulation, using Equations (3.28) - (3.46), to conclude the complete simulation of the closed loop CVS model defined for a given parameter set.

Healthy human parameters, as seen in Table 3.2, and the analytical driver function of Equation (3.51), were used to simulate the model. An example of some of the important model outputs are shown in Figure 3.11. The values shown in Equation (3.54) were used as initial conditions. The thoracic pressure (P_{th}) is set to -4mmHg, which is a typical value for a healthy human (Levitzky, 2007).

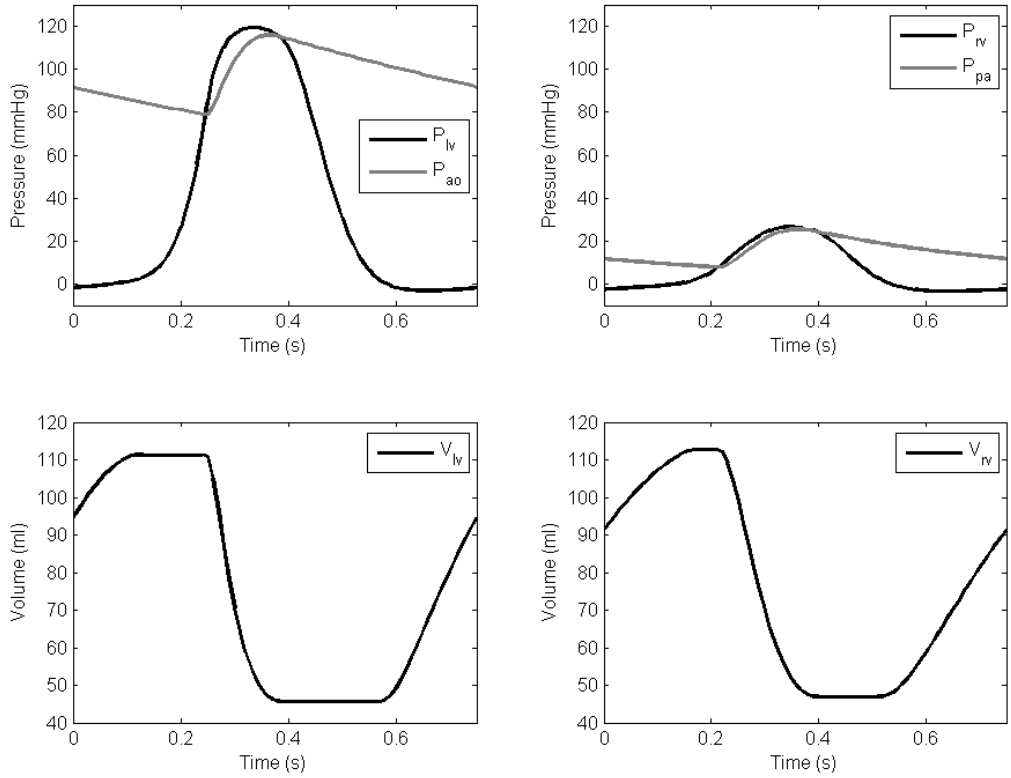

Figure 3.11: Example of some of the simulated CVS model outputs for healthy human parameters and analytically derived driver functions (e_{lv} and e_{rv}). These outputs include left ventricular pressure (P_{lv}), aortic pressure (P_{ao}), left ventricular volume (V_{lv}), right ventricular pressure (P_{rv}), pulmonary artery pressure (P_{pa}), and right ventricular volume (V_{rv}).

3.6 DISCUSSION

3.6.1 VALIDITY OF ASSUMPTIONS AND MODELLING CONCEPTS

All models, by definition, are imperfect approximations. In this work, several assumptions were made to simplify the modelling approach, as outlined in Section 3.2. The main assumptions include linear pressure-volume and linear pressure-flow relationships for peripheral flow, exclusion of atria, and that the chambers represent large sections of the CVS. It is important to be aware of these assumptions, as they impact on the physiological accuracy of the simulated outputs of the CVS model.

Physiologically, in the model, each chamber simulates a larger section of the circulation than indicated by the specific name of each chamber. The non-cardiac chambers actually represent whole regions of the circulation. For example, the aortic chamber models the effects of all the large elastic arteries. Thus, the parameters of the model define the lumped or average effects of each of the six modelled regions of the CVS.

Flow is modelled assuming a Poiseuille profile, which represents incompressible, Newtonian, laminar, axi-symmetric, fully developed flow through a rigid tube of constant cross-section. Hence, the following standard assumptions are applied to all equations governing flow:

- Blood is assumed incompressible (White, 1991).
- Although flow is not continuous in the capillaries, blood in the larger vessels is assumed to behave in a continuous Newtonian manner (Fung, 1993).
- The blood vessels are assumed to be rigid with constant cross-sectional area. This assumption is consistent with windkessel theory involving a rigid pipe and elastic chamber. The rigid pipe component simulates the fluid dynamics and the elastic chamber models the compliance of the artery walls (Tsitlik et al., 1992, Melchior et al., 1992).
- Laminar uni-directional axi symmetric flow is assumed. Although there is some flow turbulence, especially around the heart valves, it is assumed not to affect the flow profile significantly.
- Flow is assumed to be fully developed meaning the velocity profile is invariant along the vessels (Fung, 1993).

Through the use of these assumptions, vascular flow is commonly modelled using a simple electrical circuit analogy (Beyar et al., 1987, Burkhoff and Tyberg, 1993, Chung et al., 1997, Olansen et al., 2000, Smith et al., 2004), as shown by Equation (3.3).

Conversely, flow through the heart valves is pulsatile. Hence, it is not fully developed. To compensate for this issue an inertial component is added to account for the effects of the time varying flow. Thus, the inertia due to the acceleration of blood can be modelled, as defined by Equation (3.4).

All elastance, resistance, and inertance parameters in the CVS model are considered as constants. This is a commonly made assumption for this type of lumped parameter modelling (Beyar et al., 1987, Olansen et al., 2000, Ursino, 1999, Wang et al., 2003). First, elastance, which is the inverse of compliance, stays relatively constant over a physiological range of venous pressures in the venous system (Batzel and Bachar, 2010). Moreover, although it is widely accepted that lumped arterial

compliance/elastance is non-linear with respect to pressure (Batzel and Bachar, 2010, Li et al., 1990, Westerhof et al., 2009), Fogliardi et al. showed there was no advantage in using non-linear arterial compliance over linear arterial compliance in their analysis of different windkessel models (Fogliardi et al., 1996). Hence, we are justified in using a linear elastance to represent the lumped pressure volume relationship in the arterial and venous chambers in the CVS model.

Second, heart valve resistance has been suggested to be a more clinically useful than other indices of valve function (Antonini-Canterin et al., 1999). It represents a more functional index of valve impairment than the anatomical index of valve area (Antonini-Canterin et al., 1999) and has been shown to be less flow dependent in several studies (Antonini-Canterin et al., 1999) (Ford et al., 1994, Casale et al., 1992, Blitz and Herrmann, 1996, Bermejo et al., 1996, Ford et al., 1990), although these findings have been questioned (Blais et al., 2001, Mascherbauer et al., 2004). The formulation of valve resistance has the advantage that it can be easily combined with other hemodynamic calculations (Ford et al., 1994), as seen in the CVS model. Hence, the lumped valve resistance, which assumes a linear relationship between pressure difference and flow, has been used to represent valve function in the CVS model.

Third, as flow through the systemic and pulmonary capillaries is relatively steady, the resistance to flow in these regions can be considered constant, as explained above for poiseuille flow. Finally, the effects of inertia are only small in the model. Thus, calculating a variable inertance would add substantial complexity with little benefit for the model. Therefore, the elastances, resistances, and inertances of the heart valves are set as constants in the CVS model.

The ventricular pressure-volume relationship is defined by the ESPVR and EDPVR. Experimental and clinical studies have shown that the ESPVR is linear over a physiological range of loading conditions (Sagawa, 1981) (Kass et al., 1987, Grossman et al., 1977, Kass and Maughan, 1988, Kass et al., 1988, Suga et al., 1973). Therefore, ESPVR can be modelled as a linear function, as shown by Equation (3.5) and Figure 3.5. The EDPVR is most commonly modelled using an exponential function in the literature (Guyton and Hall, 2000), which provides a good approximation for the relationship over a wide range of loading conditions. Therefore, an exponential equation (Equation (3.6)) was used to model the EDPVR, as shown in Figure 3.5

The effects of the atria have been ignored in the model as they have only a small influence on cardiac and circulatory trends. In the model, the vena cava and pulmonary vein chambers represent the lumped effects of the large veins leading to the heart and atria. So, in effect, the atria are partly represented in the CVS model. However, separate atria chambers can be added to the model if the

need arises for the atria to be independently modelled, as done by Pironet et al. (Pironet et al., 2012).

3.6.2 SIMULATION

To run a simulation of the CVS model, analytical equations with respect to time are required for the driver functions, as ODE45 is a variable time-step solver. However, discrete signals are produced when the driver functions are calculated from measured data using Equations (3.48) and (3.49). Hence, when analytical formulas for the driver functions are not used, Fourier series approximations for the driver functions are created from the available discrete signals to approximate a pseudo-analytical driver function. This Fourier series function can be continuously evaluated during simulation avoiding the need for slow interpolation when evaluating the system of DEs and greatly decreasing simulation time.

3.6.3 LIMITATIONS

The main limitation of the CVS model is its lumped parameter structural definition. Due to the relative simplicity of the model it is unable to capture the micro-dynamics of the CVS. For example, the aortic notch in the aortic pressure waveform, caused by reflected pressure waves from the arterial system, is not modelled. However, the model does capture all the major dynamics of the CVS, such as changes in ventricular preload, afterload, and inotropy, which are all clinically important in managing major cardiac dysfunction and controllable with current clinical therapies.

Currently, the six-chamber model assumes that flow through the heart valves only occurs in the forward direction. However, during valvular insufficiency, backwards flow is possible through the effected valve of the patient, which fails to prevent this backward flow. Therefore, the model at its present state is unable to represent certain valvular dysfunctions, such as mitral (Paeme et al., 2011) and aortic regurgitation, without further modification.

3.7 SUMMARY

A lumped parameter model of the CVS has been created previously by Smith et al (Smith, 2004, Smith et al., 2004). The model splits the cardiovascular system into 6 sections or chambers representing the main dynamic regions which contribute to cardiovascular flow. A variety of

assumptions were used to simplify the model equations, minimising the number of parameters required. Using this minimal parameter set the model defines all the main hemodynamics of the cardiovascular system, including serial flow through the system, one-way heart valves, time-varying ventricular elastance, and parallel ventricular interaction.

CHAPTER 4: CVS MODEL PARAMETER IDENTIFICATION

For the CVS model to be clinically useful it must be personalised to each patient to accurately reflect that patient's unique cardiac and circulatory state. To do this, a parameter identification process has been created to match the dynamics of the CVS model to measurements that are easily available or inferable in an ICU setting (Hann et al., 2010, Revie et al., 2011b). This chapter presents the theory and development of the parameter identification method, used in this research, to identify patient-specific CVS models.

4.1 INTRODUCTION

The goal of this chapter is to develop a parameter identification process to match the CVS model outputs to known clinical data. The main aim is to produce a parameter identification method that can identify physiologically accurate patient-specific models of that cardiovascular system. These patient-specific models must:

- be identifiable from common ICU measurements,
- accurately reflect the patient's hemodynamics,
- provide real time feedback,
- be easy to interpret by medical staff,
- and provide additional, useful circulatory information.

In fulfilling these requirements, the parameter identification method and associated patient-specific CVS models can be used to track acute disease-dependent changes occurring in patients, and assist medical staff with monitoring the effectiveness of treatment. Hence, the goal is to combine typical clinical measurements into a clear physiological and clinically relevant picture of a patient's cardiac and circulatory status.

The starting point for the model identification method was based on the earlier method of Starfinger et al. (Starfinger, 2008, Starfinger et al., 2008a, Starfinger et al., 2008b, Starfinger et al., 2007). This integral-based parameter identification method relied on knowledge of the left and right ventricular waveforms, along with either population-based assumptions or knowledge of left and right ventricular pressures. The use of population-based assumptions limited the patient-specificity of the method. Moreover, the left and right ventricular pressure and volume waveforms are rarely

measured in the ICU. When they are, they are only measured intermittently using echocardiography, limiting the real-time ability and clinical usefulness of this earlier work (Boldt, 2002). Hence, the identification method must not rely on direct ventricular pressure or volume measurements, for the approach to be practically applied in the ICU

The improved method presented here requires only measurements that are commonly available or inferred in a typical ICU setting. These measurements include: features from the aortic and pulmonary artery pressure waveforms (P_{ao}, P_{pa}), stroke volume (SV), heart rate (HR), global end diastolic volume (GEDV), and mitral and tricuspid valve closure times (t_{mt}, t_{tc}). This measurement set is smaller than that of (Starfinger et al., 2007) as it does not require full waveforms, and is far less intensive and invasive to obtain and utilise, as these measures are typically available already.

The new model identification process has also been broken into parts, utilising smaller systemic and pulmonary circulatory models. Hence, only a sub-set of parameters are identified at any one time, leading to increased convergence stability. Thus, this research makes a significant step toward making this type of model-based approach more stable and clinically applicable without added clinical effort or burden on the patient.

The following sections outline the basic concepts and assumptions of the new identification method. The specific details of how the method is applied and works are described, and the validity and justification of the method's assumptions will be discussed.

4.2 PARAMETER IDENTIFICATION ASSUMPTIONS AND MEASUREMENTS

This section briefly outlines the main assumptions used and measurements available to identify the parameters of the six-chamber CVS model.

4.2.1 ASSUMPTIONS

Several assumptions were made to enable identification of the CVS model from the limited data set available in the ICU. These assumptions include:

- the model is at steady state
- left and right ventricular SVs are equal
- inertial effects are negligible, $L_{mt} = L_{av} = L_{tc} = L_{pv} = 0$

- $P_{lv} = P_{pu}$, at mitral valve closure
- $P_{rv} = P_{vc}$, at tricuspid valve closure
- changes in E_{lv} are proportional to changes in E_{rv} when related by the ratio of the afterloads
- GEDV ∝ LVEDV + RVEDV
- $V_{0,lv} = V_{0,rv} = V_{d,ao} = V_{d,pa} = V_{d,vc} = V_{d,pa} = 0$
- $V_{d,lvf} = V_{d,rvf} = 23$ for swine (Desaive et al., 2008) and 0 for humans
- $P_{0,lvf} = P_{0,rvf} = 0$
- heart valve resistances stay relatively constant over short time periods (<1 day)

The validity and justification of these assumptions are discussed in Section 4.6.

4.2.2 AVAILABLE AND INFERABLE ICU MEASUREMENTS

Clinically, GEDV and CO, can be measured via thermodilution techniques (Michard et al., 2003, Sakka et al., 2000, Stetz et al., 1982, Ganz et al., 1971). The aortic pressure can be estimated from radial artery pressure using one of the several transfer function methods (Westerhof et al., 2008, O'Rourke, 2004, Hope et al., 2004, Cloud et al., 2003, Pauca et al., 2001, Chen et al., 1997). Pulmonary artery indices are determined using a PAC catheter. Furthermore, the modelled P_{vc} is assumed to be equivalent to CVP, which is normally measured in the ICU. Finally, t_{mt} can be estimated from ECG. This measurement set represents all the clinically observable model outputs that can be used to identify the parameters of the six-chamber CVS model. These measurements are listed in Table 4.1 along with their equivalent or inferred model output.

Table 4.1: Typically available hemodynamic measurements in the ICU and their corresponding equivalent in the CVS model. t_{mt}, mitral valve closure time; P_{ao}, aortic pressure; P_{pa}, pulmonary artery pressure; P_{vc}, vena cava pressure; Q_{sys}, systemic flow; V_{lv}, left ventricular volume; V_{rv}, right ventricular volume.

Measurement	Description	Measured using	Equivalent or inferred model output
HR (=1/T)	Heart rate (T=period)	Electrocardiogram	t_{mt}
AP	Arterial pressure	Radial artery catheter	P_{ao}
PAP	Pulmonary artery pressure	Pulmonary artery catheter	P_{pa}
CVP	Central venous pressure	Central line catheter	P_{vc}
CO (=SVxHR)	Cardiac output	Thermodilution	$\int Q_{sys} dt$
GEDV	Global end diastolic volume	Thermodilution	$\max[V_{lv}(t)] + \max[V_{rv}(t)]$

4.3 STRUCTURAL IDENTIFIABILITY

A structural identifiability analysis was used to provide an 'a priori' indication of whether it was theoretically possible to uniquely identify the parameters of the CVS model from the available ICU measurements. The publicly available software package DAISY was used to perform this analysis on the six-chamber CVS model. This software tool uses a differential algebraic algorithm to examine global identifiability for non-linear (and linear) dynamic models with respect to observable/measurable model outputs (Bellu et al., 2007). However, please note that this purely theoretical analysis does not ensure practical identifiability as it assumes the observed measurements are noise free (Bellu et al., 2007). In reality, measurement noise is an unavoidable by-product in physiological monitoring, and thus, would have a significant effect on the identifiability of the model parameters.

Hemodynamic measurements typically available in an ICU are shown in Table 4.1. These were assumed to represent the observable measurements in the structural identification analysis. Hence, they were assigned as model outputs in DAISY.

Due to the limitations of DAISY only a simplified version of the six-chamber CVS model was analysed. The Heaviside formulation, representing the heart valve dynamics (in Equations (3.30)-(3.33)), and the equations describing ventricular interaction (Equations (3.45)-(3.46)) were removed from this simplified model description. Given these assumptions, the assumptions listed in Section 4.2.1, and list of observable measurements from Table 4.1, the following set of differential equations and model outputs were algebraically derived from Equations (3.22)-(3.39):

$$
\begin{aligned}
\dot{V}_{lv} &= \frac{\left[E_{pu}V_{pu}(t) - E_{es,lvf}\,e_{lv}(t)V_{lv}(t)\right]}{R_{mt}} - \frac{\left[E_{es,lvf}\,e_{lv}(t)V_{lv} - E_{ao}V_{ao}(t)\right]}{R_{av}} \\
\dot{V}_{ao} &= \frac{\left[E_{es,lvf}\,e_{lv}(t)V_{lv} - E_{ao}V_{ao}(t)\right]}{R_{av}} - \frac{\left[E_{ao}V_{ao}(t) - E_{vc}V_{vc}(t)\right]}{R_{sys}} \\
\dot{V}_{vc} &= \frac{\left[E_{ao}V_{ao}(t) - E_{vc}V_{vc}(t)\right]}{R_{sys}} - \frac{\left[E_{vc}V_{vc}(t) - E_{es,rvf}\,e_{rv}(t)V_{rv}(t)\right]}{R_{tc}} \\
\dot{V}_{rv} &= \frac{\left[E_{vc}V_{vc}(t) - E_{es,rvf}\,e_{rv}(t)V_{rv}(t)\right]}{R_{tc}} - \frac{\left[E_{es,rvf}\,e_{rv}(t)V_{rv}(t) - E_{pa}V_{pa}(t)\right]}{R_{pv}} \\
\dot{V}_{pa} &= \frac{\left[E_{es,rvf}\,e_{rv}(t)V_{rv} - E_{pa}V_{pa}(t)\right]}{R_{pv}} - \frac{\left[E_{pa}V_{pa}(t) - E_{pu}V_{pu}(t)\right]}{R_{pul}} \\
\dot{V}_{pu} &= \frac{\left[E_{pa}V_{pa}(t) - E_{pu}V_{pu}(t)\right]}{R_{pul}} - \frac{\left[E_{pu}V_{pu}(t) - E_{es,lvf}\,e(t)V_{lv}(t)\right]}{R_{mt}} \\
GEDV &= \max\left[V_{lv}(t)\right] + \max\left[V_{rv}(t)\right] \\
P_{ao}(t) &= E_{ao}V_{ao}(t) \\
P_{pa}(t) &= E_{pa}V_{pa}(t) \\
P_{vc}(t) &= E_{vc}V_{vc}(t) \\
CO &= \int_0^T \frac{AP(t) - CVP(t)}{R_{sys}}dt
\end{aligned}
\qquad \textbf{(4.1)}
$$

The rearranged equations of (4.1) were used to describe the simplified six-chamber CVS model in DAISY. The period of a heartbeat was set to an arbitrary value of 1. The left and right ventricular time varying elastances (e_{lv}, e_{rv}) represent the inputs of the model. GEDV, P_{ao}, P_{pa}, P_{vc}, and CO are the observable outputs of the model and volumes (V_{lv}, V_{ao}, V_{rv}, V_{pa}, and V_{pu}) are the state variables. These model variables (inputs, outputs, and state variables) need to be ranked to apply the pseudo-division algorithm used in Daisy to calculate a characteristic set of the differential ideal. The standard ranking for system identification declares that the system inputs and outputs, as known variables in this case, are the lowest ranked variables and the state variables are the highest ranking (Bellu et al., 2007). Hence, the following ranking, as denoted by '<', for the model inputs, outputs, and state variables, was used:

$$
e_{lv} < e_{rv} < GEDV < CO < P_{ao} < P_{pa} < P_{vc} < V_{lv} < V_{ao} < V_{vc} < V_{rv} < V_{pa} < V_{pu} \qquad \textbf{(4.2)}
$$

And the unknown parameter set (**P**) was defined as:

$$\mathbf{p} = \{R_{mt}, E_{es,lvf}, R_{av}, E_{ao}, R_{sys}, E_{vc}, R_{tc}, E_{es,rvf}, R_{pv}, E_{pa}, R_{pul}, E_{pu}\} \quad \textbf{(4.3)}$$

Thus, with (4.1), (4.2), and (4.3) the input file for DAISY was created, as shown in Appendix A.

Using a pseudo-division algorithm DAISY calculated the input-output relationship of the model. These relations were evaluated using a pseudo-randomly chosen set of integers, over the range of 1 to 100, for the unknown parameters. For example:

$$\mathbf{p} = \{8, 91, 28, 20, 75, 67, 83, 88, 30, 5, 35, 49\} \quad \textbf{(4.4)}$$

These values were inserted into the coefficients of the input-output relations which produced a set of non-linear algebraic equations (see Appendix A for details). This set of equations was solved using the Buchberger algorithm, providing the following Grobner basis for the parameter values of (4.4):

$$\begin{aligned} E_{ao} &= 20 \\ E_{es,lvf} &= 91 \\ E_{pa} &= 5 \\ E_{pu} &= 49 \\ E_{es,rvf} &= 88 \\ E_{vc} &= 67 \\ R_{av} &= 28 \\ R_{mt} &= 8 \\ R_{pul} &= 35 \\ R_{pv} &= 30 \\ R_{sys} &= 75 \\ R_{tc} &= 83 \end{aligned} \quad \textbf{(4.5)}$$

The Grobner basis shows that all the model parameters can be uniquely identified, as they are not functions of the other model parameters. Therefore, in theory, the simplified six-chamber CVS model is globally identifiable given the clinically observable measurement set listed in Table 4.1. Hence, in the following sections, a parameter identification method has been developed to uniquely fit subject-specific CVS models to available ICU measurement, as outlined in the following sections. A full description of the structural identification results are shown in the output file in Appendix A.

4.4 PARAMETER IDENTIFICATION CONCEPTS

Two main concepts were used to develop the parameter identification method. The first was to split the larger problem of identifying the full six-chamber model into several smaller problems using simplified models, where only sub-sets of parameters are identified at any one time. The second was the use of a proportional gain control approach to match outputs from the CVS model to known measurements, and thus, iteratively identify model parameters.

4.4.1 SIMPLIFIED MODELS

The model identification was split into pieces using smaller, simple models of the systemic and pulmonary circulations (Figure 4.1). Within each model the parameter identification was split up even further with a maximum of three parameters identified at a time. This breakdown was done to increase convergence stability. Thus, parameters that were related to each other, or trade off with each other, were identified at separate times.

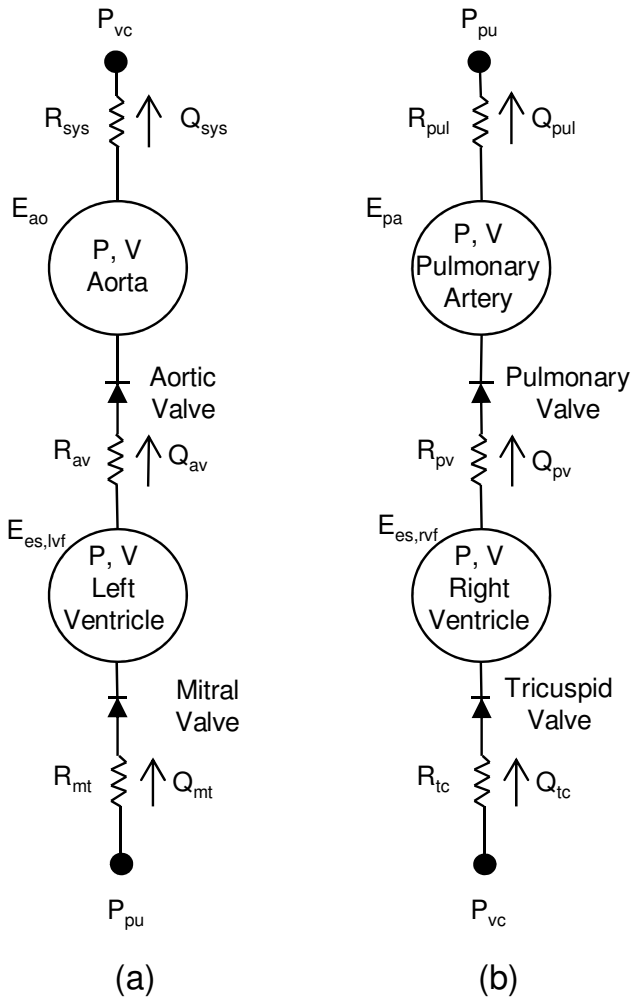

Figure 4.1: Decoupled simplified models of (a) the systemic and (b) pulmonary circulations with inertia and ventricular interaction removed. Note for comparison the orientation of the pulmonary circulation has been reversed with respect to Figure 3.1.

The systemic and pulmonary models were joined together once all parameters had converged. Ventricular coupling between the models was calculated though septum and pericardium dynamics (Hann et al., 2010, Revie et al., 2011b, Smith et al., 2004), and the vena cava and pulmonary vein chambers were identified to create a full six-chamber subject-specific CVS model. A general description of this process is shown in Figure 4.2.

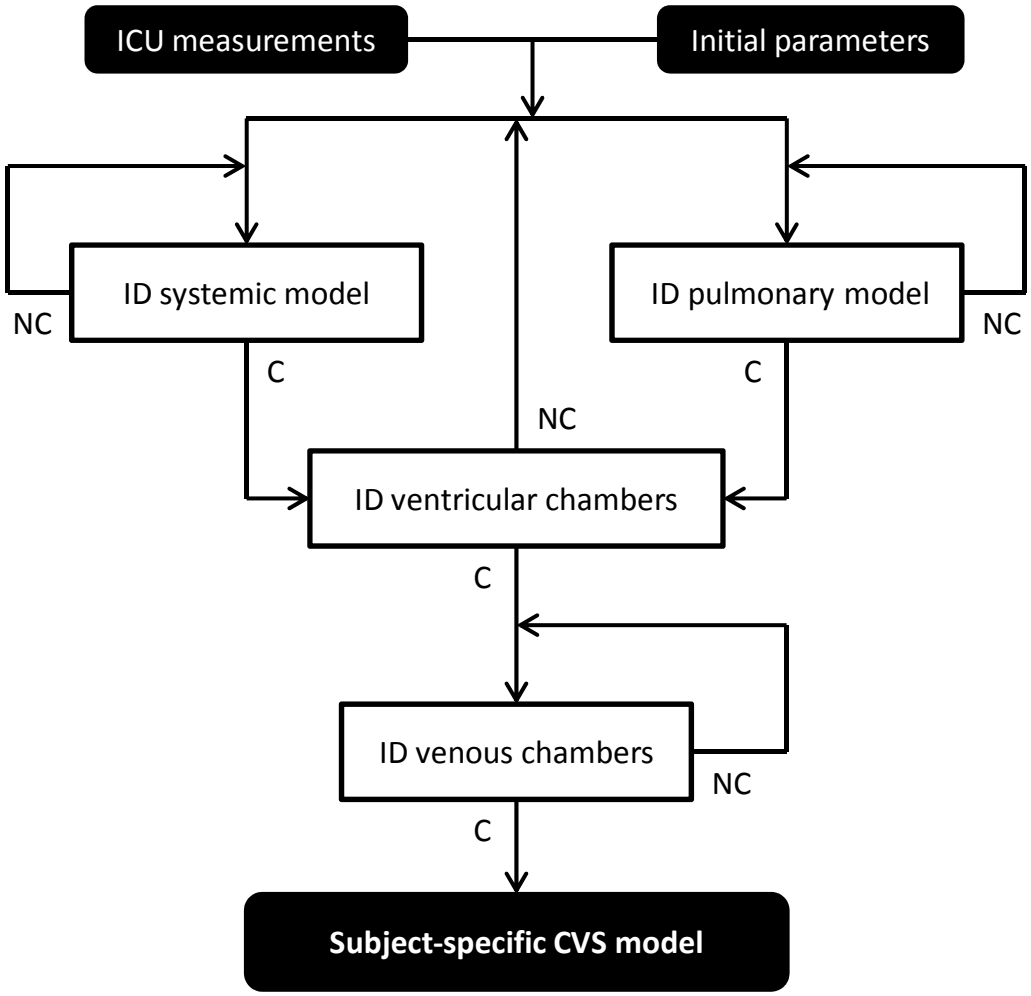

Figure 4.2: General outline of the parameter identification process. C and NC stand for if converged and if not converged.

4.4.2 PROPORTIONAL GAIN CONTROL

Most of the CVS model parameters were identified by comparing the ratio of a model output to a known measurement. To apply this method, the model output used to identify the chosen parameter must:

- be directly or inversely proportional to the parameter,
- be measureable in a clinical setting,
- and not be used already to identify another parameter.

Hence, great consideration must be taken when deciding which model output should be used to identify which parameter.

The proportional gain control method was applied once it had been decided which observable model outputs would be used to identify each specific parameter. Parameters directly proportional to a dependent model output (D_{model}) and measurement (D_{meas}) were iteratively identified using:

$$P_{new} = \frac{D_{meas}}{D_{model}} P_{old} \quad \textbf{(4.6)}$$

Similarly, inversely proportional parameters were iteratively identified with:

$$P_{new} = \frac{D_{model}}{D_{meas}} P_{old} \quad \textbf{(4.7)}$$

In the identification method, Equations (4.6) and (4.7) were used to iteratively calculate new approximations for the desired parameter from old estimates. The following steps were used to apply this iterative proportional gain approach:

1) Simulate model with initial parameter estimates.
2) Apply Equations (4.6) and (4.7) to calculate new model parameters.
3) Re-simulate model with new model parameters.
4) Repeat steps 2) and 3) until the model outputs match the measured data within tolerance.

This approach was used to simultaneously identify up to three parameters. An example of how the aortic chamber parameters are identified is shown in Section 4.4.2.1.

4.4.2.1 Aortic chamber example

In this example, the model parameters E_{ao} and R_{sys} in the systemic simplified model are identified from initial approximations. E_{ao} was found to be proportional to the amplitude of the modelled aortic pressure waveform (PP_{ao}) and R_{sys} is proportional to the mean aortic pressure ($P_{ao,mean}$). Hence, the systemic model is fitted to the mean and amplitude of the measured aortic pressure to identify these parameters. Two iterations of the proportional gain control process are shown in Figure 4.3. Note that for the demonstrative purposes of this example the other parameters of the model have been previously identified and are held constant through the iterative process. Poor initial approximations have been used for R_{sys} and E_{ao} to show the effectiveness of the method.

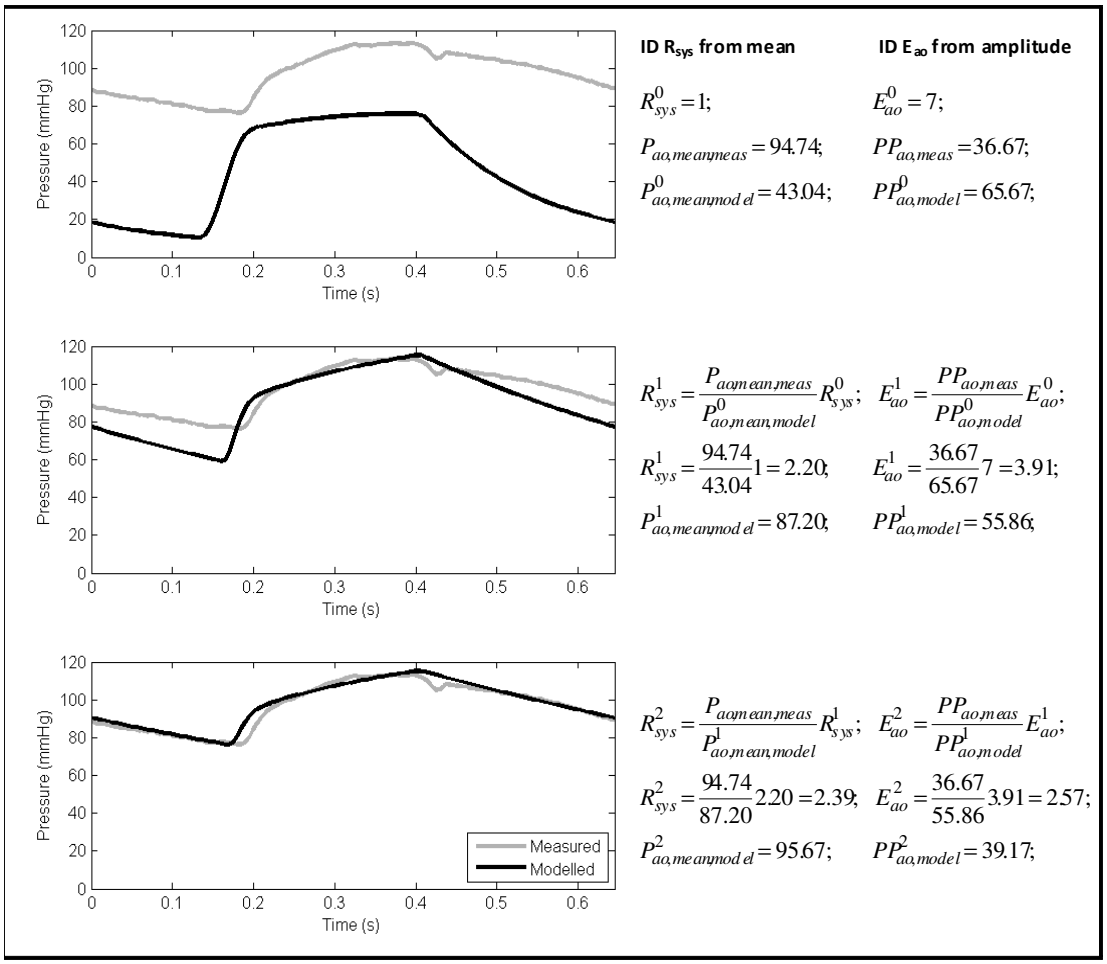

Figure 4.3: Example of the proportional gain control process iteratively fitting the mean and amplitude of the aortic pressure ($P_{ao,mean}$, PP_{ao}). The grey line in the plots represent the measured aortic pressure and the black line represents the modelled aortic pressure. Superscripts stand for iteration number. The top panel shows aortic pressure simulated from the aortic model using initial guesses for aortic elastance (E_{ao}) and systemic resistance (R_{sys}). The second and third panels show the re-simulated aortic pressure after the first and second iterations of the proportional gain control process.

As seen in Figure 4.3, the mean and amplitude of the modelled aortic pressure quickly converge to their measured counterparts. Within two iterations the error is less 1% for the mean aortic pressure and 7% for the aortic amplitude. In practice this process would be repeated until the percentage error is less than 0.5% for both measurements, and, as a result of this process, R_{sys} and E_{ao} would converge to their patient-specific value.

4.5 SPECIFICS OF PARAMETER IDENTIFICATION

The parameter identification process was split up into parts, as illustrated by Figure 4.2. The identification process used in each of these parts is shown below.

4.5.1 SYSTEMIC MODEL IDENTIFICATION

The first step in identifying the systemic model was to approximate the left ventricle driver function, $e_{lv}(t)$. The method of Stevenson et al. (Stevenson et al., 2012a, Stevenson et al., 2012b) was used to estimate $e_{rv}(t)$ from features in the measured aortic pressure waveform, $P_{ao,true}$. The systemic model parameters were then identified using a proportional gain controller that compares ratios of discrete values calculated from the model outputs (*SO*) to a set of discrete measured data (*SM*) to optimise the model parameters (*SI*), where *S* stands for systemic model and *O* = outputs, *M* = measured, and *I* = identified model parameters, as outlined by Equations (4.8)-(4.10). The initial parameter values used to simulate the systemic model, based off previous analysis of porcine data, are shown in Table 4.2.

$$SI \equiv \left\{ P_{pu}, R_{mt}, E_{es,lvf}, R_{av}, E_{ao}, R_{sys}, P_{vc} \right\} \tag{4.8}$$

$$SO \equiv \left\{ Q_{mt}, P_{lv}, V_{lv,} Q_{av}, P_{ao}, V_{ao,} Q_{sys} \right\} \tag{4.9}$$

$$SM \equiv \left\{ P_{ao,mean,true}, PP_{ao,true}, \frac{dP_{ao,\max,true}}{dt}, SV_{true}, t_{mt} \right\} \tag{4.10}$$

Table 4.2: Initial systemic model parameter inputs.

Parameter	P_{pu}	R_{mt}	$E_{es,lvf}$	R_{av}	E_{ao}	R_{sys}	P_{vc}
Initial Value	5	0.05	2	0.04	2.5	2.5	5

To start the identification algorithm, the systemic model was simulated using an initial estimate for the parameter set, *SI,* as seen in Table 4.2. At this stage, only P_{pu}, E_{ao}, R_{mt}, R_{av}, and R_{sys} of *SI* were identified, with P_{vc} identified later by the pulmonary model, and $E_{es,lvf}$ identified once the rest of the parameters of the simplified models have been fitted. Therefore, both $E_{es,lvf}$ and P_{vc} remained at their initial value, as shown in Table 4, during identification of the other systemic model parameters.

First, the mitral valve resistance (R_{mt}), aortic elastance (E_{ao}) and systemic resistance (R_{sys}) were identified by comparing the model outputs to the measured SV_{true}, $PP_{ao,true}$, and $P_{ao,mean,true}$ to find better approximations for the parameters, as shown by:

$$R_{mt,new} = \left(\frac{SV_{lv,approx}}{SV_{true}} \right) R_{mt,old} \quad \textbf{(4.11)}$$

$$E_{ao,new} = \left(\frac{PP_{ao,true}}{PP_{ao,approx}} \right) E_{ao,old} \quad \textbf{(4.12)}$$

$$R_{sys,new} = \left(\frac{P_{ao,mean,true}}{P_{ao,mean,approx}} \right) R_{sys,old} \quad \textbf{(4.13)}$$

New model outputs (*SO*) were then calculated through re-simulation of the systemic model using the new parameter approximations for R_{mt}, E_{ao}, and R_{sys}. These outputs were re-entered into Equations (4.11)-(4.13) and the process was repeated until the model outputs, $SV_{lv,approx}$, $PP_{ao,approx}$, and $P_{ao,mean,approx}$ matched the measured data to a tolerance of 0.5%.

Next, the aortic valve resistance, R_{av}, and pulmonary vein pressure, P_{pu}, were identified. R_{av} and P_{pu} were identified separately from R_{mt}, E_{ao}, and R_{sys} because they depend on the accurate convergence of these parameters. P_{pu} directly trades off with R_{mt}, as seen in Equation (3.30) when inertial effects are ignored. R_{av} is dependent on Q_{av} (Equation (3.31)) which itself is a function of stroke volume, a measured output that is matched previously through identification of E_{ao}. Hence, the reason R_{av} and P_{pu} are identified separately to R_{mt}, E_{ao}, and R_{sys}.

To calculate P_{pu} the mitral valve closure time, t_{mt} was used:

$$P_{pu} = P_{lv}(t_{mt}) \quad \textbf{(4.14)}$$

It is assumed that at the time of mitral valve closure there is no pressure difference across the valve, as shown on Figure 2.6. Therefore, at this time, P_{pu} is equal to the left ventricle pressure.

Another important feature available from the measured data was the maximum gradient or inflection point of the ascending section of the aortic pressure waveform, $dP_{ao,max,true}/dt$. In the systemic and six-chamber models, the parameter R_{av} has a significant effect on the gradient of the

ascending aortic pressure inflection point. With all other parameters held constant, changes in R_{av} cause inversely proportional changes in the maximum aortic pressure gradient.

For example, as R_{av} decreases, flow into the aorta (Q_{av}) increases, as shown by Equation (3.30). The increased Q_{av} causes the aortic volume to increase at a faster rate (Equation (3.23)) especially at the start of ejection, resulting in a sharper increase in the aortic pressure (Equation (3.34)). Hence, identification of R_{av} was achieved using the formula:

$$R_{av,new} = \left(\frac{dP_{ao,\max,approx}}{dt} \right) \Big/ \left(\frac{dP_{ao,\max,true}}{dt} \right) R_{av,old} \qquad \textbf{(4.15)}$$

where $dP_{ao,max,approx}/dt$ is the maximum ascending gradient of the model output P_{ao}. In practice, $dP_{ao,max}/dt$ is calculated by finding the first local minimum that occurs before a large ascent in the aortic pressure waveform, representing the start of ejection. The following inflection point is tehn found, representing the point of maximum gradient in the aortic pressure waveform. The change in pressure and time difference between these point (ΔP / Δt) is used to approximate $dP_{ao,max,approx}/dt$ and $dP_{ao,max,true}/dt$

With the new approximations for P_{pu} and R_{av}, the parameters R_{mt}, E_{ao}, and R_{sys} were re-identified, using Equations (4.11)-(4.13) to ensure conformity. This overall, added iterative process was repeated until $dP_{ao,max,approx}/dt$ converged to the measured data and P_{pu} stops changing between iterations, in both cases to a set tolerance of 0.5%.

Throughout identification of the systemic model, an estimate was used for the left ventricle end systolic elastance ($E_{es,lvf}$), as seen in Table 4.2, as this parameter could not be identified at this stage. However, this parameter was approximated at a later point, along with the right ventricle end systolic contractility ($E_{es,rvf}$), once the other parameters of the pulmonary model had been identified.

4.5.2 PULMONARY MODEL IDENTIFICATION

The model inputs, model outputs, and discrete measurements (calculated from the measured waveforms), which were used to identify the pulmonary model, are defined by *PI*, *PO*, and *PM,* where *P* stands for pulmonary model, as outlined by Equations (4.16)-(4.18). Table 4.3 shows the initial parameter inputs for the pulmonary model.

$$PI \equiv \left\{P_{vc}, R_{tc}, E_{es,rvf}, R_{pv}, E_{pa}, R_{sys}, P_{pu}\right\} \quad \textbf{(4.16)}$$

$$PO \equiv \left\{Q_{tc}, P_{rv}, V_{rv}, Q_{pv}, P_{pa}, V_{ao}, Q_{pul,}\right\} \quad \textbf{(4.17)}$$

$$PM \equiv \left\{P_{pa,mean,true}, PP_{pa,true}, \frac{dP_{pa,\max,true}}{dt}, SV_{true}, t_{tc}\right\} \quad \textbf{(4.18)}$$

Table 4.3: Initial pulmonary model parameter inputs.

Parameter	P_{vc}	R_{tc}	$E_{es,rvf}$	R_{pv}	E_{pa}	R_{pul}	P_{pu}
Initial Value	5	0.04	0.8	0.03	2.1	0.4	From *SI*

Identification of the pulmonary model was achieved in a similar fashion to the systemic model so only a brief description is given here. During this process, $E_{es,rvf}$ was held constant at its initial value (see Table 4.2), and was identified, along with $E_{es,lvf}$, once the other parameters of the simplified models had been identified.

First, the right ventricle driver function, $e_{rv}(t)$, was identified using the method of (Stevenson et al., 2012a, Stevenson et al., 2012b). Then Equations (4.19)-(4.21), analogous to Equations (4.8)-(4.10), were used to identify R_{tc}, E_{pa}, and R_{pul}:

$$R_{tc,new} = \left(\frac{SV_{rv,approx}}{SV_{true}}\right) R_{tc,old} \quad \textbf{(4.19)}$$

$$E_{pa,new} = \left(\frac{PP_{pa,true}}{PP_{pa,approx}}\right) E_{pa,old} \quad \textbf{(4.20)}$$

$$R_{pul,new} = \left(\frac{P_{pa,mean,true}}{P_{pa,mean,approx}}\right) R_{pul,old} \quad \textbf{(4.21)}$$

Once these parameters converged, P_{vc} and R_{pv} were calculated using:

$$P_{vc} = P_{rv}(t_{tc}) \quad \textbf{(4.22)}$$

$$R_{pv,new} = \left(\frac{dP_{pa,\max,approx}}{dt}\right) \Big/ \left(\frac{dP_{pa,\max,true}}{dt}\right) R_{pv,old} \quad \textbf{(4.23)}$$

where $dP_{ao,max,approx}/dt$ is the maximum ascending gradient of the model output P_{pa}, and these equations are analogous to Equations (4.14) and (4.15).

4.5.3 IDENTIFY VENTRICULAR CHAMBERS

The final parameters identified for the systemic and pulmonary models were $E_{es,lvf}$ and $E_{es,rvf}$. In estimating $E_{es,lvf}$ it was assumed that: the parameter R_{av} had been identified; the model output P_{ao} matched the measured data; and the systemic model stroke volume ($SV_{lv,approx}$) had converged to the measured stroke volume (SV_{true}). By analysing ohms law for fluid flow (pressure = flow·resistance or P=Q·R), the flow through valve (Q), a function of $SV_{lv,approx}$, multiplied by the resistance (R_{av}) will give a good approximation of the pressure drop across the aortic valve, ΔP_{av}. Therefore, the model should intrinsically output a relatively accurate systolic P_{lv} profile, independent of $E_{es,lvf}$, as $P_{lv} \approx P_{ao} + \Delta P_{av}$.

Given that P_{lv} was already known, changes in $E_{es,lvf}$ must trade off with left ventricle volume, as constrained by Equation (3.39), when the passive elastic recoil effects of the ventricle are ignored. Therefore, if the identified $E_{es,lvf}$ was too low then the modelled left ventricle volume, V_{lv} will be too large. Hence, knowledge of the true left ventricle volume can be used to pinpoint the correct $E_{es,lvf}$.

However, left ventricle volume is rarely measured, as it is extremely invasive to measure directly. Instead, global end diastolic volume (GEDV), which can be readily measured via thermodilution techniques (Michard et al., 2003, Sakka et al., 2000), was used to identify the sum of the ventricular elastances ($E_{es,sum} = E_{es,lvf} + E_{es,rvf}$):

$$E_{es,sum,new} = \frac{GEDV_{approx}}{GEDV_{true}} E_{es,sum,old} \quad \textbf{(4.24)}$$

where GEDV was assumed to approximately equal the sum of the left and right ventricle end diastolic volumes.

Inotropes indiscriminately affect both sides of the heart. To approximate the individual left and right ventricular contractilities ($E_{es,lvf}$ and $E_{es,rvf}$) it was assumed that any inotropic effects act evenly over the whole myocardium so the ratio of the contractilities stays constant over time. In other words, the percentage change in left ventricle elastance ($\Delta E_{es,lvf}/E_{es,lvf}$) is equal to the percentage change of the right ventricle elastance ($\Delta E_{es,rvf}/E_{es,rvf}$) over the same time period. Using this assumption, $E_{es,lvf}$

was split from $E_{es,sum}$ using a ratio of the elastances, C_E, which stays constant for each individual. The ratio C_E was identified and averaged from measurements from each patient using a ratio of the afterloads and modelled vena cava pressure, P_{vc}:

$$C_E = \frac{P_{ao,mean,true} - P_{vc}}{P_{ao,mean,true} + P_{pa,mean,true}} \approx \frac{E_{es,lvf}}{E_{es,lvf} + E_{es,rvf}} = const \quad \textbf{(4.25)}$$

This relationship is based on the Anrep effect (Anrep, 1912, Knowlton and Starling, 1912, Sarnoff and Mitchell, 1961) where increases in myocardial contractility are related to increases in afterload represented by $P_{ao,mean,true}$ on the left heart and $P_{pa,mean,true}$ on the right heart. A mean elastance ratio, $C_{E,mean}$, was averaged from the set of C_E's found for a patient. In calculating $C_{E,mean}$, only C_E's greater than 0.6 ($E_{es,lvf}/E_{es,rvf}$ > 1.5) were used to find the mean. This physiological bound ensures that the contractility of the left ventricle is always greater than the right ventricle contractility (Hosenpud and Greenberg, 2007, Konstam et al., 1985). Once $C_{E,mean}$ was calculated $E_{es,lvf}$ and $E_{es,rvf}$ were derived from $E_{es,sum}$.

$$E_{es,lvf} = C_{E,mean} E_{es,sum} \quad \textbf{(4.26)}$$

$$E_{es,rvf} = E_{es,sum,new} - E_{es,lvf} \quad \textbf{(4.27)}$$

The method for identifying the end systolic ventricle elastances is iterative and starts with initial guesses for $E_{es,lvf}$ and $E_{es,rvf}$, as shown in Table 4.2 and Table 4.3, which were used to identify the systemic and pulmonary models. Once both values had converged, the modelled ventricular volumes (V_{lv}, V_{rv}) were used to calculate $GEDV_{approx}$. The parameters $E_{es,lvf}$ and $E_{es,rvf}$ were then updated using Equations (4.24), (4.26), and (4.27) and the parameters for the systemic and pulmonary models were re-identified, as described in Sections 4.5.1 - 4.5.3. This process was repeated until $GEDV_{approx}$ had converged to the measured value.

Ventricular interaction was calculated at the same time $E_{es,lvf}$ and $E_{es,rvf}$ were identified. Initially, septum (V_{spt}) and pericardium dynamics (P_{pcd}) were set to zero in the systemic and pulmonary models. However, as new approximations for $E_{es,lvf}$ and $E_{es,rvf}$ were identified, V_{spt} and P_{pcd} were calculated using Equations (3.45) and (3.46). V_{spt} and P_{pcd} were then added to the simplified models during the next iterative step in the identification process, thus introducing ventricular interaction between the models. An in depth description on the modelling and calculation of V_{spt} and P_{pcd} can be found at Smith et al. (Smith et al., 2004).

4.5.4 IDENTIFICATION OF VENOUS CHAMBERS

The six-chamber model is the combination of the identified systemic and pulmonary models, plus two venous chambers representing the vena cava and the pulmonary vein. To fully define the model of Figure 3.1, two further parameters are required, the vena cava and pulmonary vein elastances (E_{vc}, E_{pu}). The other parameters, already identified for the systemic and pulmonary models, were fixed during identification of the six chamber model, and remain unchanged for the remainder of the identification process.

To identify E_{vc} and E_{pu} the pulmonary vein pressure, P_{pu}, identified from the systemic model, was held constant in the six-chamber model while the vena cava pressure, P_{vc}, is allowed to vary. The six-chamber model was simulated with initial guesses for E_{vc} and E_{pu}. Changes in the six-chamber model, output $P_{vc,6}$ were compared to the identified parameter, $P_{vc,simple}$, from the simplified models to calculate a better approximation for E_{vc} using:

$$E_{vc,new} = \left(\frac{P_{vc,simple}}{mean(P_{vc,6})} \right) E_{vc,old} \quad \textbf{(4.28)}$$

The model was re-simulated with the altered E_{vc} to produce a new $P_{vc,6}$. A secondary effect of altering E_{vc}, is that the simulated pulmonary volume waveform, V_{pu}, changes. This change was then utilised to identify E_{pu}:

$$E_{pu,new} = \frac{P_{pu,simple}}{mean(V_{pu})} \quad \textbf{(4.29)}$$

This process of optimising E_{vc} and E_{pu} was repeated until the mean six-chamber vena cava pressure, $P_{vc,6}$ equalled the $P_{vc,simple}$.

4.5.5 AVERAGING VALVE RESISTANCES

One of the major problems with identifying subject-specific parameters is inter-beat variability in the measured data. This variability is problematic when identifying the valve resistances (R_{mt}, R_{av}, R_{tc}, R_{pv}), which are highly sensitive to small changes in the measured data (as shown later in Section 5.3.2). However, physiologically, valve resistances stay constant between adjacent beats.

To enforce constant valve resistances, the simplified models were identified using several different periods of the measured data. The valve resistances identified for each set of measured data were stored and averaged. The medium value of the stored valve resistances was used to re-identify the other parameters of the simplified models for each set of the measured data. Equations (4.11), (4.15), (4.19), and (4.23) were no longer needed and were replaced with Equations (4.30) and (4.31):

$$P_{pu,new} = \frac{SV_{lv,approx}}{SV_{true}} P_{pu,old} \quad \textbf{(4.30)}$$

$$P_{vc,new} = \frac{SV_{rv,approx}}{SV_{true}} P_{vc,new} \quad \textbf{(4.31)}$$

Hence, the estimated t_{mt} and t_{tc} measurements were no longer required in the identification process.

4.5.6 SUMMARY

The parameter identification method was run using bounds to constrain the identified parameters within physiological limits. This helped avoid instabilities in the identification process which can occur if the parameters are allowed to become too big or small. A list of the parameter bounds are shown in Table 4.4.

Table 4.4: Parameter bounds used in the parameter identification method

Parameter	Lower Bound	Upper Bound
R_{mt}	0.005	0.5
$E_{es,lvf}$	0.1	10
R_{av}	0.005	0.5
E_{ao}	0.1	10
R_{sys}	0.1	10
E_{vc}	-	-
P_{vc}	1	minimum of 15 or ($P_{ao,min,true}$ – 2)
R_{tc}	0.005	0.5
$E_{es,rvf}$	0.1	10
R_{pv}	0.005	0.5
E_{pa}	0.1	10
R_{pul}	0.05	10
E_{pu}	-	-
P_{pu}	1	minimum of 15 or ($P_{pa,min,true}$ – 2)

A highly iterative process, involving six feedback loops was used to identify the parameters of the six-chamber model. This model identification system was run on a 2.13 GHz dual core machine with 3GB of ram. Since this research is still in the development stages the model identification had been run using the development-orientated but relatively slow Matlab software (MathWorks, Natwick, MA, USA). Using one processor the identification method took on average 6 minutes and 24 seconds to identify a subject-specific model of the CVS. Preliminary tests using the C programming language, which is better suited for real time applications, have suggested the simulation time of the six-chamber model can be reduced by a factor of 100, to approximately 3 seconds per identified model, which is an acceptable run time in a clinical environment.

The approach presented has been changed dramatically from that in Starfinger et al. (Starfinger et al., 2007), as the method now only requires a minimal set of measurements that are typically available in the ICU. In contrast, Starfinger et al. (Starfinger et al., 2007) required a larger set of invasive measurements and assumptions based on population trends. Hence, this approach is far more general. The step-wise process, including iterative feedback loops, of the new algorithm is summarised in Table 4.5.

Table 4.5: Step-wise parameter identification process of the six-chamber cardiovascular system model.

Step 1: Input set of measured data.

Step 2: Approximate left and right ventricle driver functions.

Step 3: Estimate an initial set of input parameters for systemic and pulmonary models as shown in Table 4 and 5.

Step 4: Identify systemic model of Figure 2 (a).

- **Step 4.1**: Simulate systemic model.
- **Step 4.2**: Identify R_{mt}, E_{ao}, and R_{sys} with **Equations (4.11) - (4.13)**.
- **Step 4.3**: Re-simulate the systemic model with new parameters.
- **Step 4.4**: If $SV_{lv,approx}$, $PP_{ao,approx}$, and $P_{ao,mean,approx}$ have converged within a tolerance of 0.5% go to **Step 4.5** otherwise go back to **Step 4.2**.
- **Step 4.5**: Identify P_{pu} and R_{av} with **Equations (4.14) and (4.15)**.
- **Step 4.6**: If P_{pu} and $dP_{ao.\max approx}/dt$ have converged within a tolerance of 0.5% go to **Step 5** otherwise go back to **Step 4.2**.

Step 5: Identify pulmonary model.

- **Step 5.1**: Simulate pulmonary model.
- **Step 5.2**: Identify R_{tc}, E_{pa}, and R_{pul} for the **Equations (4.19) - (4.21)**.
- **Step 5.3**: Re-simulate the pulmonary model with new parameters.
- **Step 5.4**: If $SV_{rv,approx}$, $PP_{pa,approx}$, and $P_{pa,mean,approx}$ have converged within a tolerance of 0.5% go to **Step 5.5** otherwise go back to **Step 5.2**.
- **Step 5.5**: Identify P_{vc} and R_{pv} with **Equations (4.22) and (4.23)**.
- **Step 5.6**: If P_{vc} and $dP_{pa,\max approx}/dt$ have converged within a tolerance of 0.5% go to Step 6 otherwise go back to Step 5.2.

Step 6: Identify $E_{es,lvf}$ and $E_{es,rvf}$ with **Equations (4.24), (4.26), and (4.27)** and calculate V_{spt} and P_{pcd} with **Equations (3.45) and (3.46)**. If $GEDV_{approx}$, V_{spt}, and P_{pcd} have converged within a tolerance of 0.5% go to **Step 6** otherwise go back to **Step 4**.

Step 7: Repeat **Steps 1 to 6** with different sets of the measured data and store and average the identified valve resistance.

Step 8: Repeat **Steps 1 to 6** using the averaged/fixed valve resistances (ie without identifying R_{mt}, R_{av}, R_{tc} and R_{pv}) and **Equations (4.30) - (4.31)**.

Step 9: Identify six-chamber model.

- **Step 9.1**: Simulate six-chamber model.
- **Step 9.2**: Identify E_{vc} and E_{pu} with **Equations (4.28) - (4.29).**
- **Step 9.3**: Re-simulate six-chamber model with new parameters.
- **Step 9.4**: If P_{vc} has converged within a tolerance of 0.5% go to **Step 10** otherwise go back to **Step 9.2**.

Step 10: Output six-chamber parameters and model outputs

4.6 DISCUSSION

4.6.1 VALIDITY AND JUSTICATION OF ASSUMPTIONS

The first assumption made by the identification method is that the measurement set used in the identification process represent steady state hemodynamics. Hence, it is assumed the SVs of the left and the right ventricles are the same. This assumption is physiologically reasonable as serial interaction between the ventricles, due to the Frank Starling mechanism, maintains the balance of ejected volume from both pumps.

Second, inertial effects of the blood were ignored. Inertia, represented by the inertance parameters in the model, was found to contribute less than 1% to the outputs of the CVS model. Hence, it was removed from Equations (3.30)-(3.33), simplifying these equations, and decreasing the number of parameters required for identification.

Third, it was assumed that the venous filling pressures, P_{pu} and P_{vc}, were equal to the pressures in the left and right ventricles, P_{lv} and P_{rv}, at the time of mitral and tricuspid valve closure. In the CVS model, P_{pu} and P_{vc} act as the filling pressures to ventricles, as the left and right atrium are not modelled. Since inertia of blood is ignored, the heart valves close when there is a negative pressure gradient, which prevents backwards flow through the valve. Hence, the valves close as soon as ventricular pressure rises above the venous press and at this point $P_{pu} \approx P_{lv}$ and $P_{vc} \approx P_{rv}$. This assumption is used to identify P_{pu} and P_{vc} in the identification process.

In the ICU, few measurements are taken directly from the heart. There are not enough available measurements to directly identify $E_{es,lvf}$ and $E_{es,rvf}$. Hence, in the identification process an empirical coefficient (C_E), based on Equation (4.25), was used as added piece of information to calculate $E_{es,lvf}$ and $E_{es,rvf}$. Equation (4.26), which uses C_E, is based off a strong relationship ($R^2 = 0.80$) between $E_{es,lvf}$ and the sum contractilities, $E_{es,sum}$, where $E_{es,sum}$ is identified beforehand using GEDV. This relationship was discovered during preliminary development of the model identification process where left and right ventricular volume measurements from porcine studies (Ghuysen et al., 2008, Lambermont et al., 2006) were used to fit subject-specific CVS models. The relationship is shown in Figure 4.4. Although applying the empirical relation requires extra iterations during the identification process it enables accurate approximation of left and right ventricular function without the need for highly invasive measures. In practice, measurement of $E_{es,lvf}$ and $E_{es,rvf}$ require highly invasive cardiac catheterisation combined with a vena cava occlusion manoeuvre or expensive equipment needed for echocardiography. Importantly, these latter methods, while accurate, do not provide continuous measurements and are clinically impractical, limiting their utility.

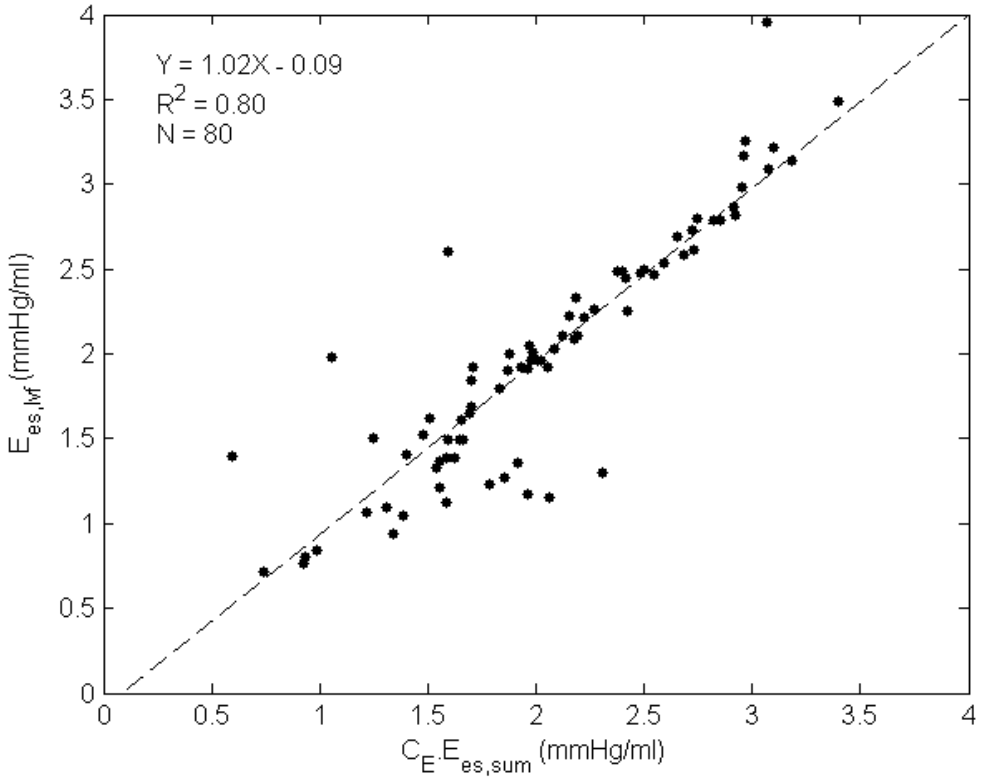

Figure 4.4: Relationship used to separate the end systolic left ventricular elastance ($E_{es,lvf}$) from the sum of the ventricular elastances ($E_{es,sum}$). The coefficient C_E is calculated from the mean aortic, mean pulmonary artery, and vena cava pressures using Equation (4.25).

The fifth assumption assumes the maximum heart volume (GEDV) is directly proportional to the sum of the maximum left and right ventricles. In the ICU GEDV is normally calculated from thermodilution measurements. The assumption of proportionality is logical because at the end of filling most of the volume from the left and right atriums has been ejected into the ventricles. This assumption is also backed up by experimental evidence (Sakka et al., 2000). Therefore, the main determinant of GEDV will be LVEDV and RVEDV, and the small amount of volume left in the atriums at the end of filling will generally be proportional to these volumes.

The less important model parameters are not identified during the identification process. This choice is simply due to the lack of available unique ICU measurements. These parameters, such as unstressed volumes of the six model chamber ($V_{d,lvf}$, $V_{d,rvf}$, $V_{d,ao}$, $V_{d,pa}$, $V_{d,vc}$, and $V_{d,pu}$) and the zero volume left and right ventricular pressures, are set as constants in the CVS model so the identification method can focus on identifying the more important metrics which define the main dynamics of the cardiovascular flow. In general, this choice ensures identifiability of the more physiologically and clinically relevant parameters.

The final assumption made by the identification process is that the valve resistances stay relatively constant. Calcification of the heart valves, the main cause of stenosis, normally develops slowly. Hence, it is assumed that the resistant state of the heart valves do not change over short time periods (<1 day). In the identification method several patient-specific models are identified from different sets of data and the heart valve resistances are averaged. The CVS models are then re-identified using these averaged and now constant valve resistances. The use of this process removes the inter-beat variability in the identified valve resistances, which are highly sensitive to noise in the measured data. Thus, facilitating identification of more accurate CVS models.

4.6.2 SIMPLIFIED MODELS

Before the identification process, the systemic and pulmonary side of the six-chamber CVS model are separated from each other. These simplified models are mathematically decoupled by removing the ventricular interaction and replacing the vena cava and pulmonary vein chambers with constant pressure sources, P_{vc} and P_{pu}. Although the models are mathematical decoupled there still remains an intrinsic coupling between the models as they both share the same upstream and downstream pressure, P_{vc} and P_{pu}, and they are identified using the same SV.

The use of the simplified models increases the convergence stability of the identification process, as only subsets of the total number of parameters need to be identified at any one time. This results in less interaction between parameters during identification, smoothing convergence. The setup with the simplified models also makes the identification process easy to program, as the larger problem of identifying the full six-chamber model is broken into smaller and easier to understand modules.

4.6.3 PARAMETER IDENTIFICATION LIMITATIONS

The main limitation of model identification method is its reliance on knowing the pulmonary artery pressure, which is not widely measured. The use of the pulmonary artery catheter (PAC) has gone out of fashion in recent times (Johnston et al., 2008b, Wiener and Welch, 2007) as it has been associated with little or even deleterious effects on mortality rates (Binanay et al., 2005, Shah et al., 2005). Some investigators (Shah et al., 2005) have suggested the use of the PAC by itself may not be the problem. Instead, incorrect interpretation of the waveform and the use of sub-optimal therapies triggered from data obtained from the PAC may be the cause of these poor results. In such cases, patient-specific models could be used to standardise interpretation of the measurement.

Features of the pulmonary artery waveform in conjunction with other measurements can be converted into easy to understand metrics representing ventricular contractility, preload, vascular stiffness and resistance which are directly controllable with current clinical treatments (fluid resuscitation, inotropes, vasopressors, and vasodilators), providing a better platform for therapy to be based from. Given the potential, and only small added risks associated with the PAC (Berenholtz et al., 2004, Johnston et al., 2008a, Mermel et al., 1991, Ramritu et al., 2008, Safdar et al., 2002, Weil, 1998), this compromise favours improved patient outcome, as well as ease of use. Alternatively, the model identification method could easily be adapted to use echocardiography measurements to identify parameters of the pulmonary circulation, although, this approach would reduce the frequency at which the CVS models could be identified.

The model also assumes $V_{d,lvf} = V_{d,rvf} = 0$, though in most cases this assumption is not accurate. When the true $V_{d,lvf}$ or $V_{d,rvf} \neq 0$, $E_{es,lvf}$ and $E_{es,rvf}$ will not quantitatively represent the gold standard definition of ventricular contractility as defined by Sugawa et al. (Sagawa et al., 1977), as represented by Equation (3.7). However, physiologically $V_{d,lvf}$ and $V_{d,rvf}$ stay relatively constant over the range of normal loading conditions and short time periods. Therefore, as the CVS model is a lumped parameter model the effects of a non-zero $V_{d,lvf}$ or $V_{d,rvf}$ will be taken into account during the identification of $E_{es,lvf}$ and $E_{es,rvf}$. In other words, if there is a sharp increase in the contractile state of the heart, a sharp increase will be noticed in the identified $E_{es,lvf}$ and $E_{es,rvf}$. Thus, importantly, although the value of modelled $E_{es,lvf}$ and $E_{es,rvf}$ may differ from the gold standard measurement the qualitative trends of these parameters should still represent the changes in the patient's state. Preliminary testing has indicated that changes in the estimated driver function may be used to identify $V_{d,lvf}$, which could be incorporated in future versions of the modelling identification method.

Further limitations in identifying the ventricular contractilities arise from the assumption that the ratio of the contractilities, C_E, stays constant over the duration of the trial. It would seem logical that if one side of the heart was badly damaged or highly distended then the relationship between $E_{es,lvf}$ and $E_{es,sum}$ may no longer be linear and the ratio may not stay greater than 0.6. It should be noted that such patients might well be close to death. No useful literature was found comparing inotropic effects on both the left and right ventricle simultaneously. Hence, the assumption of a constant C_E was based off measurements from the nine pigs with induced pulmonary embolism (N=5) or induced septic shock (N=4) where C_E was found to stay relatively constant in this range for each animal over a wide range of inotropic states and loading conditions (see Figure 4.4). For use in humans, this ratio will have to be further confirmed in trends that controllably change the inotropic state of the heart with dobutamine or a similar infusion.

4.7 SUMMARY

A parameter identification method for identifying patient-specific models cardiovascular models has been created. The models can be identified from readily ICU measurements through the use simplified models and proportional gain control. This work is an improvement on previous work as this process now enables real-time monitoring of cardiovascular dynamics in a clinical setting.

CHAPTER 5: PARAMETER IDENTIFICATION VALIDATION

The parameter identification method outlined in Chapter 4 must now be tested and validated. In this chapter, subject-specific CVS models are identified using porcine data from animal trials. The convergence, sensitivity, repeatability, and accuracy of these models is tested and analysed to validate the method and its performance and limitations.

5.1 INTRODUCTION

This chapter examines the ability of the parameter identification method to accurately identify subject-specific CVS models from realistically available clinical data. Verification and validation of the identified models was done by analysing:

1) model convergence,
2) parameter sensitivity,
3) repeatability of model identification,
4) and accuracy of the model outputs against independent measurements not used in the identification method.

These analyses provide quantitative information on the strengths and weaknesses of the parameter identification method.

These verification and validation analyses were tested using measurements from two porcine studies on acute pulmonary embolism (PE) and septic shock (SS). The convergence, parameter sensitivity, and repeatability of the model identification process were tested using measurements from the PE study. Validation against independent measurements was analysed using identified models for both PE and SS. The details and results of the validation analyses are outlined in the following sections.

5.2 METHODS

5.2.1 PORCINE MEASUREMENTS

To validate of the model identification method, subject-specific CVS models were identified retrospectively from measurements recorded in experimental pig studies on PE and SS. In the PE study, autologous blood clots were inserted into 5 pigs to induce pulmonary embolism (Ghuysen et al., 2008). Continuous measurements over 6 - 12 heartbeats of aortic pressure, pulmonary artery pressure, and left and right ventricular pressures and volumes were measured. Measurements were recorded at 30 minute intervals up to 4.5 hours with an extra set of measurements taken 5 minutes before the end of the trials (T0, T30,....,T210, T240, T265, T270).

In the SS study, an endotoxin infusion over the first 30 minutes was used to induce septic shock in 4 pigs (Lambermont et al., 2006). The same measurements as in the porcine study were recorded. However, in this study measurements were only recorded up to 4 hours (T0, T30,..., T210, T240). Further details on the experimental protocol used in both these studies can be found in the Sections 6.2.1 and 7.2.1 or in (Ghuysen et al., 2008, Lambermont et al., 2006).

5.2.2 MODEL IDENTIFICATION ANALYSES

First, model convergence was checked to ensure the model outputs correctly converged to the convergence set points. These set points represent measurements of hemodynamic vital signs recorded for one heartbeat (ie, MAP and SV), as shown in Table 4.1, Section 4.2.2. The convergence of the identified CVS models was analysed by observing whether or not the model outputs converged to their corresponding set points to within the desired tolerance (normally +/- 0.5%) for the systemic and pulmonary sub models and for the full six chamber model identified in the PE study.

Second, the sensitivity of the model parameters to changes in the convergence set points used in the identification method was analysed. Each convergence set point was changed by +/-10%, while the other set points were left at their measured value. CVS models were identified for every combination of the altered convergence set points, and the effect on the identified parameters was analysed for Pig 1, in the PE study, in a healthy (at T0) and diseased state (at T150).

Third, the repeatability of the model identification method was examined. In the porcine studies, the subject-specific CVS models were identified from hemodynamic measurements recorded over one heartbeat. Hence, to test the repeatability of the identification method, subject-specific CVS models

were identified from measurements obtained from three adjacent heartbeats. The change in the subject-specific models was analysed to see how the identified parameters varied between heartbeats. Thus, this analysis provides an indication of the repeatability of the parameter identification process.

Finally, the ability of the subject-specific models to accurately identify cardiac measurements not used as convergence set points in the model identification process was explored. Modelled left and right ventricular pressures and volume outputs were compared to measured values. Hence, the ability of the subject-specific CVS models to predict dynamics of the CVS that were assumed unknown beforehand is tested. This independent measurement validation assesses the ability of the identified subject-specific CVS models to interpolate cardiac dynamics from the available circulatory measurements.

5.2.3 DATA ANALYSIS

In the convergence and repeatability analyses data is presented as mean bias plus or minus two standard deviations (mean +/- 2SD) of the percentage error. In the sensitivity analysis data is presented in pairs showing the percentage deviation in the parameter due to changing the convergence setting input by +/- 10% (or +/-0.005s for temporal inputs). To analyse the repeatability of the model identification method the percentage change in the identified parameters between beats was analysed. Bland-Altman analysis (Bland and Altman, 1986) was used to illustrate the accuracy of the identification method against independent measurements. Median, 5^{th}, and 95^{th} percentile percentage errors are also used to quantify accuracy against the independent measurements. A percentage error less than 20% was regarded as an acceptable result, because the clinical measurement of physiological variables often lack precision, with errors of +/- 10 to 20% not uncommon (Clancy et al., 1991, Critchley and Critchley, 1999, Salandin et al., 1988).

5.3 RESULTS

5.3.1 CONVERGENCE

The convergence of the identified models was verified for the PE data by checking whether or not the model outputs matched the convergence criteria within the given tolerance. Table 5.1 shows the bias and spread (mean +/- 2 SD) of the errors in the model outputs used in the identification process. In 93% of the subject-specific models all the model outputs converged to the measured value within

the tolerance range. However, the model outputs of 4 of the identified systemic sub-models, 3 of the pulmonary sub-models, and 4 of the six-chamber models did not converge within their set tolerances. The larger errors seen in Table 5.1 are solely due to four (of 51) identified models that had not fully converged during the identification process. For all the other models, the model outputs converged to within 0.5% of the convergence criteria.

Table 5.1: Convergence analysis of the parameters of the systemic and pulmonary sub-models and six-chamber model for the PE case. Data presented for 51 subject-specific CVS models compares the model output to measured data to a bias +/- 2SD.

	Bias +/- 2SD		
	Systemic	**Pulmonary**	**Six**
$P_{ao,mean}$	-0.03 +/- 0.62%	-	-0.00 +/- 0.66%
PP_{ao}	-0.09 +/- 1.60%	-	-0.07 +/- 1.55%
max dP_{ao}/dt	-0.33 +/- 4.39%	-	-0.04 +/- 3.75%
SV_{lv}	0.00 +/- 0.32%	-	-0.03 +/- 0.42%
$P_{pa,mean}$	-	0.08 +/- 0.65%	-0.01 +/- 1.05%
PP_{pa}	-	-0.41 +/- 1.37%	-0.54 +/- 1.98%
max dP_{pa}/dt	-	-0.59 +/- 7.98%	-0.18 +/- 10.3%
SV_{rv}	-	0.00 +/- 0.10%	-0.04 +/- 0.97%
$GEDV$	-	-	-0.08 +/- 0.70%
E_{rat}	-	-	-0.02 +/- 0.35%
$P_{pu,mean}$	-	-	0.02 +/- 0.18%
$P_{vc,mean}$	-	-	0.00 +/- 0.05%

5.3.2 SENSITIVITY ANALYSIS

A sensitivity analysis was done using one heartbeat's worth of pig measurements, for Pig 1 in a healthy state (at T0) and diseased state (at T150 after 2 injected emboli). The measurement of mean arterial pressure ($P_{ao,mean,true}$) used in the identification process was altered by +/- 10%, while the other measurements were kept at their normal values. A subject-specific CVS model was identified, and the effect of changing $P_{ao,mean,true}$ on the identified parameters was observed. This process was repeated for the other measurements used to identify subject-specific CVS models. All pressure, pressure gradient, and volume measurements were changed by +/- 10%, and time measurements were altered by +/- 0.005s. Please note that during the identification process the valve resistances were not averaged, as described in Section 4.4.5, so that the sensitivity of these parameters could also be analysed. The results of the sensitivity analysis are shown in Table 5.2 and Table 5.3 for Pig 1 in a healthy state at T0 and Pig 1 in a diseased state at T150 during the trial.

Table 5.2 shows that the parameters on the pulmonary side of the model are insensitive to convergence inputs relating to the other side of the circulation, i.e. R_{tc}, E_{rv}, R_{pv}, E_{pa}, and R_{pul} only change by a small amount when PP_{ao} is altered. A parameter was considered highly sensitive if it changed by greater than 25%. The valve resistances, E_{vc}, and E_{pu} were the most sensitive parameters, with the parameter changing as much as 50%. R_{mt} was highly sensitive to t_{mt}; R_{av} was highly sensitive to PP_{ao}, *SV*, and *GEDV*; R_{tc} was highly sensitive to t_{tc}; R_{pv} was highly sensitive PP_{pa}, and moderately sensitive to max dP_{pa}/dt and *GEDV;* E_{vc} was highly sensitive to t_{tc}; and E_{pu} was highly sensitive to t_{mt}.

The results for the diseased state at T150, as shown in Table 5.3, are similar to the healthy state results. The valve resistance and venous chamber elastances were again the most sensitive parameters. In the diseased state, maximum changes of up to 180% were noticed for some of the parameters, although R_{av} and R_{pv} were a lot less sensitive to *SV* and *GEDV*. The results shown in Table 5.2 and Table 5.3 indicate the need for accurate measurements and averaging when identifying valve resistances in the CVS model.

5.3.3 REPEATABILITY OF MODEL IDENTIFICATION ANALYSIS

The repeatability of the model identification process was tested by identifying subject-specific CVS models for three adjacent heartbeats. The analysis was performed for the same pig (Pig 1) and at the same times (T0 and T150) as the sensitivity analysis, although, different heartbeats from the recorded measurements were used. The adjacent heartbeats reflect steady state hemodynamics, and thus, there are only minor differences due to the natural variability between the measurements of each beat. The identified parameters for the different heartbeats and their percentage change from the first heartbeat are shown in Table 5.4. Again, the heart valve resistances were not averaged, to allow analysis of their inter-beat sensitivity.

The results in Table 5.4 are similar to the sensitivity analysis in that the valve resistances, E_{vc}, and E_{pu} seem to be the most sensitive to small changes in the measurements. All the other parameters change by less than 9% between beats. A maximum change of 105% is seen for the R_{mt} identified from the 3rd beat at T150. These results indicate that the measurements used as convergence criteria in the parameter identification process should be averaged to reduce inter beat variability in the identified parameters.

Table 5.2: Parameter sensitivity analysis of Pig 1 at T0 showing identified parameters for +/-10% (or -/+ 0.005s for t_{mt} and t_{tc}) change in the measured input value used in the identification method. 'ID value' indicates the parameter value identified when the inputs of the identification process were not altered.

		R_{mt} [mmHg.s/ml]	E_{lv} [mmHg/ml]	R_{av} [mmHg.s/ml]	E_{ao} [mmHg/ml]	R_{sys} [mmHg.s/ml]	E_{vc} [mmHg/ml]	R_{tc} [mmHg.s/ml]	E_{rv} [mmHg/ml]	R_{pv} [mmHg.s/ml]	E_{pa} [mmHg/ml]	R_{pul} [mmHg.s/ml]	E_{pu} [mmHg/ml]
	ID value	0.025	2.572	0.058	2.662	3.467	0.005	0.065	0.478	0.010	0.741	0.429	0.015
%	$P_{ao,mean}$	-9.6|7.9	-10.1|8.6	15.6|-16.4	1.9|-0.6	-10.9|9.5	0.5|0.4	0.3|-0.2	1.4|-1	0.6|-0.3	-0.2|0.2	2.2|-2.2	-15.4|8.5
	PP_{ao}	-1.7|1.7	-0.9|1.1	-55|32.1	-12.4|10.6	0.2|0.2	0.4|0	-0.4|0.4	-1|1.3	-1.5|1.4	-0.1|0	0.4|-0.4	-3.1|1.7
	max dP_{ao}/dt	0.3|-0.1	0.2|-0.1	16|-11.4	0.7|0.6	0|0.3	0.4|0.8	0.1|0	0.2|-0.1	0.2|-0.2	0|0	-0.1|0.1	-1.3|-4.7
	t_{mt}	-50.8|32.1	0.1|0.1	0.9|1.3	0.4|0.4	0.4|0.1	0.6|0.4	0|0	0.1|0.1	-1|1.6	-0.7|1.2	6.6|-10.4	-53.3|29.2
	$P_{pa,mean}$	0.3|-0.6	1.3|-0.9	6.3|0.7	0.5|0.4	0.4|-0.1	-8.8|8.5	-8.8|7.3	-9.7|8.3	4.6|-4	1.9|-2	-13.5|10.7	-3.8|-2.3
	PP_{pa}	-0.2|0	-0.9|1	-2|5.8	0.3|0.6	0.2|0	-1.9|2.8	-2.2|2	-1.5|1.6	-42.4|26.6	-13.4|10.3	-0.2|0.2	-1.2|-3.2
	max dP_{pa}/dt	-0.1|-0.1	0.2|0	3.8|0.4	0.6|0.2	0.1|0.2	0.5|-0.2	0.3|-0.3	0.3|-0.1	17.1|-21	-0.1|0	-0.1|0.2	-0.8|-0.6
	t_{tc}	1.1|-1.5	3.9|-4.4	11.4|-11	1.1|0.3	1.5|-1.3	-42.9|27.9	-44.1|28.7	-4.3|5.2	-5.1|6.1	-0.4|-0.1	-0.3|0.6	0.5|-4.4
	SV	6.1|-5.2	-3.9|3.8	-40.9|20.6	8.7|-8.5	9.7|-9.7	-5.9|6.7	5.3|-4.3	-5.3|5.2	-10.3|9.2	8.8|-9.6	10.5|-10.7	-3.4|-1
	GEDV	4.3|-3.6	13.8|-13.8	30.8|-49.9	1.7|-1.1	0.3|0.2	5.7|-3.1	5.8|-4.3	15.2|-14.9	19.8|-18	0.4|-1.2	-0.6|0.2	-3.9|2.3

Table 5.3: Parameter sensitivity analysis of Pig 1 at T150 showing identified parameters for +/-10% (or -/+ 0.005s for t_{mt} and t_{tc}) change in the measured input value used in the identification method. 'ID value' indicates the parameter value identified when the inputs of the identification process were not altered.

		R_{mt} [mmHg.s/ml]	E_{lv} [mmHg/ml]	R_{av} [mmHg.s/ml]	E_{ao} [mmHg/ml]	R_{sys} [mmHg.s/ml]	E_{vc} [mmHg/ml]	R_{tc} [mmHg.s/ml]	E_{rv} [mmHg/ml]	R_{pv} [mmHg.s/ml]	E_{pa} [mmHg/ml]	R_{pul} [mmHg.s/ml]	E_{pu} [mmHg/ml]
	ID value	0.075	2.307	0.027	2.821	2.158	0.013	0.051	1.239	0.240	3.841	0.611	0.063
%	$P_{ao,mean}$	1.5|-3.4	-5.1|9.4	-5.9|9.3	2.5|1.2	-12.4|9.4	-4.3|-1.3	-1.9|0.2	-4.8|-0.8	-3.7|-0.9	0.1|-0.1	-0.1|-0.1	9.5|8
	PP_{ao}	-0.4|-1.2	-0.4|0.7	-41.6|25	-10.7|10.4	-0.4|-0.4	-1.1|-1.8	-0.2|0.3	-0.5|0.8	-0.5|0.6	0|0	0|0	5.9|7.6
	max dP_{ao}/dt	-0.9|-0.3	0.2|-0.2	12.1|-36.9	0.8|0.4	-0.6|-0.1	-1.5|-0.8	0.1|-0.1	0.2|-0.2	0.2|-0.2	0|0	0|0	7.2|3.2
	t_{mt}	-193.1|0	-1.3|0	-8.6|0	0|0	-0.1|0	-4.4|0	-3|0	-2.5|0	-12.6|0	-3.8|0	21.1|0	-126.4|0
	$P_{pa,mean}$	0.6|0.2	1.6|1.6	-1.4|-5.4	-1.3|0.3	0.4|-0.1	-6.4|3.7	-7|3.3	-9.4|1.8	-2.5|-10.1	4.3|-3.3	-16.2|12.1	-4.1|-0.9
	PP_{pa}	-0.3|-1	-3.6|4.3	-4.3|-5.2	0.3|2	0.8|-1.6	-11.2|6	-10|7.6	-7.1|4.6	-48.5|22.2	-15.8|13	-0.2|0.4	3.7|8.5
	max dP_{pa}/dt	-0.3|-1	3.9|-1.6	-1.8|-5	1.1|1.2	-0.5|0	6.8|-7.5	7|-5.1	4.1|-3.5	22.7|-25.1	2|-1.1	-0.6|0.4	1.9|8.9
	t_{tc}	-0.3|-0.7	9.8|-0.1	5.1|-0.8	0.3|0.8	6.8|-1.4	-130.2|7	180.7|10.6	-11|0.1	-7.3|-0.7	-0.2|0	-0.3|0	-0.4|6.2
	SV	9.8|-11.3	-2.5|3.2	-7.6|-3.9	10.9|-7	10.2|-10.6	-5.5|2.4	6.1|-5.2	-4|3.5	1.6|-2.4	9.7|-9.6	9.6|-9.8	4.6|8.3
	GEDV	0.3|-0.9	12.9|-12.6	7.7|-13.7	-0.2|0.5	0.1|-0.2	4.8|-4.8	5.2|-4.6	13.2|-14	7.7|-7.7	0.2|0	0.1|-0.2	-8.1|11.2

Table 5.4: Identified parameters of the CVS model from measurements obtained from three adjacent beats. The table shows the parameter values and the percentage change in brackets for beats 2 and 3 in the parameter value in comparison to beat 1.

		R_{mt} [mmHg.s/ml]	E_{lv} [mmHg/ml]	R_{av} [mmHg.s/ml]	E_{ao} [mmHg/ml]	R_{sys} [mmHg.s/ml]	E_{vc} [mmHg/ml]	R_{tc} [mmHg.s/ml]	E_{rv} [mmHg/ml]	R_{pv} [mmHg.s/ml]	E_{pa} [mmHg/ml]	R_{pul} [mmHg.s/ml]	E_{pu} [mmHg/ml]
t000	**Beat 1**	0.033	2.6	0.22	2.6	3.4	0.003	0.038	0.41	0.008	0.56	0.26	0.025
	Beat 2	0.035 (6.5)	2.6 (-1.4)	0.18 (-17)	2.7 (1.9)	3.4 (1.3)	0.003 (5.6)	0.041 (7.8)	0.40 (-1.7)	0.006 (-23)	0.54 (-2.5)	0.24 (-6.5)	0.028 (8.2)
	Beat 3	0.034 (3.0)	2.6 (0.4)	0.2 (-7.1)	2.7 (2.2)	3.4 (0.8)	0.003 (0.1)	0.037 (-1.2	0.40 (-1.4)	0.005 (-35)	0.56 (-1.0)	0.25 (-4.0)	0.026 (1.8)
t150	**Beat 1**	0.018	2.3	0.11	2.3	2.3	0.008	0.047	1.0	0.11	2.6	0.75	0.024
	Beat 2	0.029 (55)	2.3 (-0.0)	0.12 (7.1)	2.5 (4.9)	2.4 (1.9)	0.009 (16)	0.060 (28)	1.1 (3.3)	0.12 (18)	2.7 (3.6)	0.73 (-2.8)	0.032 (34)
	Beat 3	0.037 (105)	2.3 (0.0)	0.09 (-11)	2.4 (2.9)	2.3 (-1.0)	0.011 (41)	0.071 (53)	1.1 (8.6)	0.17 (60)	2.6 (2.9)	0.68 (-9.0)	0.039 (64)

5.3.4 VALIDATION AGAINST INDEPENDENT MEASUREMENTS

Validation was achieved by comparing the other model outputs to measurements that were not used in the identification process (left and right ventricular end diastolic volumes [LVEDV, RVEDV] and maximum left and right ventricular pressures [$P_{lv,max}$, $P_{rv,max}$]). Bias, precision, absolute percentage errors and correlation metrics were used to analyse accuracy. These metrics were analysed in both the pulmonary (PE) and septic shock (SS) studies.

5.3.4.1 *Pulmonary embolism*

Table 5.5 shows that the modelled outputs, LVEDV, RVEDV, $P_{lv,max}$, and $P_{rv,max}$ correlated well with their corresponding independent measurements, with $R^2 > 0.84$ in all cases. All percentage errors were less than 15% except for those for $P_{rv,max}$. Modelled LVEDV, RVEDV, and $P_{lv,max}$ all had a small bias (-1.1 ml, 1.0 ml, and -0.6 mmHg). However, a larger bias of 6 mmHg was seen for $P_{rv,max}$. Two standard deviations of the modelled LVEDV and RVEDV fell with 6ml of the measured values. Whereas, two standard deviations of $P_{lv,max}$ and $P_{rv,max}$ fell within a larger range of 18.5 mmHg and 23.4 mmHg, respectively. Figure 5.1 and Figure 5.2 show the regression and Bland-Altman plots for LVEDV and RVEDV.

Table 5.5: Mean, bias and precision metrics, median absolute percentage errors with 5th and 95th percentile bounds, and correlation coefficients of the measurements used for validation of the model identification process in the pulmonary embolism pig study.

	Mean	Bias +/- 2SD	% Error (5^{th} - 95^{th} percentile)	R^2
LVEDV	79.6 ml	-1.1 +/- 5.4 ml	1.6% (0.1% - 8.6%)	0.96
RVEDV	71.8 ml	1.0 +/- 5.7 ml	1.7% (0.1% - 10.4%)	0.89
$P_{lv,max}$	127.7 mmHg	-0.6 +/- 18.5 mmHg	3.6% (0.3% - 14.6%)	0.86
$P_{rv,max}$	47.4 mmHg	6.6 +/- 23.4 mmHg	16.0% (2.4% - 54.1%)	0.84

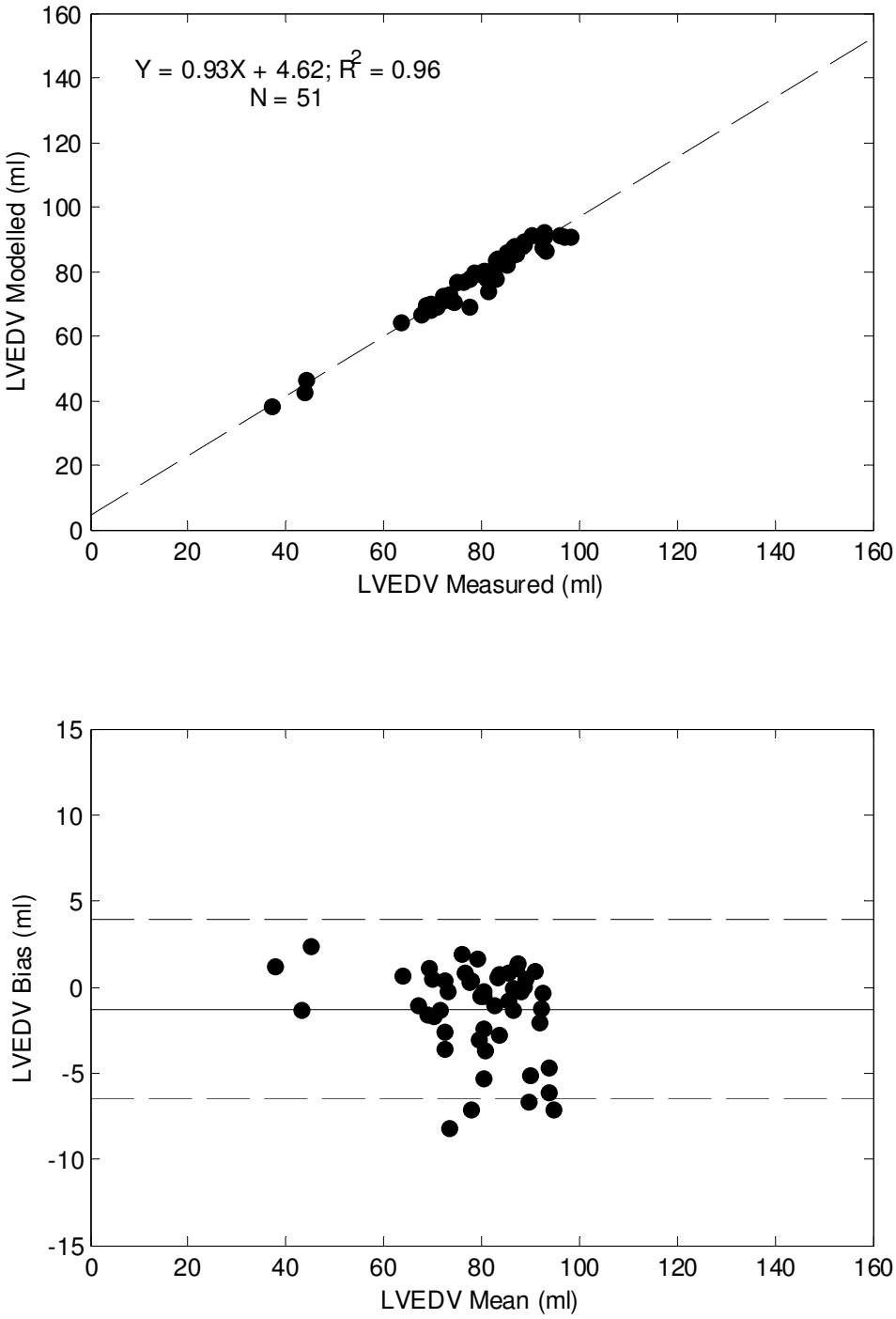

Figure 5.1: Regression (top) and Bland-Altman analysis showing 2 standard deviation limits (bottom) of the modelled and measured left ventricular end diastolic volume (LVEDV) in the pulmonary embolism study.

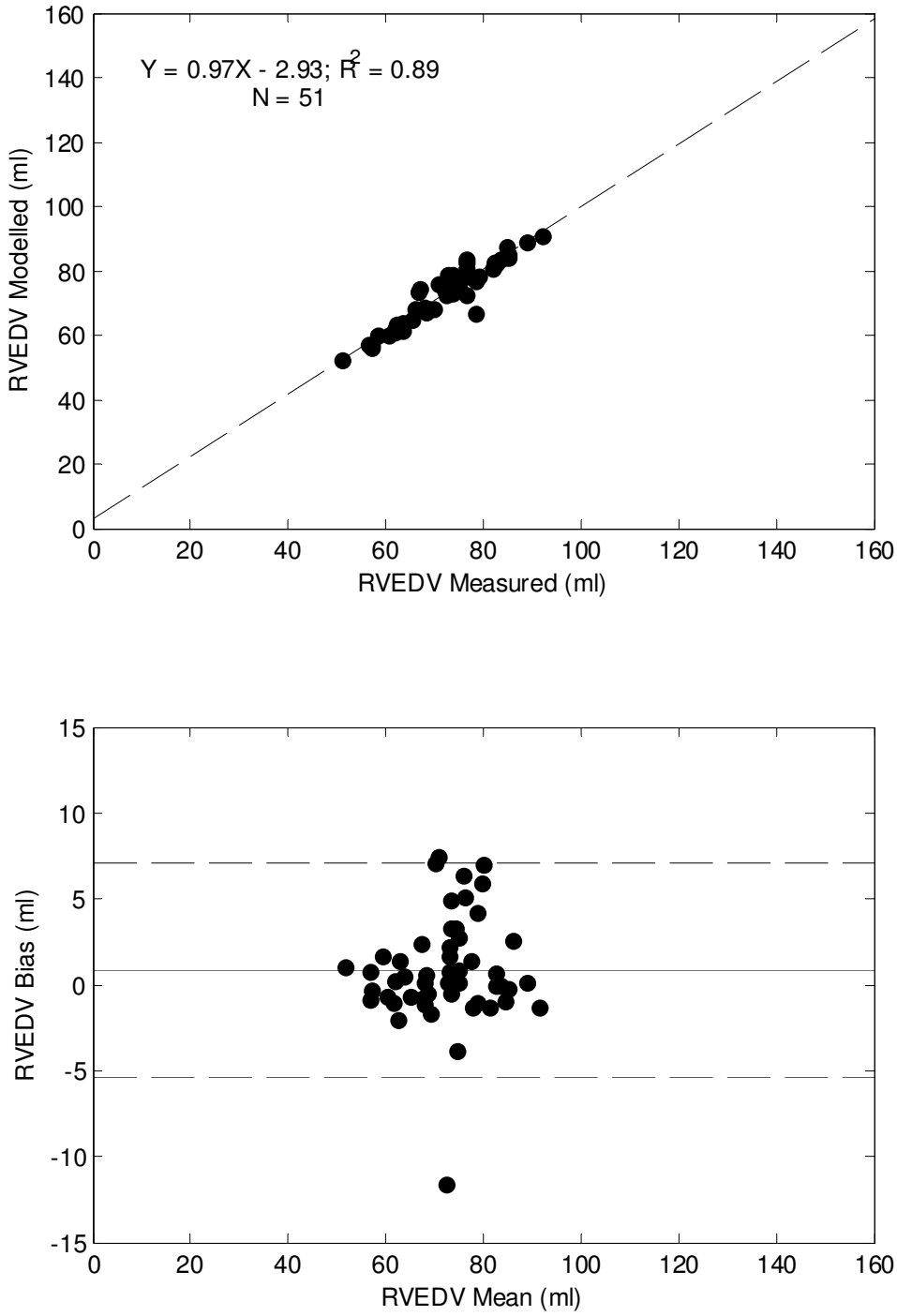

Figure 5.2: Regression (top) and Bland-Altman analysis showing 2 standard deviation limits (bottom) of the modelled and measured right ventricular end diastolic volume (RVEDV) in the pulmonary embolism study.

5.3.4.2 Septic shock

In the septic shock study all four modelled outputs (LVEDV, REVDV, $P_{lv,max}$, $P_{rv,max}$) correlated well with the measured data ($R^2 \geq 0.78$), as seen in Table 5.6. Modelled left ventricular outputs (LVEDV, $P_{lv,max}$) had a small negative bias (-5.4 ml, and -1.4 mmHg) whereas right ventricular outputs (RVEDV, $P_{rv,max}$) tended to slightly overestimate (4.9 ml, and 0.5 mmHg) the true measurement. The precision (2 standard deviations) of the LVEDV and RVEDV predictions were 13.9ml and 14.1ml, and 10.6 mmHg and 10.1 mmHg for $P_{lv,max}$ and $P_{rv,max}$. All percentage errors were within an acceptable range (<20%), except for the 95th percentile error in the modelled maximum right ventricular pressure. Figure 5.3 and Figure 5.4 show regression and Bland-Altman plots for LVEDV and RVEDV.

Table 5.6: Mean, bias and precision metrics, median absolute percentage errors with 5th and 95th percentile bounds, and correlation coefficients of the measurements used for validation of the model identification process in the septic shock pig study.

	Mean	**Bias +/- 2SD**	**% Error (5th - 95th percentile)**	**R^2**
LVEDV	93.7 ml	-5.4 +/- 13.9 ml	7.5% (0.5% - 13.8%)	0.94
RVEDV	84.4 ml	4.9 +/- 14.1 ml	7.4% (0.5% - 18.1%)	0.91
$P_{lv,max}$	87.8 mmHg	-1.4 +/- 10.6 mmHg	4.5% (0.3% - 15.2%)	0.93
$P_{rv,max}$	39.7 mmHg	0.5 +/- 10.1 mmHg	6.2% (0.6% - 26.6%)	0.78

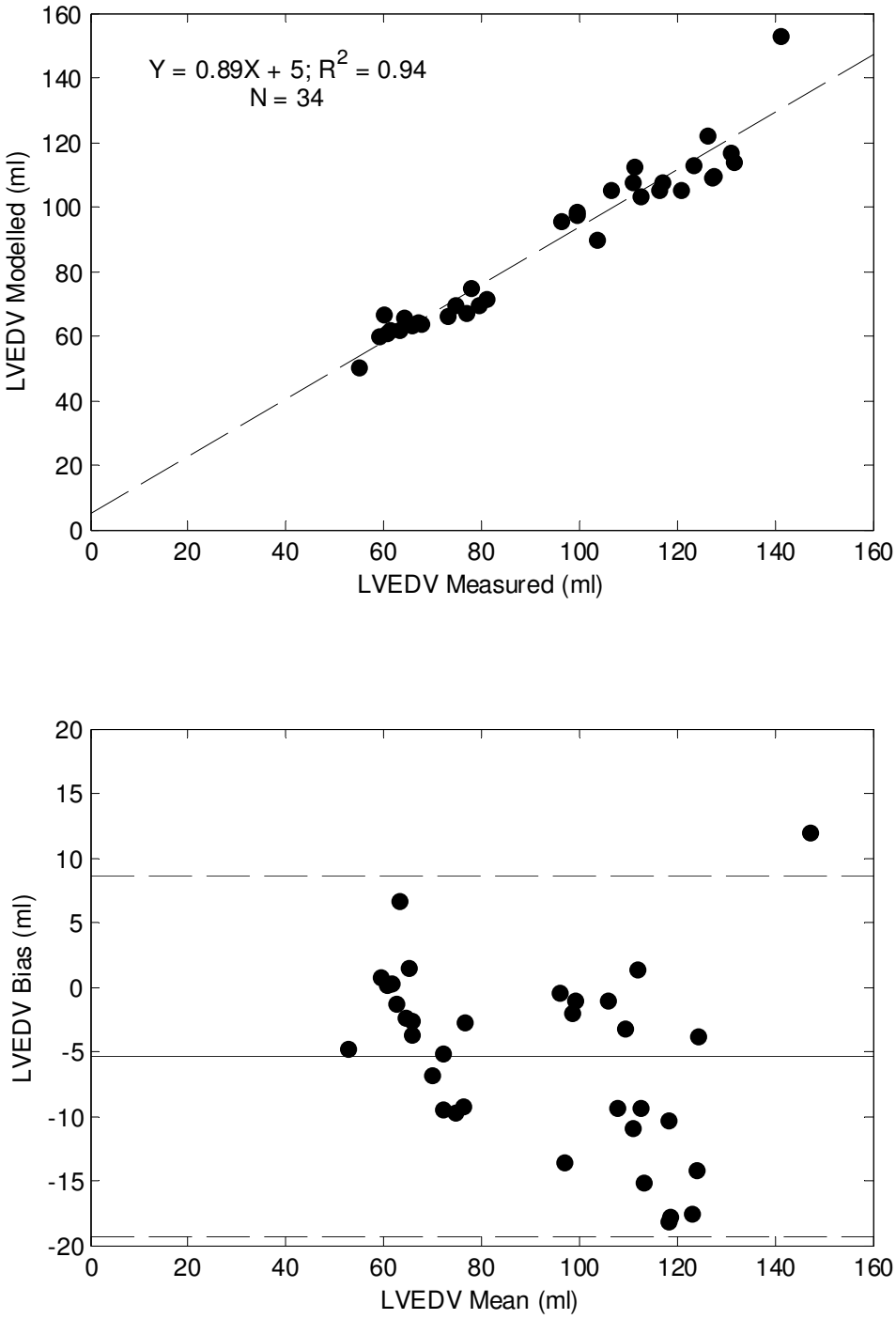

Figure 5.3: Regression (top) and Bland-Altman analysis showing 2 standard deviation limits (bottom) of the modelled and measured left ventricular end diastolic volume (LVEDV) in the septic shock study.

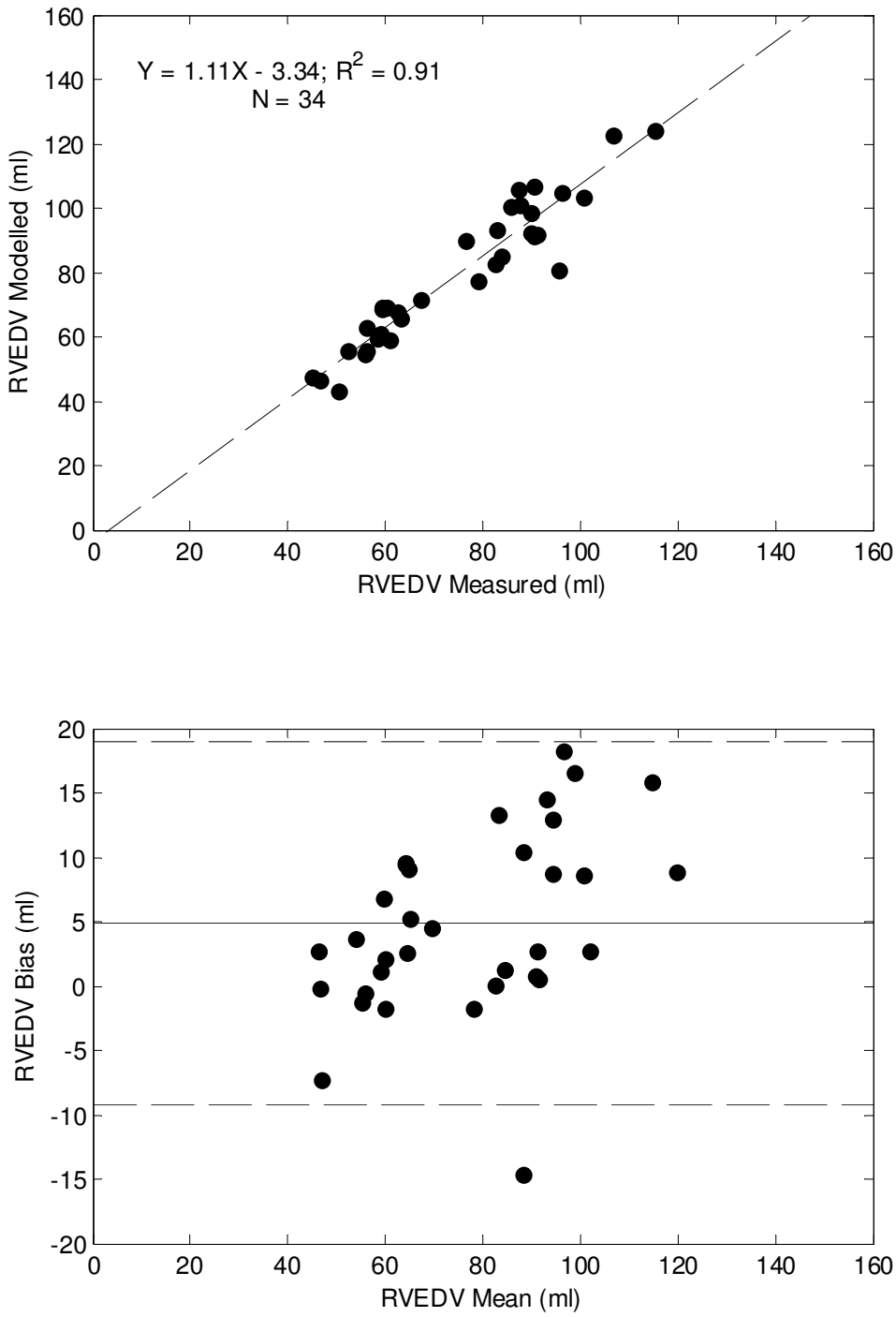

Figure 5.4: Regression (top) and Bland-Altman analysis showing 2 standard deviation limits (bottom) of the modelled and measured right ventricular end diastolic volume (RVEDV) in the septic shock study.

5.4 DISCUSSION

5.4.1 CONVERGENCE

All the controlled outputs of the systemic and pulmonary sub-models converged towards their measured values during the identification process. However, in a few cases (three systemic and four pulmonary sub-models) some of the outputs did not converge to within the desired tolerance. These cases occurred because: 1) the parameter being identified had reached its upper or lower limit, causing the output to stop converging closer to its target value; or 2) the simulation of the CVS model was not run for enough time to reach steady state for the given parameter set, which is required for correct parameter identification.

Scenario 1) was mostly a problem when identifying R_{av} and R_{pv} using the measurements of maximum dP_{ao}/dt and maximum dP_{pa}/dt. R_{av} and R_{pv} are highly interdependent on $E_{es,lvf}$ and $E_{es,rvf}$ being accurate. However, at first, when identifying the simplified sub-models only initial estimates for $E_{es,lvf}$ and $E_{es,lvf}$ are used. Thus, in some cases large errors in $E_{es,lvf}$ and $E_{es,rvf}$, used to initially identify the sub-models, can cause R_{av} and R_{pv} to converge to unphysiological values that are below the allowable limits set in the identification method (see Table 4.4, Section 4.7). In such cases the identification method tries to reduce R_{av} and R_{pv} so the model matches the measured maximum aortic and pulmonary artery pressure gradients. However, the imposed lower limits for R_{av} and R_{pv} in the identification method stop the maximum dP_{ao}/dt and dP_{pa}/dt outputs reaching their measured value. Thus, these outputs do not converge to within the set tolerance during parameter identification. However, this is generally not a problem when identifying the six-chamber model because $E_{es,lvf}$ and $E_{es,rvf}$ are identified.

Scenario 2) occurs when the initial estimates of the model outputs, as shown in Table 4.2 and Table 4.3, in Sections 4.5.1 and 4.5.2 (different to the initial parameter estimates for the parameter identification method), are vastly different to the steady state model outputs. During simulation of the CVS model, the poor initial conditions cause there to be a long transient period before steady state conditions are reached. However, in the parameter identification method a maximum time limit is set to limit the amount of computational time spent on any one simulation of CVS model. Thus, sometimes, the maximum time limit of the simulation is reached before steady state conditions in the simulation are achieved. In such cases, the model outputs taken from the simulation do not reflect steady state conditions which are required for identifying subject-specific models. Therefore, the parameters identified for the systemic and pulmonary sub-models may not reflect steady state, and when used to simulate six-chamber model may cause errors in the model outputs. To reduce this problem, when simulating the CVS models, it is checked if the models have

reached steady state over the set time span in the ODE solver. If the models have not reached the steady state, the models are re-simulated using the end conditions of the previous simulation as the initial conditions for the new simulation, to allow more time for steady-state solution to be reached.

For 93% of the 51 identified model cases in the PE analysis all of the parameters converged to their set points within the desired tolerance. In the 7% of models that did not converge most of the model outputs had converged to set points and the model outputs that had not fully converged were still close to their measured value with errors < 10% most of the time. These results are acceptable and still good for this type of physiological monitoring (Clancy et al., 1991, Critchley and Critchley, 1999, Salandin et al., 1988). Hence, these identified models could still be used to base therapy decisions from.

5.4.2 PARAMETER SENSITIVITY

The most sensitive parameters to changes in the measured inputs were the valve resistance (R_{mt}, R_{av}, R_{tc}, and R_{pv}) and the venous elastances (E_{vc} and E_{pu}). R_{mt} was highly sensitive to the mitral valve closure times (t_{mt}). A change in the mitral valve closure time can significantly change P_{pu}. Identified R_{mt} is a function of pressure difference between the P_{pu} and the diastolic left ventricular pressure during filling of the left heart. Hence, a change in the mitral valve closure time causes a large change in P_{pu} which consequentially causes a large change in R_{mt}. The same logic holds true for the sensitivity of R_{tc} in relation to t_{tc}.

R_{av} was very sensitive to changes in the measured maximum dP_{ao}/dt, PP_{ao}, SV, and GEDV. Once inertial effects are ignored, R_{av} is defined by a rearranged version of Equation (3.31):

$$R_{av} = \frac{P_{lv}(t) - P_{ao}(t)}{Q_{av}(t)} \qquad \textbf{(5.1)}$$

The difference between P_{lv} and P_{ao} is only small during left ventricular ejection, resulting in the numerator of Equation (5.1) being substantially smaller than the magnitude of Q_{av}. Hence, small changes in the features of the aortic pressure waveform (maximum dP_{ao}/dt and PP_{ao}) can cause relatively large changes in this numerator and consequentially cause large changes in R_{av}. Q_{av} and P_{ao} are both products of SV, and SV is a function of P_{lv} in the model. Hence, R_{av} is also highly sensitive to SV. Finally, P_{lv} is defined by $E_{es,lvf}$ (Equation (3.38)), which is identified using GEDV in the parameter identification method. As mentioned earlier R_{av} is interdependent with $E_{es,lvf}$ and small changes in

$E_{es,lvf}$ can cause large changes in R_{av}. Thus, R_{av} is also highly sensitive to changes in GEDV. The same principles can be used to explain why identified R_{pv} is sensitive to dP_{pa}/dt, PP_{pa}, SV, and GEDV.

Lastly, E_{vc} and E_{pu} are very sensitive to changes in t_{mt} and t_{tc}. This result occurs because E_{vc} and E_{pu} are fitted using P_{vc} and P_{pu}, which are identified from the systemic and pulmonary sub-models. Small changes in t_{mt} and t_{tc} can cause large changes in the identified P_{pu} and P_{vc} in the sub-models. Hence, E_{vc} and E_{pu} vary a lot when t_{mt} and t_{tc} are changed in the parameter identification method.

To minimise the variance in the identified parameters due to perturbations in the measurements, the highly sensitive parameters can be averaged over several identified models. By averaging the parameters, over several identifications in a given period, the negative flow-on effects of measurement noise, or other irregularities due to sensor issues, on these highly sensitive parameters would be reduced. Thus, this approach would produce more physiologically accurate subject-specific models of the CVS. For example, averaging valve resistances, as done in Chapters 6, 7, and 8 and in (Revie et al., 2011b), and averaging E_{vc} and E_{pu} over several identified models can be done using the approach.

5.4.3 INTER-BEAT REPEATABILITY

The ability of the identification method to repeatedly identify subject-specific CVS models from sets of data from adjacent heartbeats, was also analysed. This analysis represents a more realistic sensitivity analysis than the previous section as: 1) there are slight changes in all the measurements between heartbeats, not just a change in one measurement as there was in Section 5.4.2; and 2) these changes represent realistic inter-beat variability in the measurements and hemodynamics, rather than an arbitrary potentially unrealistic change of +/- 10% used in Section 5.4.2. Moreover, the measurements used to identify the subject-specific CVS models were taken in steady state. Therefore, it can be assumed that there is very little beat-to-beat change in hemodynamics and that most of the inter-beat variability in the measurements is thus due to measurement noise. Hence, this analysis also shows how repeatable the model identification method in response to measurement noise.

The results of this repeatability analysis were similar to the previous parameter sensitivity analysis. The identified heart valve resistances (R_{mt}, R_{av}, R_{tc}, R_{pv}) and the elastance of the venous chambers (E_{vc}, E_{pu}) were the most variable parameters between heartbeats. Inter-beat variability is in the identified model parameters was noticeably smaller for Pig 1 in a healthy state, whereas larger

errors were seen at T150 after pulmonary embolism was induced. The largest change of 105% was seen for the identified R_{mt} between beat 1 and beat 3 for Pig 1 at T150.

To eliminate the effects of measurement noise, the subject-specific CVS models could be identified from a set of averaged measurements. The measurements used as the convergence criteria in the identification method could be averaged over several heartbeats to reduce the effects of measurement noise, increasing the repeatability of the model identification process between heartbeats. This recommendation is implemented in Chapter 8, where the measurements used to identify patient-specific CVS models were averaged over two breathing cycles (approximately 6-12 heartbeats).

5.4.4 VALIDATION AGAINST INDEPENDENT METRICS

Modelled cardiac metrics of LVEDV, RVEDV, $P_{lv,max}$, and $P_{rv,max}$, for both PE and SS, correlated well against their measured values, with all but $P_{rv,max}$ of 0.78 with R^2 value greater than 0.9. LVEDV and RVEDV were modelled accurately in both studies with averaged absolute percentage errors less than 8%. $P_{lv,max}$ was also modelled accurately in both studies with median absolute percentage errors less than 6.5%. Modelled $P_{rv,max}$ was the least accurate metric, especially in PE, with median absolute percentage errors of 16%, although there was only an average error of 6.2% in the SS study. In the PE study, LVEDV and RVEDV were identified more accurately. However, the maximum pressures were more accurate in the SS study. These results indicate that there appears to be a trade off in the accuracy of the maximum ventricular volumes (LVEDV, RVEDV) and the maximum ventricular pressures ($P_{lv,max}$, $P_{rv,max}$) in the identified models. Most errors were less than 10% and the majority were less than 20% which is acceptable for this type of physiological monitoring (Clancy et al., 1991, Critchley and Critchley, 1999, Salandin et al., 1988).

A primary cause of some of the larger errors and difference in polarity of the modelled bias between the left and right ventricle measurements, as seen in Table 5.5 and Table 5.6, is due to the difficulties in measuring and calculating the right ventricular volume experimentally with a conductance catheter. Due to the right ventricle's complex shape the volume measurements were underestimated in most of the pigs, where the left ventricular SV was greater than two times the right ventricular SV, which is not physiologically accurate for steady state hemodynamics.

The SV of both ventricles in the CVS model is assumed to be equal, so an average of the measured left and right ventricular stoke volumes was used in the identification process. Therefore, once converged, the identified models generally underestimated the measured left ventricular stroke

volume and overestimated the measured right ventricular stroke volume. This issue caused the LVEDV and, consequentially, the left ventricular pressure in the model to be underestimated relative to the measurements taken in the experiment, with the opposite occurring in the right ventricle. However, more importantly, these errors were generally systematic so the trends associated with these measurements are still clearly identified and accurate, as indicated by the good correlations seen in Table 5.5 and Table 5.6.

5.5 SUMMARY

In 93% of cases the outputs of the identified models converged to their set-points. In the remaining cases the models still converged towards their set points but did not reach them due to parameter limits in the parameter identification method or because the CVS models were not simulated over a long enough time span to reach steady state. The heart valve resistances and venous elastances were found to be the most sensitive parameters to changes in the model identification set points. However, these parameters could be averaged over several identified CVS models and averaged measurements could be used to fit the subject specific models to reduce the sensitivity of these parameters and improve the repeatability of the identification method. Finally, the subject-specific models could generally predict cardiac volume and pressure measurements to percentage errors less than 20%, which is acceptable for this type physiological monitoring.

CHAPTER 6: MODEL-BASED MONITORING OF PULMONARY EMBOLISM

The subject-specific models have been shown to robustly and accurately represent cardiovascular dynamics. Now, the ability of these models to monitor and track the cardiac and circulatory response to common cardiovascular diseases is tested. In this chapter, the clinical potential of the approach to monitor hemodynamic changes due to acute pulmonary embolism in porcine trials is examined (Revie et al., 2011a).

6.1 INTRODUCTION

Pulmonary embolism (PE) is an acute, life threatening disease thought to be responsible for around 15% of all sudden deaths (Kasper and Harrison, 2005). In one study, untreated mortality was found to be 26% (Barritt and Jordan, 1960). Other studies have shown that pulmonary embolism is responsible for, or contributes to, around 15% of in-hospital deaths (Smulders, 2000, Dalen and Alpert, 1975, Morrell and Dunnill, 1968, Uhland and Goldberg, 1964). In particular, the dysfunction is a major problem in intensive care due to factors such as: the insertion of catheters, admission of post cardiac surgery patients, prolonged bed rest, and compromised anticoagulant state of the typical ICU patient (Cook et al., 2005, Heit et al., 2000, Anderson and Spencer, 2003) . Further exacerbating the problem is the fact that PE often goes unrecognised, with studies showing that only around one third of all patients that died from this dysfunction were correctly diagnosed before death (Goldhaber et al., 1982, Stein and Henry, 1995).

Due to the fast acting and deadly nature of PE it is important to diagnose and treat as soon as possible. Mortality increases if diagnosis is delayed and/or if correct treatment is not administered in a timely fashion. When pulmonary embolism is diagnosed and treated correctly, mortality rates drop from around 30%, in untreated patients, to 2.5% (Carson et al., 1992, Smulders, 2000). Hence, real time monitoring is required to ensure symptoms of pulmonary embolism are identified before irreversible damage is done.

This chapter analyses the monitoring ability of subject-specific CVS models to track the onset and evaluation of pulmonary embolism. The parameter identification method, outlined in Chapter 4, was retrospectively tested using measurements from a porcine study on pulmonary embolism (Ghuysen et al., 2008). In this animal study, a wide range of hemodynamic measurements were recorded and

autologous blood clots were used to induce PE. Subject-specific CVS models were identified from clinically available data derived from the porcine measurements. The performance of the model identification method in PE was assessed against independent measurements not used for identification (Chapter 5), experimentally derived metrics (Ghuysen et al., 2008), and clinically expected trends from the literature (Elliott, 1992, Wauthy et al., 2004). Hence, the overall goal of this work was to demonstrate the clinical relevance and prove the concept (and potential) of computer-based clinical monitoring of CVS status for the acute CVS dysfunction.

6.1.1 PATHO-PHYSIOLOGY AND TREATMENT OF PULMONARY EMBOLISM

Pulmonary embolism is the blockage of the pulmonary artery or one of its distal branches due to an embolism. Emboli are generally blood clots (thrombus) originating from the deep veins of the legs and pelvis. The thrombi break off from the walls of the deep veins, travel through the right heart, and get stuck in the pulmonary circulation. The main cause of pulmonary embolism is deep vein thrombosis (DVT). Other causes of pulmonary embolism include air bubbles, fat deposits, talc, or amniotic fluid. The severity of pulmonary embolism depends on the size of these emboli, as well as, coexistent cardiopulmonary disease, and the magnitude of counterproductive neural and humoral reflex responses (Goldhaber, 2002).

Pulmonary embolism symptoms result from the obstruction to blood flow in the lungs which causes pressure to build up in the right ventricle (Wauthy et al., 2004). Clinical signs of PE include low blood oxygen saturation, rapid breathing, and a rapid heart rate. Diagnosis is based off these findings, which may lead to a D-dimer test and/or chest CT scan for confirmation (Goldhaber and Elliott, 2003a). Treatment generally consists of anticoagulant medication, and, in severe cases, thrombolysis or surgical intervention (pulmonary thrombectomy) (Goldhaber and Elliott, 2003b).

From a hemodynamic perspective, the obstruction in the pulmonary vasculature initiates the release of vasoactive agents, such as serotonin and platelets, which increase pulmonary arterial tone (Goldhaber and Elliott, 2003a). As a result, pulmonary vascular resistance increases due to the mechanical obstruction of the emboli and pulmonary vasoconstriction (Goldhaber and Elliott, 2003a). Systemic vascular resistance also increases as a reflex response (Klabunde, 2004) to maintain mean arterial pressure and preload on the left ventricle. Alveolar dead space increases in the lungs due to under-perfused alveoli capillaries. Bronchoconstriction reflexes cause elevated airway resistance and pulmonary edema decreases pulmonary compliance. The combinations of these factors result in increased right ventricular afterload and subsequent dilation of the right ventricle

with excess volume (Goldhaber, 1998). Follow on effects include: decreased venous return, a subsequent drop in left ventricle preload, and ischemia due to compromised cardiovascular and pulmonary function (Goldhaber and Elliott, 2003a).

This hemodynamic profile summarises the causes and effects of pulmonary embolism:

- Thrombotic
    - Clots form in deep veins and embolise to pulmonary arteries (Goldhaber, 1998)
- Obstructive
    - Mechanical obstruction of blood flow to the lungs from blood clots (Goldhaber, 1998)
    - Pulmonary vascular vasoconstriction (reflex response) due to release of vasoactive agents (Goldhaber and Elliott, 2003a)
    - Increased pulmonary vascular resistance (reflex response and physical obstruction) (Goldhaber and Elliott, 2003a)
    - Initial increase in systemic vascular resistance increases (reflex response) to maintain MAP and left ventricle preload (Klabunde, 2004)
- Distributive
    - Right ventricle dilation (Goldhaber and Elliott, 2003a, Gan et al., 2006, Lualdi and Goldhaber, 1995)
    - Decreased left ventricle filling due to reduced return from pulmonary circulation (Goldhaber and Elliott, 2003a)
    - Decreased left ventricle preload (Goldhaber and Elliott, 2003a, Gan et al., 2006, Lualdi and Goldhaber, 1995)
- Cardiogenic
    - Initial increase in contractility (reflex response) to maintain CO (Burkhoff and Tyberg, 1993, Klabunde, 2004)
    - Eventual decrease in contractility due to decreased oxygen supply to heart (Goldhaber and Elliott, 2003a)
    - Leftward shift in intra-ventricular septum due to right ventricule dilation and decreased left ventricle preload (Goldhaber and Elliott, 2003a, Gan et al., 2006, Lualdi and Goldhaber, 1995)
- Chronotropic
    - Increased heart rate (reflex response) to increase CO and maintain tissue perfusion (Goldhaber and Morrison, 2002)

6.2 METHODS

6.2.1 PORCINE EXPERIMENTS AND DATA

All procedures and protocols used in the porcine experiments were reviewed and approved by the Ethics Committee of the Medical Faculty at the University of Liege (Belgium). Six pure Pietrain pigs were pre-medicated and anesthetised as explained in (Ghuysen et al., 2008). 10 ml/kg volume-cycle ventilation was provided after endotracheal intubation through a cervical tracheostomy at a respiratory rate of 20 breaths per minute. Inspired oxygen fraction was set to 40% and the respiratory settings were adjusted to maintain CO_2 between 30 and 35 mmHg. Access to the cardiac chambers and pulmonary truck was achieved via median sternotomy. A micromanometer-tipped catheter was inserted into the pulmonary artery through an incision in the right ventricle outflow track and was adjusted to be 2cm downstream from the pulmonary valve. Another micromanometer-tipped catheter was descended into the thoracic aorta through the femoral artery. Furthermore, 7F, 12 electrode conductance micromanometer-tipped catheters were positioned in the left and right ventricle so that all electrodes were within these cavities.

To simulate PE three autologous blood clots of decreasing size (0.25, 0.125, and 0.0625 g kg^{-1}) were inserted into the external jugular vein at 0, 120 and 240 minutes into the trials. From the catheters, continuous waveforms over 6 to 12 heartbeats were obtained every 30 minutes (T0 to T270) of left and right ventricular pressures and volumes (P_{lv}, P_{rv}, V_{lv}, V_{rv}), aortic pressure (P_{ao}), and pulmonary artery pressure (P_{pa}). This research uses 51 sets of data from five of the pigs (Pig 1, Pig 2, Pig 3, Pig 4, and Pig 5) from the study (Ghuysen et al., 2008). Measurements from the sixth pig were omitted as it died very early in the trial and only a partial set of measurements were available for Pig 2 as it died at T180.

6.2.2 MODEL IDENTIFICATION

The model identification method outlined in Chapter 4 was used to identify the subject-specific models of pulmonary embolism. In this study GEDV was assumed to be equal to the sum of the maximum left and right ventricular volumes (GEDV = max(Vlv) + max(Vrv) = LVEDV + RVEDV). The mitral and tricuspid valve closure times were estimated from the approximated left and right ventricular functions ($e_{lv}(t)$ and $e_{rv}(t)$) from (Stevenson et al., 2012a, Stevenson et al., 2012b) as central venous pressure and ECG were not measured in this study.

6.2.3 DATA AND STATISTICAL ANALYSIS

Data is presented as mean +/- standard deviation (SD) unless stated otherwise. A paired-sample t-test was used to check temporal variance over T0 – T60, T120 – T150, and T240 - T265 to analyse the effect of the injected emboli. A value of $p < 0.05$ was considered a statistically significant result. Percentage errors, and bias and precision metrics were used to compare the relationship of the modelled to experimentally derived metrics. A percentage error less than 20% was regarded as an acceptable result as measurement of physiological variables often lack similar precision, with errors of +/- 10-20% not uncommon (Clancy et al., 1991, Critchley and Critchley, 1999, Salandin et al., 1988).

6.3 RESULTS

Data sets were recorded every 30 minutes, and once 5 minutes before the end of the experiments (T0, T30, T60,... , T240, T265, T270) in each of the four and half hour long trials. From each of the data sets, subject-specific models were retrospectively fitted for each of the pigs. Hence, a total 51 subject-specific CVS models were identified and analysed.

In this study each animal acts as its own control with baseline measurements taken at T0 reflecting the undiseased state of the pig, prior to the injection of the autologous blood clots. Statistically significant changes ($p<0.05$) were seen in the measured systolic and diastolic aortic and pulmonary artery pressures, and left and right ventricular end diastolic volume over T0-T60, showing the deviation from baseline circulatory dynamics due to the insertion of the initial blood clot after T0. Further changes were also noted after insertion of later blood clots at T120 and T1240. A summary of these main hemodynamic measurements is seen in Figure 6.1.

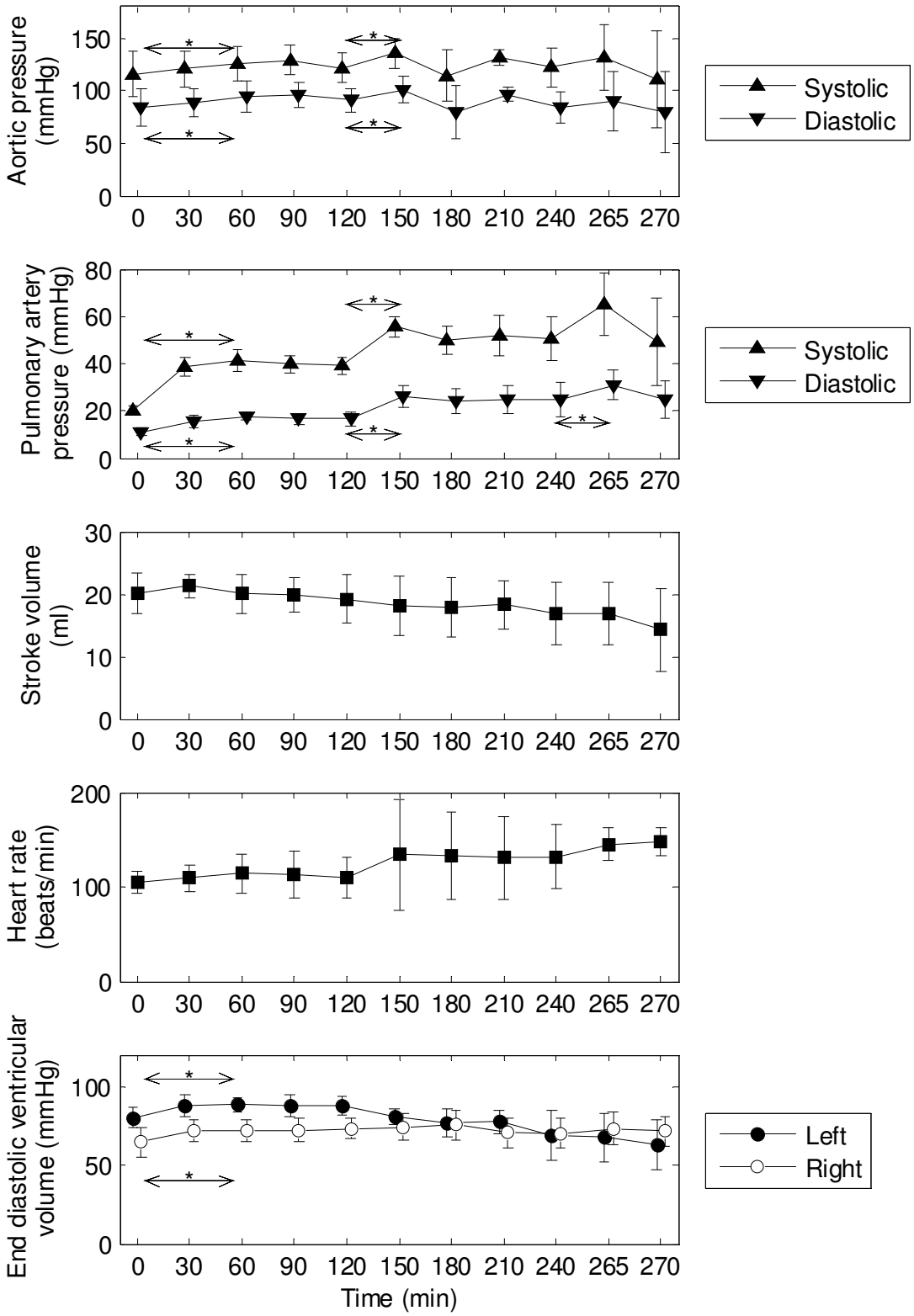

Figure 6.1: Evolution of the averaged hemodynamic measurements recorded during the trials. * indicates P<0.05 for indicating a significant temporal change over T0-T60, T120-T150, or T240-T265 after the insertion of emboli. The data is presented as mean +/- SD.

6.3.1 COMPARISON TO EXPERIMENTALLY DERIVED METRICS

For further validation, on top of the validations shown in Chapter 5, the identified pulmonary afterload, right ventricular end systolic elastance, and right ventricular vascular coupling (RVVC) from the model were compared to corresponding metrics (E_a, E_{es}, E_{es}/E_a) derived experimentally using pressure-volume loop analysis from the same measurements (Ghuysen et al., 2008). The afterload on the right ventricle in the model is the pulmonary vascular resistance divided by the period of one heartbeat ($E_{a,model} = R_{pvl}/T$).

Bias, precision, and correlation indices for pulmonary afterload and coupling are shown in Table 6.1 and the temporal trends for these indices are shown in Figure 6.2, Figure 6.3, and Figure 6.4. The model matched pulmonary afterload closely with a bias and precision (2 SD) of -0.06 +/- 0.68 mmHg/ml and correlation of R^2 = 0.86. The model parameter $E_{es,rvf}$ is directly comparable to experimentally derived right ventricular end systolic elastance and was found to have bias of and precision of -0.87+/-1.00 mmHg/ml (R^2=0.51). Furthermore, a bias and spread of -0.73 +/- 0.83 was observed for the RVVC with correlation of R^2 = 0.83 as seen in Figure 6.4.

Table 6.1: Bias, precision, and correlation metrics comparing the modelled to experimentally derived indices of afterload, contractility, and right ventricular vascular coupling (RVVC).

Metric	Bias	Precision (2SD)	R^2
Afterload (E_a)	-0.06 mmHg/ml	0.68 mmHg/ml	0.86
Contractility (E_{es})	-0.87 mmHg/ml	1.00 mmHg/ml	0.51
RVVC (E_{es}/E_a)	-0.73	0.83	0.83

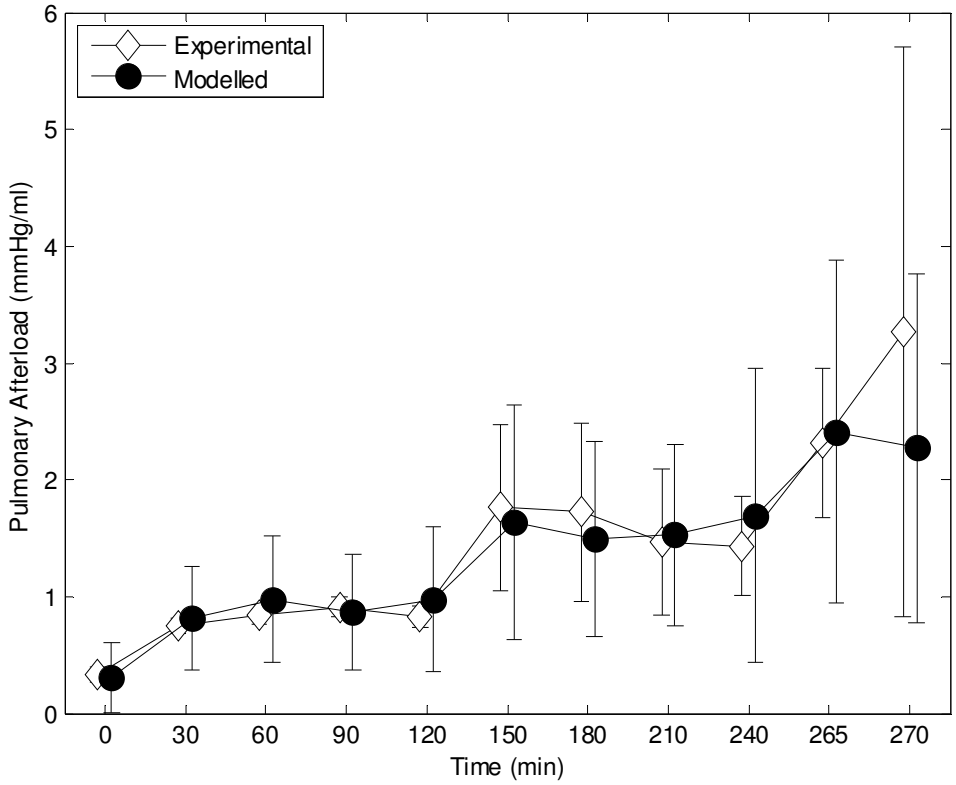

Figure 6.2: Comparison of the experimentally derived (Ghuysen et al., 2008) and modelled pulmonary afterload. The data is presented as mean +/- SD.

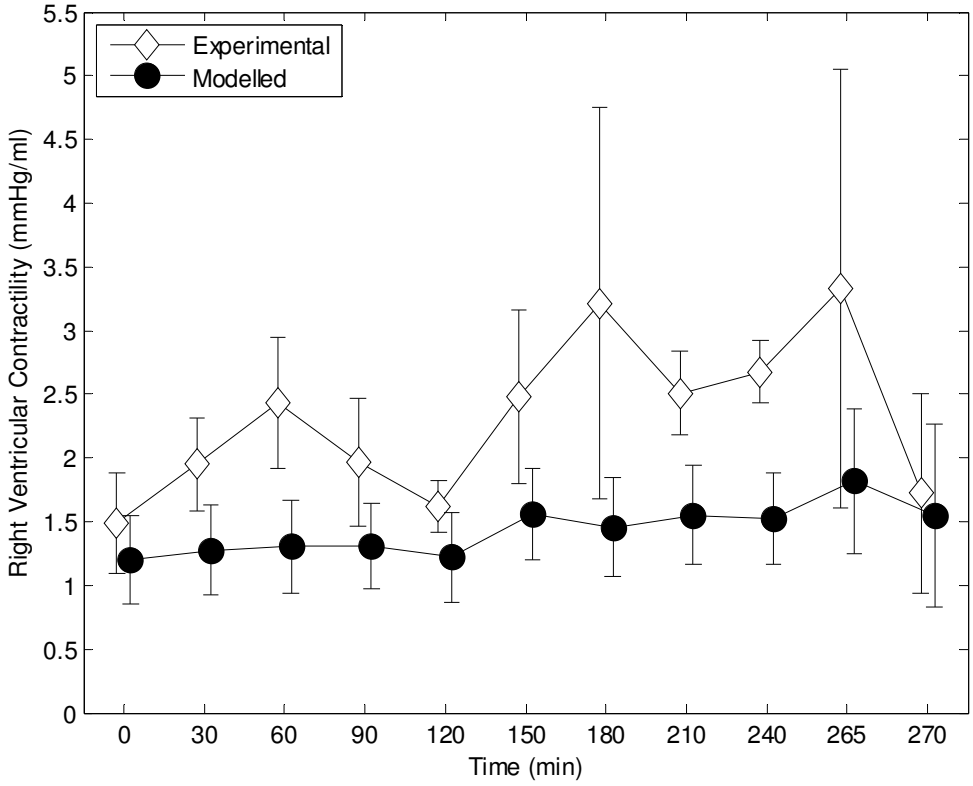

Figure 6.3: Comparison of the experimentally derived (Ghuysen et al., 2008) and modelled right ventricular end systolic elastance ($E_{es,rvf}$). The data is presented as mean +/- SD.

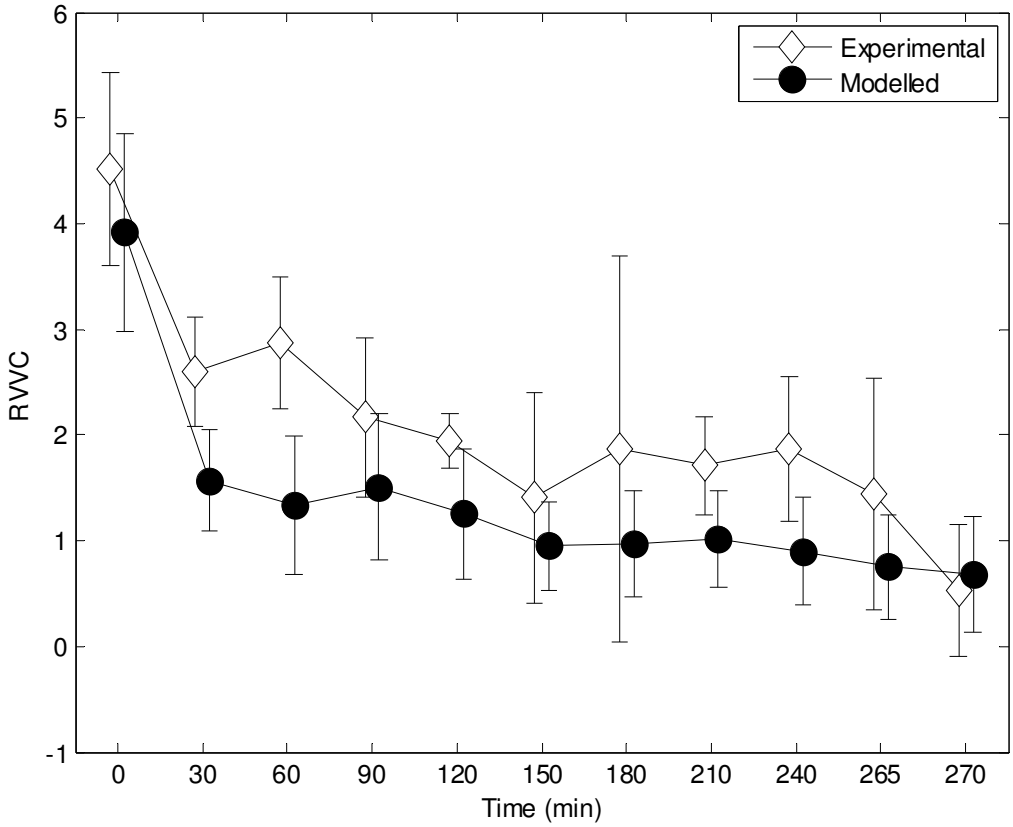

Figure 6.4: Comparison of the experimentally derived (Ghuysen et al., 2008) and modelled right ventricular-vascular coupling (RVVC or E_{es}/E_a). The data is presented as mean +/- SD.

6.3.2 PULMONARY EMBOLISM TRENDS

6.3.2.1 Afterload

The model parameters for systemic and pulmonary vascular resistance (R_{sys}, R_{pul}) represent the main components of afterload on the left and right ventricles, respectively. The averaged time varying trends for these parameters are shown in Figure 6.5. Average R_{sys} stays relatively constant throughout the study, ranging between 2.5 and 3 mmHg.s/ml, except for a drop at T180, which is largely influenced by the near death state of Pig 2. In contrast, the averaged R_{pul} value steadily increases to 243% above the baseline value by the end of the study, with noticeable increases seen after T0, T120, and T240 when the autologous blood clots were introduced to the circulation. These results match clinically expected trends (Goldhaber and Elliott, 2003a).

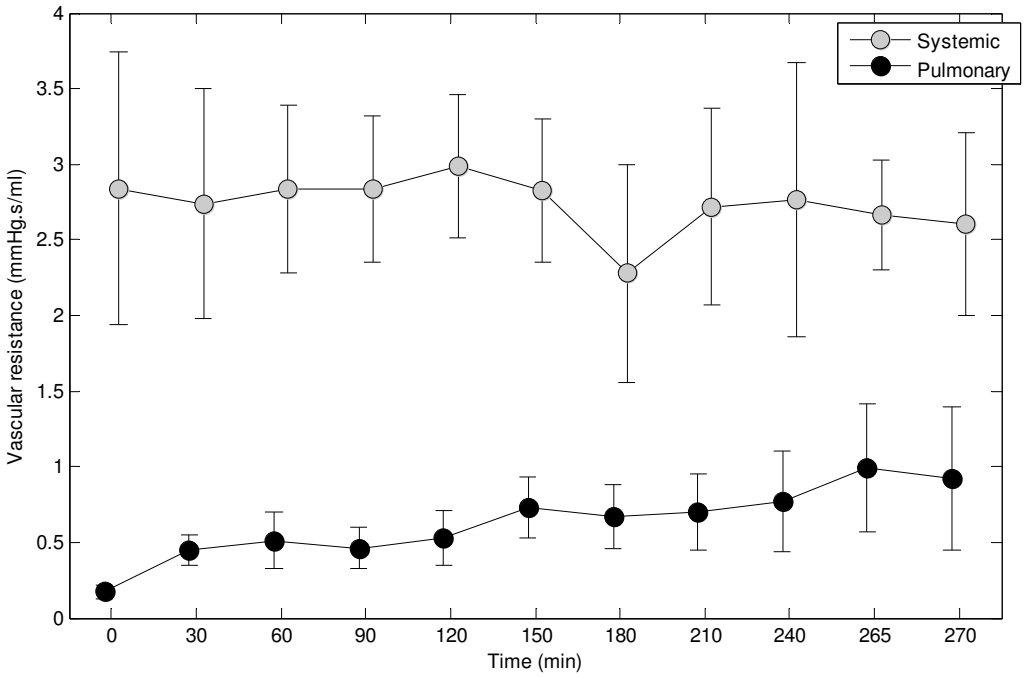

Figure 6.5: Modelled left and right ventricular afterload. The data is presented as mean +/- SD.

6.3.2.2 Preload

Ventricular preload in the model is represented by ventricular end diastolic volume (LVEDV, RVEDV). Averaged LVEDV and RVEDV over all the pigs are seen in Figure 6.6. The averaged RVEDV increases slightly above baseline throughout the study indicating right ventricular distension. On the other hand, LVEDV decreases dramatically most likely due to a decrease in venous return (Gan et al., 2006, Goldhaber and Elliott, 2003a).

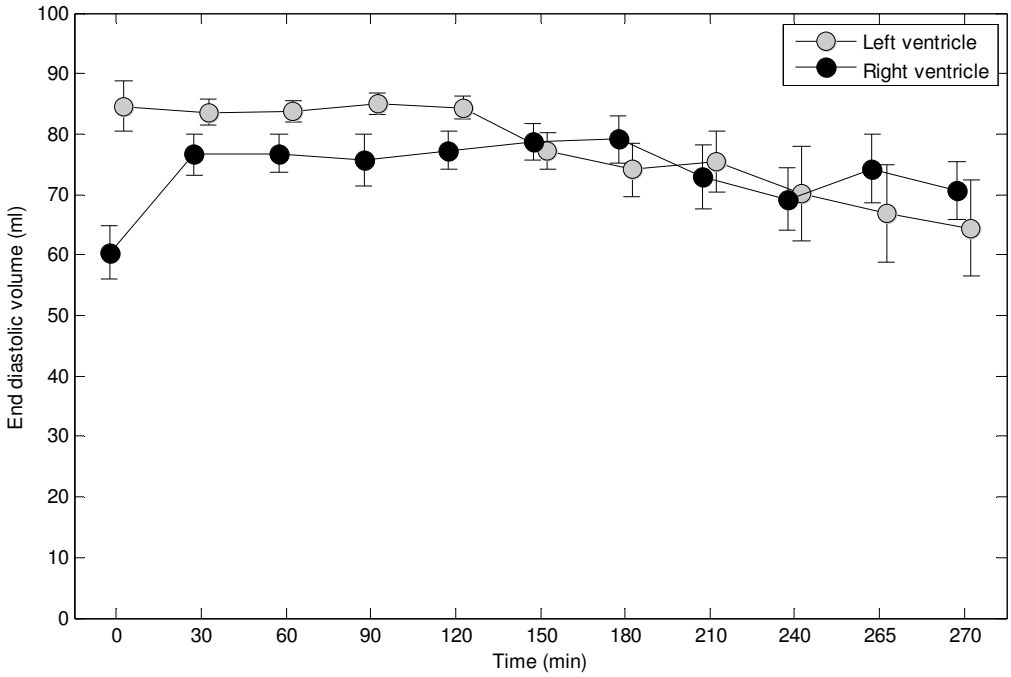

Figure 6.6: Modelled left and right ventricular end diastolic volume (LVEDV, RVEDV). The data is presented as mean +/- SS.

6.3.2.3 Contractility

Parameters of left and right ventricular end systolic elastances define the inotropic state of the ventricles in the CVS model. The evolution of model parameters, $E_{es,lvf}$ and $E_{es,rvf}$, through time is shown in Figure 6.7. Both parameters increase for most of the study. However, large drops are seen after T265 when the pigs are near death. As with R_{pul}, large increases in $E_{es,rvf}$ are seen after T0, T120, and T240 indicating a reflex response in the pigs to counteract the increased resistance of the pulmonary system (Klabunde, 2004).

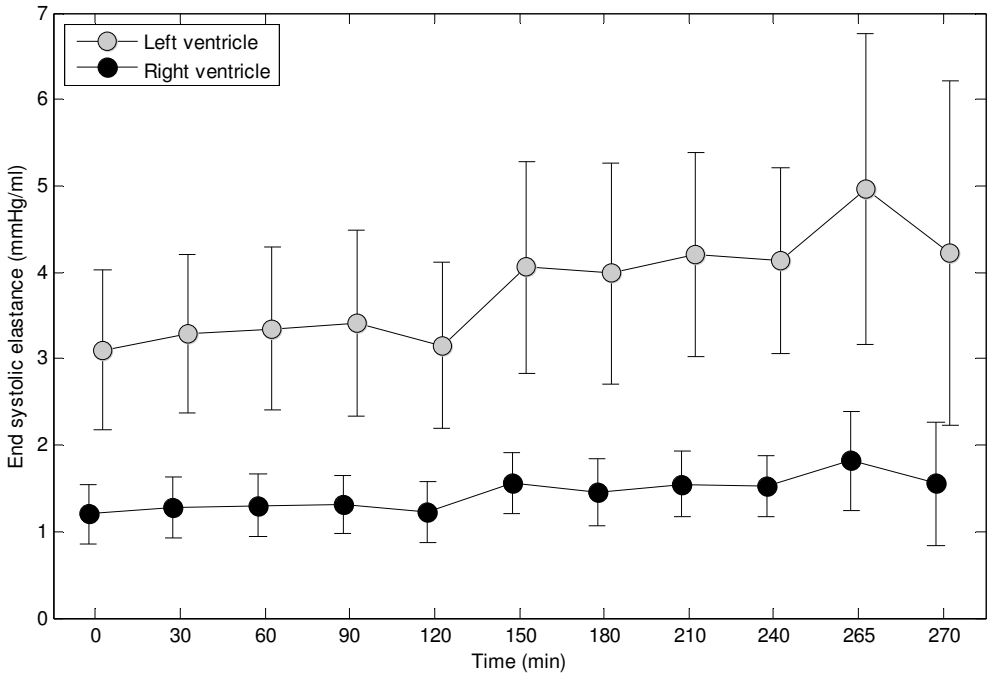

Figure 6.7: Modelled left and right ventricular end systolic elastance ($E_{es,lvf}$, $E_{es,rvf}$). The data is presented as mean +/- SD.

6.3.3 SUBJECT-SPECIFIC RESPONSE

Although the average results seen in the previous section show that the model is capable of identifying the hemodynamic trends of the induced disease over a cohort, inter-patient variability can be significant. It is important to know how each subject responds to the disorder. Hence, it is essential to analyse the individual time varying trends for each pig, not just the averaged trends of the disease.

The time varying profile of some of the measurements used to identified the subject-specific CVS models are shown in Figure 6.8. The subject-specific parameters identified from these measurements can be seen in Figure 6.9. For all the pigs an increase in pulmonary vascular resistance was noticed at T0, the main consequence of PE. This increase in pulmonary resistance would have been responsible for the increase in mean pulmonary artery pressures observed in the pigs. The identified increases in R_{pul} indicate that PE was successfully induced in each pig.

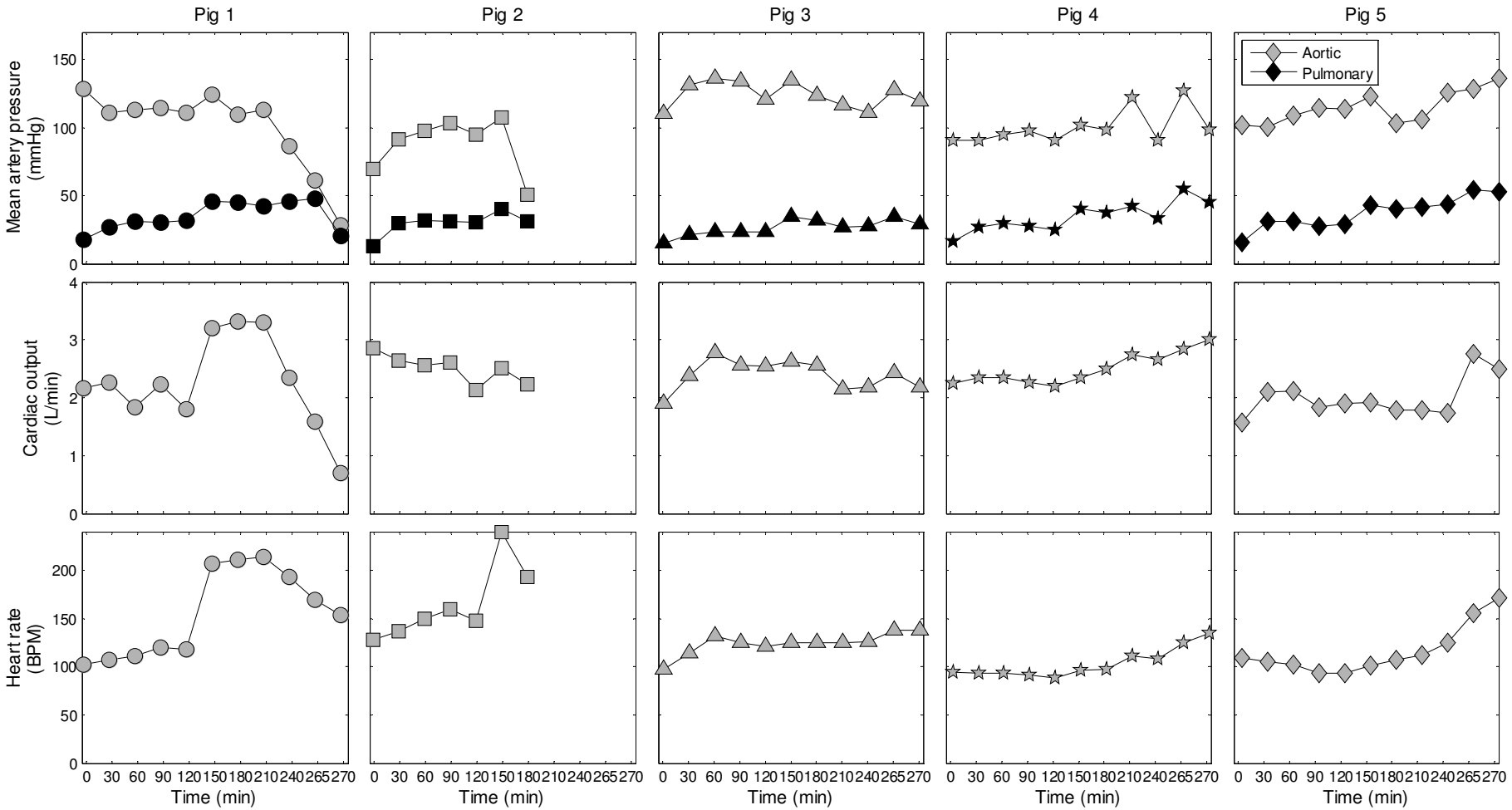

Figure 6.8: Temporal evolution of the subject-specific hemodynamic measurement recorded during the porcine trials and used to identify the subject-specific CVS models.

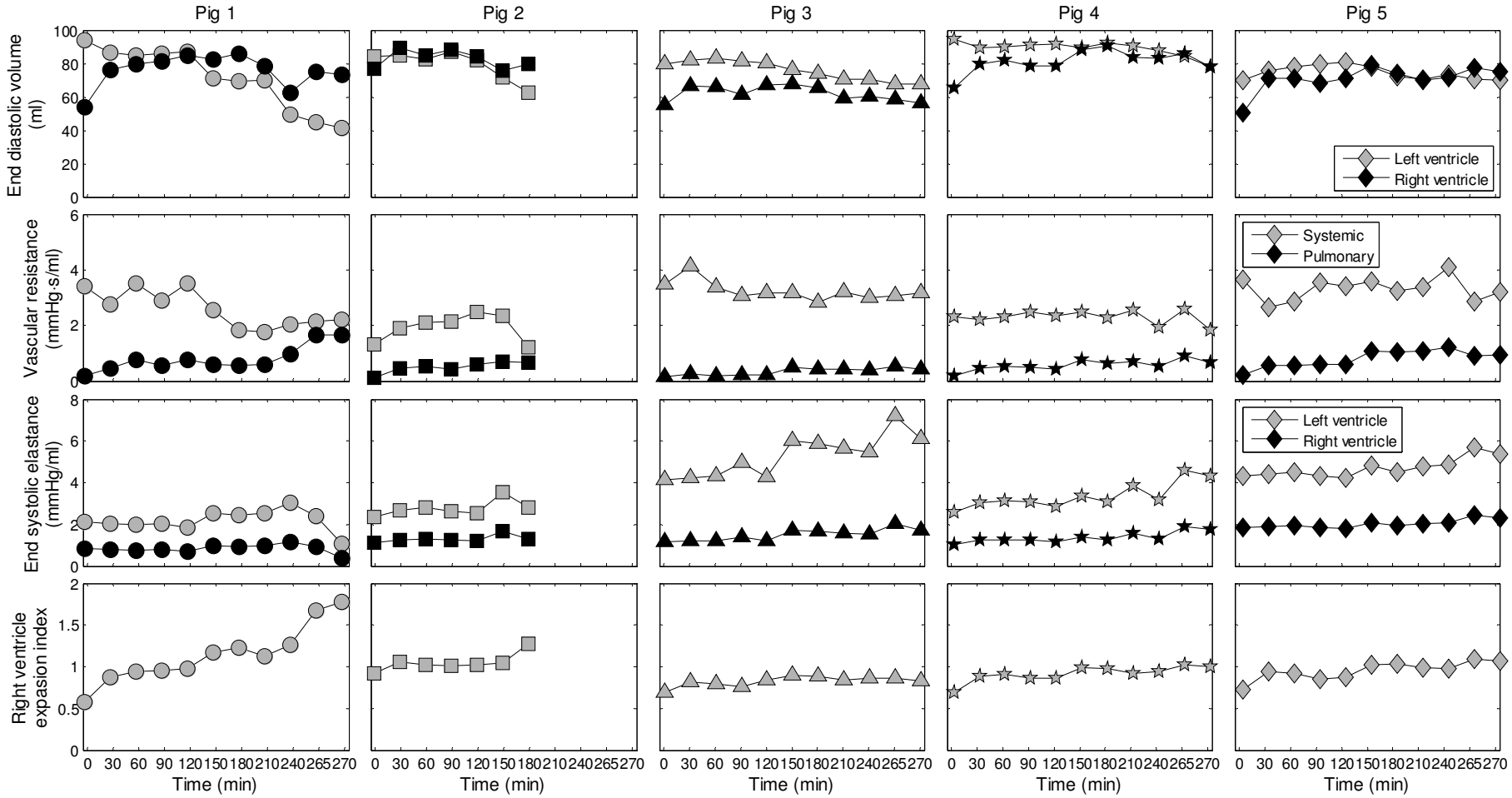

Figure 6.9: Identified subject-specific metrics of preload (LEVDV, RVEDV), afterload (R_{sys}, R_{pul}), contractility ($E_{es,lvf}$, $E_{es,rvf}$), and right ventricular vascular index (RVEDV/LVEDV).

To counteract the increased resistance of the pulmonary circulation the right ventricle contracts with greater force to maintain cardiac output. This result is captured by monitoring the modelled $E_{es,rvf}$, which represents the contractile state of the right ventricle Figure 6.9 shows the time varying trend of the modelled $E_{es,rvf}$ in each pig. In all the pigs, except Pig 1, the change $E_{es,rvf}$ closely matches the change in R_{pul}, indicating that increasing contractility is a internal reflex response to increased afterload.

The pigs' conditions begin to deteriorate when the response of the cardiovascular (such as increased $E_{es,rvf}$) can no longer adequately compensate for the effects PE. The obstruction in the pulmonary circulation cause decreased venous return to the left heart and a rise in pressure and volume in the right heart (Goldhaber and Elliott, 2003a). To analyse the magnitude of these effects the right ventricle expansion index (RVEI) is used, which is the ratio of the right to left end diastolic volumes (RVEDV/LVEDV). The individual response of the modelled RVEI for each pig is shown in Figure 6.9. RVEI increases for each pig throughout the study. The largest increases are noticed for Pigs 1 and 2, which both die during the study. Hence, RVEI can be used as an indicator of the severity of PE and the ability of the pig's internal reflexes to respond to the disorder.

6.4 DISCUSSION

6.4.1 COMPARISON WITH CLINICALLY DERIVED METRICS

Modelled pulmonary afterload closely matched the clinically derived metric with an R^2 = 0.86 and bias of -0.06 mmHg/ml. The trends for the modelled right ventricle contractility and right ventricular vascular coupling also followed the trends of the clinically derived metrics (R^2 = 0.51, R^2 = 0.83) although a large negative bias was observed (-0.87 mmHg/ml and -0.73 mmHg/ml). The main reason for this bias was due to the use of the constant $V_{d,rvf}$ = 23 ml to define the pressure volume relationship in the right ventricle (Equation (3.39)), as recommended for pigs in (Desaive et al., 2008). However, this value was deduced from a porcine model of septic shock and may not optimally represent right ventricle dynamics in pulmonary embolism. Though, more importantly, this bias from the use of $V_{d,rvf}$ = 23 ml represents a relatively systematic error in the modelled metrics meaning that disease-dependent trends in these indices were still captured. Hence, the identified model parameters can still be used to monitor the progression (trends) of disease in the subjects.

6.4.2 DETECTING ACUTE PULMONARY EMBOLISM

The subject-specific CVS models captured the main hemodynamic trends of PE. Increased pulmonary vascular resistance, a main sign of PE (Goldhaber, 1998, Goldhaber and Elliott, 2003a, Lualdi and Goldhaber, 1995), was observed in this study, indicating the presence of pulmonary emboli. The increased resistance in the pulmonary vasculature caused the pressure and volume in the right heart to increase (Goldhaber and Elliott, 2003a, Lualdi and Goldhaber, 1995, Wauthy et al., 2004), as shown in Figure 6.1. The obstruction also resulted in less blood returning to the left ventricle. Hence, the volume (or preload) of the left ventricle decreased (Figure 6.1). Right ventricular contractility increased, as R_{pul} increased, in an attempt to expel a build up of volume in the right ventricle and to maintain stroke volume (Figure 6.1). These trends were tracked well by the subject-specific models as shown by the validation analysis performed in Chapter 5 and the results in Section 6.3.1.

Left and right end diastolic ventricular volume and pressure, pulmonary vascular resistance, and end systolic elastance are rarely measured in intensive care as they are highly invasive to measure. However, the use of these metrics can provide great insight into cardiac and circulatory status during PE. To calculate these metrics the model-based approach only utilises measurements that are already taken in the ICU. Thus, this method provides a means of identifying these parameters without the need for direct cardiac measurement. Therefore, identified subject-specific models can be used to provide important information on a patient's cardiovascular health without any added risk.

6.4.3 SUBJECT-SPECIFIC MODELLING

The averaged results show that the model is capable of identifying the hemodynamic trends of PE. However, it is important to know how each subject (or patient) responds to the disorder to optimise treatment for the individual. Hence, in this research the time varying trends for each pig were also analysed.

Pulmonary vascular resistance (R_{pul}) increased in all the pigs (Figure 6.9), as expected, indicating that the PE was successfully induced in each of the subjects in this study. An increase in right ventricular contractility ($E_{es,rvf}$), reflecting one of the CVS compensatory reflex mechanisms to the pulmonary blockage, was also detected by the identification process. These results, as shown in Figure 6.9, illustrate how the subject-specific models were able to monitor the effect of the obtrusive blood clots, and identify the magnitude of each pig's compensatory reflex response to PE.

When the reflex responses of the pigs can no longer handle the effects of the pulmonary embolism the right ventricle begins to distend and the preload of the left ventricle begins to decrease quickly. Thus, the right ventricle expansion index in the model was used as an indicator of the severity of PE. Large increases in RVEI were seen near death in Pigs 1 and 2, as shown on Figure 6.9, indicating that the subject-specific models are capable of identifying the severity of the PE.

6.4.4 LIMITATIONS

Most of the limitations are the same as stated in Section 4.6.3. One major limitation of this type of research is the uncertainty regarding whether the animal model of the PE reflects the true disease. However, it is pretty obvious from the measurements recorded in this animal study and corresponding identified CVS models that pulmonary vascular resistance increased after the insertion of blood clots. Indicating that the blood clots most likely did embolise from their insertion point in jugular vein to the pulmonary circulation where they obstructed blood flow. Thus, the effects of the induced PE in the animal study closely matched the known effects of the actual disease.

One assumption used in the parameter identification method in this chapter was that the global end diastolic volume (GEDV) is equal to the sum of the left and right end diastolic volumes (LEVDV+RVEDV). This is not true in reality as GEDV represents the volume of the whole heart and not just the ventricles. When measured in practice GEDV also represents the volume of the initial part of the arterial system. However, GEDV has been found to be highly related to cardiac preload (Michard et al., 2003), which is primarily dominated by the left ventricle and right ventricle. Changes in GEDV mostly reflect changes in LVEDV and RVEDV, and hence, if required, a simple relationship can be used to relate the measured GEDV to the GEDV used in the parameter identification process.

6.5 SUMMARY

The identified subject-specific CVS models correctly estimated the known physiological responses to PE. An increase in right ventricle afterload (R_{pul}), the main hemodynamic consequence of PE, related well to the experimentally derived pulmonary vascular resistance. The individualised models also captured a loss of autonomous control of important reflex responses, R_{sys} and $E_{es,rvf}$, in Pigs 1 and 2 leading to cardiovascular failure. Furthermore, the identified RVEI increased as emboli were inserted into the pigs, indicating a leftward shift in the intra-ventricular septum, which accurately matched

the changes in the measured RVEI. These results clearly show that subject-specific models can be used to identify clinically useful and relevant cardiac and circulatory information in PE by accurate regular assessment of (model-based) subject-specific CVS status. Hence, this research demonstrates and proves the clinical relevance, concept and potential of this model-based approach to CVS monitoring and diagnosis of PE.

CHAPTER 7: MODEL-BASED MONITORING OF SEPTIC SHOCK

Septic shock is a common and serious dysfunction in the ICU affecting the heart and circulation. Thus, it is important to test the ability of the parameter identification method to track the hemodynamic changes due to septic shock. This chapter examines the ability of subject-specific CVS models to monitor the effects of septic shock in pigs (Revie et al., 2012).

7.1 INTRODUCTION

Sepsis is one of the most prevalent diseases in the ICU contributing to 10.4% of ICU admissions in the United States (Martin et al., 2003). Septic shock is the more severe form of sepsis accounting for 9% of ICU patients, with mortality rates ranging between 25-80% (Brun-Buisson, 2000, Angus et al., 2001). The disease is caused by a harmful systemic inflammatory response to an infection. Its effects are wide reaching due to decreased oxygen delivery, which can result in multiple organ failure (Dellinger, 2003). The mortality rates are high, especially for the acute form of the disease, which is most prevalent in elderly (Girard et al., 2005) or immune-compromised individuals. In such patients, a weakened immune system cannot deal with the underlying infection as effectively as a healthy person. Hence, these patients usually die unless the underlying infection is controlled.

To increase the chances of survival it is important to diagnose, monitor, and treat septic shock, as early as possible. In recent times, it has been shown that early detection and application of goal directed therapy can help improve outcomes in response to the disease (Rivers et al., 2001). The use of an automated model-based monitoring system could help track more direct and controllable targets for treatment. Hence, the combination of a model-based monitoring and goal directed therapy could provide a means to further standardise therapy and improve patient outcomes.

This chapter analyses the ability of subject-specific CVS models to track metrics of cardiovascular health during septic shock. The model identification method, outlined in Chapter 4, is retrospectively tested using measurements from a porcine study on septic shock (Lambermont et al., 2006). In this animal study, endotoxin infusions were used to induce septic shock and the pigs were then treated with a newly developed large pore hemofiltration therapy (LPHF). A range of hemodynamic measurements were recorded, and it was hypothesised that the filtration of small to medium sized water soluble cytokine molecules from the blood stream would reduce the systemic inflammatory

effects of septic shock resulting in improved circulatory dynamics. However, the aim of this study is not to test the effectiveness of the LPHF, but to assess the ability of the system to track the disease dependent hemodynamic changes resulting from endotoxin infusion and the resulting LPHF treatment.

Subject-specific CVS models are again identified from clinically available data derived from the porcine measurements. The performance of the model identification method in septic shock is assessed against independent measurements not used for identification (Chapter 5), experimentally derived metrics (Lambermont et al., 2006), and clinically expected trends from the literature (Chan and Klinger, 2008, Dellinger, 2003, Merx and Weber, 2007, Parker et al., 1984, Schneider et al., 1988, Vincent et al., 1992, Groeneveld et al., 1988). Hence, the overall goal of this work is to demonstrate the clinical relevance and prove the concept (and potential) of computer-based clinical monitoring of: 1) CVS status; 2) septic shock; and 3) the effect of treatment.

7.1.1 PATHO-PHYSIOLOGY AND TREATMENT OF SEPTIC SHOCK

Septic shock is commonly caused by a Gram-negative bacterial infection which produces endotoxins (Werdan, 2001). High levels of endotoxins in the blood activate a systemic inflammatory response leading to systemic vasodilation (Werdan, 2001), myocardial depression (Vincent et al., 1992), widespread endothelial injury (Mutunga et al., 2001), and disseminated intravascular coagulation (Fourrier et al., 1992). The combination of these effects causes hypoperfusion leading to multiple organ dysfunction syndrome (Werdan, 2001). Treatment normally consists of aggressive fluid resuscitation, antibiotic administration, early goal directed therapy, and organ support (positive pressure ventilation, dialysis, etc) (Dellinger, 2003, Rivers et al., 2001). Vasopressors, such as norepinephrine or dopamine, are commonly used to increase blood pressure, and inotropes (e.g. dobutamine) may be used to assist cardiac function (Dellinger, 2003).

Figure 7.1 from Dellinger (Dellinger, 2003) outlines the main effects of septic shock from a hemodynamic perspective. In untreated septic shock (Figure 7.1, A) left ventricular venous return decreases due to capillary leakage, increased venous capacitance, and increased pulmonary vascular resistance. Stroke volume is further compromised by decreased left and right ventricular contractility. HR and left ventricular compliance increase to partially restore CO and left ventricle preload. However, CO and LVEDV may remain below normal levels. Finally, systemic vascular resistance decreases to enables a higher SV at the cost of lower blood pressure, and thus, can lead to severe hypotension.

Aggressive fluid loading (Figure 7.1, C) increases venous return by counteracting the effects of capillary leak, increased venous compliance, and increased pulmonary vascular resistance. Cardiac function improves as left ventricular preload increases. Due to the combination of these factors, most patients exhibit a hyperdynamic state, after fluid resuscitation, with high CO and low systemic resistance.

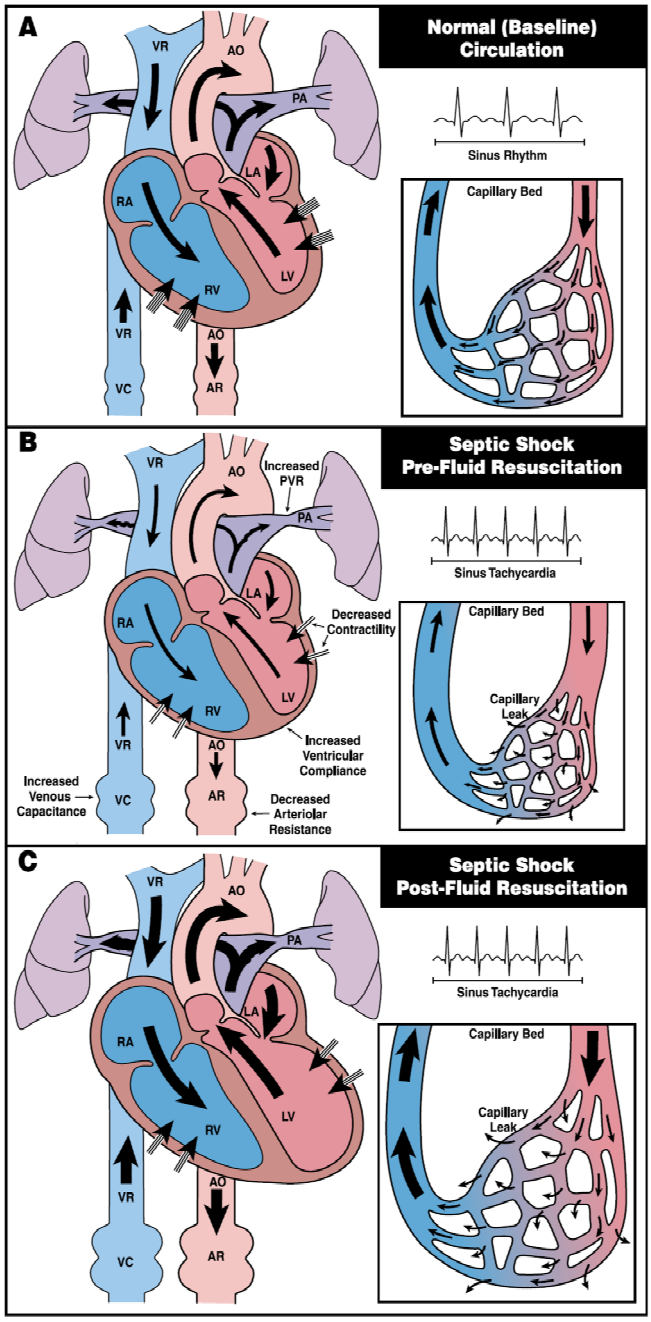

Figure 7.1: Illustration of the effects of septic shock before and after fluid resuscitation, from Dellinger (Dellinger, 2003). VR, venous return; VC, venous capacitance; AO, aorta; AR, arteriolar resistance; RA, right atrium; LA, left atrium; RV, right ventricle; LV, left ventricle; PA, pulmonary artery.

The hemodynamic profile of the effects of septic shock is summarised below:

- Hypovolemic
    - Capillary leak (Dellinger, 2003)
    - Venous dilation (Dellinger, 2003)
    - Decreased venous return (Chan and Klinger, 2008)
- Cardiogenic
    - Decreased ventricular contractility (Chan and Klinger, 2008, Dellinger, 2003, Vincent et al., 1992, Merx and Weber, 2007)
    - Left-ward shift in inter ventricular septum (Chan and Klinger, 2008)
- Hypoperfusion (despite adequate CO)
    - Decreased systemic resistance (Chan and Klinger, 2008, Parrillo et al., 1990)
- Obstructive
    - Increased pulmonary vascular resistance (Chan and Klinger, 2008)
    - Activation of coagulation mechanisms (Chan and Klinger, 2008, Fourrier et al., 1992)
- Distributive
    - Right ventricle dilation (Chan and Klinger, 2008)
    - Shunting (Dellinger, 2003)
    - Decreased splanchic blood flow (Dellinger, 2003)
- Cytoxic
    - Inability of tissues to utilise O_2 despite sufficient supply (Dellinger, 2003)

7.2 METHODS

7.2.1 PORCINE EXPERIMENTS AND DATA

All procedures and protocols used in the porcine experiments were reviewed and approved by the Ethics Committee of the Medical Faculty at the University of Liege (Belgium). Four pure Pietrain pigs weighing 20-30kg were premedicated and anesthetised as described in (Lambermont et al., 2003, Lambermont et al., 2006). After endotracheal intubation, through a cervical tracheostomy, the pigs were connected to a volume cycle ventilator (Evita 2, Drager, Lubeck, Germany) set to deliver a tidal volume of 10ml/kg, with a fraction of inspired oxygen (FiO_2) of 0.4, at a respiratory rate of 20 breaths/min. Respiratory settings were adjusted so the end tidal CO_2 pressure ranged between 30 and 35 mmHg. The animals received a 0.5-mg/kg endotoxin infusion (lipopolysaccharide from Escherichia coli serotype 0127:B8; Sigma Chemical, St. Louis, MO, U.S.A) over 30 minutes from T0 to

T30. From T60 onwards the pigs underwent a zero balance continuous veno-venous hemofiltration at a rate of 45 ml/kg/h with a 0.7 m^2 large-pore (78 Å) membrane with a cutoff of 80 kDa (Sureflux FH 70, Nipro, Osaka, Japan) and a BaxterBM 25-BM 14 hemofiltration device (Baxter Health Care, Munich, Germany). Ultrafiltrate was replaced in the post dilution mode by a bicarbonate-buffered hemofiltration fluid (Na^+: 150 mM; K^+: 3 mM; bicarbonate: 30 mM) at a temperature of 37°C. Anticoagulation of the extracorporeal circuit was achieved using a loading dose of 5000 IU of heparin followed by an anticoagulation regimen based on the activated clotting time (100 - 200s).

The pulmonary trunk was accessed via medial sternotomy and a micromanometer-tipped catheter (Sentron, Cordis, Miami, FL) was inserted into the main pulmonary artery through a stab wound in the RV outflow tract and positioned approximately 2 cm downstream of the pulmonary valve. Aortic pressure was measured using a micromanometer-tipped catheter inserted into the descending thoracic aorta through the right femoral artery. 7F, 12 electrode conductance micromanometer-tipped catheters (CD Leycom, Zoetermeer, Holland) were positioned in the left and right ventricles so that all electrodes were in their respective cavities. From these four catheters continuous measurements over 6 to 12 heartbeats were recorded every 30 minutes (T0 to T240) of the aortic and pulmonary pressure waveforms (P_{ao}, P_{pa}), and the left and right ventricular pressure and volume waveforms (P_{lv}, V_{lv}, P_{rv}, V_{rv}) at a sampling rate of 200 Hz. In this study, 34 sets of measurements from the four pigs were used. Further details on the trials can be found in (Lambermont et al., 2006).

7.2.2 MODEL IDENTIFICATION

The model identification method outlined in Chapter 4 was used to identify the subject-specific models of septic shock. In this study GEDV was assumed to be equal to the sum of the maximum left and right ventricular volumes. A left and right ventricle deadspace volume of 23 ml ($V_{d,lvf} = V_{d,rvf} = 23$ ml) was used to simulate the CVS model as suggested by Desaive et al. (Desaive et al., 2008) . The mitral and tricuspid valve closure times were estimated from the approximated left and right ventricular functions ($e_{lv}(t)$ and $e_{rv}(t)$) from (Stevenson et al., 2012a, Stevenson et al., 2012b), as central venous pressure and ECG were not measured in this study.

7.2.3 DATA AND STATISTICAL ANALYSIS

Data is presented as mean +/- 1 standard deviation (SD) unless stated otherwise. A paired-sample t-test was used to check temporal variance over T0 - T60 to analyse the effect of the endotoxin intervention. $P < 0.05$ was considered a statistically significant result. Percentage errors, and bias

and precision metrics were used to compare the relationship of the modelled to experimentally derived metrics. A percentage error less than 20% was regarded as an acceptable result as measurement of physiological variables often lack precision, with errors of +/- 10-20% not uncommon (Clancy et al., 1991, Critchley and Critchley, 1999, Salandin et al., 1988).

7.3 RESULTS

Data sets were recorded every 30 minutes (T0, T30, T60,... ...,T240) in each of the four hour long trials. From each of the data sets, subject-specific models were retrospectively fitted for each of the pigs. Hence, a total 34 subject-specific CVS models were identified and analysed.

In this study, each animal acts as their own control with baseline (T0) measurements reflecting the undiseased state of the pig. The temporal variance in the measurements of the cohort were analysed between T0-T30, as well as T0-T60 and T30-T60. The reason temporal variance was analysed over T0-T60 and T30-T60 is because sometimes the symptoms of septic shock do not manifest immediately after the endotoxin infusion at T30. Statistically significant temporal changes ($P<0.005$) were noticed in the measured systolic and diastolic aortic and pulmonary artery pressures, left and ventricular end diastolic volume (LVEDV, RVEDV), heart rate (HR), and maximum left ventricular pressure ($P_{lv,max}$) over the first hour, underlining the pathological changes occurring in the animals due to the endotoxin infusion. A summary of the main hemodynamic measurements is seen in Figure 7.2.

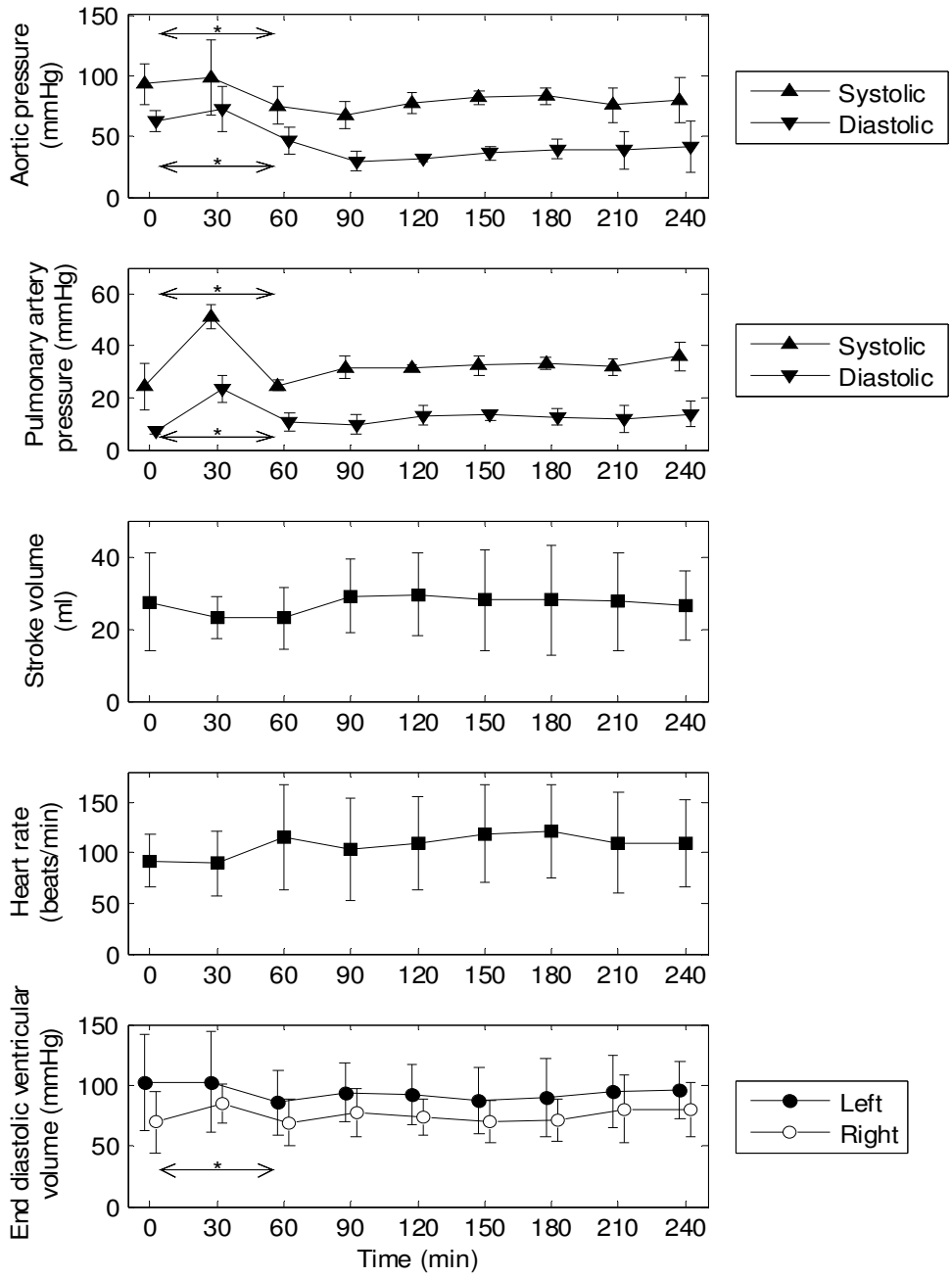

Figure 7.2: Evolution of the averaged hemodynamic measurements recorded during the trials. * indicates P<0.05 for expected temporal changes over T0-T60 due to the induction of septic shock. The data is presented as mean +/- SD.

7.3.1 COMPARISON TO EXPERIMENTALLY DERIVED METRICS

For further validation (on top of the validations shown in Chapter 5), the identified pulmonary afterload, right ventricular end systolic elastance, and right ventricular vascular coupling (RVVC) from the model were compared to corresponding metrics (E_a, E_{es}, E_{es}/E_a) derived experimentally using pressure-volume loop analysis from the same measurements (Lambermont et al., 2006). The

afterload on the right ventricle in the model is the pulmonary vascular resistance divided by the period of one heartbeat ($E_{a,model} = R_{pul}/T$). Bias, precision, and correlation indices for pulmonary afterload and coupling are shown in Table 7.1 and the temporal trends for these indices are shown in Figure 7.3, Figure 7.4, and Figure 7.5 . The model matched the changes in pulmonary afterload accurately ($R^2 = 0.86$) although there was a noticeable bias of -0.06 mmHg/ml. The model parameter $E_{es,rvf}$ is directly comparable to experimentally derived right ventricular end systolic elastance and was found to have bias of and precision of -0.48 +/- 0.40 mmHg/ml (R^2= 0.66). Furthermore, a relatively small bias and spread of -0.73 +/- 0.83 was observed for the RVVC with correlation of R^2 = 0.83 as seen in Figure 7.

Table 7.1: Bias, precision, and correlation metrics comparing the modelled to experimentally derived indices of afterload, contractility, and right ventricular vascular coupling (RVVC).

Metric	Bias	Precision (2SD)	R^2
Afterload (E_a)	-0.27mmHg/ml	0.48 mmHg/ml	0.94
Contractility (E_{es})	-0.48 mmHg/ml	0.40 mmHg/ml	0.66
RVVC (E_{es}/E_a)	-0.14	0.67	0.71

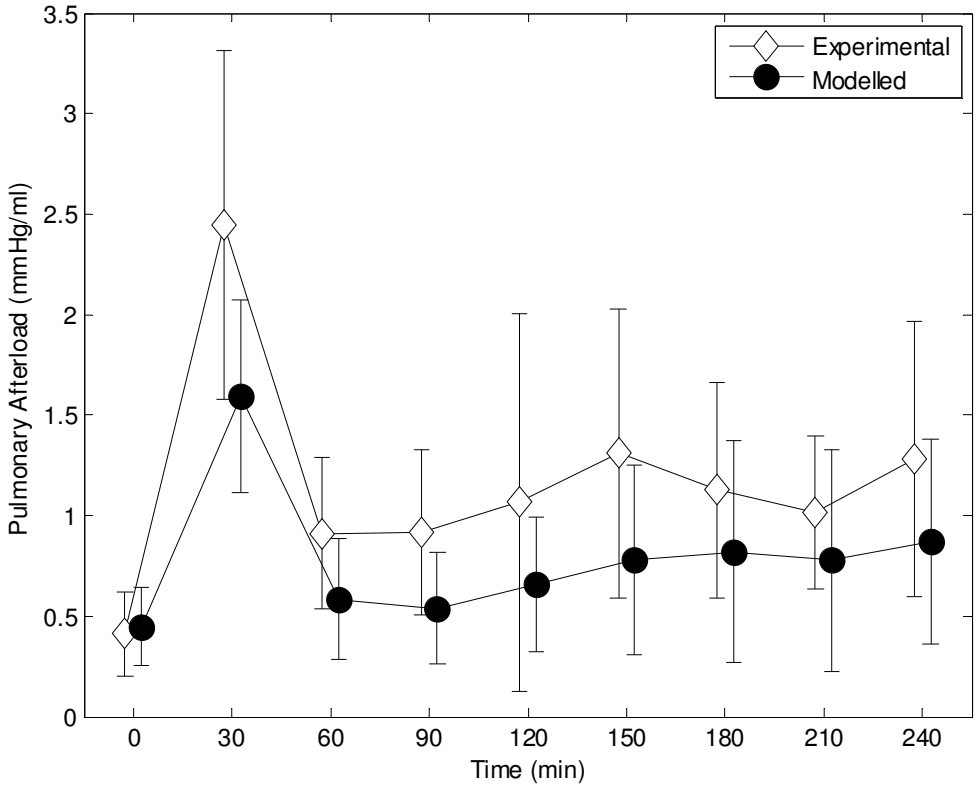

Figure 7.3: Comparison of the experimentally derived (Lambermont et al., 2006) and modelled pulmonary afterload. The data is presented as mean +/- SD.

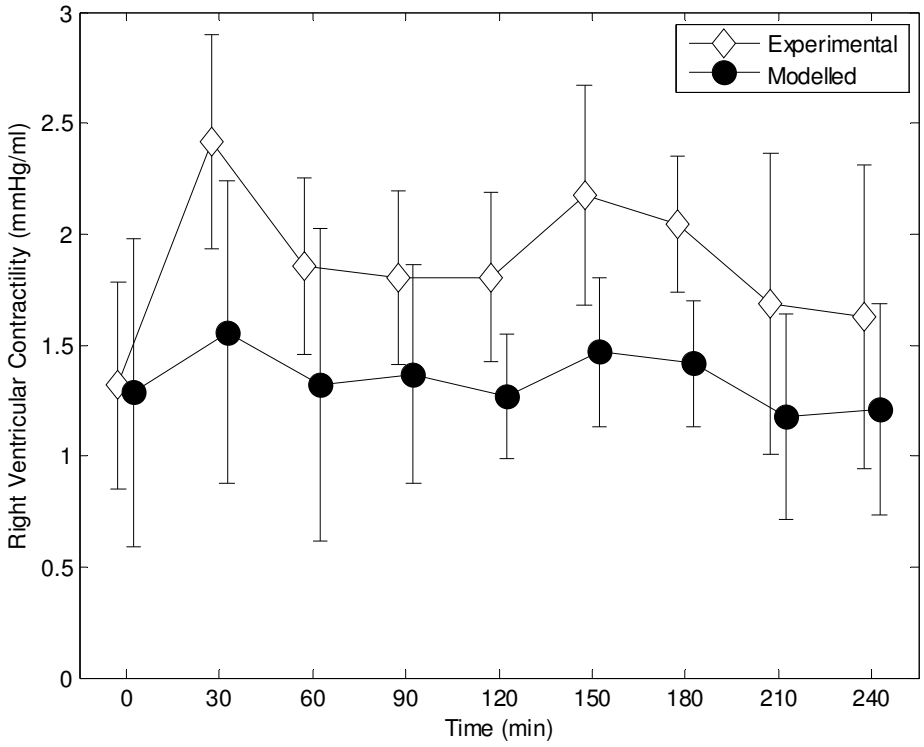

Figure 7.4: Comparison of the experimentally derived (Lambermont et al., 2006) and modelled right ventricular end systolic elastance ($E_{es,rvf}$). The data is presented as mean +/- SD.

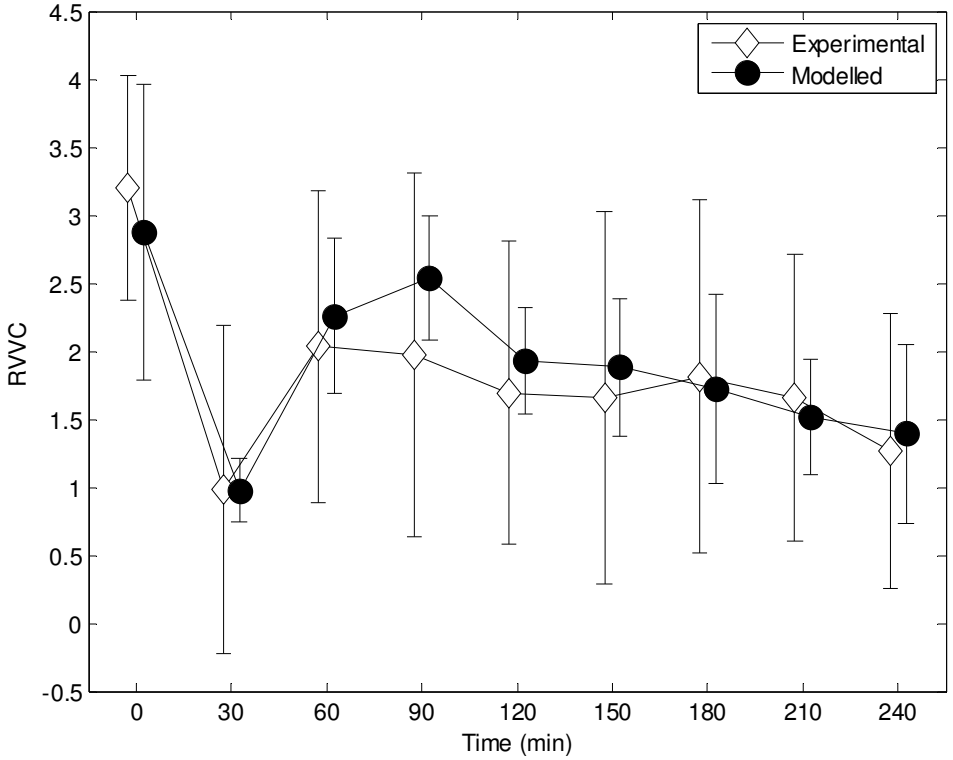

Figure 7.5: Comparison of the experimentally derived (Lambermont et al., 2006) and modelled right ventricular-vascular coupling (RVVC). The data is presented as mean +/- SD.

7.3.2 SEPTIC SHOCK TRENDS

Global hemodynamic trends during septic shock were examined through analysis using identified metrics of preload, afterload and contractility from the subject-specific CVS models.

7.3.2.1 Preload

Ventricular preload in the model is represented by ventricular end diastolic volume (LVEDV, RVEDV). Averaged LVEDV and RVEDV over all the pigs are seen in Figure 7.6. The averaged RVEDV increases throughout the study indicating right ventricular distension. LVEDV remains 10 ml to 15 ml below its baseline (T0) durind the trial, as expected (Chan and Klinger, 2008, Schneider et al., 1988).

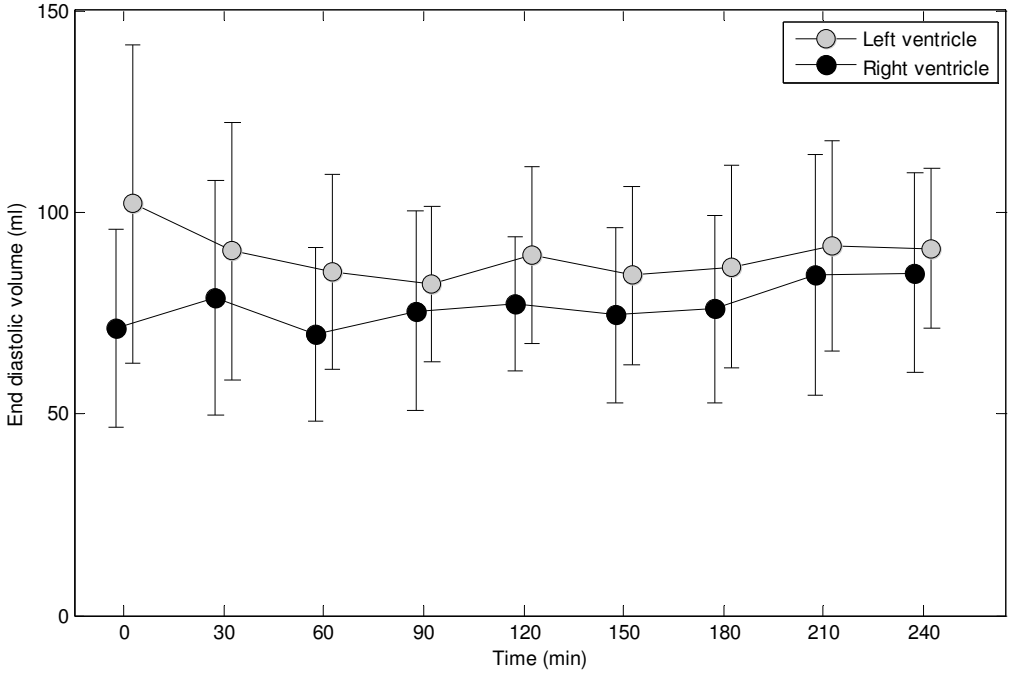

Figure 7.6: Modelled left and right ventricular end diastolic volume (LVEDV, RVEDV). The data is presented as mean +/- SD.

7.3.2.2 Afterload

The model parameters for systemic and pulmonary vascular resistance (R_{sys}, R_{pul}) represent the main components of afterload on the left and right ventricles, respectively. The average time varying trends for these parameters are shown in Figure 7.7. Noticeably, the average R_{sys} drops to 40.1% below the baseline level at T120 and where it stabilised to a level around 20% below baseline by the end of the experiment. In contrast, the average R_{pul} value increased steadily to 86% above the

baseline value by the end of the study after an initial spike at T30. These results match clinically expected trends (Dellinger, 2003, Groeneveld et al., 1988, Vincent et al., 1992).

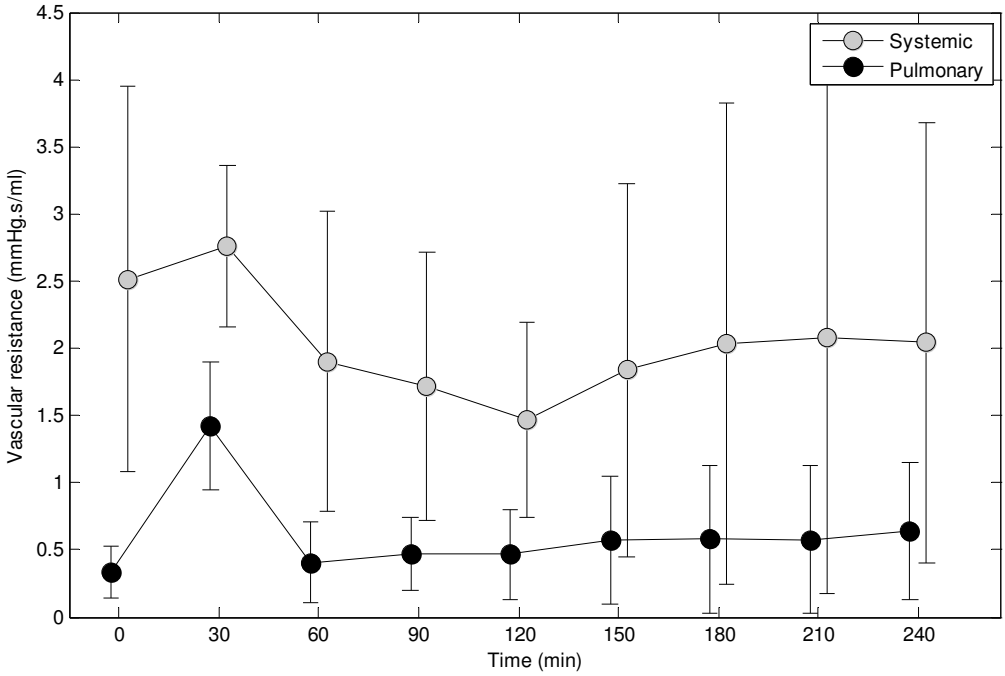

Figure 7.7: Modelled left and right ventricular afterload. The data is presented as mean +/- SD.

7.3.2.3 Contractility

Parameters of left and right ventricular end systolic elastances define the inotropic state of the ventricles. The evolution of model parameters, $E_{es,lvf}$ and $E_{es,rvf}$, through time is shown in Figure 7.8. An initial spike in both parameters is seen at T30, where afterwards the parameters increase and then start decreasing at the end of study (T150 onwards).

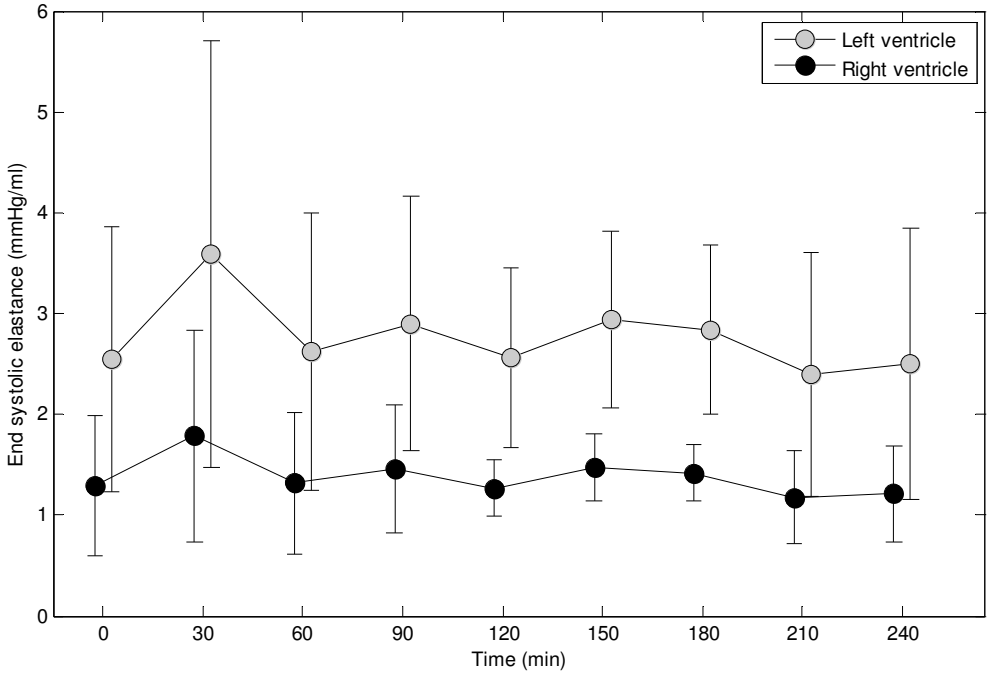

Figure 7.8: Modelled left and right ventricular end systolic elastance ($E_{es,lvf}$, $E_{es,rvf}$). The data is presented as mean +/- SD.

7.3.3 SUBJECT-SPECIFIC RESPONSE

Although the averaged results, seen previously, show that the model is capable of identifying the hemodynamic trends of the induced disease over a cohort, inter-patient variability can be significant. It is important to know how each subject responds to the disorder and corresponding treatment. Hence, it is essential to analyse the individual time varying trends for each pig, not just the averaged trends of the disease.

Figure 7.9 shows the subject-specific trends in the measured data for the pigs. The mean aortic pressure decreases initially in all the pigs, consistent with the known signs of septic shock. However, a restoration of mean aortic pressure is seen in Pigs 1 and 2 during the second half of the trials, whereas aortic pressure remains well below the baseline value in Pigs 3 and 4 at the end of the experiment. Mean pulmonary artery pressure increases during the trials in Pigs 1, 2, and 3 and hyperdynamic cardiac states are observed in Pigs 3 and 4 with large increases in cardiac output.

The identified model parameters are shown in Figure 7.10. In the identified models, the main reason mean aortic pressures is restored in Pigs 1 and 2 is due to an increase is systemic vascular resistance, as there is no significant change in cardiac output. However, this result appears to come at the cost

of higher pulmonary resistances and pressures and may lead to decoupling of the right ventricle and pulmonary circulation.

In the CVS models, the hyperdynamic states observed in Pigs 3 and 4 are caused by an initial increase in left ventricle contractility and a decrease in systemic resistance. In the absence of fluid resuscitation, cardiac output decreases at the end of the trials along with the identified left ventricular end systolic elastance, indicating the onset of myocardial depression. These results represent the known pathophysiological state of septic shock (Dellinger, 2003, Vincent et al., 1992).

These findings, as expected, show there is significant inter-patient variability in response to the endotoxin and corresponding large-pore hemofiltration therapy. On average, systemic resistance drops by 20.3% across the four pigs over the duration of the trials. However, when analysing the individual response of each of the pigs, it is seen that the R_{sys} returns to baseline for Pig 2, and a substantial improvement is observed in Pig 1 after LPHF treatment (T60 onwards). Whereas, there are large drops in R_{sys} with no apparent improvement with treatment in Pigs 3 and 4, indicating the difference response to septic shock and therapy between the pigs.

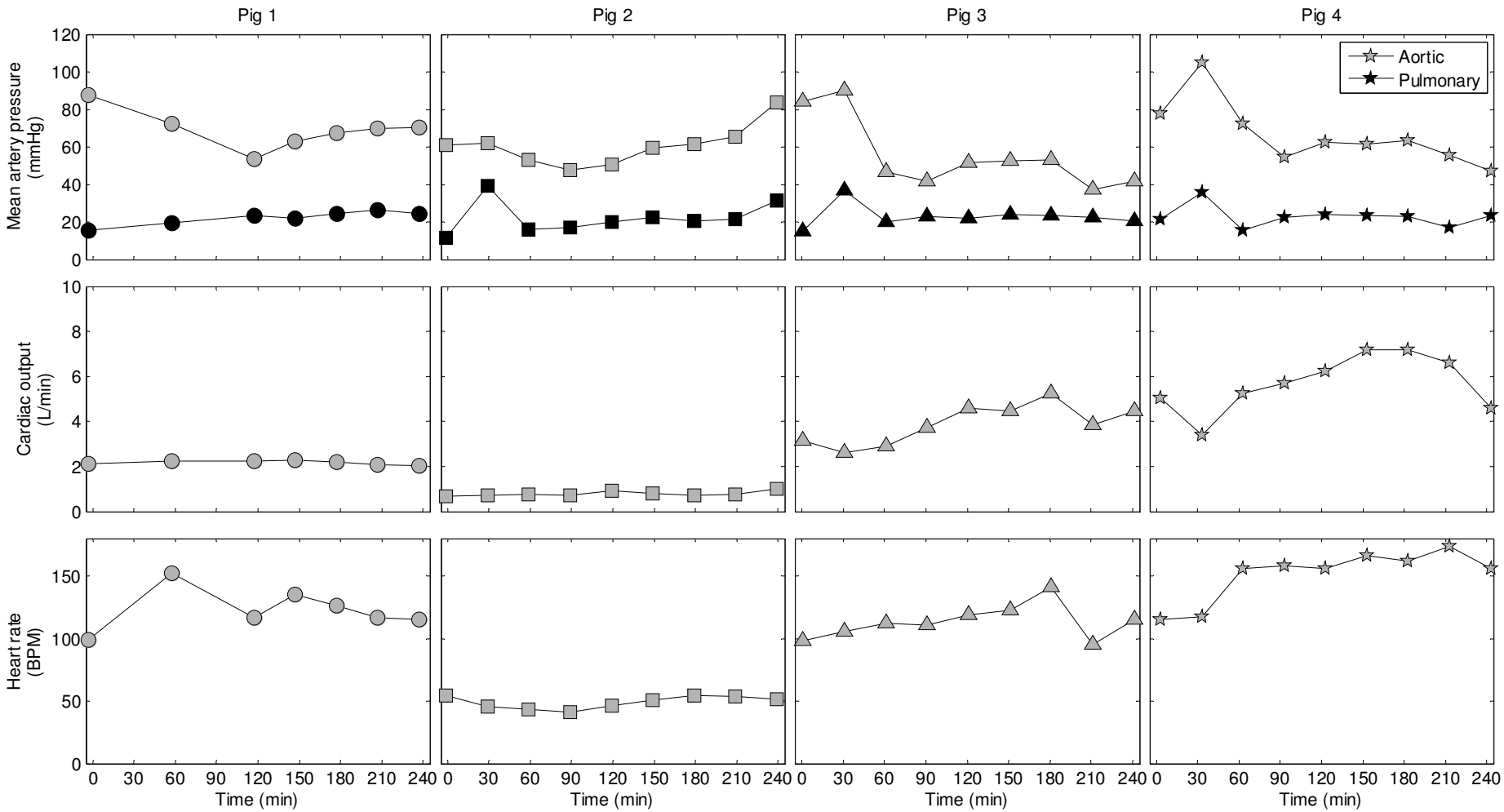

Figure 7.9: Temporal evolution of the subject-specific hemodynamic measurement recorded during the porcine trials and used to identify the subject-specific CVS models.

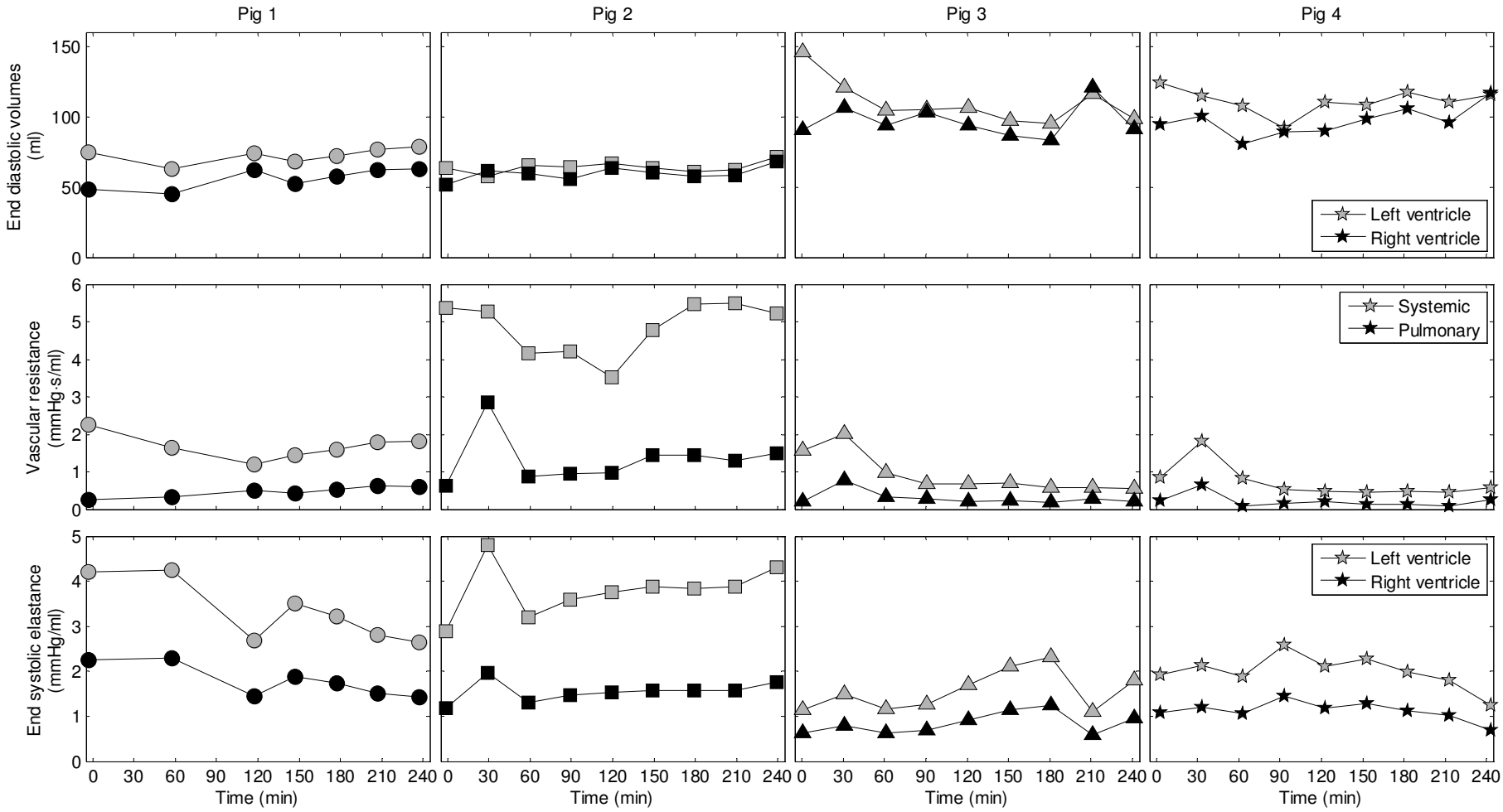

Figure 7.10: Identified subject-specific metrics of preload (LEVDV, RVEDV), afterload (R_{sys}, R_{pul}), and contractility ($E_{es,lvf}$, $E_{es,rvf}$).

7.4 DISCUSSION

7.4.1 DETECTING SEPTIC SHOCK

The subject-specific models of the CVS captured the main hemodynamic trends of septic shock. A drop in systemic vascular resistance, corresponding to a loss of vascular tone in the arterial system (Parrillo et al., 1990, Dellinger, 2003, Chan and Klinger, 2008), and an increase in pulmonary vascular resistance were noticed, a known result of the disease (Chan and Klinger, 2008, Dellinger, 2003). Initially, for Pigs 3 and 4 a decrease in R_{sys} leads to an increase in cardiac output, reflective of warm septic shock. Later in the trials, the decreasing ratio of the left to right ventricular afterload caused dilation of the right ventricle and a decrease in left ventricular preload (LVEDV). These two factors would have resulted in a flattening of the intra-ventricular septum and a decrease in the left ventricular function (Chan and Klinger, 2008). This point is reinforced through analysis of left ventricular contractility, $E_{es,lvf}$, which increases initially, but starts to drop in the later stage of the trials. Hence, the model appears to be accurately capturing the expected trends of septic shock in the pigs.

7.4.2 COMPARISON TO EXPERIMENTALLY DERIVED METRICS

The modelled metric of afterload (R_{pul}/T) underestimated the experimentally derived value, as seen on Figure 7.3. This result is expected as R_{pul}/T only represents the averaged steady state resistive component of afterload and does not take into account the pulsatile component of afterload due to the dynamic impact of stiffness in the circuit (Hunter et al., 2008). However, despite these limitations, the modelled afterload still captured the changes in afterload observed in the pigs with correlation of $R^2 = 0.86$.

Similarly, the modelled right ventricular contractility ($E_{es,rvf}$) underestimated the experimentally derived value calculated from regressive pressure volume loops. This finding is most likely the result of using a constant right ventricle deadspace volume ($V_{d,rvf}$) of 23 ml for the ESPVR in the model. In reality the deadspace volume would change as inotropic state changes in the pigs. However, due to the lack of available measurements it cannot be identified and is kept as a constant in the fitting process. However, by keeping $V_{d,rvf}$ constant, changes in modelled $E_{es,rvf}$ were accurately identified as shown by the good correlation of $R^2 = 0.66$ with the true value, which is of greater importance clinically.

In the calculation of modelled right ventricular vascular coupling the systematic errors observed in $E_{es,rvf}$ and R_{pul}/T are cancelled out. Hence, there is only an average bias of -0.73 in the modelled right ventricular vascular coupling metric. Because the trends the modelled $E_{es,rvf}$ and R_{pul}/T are the calculated trend in RVVC is also good with R^2 = 0.83. These examples illustrate how the subject-specific CVS models can accurately monitor disease-dependent changes in right ventricular function.

7.4.3 HEMODYNAMIC EFFECTS OF LARGE PORE HEMOFILTRATION

Systemic vascular resistance began to increase one hour after the treatment was started (T120) in Pigs 1 and 2. As a result, mean aortic pressure increased in these two pigs independent of changes in cardiac output. These results tentatively suggest that LPHF was responsible for increasing systemic vascular resistance through the removal of inflammatory molecules in Pigs 1 and 2. Thus, the treatment helped maintain coupling between the left ventricle and arterial system. Although, the treatment appeared to have little effect on the other two pigs. Larger trials would be required before a more substantiated conclusion on this therapy could be made, which was not the goal of this research. However, it is clear the model has accurately segregated those subjects who did (and did not) respond positively to the endotoxin insult, due either to internal cardiovascular reflexes or because of the effects of this therapy.

7.4.4 SUBJECT-SPECIFIC MODELLING

Section 7.3.2 shows that personalised CVS models can be used to accurately match and predict important hemodynamic markers of afterload (R_{sys}, R_{pul}), preload (LVEDV, RVEDV), and inotropy ($E_{es,lvf}$, $E_{es,rvf}$). The subject-specific models were also able to track the main hemodynamic changes in resulting from induced septic shock. The results show that the new model identification method utilised is capable of accurately identifying markers of cardiovascular health, like the previous integral-based method (Starfinger et al., 2008a, Starfinger et al., 2007). However, this improved method is clinically more relevant, as it requires a much smaller, more clinically available set of measurements including features from the aortic and pulmonary artery pressures, SV, GEDV, and the mitral and tricuspid valve closure times. Hence, the method is a significant improvement on previous work (Starfinger et al., 2008a, Starfinger et al., 2007), especially with respect to clinical feasibility.

Although the measurements in this study were only taken intermittently every 30 minutes, the system has the potential to provide continuous real time information to medical staff. Accurate

model identification can be achieved using low fidelity pressure measurements, as only the main features of the aortic and pulmonary artery pressure are required such as the mean, amplitude and maximum gradient. In practice, the aortic pressure could be inferred from the radial artery pressure using several possible methods (Chen et al., 1997, Hope et al., 2004, Pauca et al., 2001, Westerhof et al., 2008). The method could also be implemented in the ICU at little extra cost as it only uses measurements already taken in the ICU. Thus, adding no further invasive burden to the patient or staff. In addition, the system can be easily automated so that a full picture of a patient's hemodynamic state is available to clinicians with little extra effort required from medical staff.

7.4.5 LIMITATIONS

Most of the limitations are the same as stated in Section 4.6.3. In this chapter, subject-specific CVS models were matched to measurements from an experimental animal model of septic shock with LPHF. It is difficult to known if this animal model accurately represents the same dynamics that are seen in a septic shock patient. However, the measurements shown in Figure 7.2 are consistent with known trends of the disease. It is also difficult to separate the effects of the hemofiltration therapy from the subject's internal recuperative response to septic shock. Though, it is clear, through analysis of the results, that the method can track if the patient is getting better (or not), which is of greater importance.

Systemic and pulmonary vascular resistance were used to analyse afterload in the subject-specific CVS models. Although it is widely accepted the systemic vascular resistance and pulmonary vascular resistance are not the best measures of ventricular afterload (Tibby and Murdoch, 2003, Lang et al., 1986, Naeije, 2003, Hunter et al., 2008) they are still the most commonly surrogates of afterloads (Tibby and Murdoch, 2003). Hence, the systemic and pulmonary vascular resistance were chosen for examination of afterload in this study.

7.5 SUMMARY

The CVS monitoring system accurately estimated the known physiological responses to septic shock and tracked the effectiveness of continuous veno-venous LPHF. A decrease in systemic vascular resistance and increase in pulmonary vascular resistance was identified by the model, both well known trends of septic shock. RVVC in the model related closely to the experimentally derived metric calculated from the same measurement. Furthermore, restoration of systematic vascular

resistance was observed in two of the pigs, possibly due to the LPHF treatment, with no significant drop in mean aortic pressure noticed in these pigs. However, large drops in systemic resistance in Pigs 3 and 4 resulted in hyperdynamic states with hypotension. These results clearly show that subject-specific models can be used to accurately identify and discriminate clinically useful and relevant cardiac and circulatory information in acute CVS dysfunction by accurate regular assessment of (model-based) subject-specific CVS status. The ability to accurately segregate between successful and unsuccessful response to therapy is a further significant validation of this model and method. Hence, this research demonstrates and proves the clinical relevance, concept and potential of this model-based approach for hemodynamic monitoring and diagnosis of septic shock.

CHAPTER 8: MODEL-BASED MONITORING OF RECOVERY POST MITRAL VALVE SURGERY

This chapter looks at using a model-based parameter identification approach to retrospectively analyse the initial recovery from mitral valve repair or replacement in the ICU. The aim of this work is to use patient-specific CVS models to monitor hemodynamic recovery post mitral valve surgery. The results of this chapter provide the first clinical proof of concept of this model-based approach on human measurements.

8.1 INTRODUCTION

Mitral regurgitation is one of the most common forms of valvular heart disease affecting approximately 2% of the population (Nkomo et al., 2006). Because of this high prevalence, mitral valve replacement and repair are regularly-performed surgical procedures in the hospital. Operative mortality rates for the mitral valve replacement are estimated to be 5% in elderly patients (>75 years) (Detaint et al., 2006) and 8% when performed in tandem with coronary artery bypass surgery (CABG)(Edwards et al., 2001). There are high risks of post-operation complications in patients undergoing mitral valve surgery. Hence, they are often admitted to the ICU during the first one-to-two days post-surgery. During this period, it is essential to accurately monitor and track important signs of cardiac and circulatory health to ensure hemodynamic recovery.

This chapter examines the ability of the parameter identification method of Chapter 4 to capture the state of global hemodynamic recovery post mitral valve surgery using the circulatory measurements taken as part of normal care. To do this, hemodynamic measurements were retrospectively collected from the Christchurch hospital ICU electronic patient database. These measurements reflect a realistic uncontrolled clinical scenario. Hence, they provide the perfect backdrop for the first human clinical test of this model-based monitoring method.

The overall objective of this chapter is to test the ability of a model-based method to track clinically relevant signs of hemodynamic recovery. Patient-specific CVS models are identified using data recorded from the first 12 hours of ICU admission. Parameters and metrics derived from the patient-specific models are examined to analyse the performance of the approach.

8.1.1 MITRAL REGURGITATION, REPAIR, REPLACEMENT, AND RECOVERY

Mitral valve regurgitation occurs when the mitral valve does not close properly after left ventricular filling. Blood leaks backwards through the valve during left ventricular contraction and ejection due to the failure of the valve to fully close. This phenomenon is known as regurgitation (Stouffer, 2008).

The most common cause of primary mitral regurgitation is mitral valve prolapse due to myxomatous degeneration (Hayek et al., 2005). Myxomatous degeneration causes the valve leaflets and chordae tendineae to stretch (Hayek et al., 2005, Devereux et al., 1976). The elongated leaflets and chordae tendineae prevent the valve leaflets from fully sealing when the valve is closed, causing the leaflet to prolapse into the left atrium, as shown in Figure 8.1. Other causes of primary mitral regurgitation include ischemic heart disease (Martinez-Selles et al., 2009), rheumatic fever (Martinez-Selles et al., 2009), and Marfan Syndrome (Devereux et al., 1976). Secondary mitral regurgitation results from systolic left ventricular dysfunction, in the presence of normal valvular structure (Yiu et al., 2000). Acute mitral regurgitation is commonly caused by endocarditis (Mokadam et al., 2011).

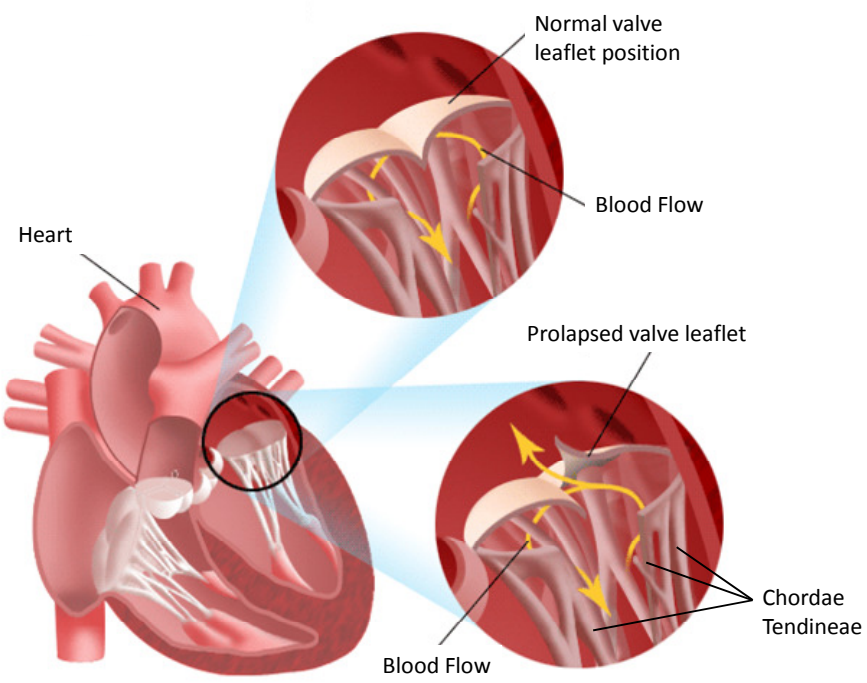

Figure 8.1: Illustration of a normal and prolapsed mitral valve leaflet (yalemedicalgroup.org, 2012).

The patho-physiology of mitral regurgitation can be broken into three phases: the acute phase, the chronic compensated phase, and the chronic decompensated phase (Bonow et al., 2006, Otto, 2001, Carabello, 2008, Kusiak and Brest, 1986). In the acute phase, the left ventricle and atrium experience a volume overload (Bonow et al., 2006). The ventricle has to pump the sum of the forward flow, into

the aorta, and the regurgitant flow, into the atrium. Hence, the total stoke volume (combination of forward and backwards flow) of the ventricle is increased in the acute setting, normally due to more complete emptying of the heart (decreased LVESV). As a result, the ejection fraction increases. However, forward flow is normally decreased (Bonow et al., 2006). As the disorder progresses the left ventricular volume increases and contractile function deteriorates, leading to decreased ejection fraction. The regurgitant flow also causes a pressure and volume overload in the left atrium (Bonow et al., 2006). The increased atrial pressure inhibits the venous return from the lungs and causes pulmonary congestion (Bonow et al., 2006).

In the chronic compensated phase, mitral regurgitation develops slowly over months to years giving the heart time to adapt to the disorder. The left ventricle develops eccentric hypertrophy (enlargement of the ventricular muscle) to compensate for the increased SV and LVEDV (Bonow et al., 2006). The eccentric hypertrophy and increased LVEDV help maintain cardiac output at near normal levels (Bonow et al., 2006). The left atrium also adapts by enlarging, allowing the filling pressure in the chamber to decrease (Bonow et al., 2006). This decreased filling pressure improves venous return from the lungs, alleviating the effects of pulmonary congestion (Bonow et al., 2006). Due to these compensatory mechanisms, individuals with chronic compensated mitral regurgitation may be asymptomatic.

Eventually, maybe after many years, an individual in the compensated phase will develop left ventricular dysfunction (Bonow et al., 2006), a sign of the decompensated phase of the disease. In the chronic decompensated phase, the contractility of the myocardium can no longer compensate for the regurgitant volume, leading to a decrease in total SV (Bonow et al., 2006). Decreased total SV results in decreased forward flow and an increase in LVESV (Bonow et al., 2006). The increased filling volume translates to increased filling pressures in the ventricle and atrium, leading to increased pulmonary congestion (Bonow et al., 2006). The left ventricle also begins to dilate in this phase, resulting in dilation of the mitral annulus, further worsening the effects of mitral regurgitation. As a result of these factors, ejection fraction normally decreases, although it may still remain in a normal range (Bonow et al., 2006).

Mitral valve surgery is the recommended treatment for severe mitral regurgitation (Bonow et al., 2006). This can include mitral valve repair or replacement (MVR). Valve replacement involves a substitution of the diseased valve with a mechanical or bioprosthetic valve, via surgery. Alternatively, the mitral valve can be repaired, especially if it is only minimally damaged. Advantages of mitral valve repair include lower surgical mortality and improved long term survival (Enriquez-

Sarano et al., 1995). Surgical mortality rates range between 3.8% for valve replacement and 1.4% for valve repair (Gammie et al., 2009).

After surgery patients are admitted to the ICU for close monitoring. Post-operative risks of mitral valve surgery include atrial fibrillation, pulmonary edema, ARDS, and pulmonary embolism. Hence, in this early stage of recovery, inotropic, fluid resuscitation, and ventilator support are normally required to assist respiratory and cardiac function.

Given this information, the expected hemodynamic recovery profile post-mitral valve surgery can be summarised as:

- Valvular
    - Decreased mitral valve regurgitation (Flameng et al., 2003, Foster et al., 2007, Bolling et al., 1998)
- Cardiogenic
    - Increased left ventricle contractility (Starling, 1995)
    - Increased cardiac output (Bolling et al., 1998, Braunwald et al., 1965)
- Distributive
    - Decreased left ventricle volume (although may be masked by fluid resuscitation) (Bolling et al., 1998) (Starling, 1995)
    - Decreased right ventricle volume (although may be masked by fluid resuscitation) (Grapsa et al., 2012)
- Circulatory pressures
    - Decreased right ventricle and pulmonary artery pressure (Braunwald et al., 1965, Foltz et al., 1984)
    - Decreased left ventricle filling pressure (Starling, 1995, Braunwald et al., 1965, Foltz et al., 1984)
- Obstructive
    - Decreased pulmonary vascular resistance (Braunwald et al., 1965, Foltz et al., 1984)

The CVS model has parameters to reflect these conditions, and should thus be able to capture the overall broad profile, or, critically deviations from the desired profile.

8.2 METHODS

8.2.1 CLINICAL STUDY

The clinical study was a retrospective, observational, single centre study performed at the Christchurch Hospital mixed medical-surgical ICU. Auditing ethics was obtained for this observation study from the Upper South A Regional Ethics Committee (REF: URA/12/EXP/023). The study used data collected over a six month period from the 1st February to the 1st July 2012.

8.2.2 PATIENTS

The inclusion criteria for patients in the study included:

- Diagnosed mitral valve regurgitation
- Underwent mitral valve replacement or repair surgery
- Immediate admission to the ICU post operation
- Swan-Ganz catheterisation for > 12 hours after ICU admission

Over the six month period four patients fulfilled these criteria. The demographics of these four patients are shown in Table 8.1. Overall they represent a normal range of cardiovascular disorders, as well as mitral valve surgeries. Hence, they should provide a suitable initial test of the model capability in a clinical setting.

Table 8.1: Demographics of patients who underwent mitral valve (MV) surgery. CABG, coronary artery bypass surgery; AV, aortic valve; CAD, coronary artery disease; IHD, ischemic heart disease; AF, atrial fibrillation. Note CABGx2 or x4 refers to double or quadruple coronary artery bypass graft.

Patient #	**1**	**2**	**3**	**4**
Age	75	64	82	75
Sex (M/F)	M	M	M	M
Height (cm)	187	155	160	164
Weight (kg)	96	56.5	65	69
BMI (kg/m^2)	27.5	23.5	25.3	25.6
Surgery	MV repair and CABG x2	MV replacement	MV repair and CABGx4	MV repair and AV replacement
Reason for MV surgery	MV regurgitation and CAD	MV regurgitation	MV regurgitation and IHD	MV and AV regurgitation
Other diagnoses	CAD, hypertension		IHD, pulmonary hypertension, hypertension, dyslipidaemia	AV regurgitation, transient ischemic attack, AF, pneumonia, hypertension

8.2.3 MEASURED DATA

Hemodynamic measurements from the first 12 hours of ICU admission were retrospectively obtained from a secure ICU database. Swan-Ganz derived measurements of cardiac output (CO) and the pulmonary artery pressure waveform (P_{pa}) were collected. Other data collected included:

a) Hemodynamic measurements of radial arterial pressure (AP), central venous pressure (CVP) and ECG waveforms.
b) Measures of respiratory function, peak inspiratory pressure (PIP), positive end expiratory pressure (PEEP), fraction of expired oxygen (FiO2), and oxygen saturation (SpO2).
c) Administered vasoactive drugs and fluids, and urine output.
d) Patient demographics.

8.2.4 INFERRED DATA

Further data required by the parameter identification method, was inferred from each patient's demographics data or from the available measurements. A baseline total blood volume (TBV) estimation was calculated using the Nadler formula (Nadler et al., 1962). Hence, for males, TBV was calculated using:

$$TBV = 0.3669 \times height^3 + 0.03219 \times weight + 0.6041 \quad \textbf{(8.1)}$$

and for females using,

$$TBV = 0.3561 \times height^3 + 0.03308 \times weight + 0.1833 \quad \textbf{(8.2)}$$

where height is in metres and weight is in kilograms. Changes in TBV from baseline were assumed to be equal to the balance of fluid entering and exiting the patient. The total blood volume in the heart (HBV) was estimated to account for 7% of the blood in the CVS (Guyton and Hall, 2000). Furthermore, approximately 70% of the blood in the heart resides in the ventricles. Using these assumptions the total volume in the ventricles (GEDV) can be calculated from TBV using:

$$GEDV = 0.7 \times 0.07 \times TBV \quad \textbf{(8.3)}$$

In this research GEDV is refers to the sum of the maximum left and right ventricle volumes (GEDV=LVEDV+RVEDV)

Moreover, the aortic pressure waveform was derived from radial pressure using the general transfer function from the work of (Chen et al., 1997), and changes in intrathoracic pressure (P_{th}) in the model were estimated using a linear relationship with PEEP, as derived from the results of (Smiseth et al., 1996):

$$P_{th} = \frac{PEEP}{1.85} \tag{8.4}$$

where both PEEP and P_{th} are in millimetres of mercury.

8.2.5 PARAMETER IDENTIFICATION

The parameter identification method outlined in Chapter 4 was used to identify the subject-specific CVS models. Measurements used as convergence criteria for the parameter identification method were averaged over two breathing cycles. Analytical time varying elastance functions, defined by Equation (3.51), were used to represent $e_{lv}(t)$ and $e_{rv}(t)$. The tricuspid valve closure time was not required as CVP was measured. CVP was assumed to be equal to P_{vc} in the model. The closure time of the mitral and tricuspid valves were assumed to be the same. Hence, the intercept between the modelled P_{vc} and right ventricle pressure (P_{rv}) was assumed to be equal to the mitral valve closure time in the parameter identification.

In the parameter identification method, Equation (4.25) was slightly modified to better match human data (instead of pig data). To do this, P_{vc} was removed from the equation as central venous pressure does not a significant effect on left ventricle afterload in humans, and therefore, does not influence left ventricle contractility. Hence, the following equation is now used to calculate C_E:

$$C_E = \frac{P_{ao,mean,true}}{P_{ao,mean,true} + P_{pa,mean,true}} \approx \frac{E_{es,lvf}}{E_{es,lvf} + E_{es,rvf}} \tag{8.5}$$

In this study, C_E was allowed to vary with time, and thus, was not enforced as a constant for each patient in the parameter identification process, as had been done in the pigs studies of Chapters 6

and 7. This was done to allow for the possibility that C_E could change over the longer 12 hour observational period used in the human study, as opposed to relatively short 4 hour pig trials.

Through these assumptions, subject-specific CVS models were matched to the clinically obtained hemodynamic measurements. Models were identified from the clinical data at hourly intervals, from T0, representing admission to the ICU, to T12, 12 hours later. Hence, 52 subject-specific CVS models were identified for the four patients.

8.3 RESULTS

8.3.1 RECORDED DATA

All the patients initially required ventilator support on their admission to the ICU. Heart stimulants (inotropes) and fluid resuscitation were used to improve cardiac and circulatory function in conjunction with hemodynamic monitoring. These were dosed by the attending clinician. An overview of the administered therapies for each patient can be seen in Appendix B

For this research, hemodynamic measurements were recorded every hour over the first 12 hours (T0, T1, T2,... , T11, T12) after admission to the ICU. These measurement sets were pre-processed and averaged over 2 breathing cycles (approximately 6 – 12 heartbeats) before they are used in the parameter identification method. Figure 8.2 summarises these main hemodynamic measurements for each patient.

On average, mean aortic pressure increased from 78.0 to 89.3 mmHg, mean pulmonary artery pressure dropped from to 33.3 to 23.8 mmHg, stroke volume improved from 48.6 to 65.0 ml, and heart rate decreased from 83.2 to 73.3 bpm, over the 12 hour period. Individually, Patients 1, 2, and 3 had similar trends including a relatively constant aortic pressure, decreasing pulmonary artery pressure, increasing stroke volume, and decreasing heart rate. In contrast, a large increase in aortic pressure and a drop in stroke volume are noticed for Patient 4, as seen on Figure 8.2. Hence, Patients 1-3 were following the clinically desired path, while Patient 4 was less stable or certain in recovery.

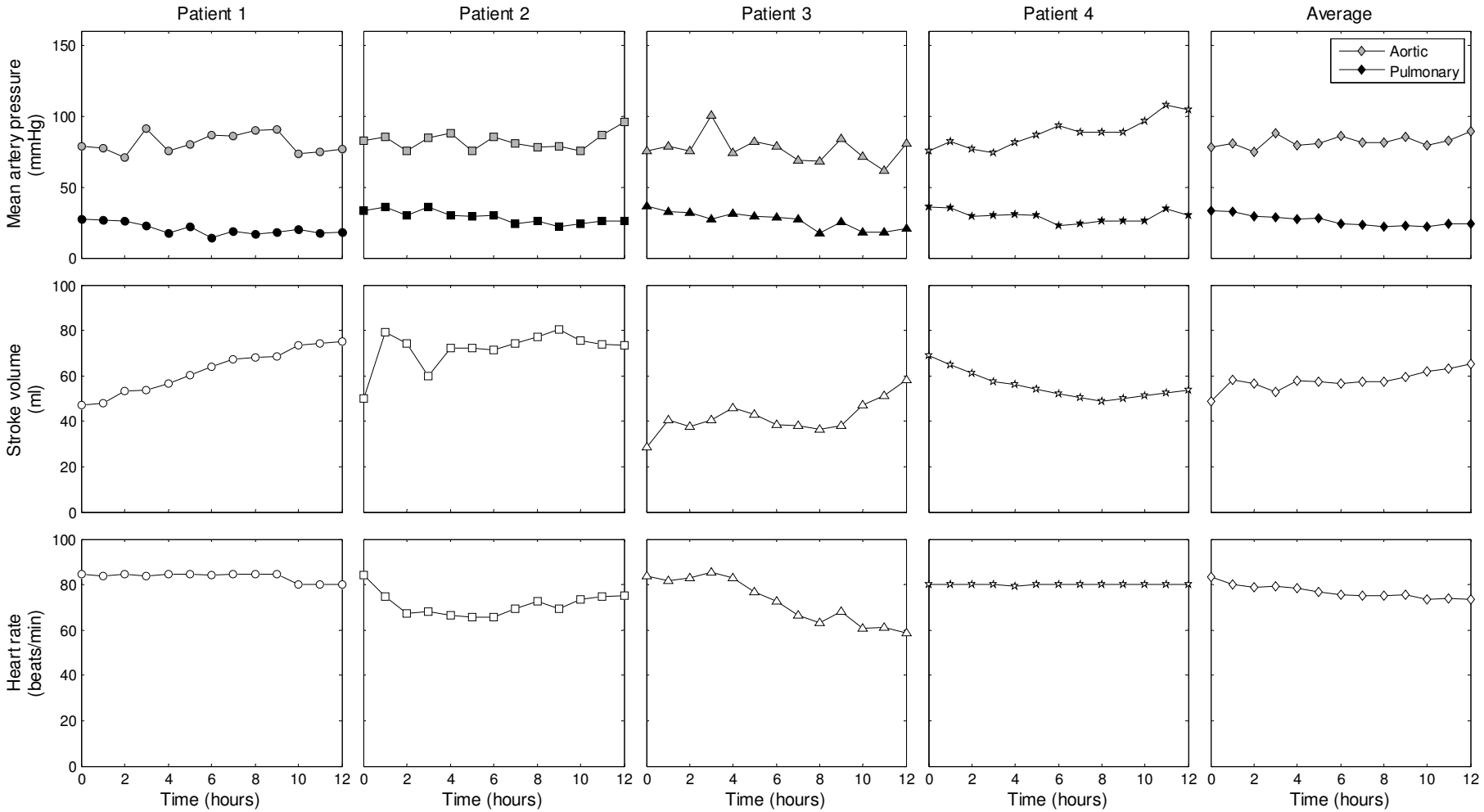

Figure 8.2: Evolution of the patient-specific hemodynamic vital signs recorded during the first 12 hours post mitral valve surgery.

8.3.2 PATIENT-SPECIFIC MODELS

Patient-specific CVS models were fitted to the data sets at one hour intervals (T0-T12, 13 per patient). Modelled indices of preload (LVEDV, RVEDV), afterload, (R_{sys}, R_{pul}), and contractility ($E_{es,lvf}$, $E_{es,rvf}$) were analysed along with the left ventricle filling pressure (P_{pu}) of the left ventricle, as shown in Figure 8.3.

8.3.2.1 Preload

Left and right ventricle preload, as analysed through the modelled LVEDV and RVEDV, increased in all patients. This result was expected as all patients had been administered fluids and had a positive fluid balance after 12 hours of admission to the ICU (see Appendix B). The increased preload partially explains the average increase in measured SV seen in these patients, as shown on Figure 8.1.

8.3.2.2 Afterload

Left ventricle afterload, represented by R_{sys} in the model, stayed relatively constant in Patients 1, 2, and 3. In Patient 4, R_{sys} increased constantly throughout the 12 hours. The resulting increase in left ventricle afterload was most likely responsible for the observed increase in mean aortic pressure, and the decrease in SV, which is consistent with the known ventricular response to increased afterload (Klabunde, 2004).

In contrast, right ventricle afterload, represented by R_{pul} in the model, decreased for Patients 1, 2, and 3. These findings are expected due to the inhibition of pulmonary arteriolar vasoconstriction mechanisms post surgery (Foltz et al., 1984). The decrease in R_{pul} is partially responsible for the decrease in the measured pulmonary artery pressures in these patients. No substantial change in R_{pul} was observed in Patient 4 throughout the 12 hour period. This result explains why there was only a minor drop in mean pulmonary artery pressure in Patient 4.

8.3.2.3 Contractility

Identified left ventricular contractility ($E_{es,lvf}$) increased in Patients 1, 2, and 3, indicating improved contractile state. In Patient 4, $E_{es,lvf}$ decreased, signifying a depressed cardiac state. These changes in left ventricle contractility partially account for the increase in SV seen in Patients 1-3 and the decrease in SV seen in Patient 4.

For Patients 1, 2, and 3 no substantial change was seen in right ventricular contractility ($E_{es,rvf}$). However a large drop was observed in Patient 4. This result further suggests the cardiac state of Patient 4 is depressed post mitral valve repair.

8.3.2.4 Left ventricle filling pressure

In the model, the left ventricle filling pressure is represented by the pulmonary vein pressure (P_{pu}). P_{pu} is highly rated to the end systolic pressures in the left ventricle, which are elevated during mitral regurgitation. Thus, a drop in P_{pu} should occur as the cardiovascular system adapts to the cessation of regurgitant flow post mitral valve correction (Foltz et al., 1984). As expected, P_{pu} decreased in all patients 12 hours after admission to the ICU. This drop in pulmonary vein pressure is partially responsible for the decline in pulmonary artery pressures, indicating a decreased likelihood of pulmonary congestion in these patients

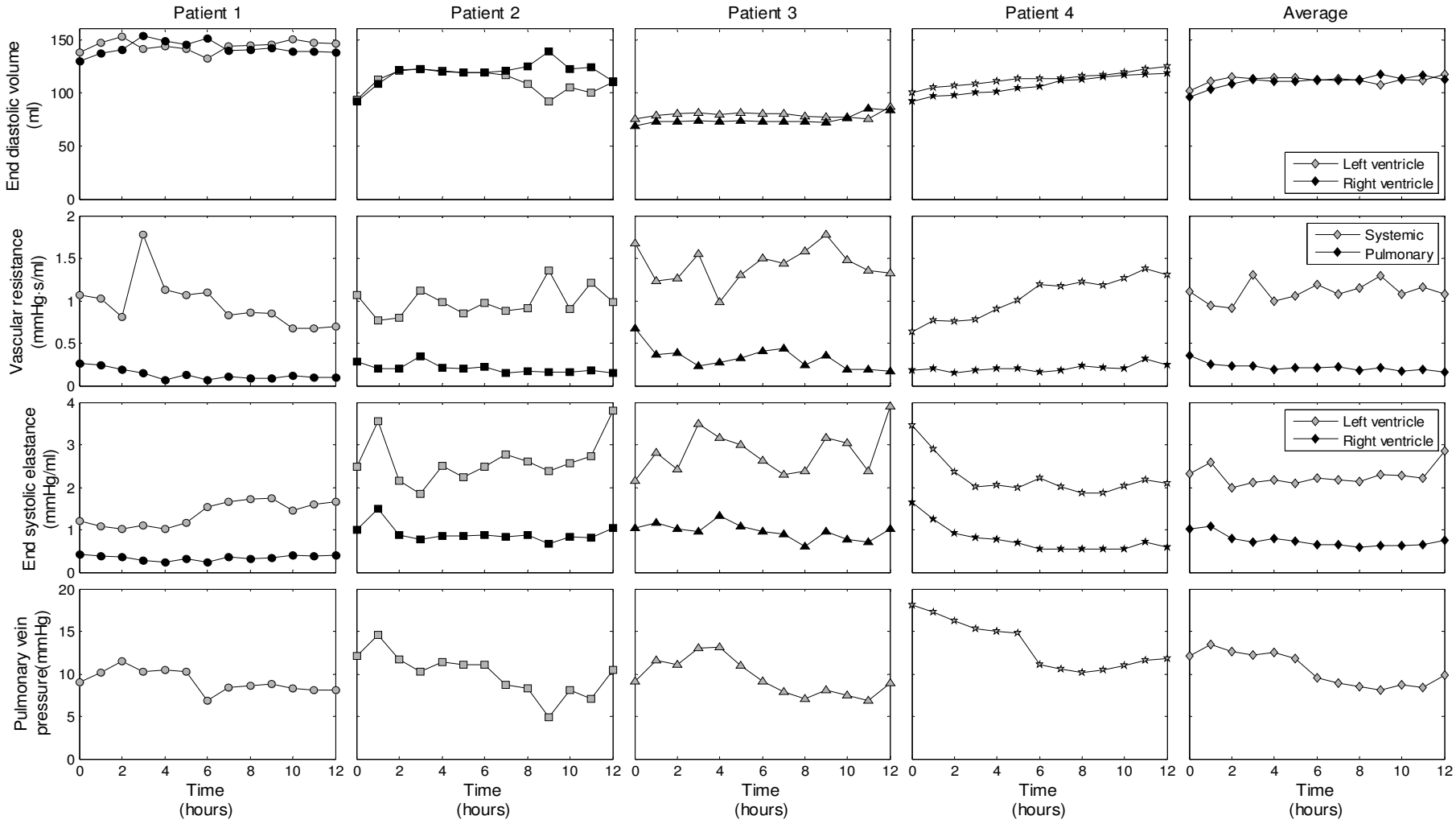

Figure 8.3: Evolution of the patient-specific metrics of preload (left and right end diastolic volumes), afterload (systemic and pulmonary vascular resistance), contractility (left and right ventricular end diastolic elastances), and ventricular filling pressures (pulmonary vein pressure) identified from the CVS model.

8.4 DISCUSSION

8.4.1 MODEL-BASED APPROACH

The model-based approach used in this chapter provides a way of approximating metrics of preload (LVEDV, RVEDV), afterload (R_{sys}, R_{pul}), and contractility ($E_{es,lvf}$, $E_{es,rvf}$), post mitral valve operation. Metrics specific to mitral insufficiency could also be tracked, such as pulmonary vein pressure, an important metric of mitral regurgitation and pulmonary congestion. Thus, the identified CVS models can be used to reveal the hemodynamic reasons why the patients react differently to the mitral valve correction.

The parameter identification method only used measurements that were taken as part of normal clinical care. Thus, these measurements reflect a realistic uncontrolled clinical scenario. Most of these measurements, except for the patient demographic data, can be continuously measured and electronically stored to a database. Hence, the approach has the potential to be automated and to provide real time information to make therapeutic decisions. Further potential benefits of the approach are that it could be implemented at little extra cost and effort as it does not require any additional hardware, measurements, or interventions from the medical staff.

8.4.2 PATIENT-SPECIFIC MODELLING OF HEMODYNAMIC RECOVERY

The patient-specific models observed a decrease in pulmonary vein pressure and a decrease in R_{pul} over the duration of the study. The combination of these factors explains the decrease in pulmonary artery pressure in the patients. These results are consistent with the findings of Foltz et al. (Foltz et al., 1984) whom found that mitral regurgitation-induced elevated left ventricle filling pressures and pulmonary vasoconstriction are rapidly reversed post mitral valve surgery.

The patient-specific CVS models observed clinically relevant signs of cardiac recovery in 3 of the 4 patients in the study (Patients 1, 2, and 3). Left ventricle filling pressures decreased (Braunwald et al., 1965, Starling, 1995) and left ventricular contractility increased (Starling, 1995), leading to increased cardiac output in these patients. These results indicate the cardiovascular system is compensating well to the alterations in mitral valve function.

In the other patient (Patient 4), a decreased left and right ventricle contractility and increased systemic resistance was noticed, contributing to a decrease in stroke volume and increase in aortic pressure. The combination of these factors caused left ventricle dilation. This effect is symptomatic of patients with decompensated hearts, where an increase in left ventricle afterload after valve

replacement leads to a decline in ejection fraction (Goldfine et al., 1998, Zile et al., 1985). The mitral valve surgery has effectively removed the low resistance conduit for backwards ejected flow from the ventricle. Thus, the left ventricle can only eject through the high resistance conduit of the systemic circulation. The weakened contractile state of the left ventricle in Patient 4 does not appear to be able to compensate for this apparent increase in afterload (Leung et al., 1996, Zile et al., 1985, Goldfine et al., 1998). Hence, the CVS model of Patient 4 indicates that ventricular dilation and decreased left ventricular end systolic elastance are responsible for the decrease in stroke volume, leading to decreased ejection fraction, which is common after surgical correction of the mitral valve (Suri et al., 2008). The identified model parameters for Patient 4 also show a decoupling between the ventricular and arterial system due to decreased left ventricular function an increased left ventricular afterload. This decoupling indicates the transfer of blood between the ventricle and arterial system is becoming less efficient. These examples illustrate how patient-specific models can be used differentiate patients with compensated cardiac function from patients with decompensated cardiac function after mitral valve repair or replacement. Hence, the model can be used to track the progression of recovery in ICU patients post mitral valve surgery.

8.4.3 LIMITATIONS

The heart valves in the CVS model do not allow backwards flow. Hence, the model is unable to simulate the effects of residual mitral regurgitation post surgery. However, in most cases this is not a problem as the regurgitation is normally minimal or non-existent immediately after mitral valve replacement or repair (Bolling et al., 1998, Flameng et al., 2003, Foster et al., 2007).

Population-based empirical equations were used to estimate the total blood volume and global end diastolic volume. These equations are not dependent on the cardiovascular state of the patient, and thus, may not precisely reflect the true value. However, they provide good initial approximations for the baseline (T0) convergence criteria and can be used in conjunction with the known fluid balance to interpret trends in the later identified CVS models (T1, T2, ...,T12).

8.5 SUMMARY

Patient-specific CVS models were retrospectively fitted to hemodynamic measurements taken from patients recovering from mitral valve surgery in the ICU. The model-based approach was able to track known trends in preload, afterload, and contractility in the patients, post mitral valve surgery.

A decrease in pulmonary artery pressure was observed due to a decrease in pulmonary vein pressure and pulmonary vascular resistance, a known response to mitral valve correction, leading to decreased pulmonary congestion. Furthermore, through analysis of contractility and preload, the approach was able to differentiate between patients with compensated and decompensated hearts. Thus, the method was able to discriminate between patients who responded positively against patients who responded negatively to the surgery during the first 12 hours of recovery. Hence, this chapter illustrates the clinical potential of patient-specific models in an ICU setting.

CHAPTER 9: AORTA MODEL

A model of arterial dynamics is used to describe the relationship between pressure and flow in the arterial system. The arterial model provides a more detailed description of arterial flow than the six-chamber model of Chapter 3, but is a less comprehensive description of global cardiovascular dynamics. Hence, the arterial flow model is introduced in this chapter as an alternative modelling modality that can be used when modelling arterial dynamics is more important than simulating the hemodynamics of the whole CVS.

9.1 INTRODUCTION

A better understanding of the factors contributing to morphological changes in the aortic pressure waveform may help assist with analysing disease and treatment dependent hemodynamic changes that occur in the ICU patient (Mitchell et al., 2004, Hope et al., 2005, Thiele and Durieux, 2011). Model-based approaches can be used to help provide insights into the components that contribute to the shape of the aortic waveform. In 2003, Wang et al. (Wang et al., 2003) combined windkessel (Frank, 1898) and wave theories (Parker and Jones, 1990) to create a model of aortic hemodynamics that described the main components that make up the aortic pressure pulse. This model was able to account for the difference in shape between the aortic pressure and flow waveforms (Davies et al., 2007, Wang et al., 2003), and suggested wave reflections only make a minor contribution to the shape of the aortic pressure waveform (Davies et al., 2010, Wang et al., 2003).

This model was initially derived from windkessel theory (Frank, 1898), which treats the arterial system as an elastic reservoir. This reservoir acts as a hydraulic integrator, storing the flow going into the arterial system as volume. The changes in volume (ΔV_{wk}) of the arterial reservoir are related to changes in pressure (ΔP_{wk}) by the lumped compliance (C) of the arterial system, where ΔV_{wk} is simply the difference between the flow in (Q_{in}) and out (Q_{out}) of the arterial system.

Following the windkessel theory, Lighthill (Lighthill, 1978) suggested that the difference between the pressure generated by the 2-element windkessel model and the measured aortic pressure could be the result of pressure generated due to wave motion. He named this difference the excess pressure (P_{ex}). Hence, excess pressure is defined as the difference between the aortic pressure and reservoir pressure ($P_{ex} = P_{ao} - P_{wk}$). By combining these two theories in a model, Wang et al. (Wang et al.,

2003) found that the shape of the P_{ex} closely matched the shape of Q_{in}, indicating the two variables were related by the proximal resistance of the aorta ($R_{prox} = Q_{in}/P_{ex}$). Hence, through consideration of these findings, the following model representing flow and pressure in the aorta can be derived, as shown in Figure 9.1. In Figure 9.1, P_∞ represents the downstream pressure to which the aortic diastolic pressure decays, R symbolises the peripheral systemic resistance, and C is the lumped compliance or capacitance of the arterial system.

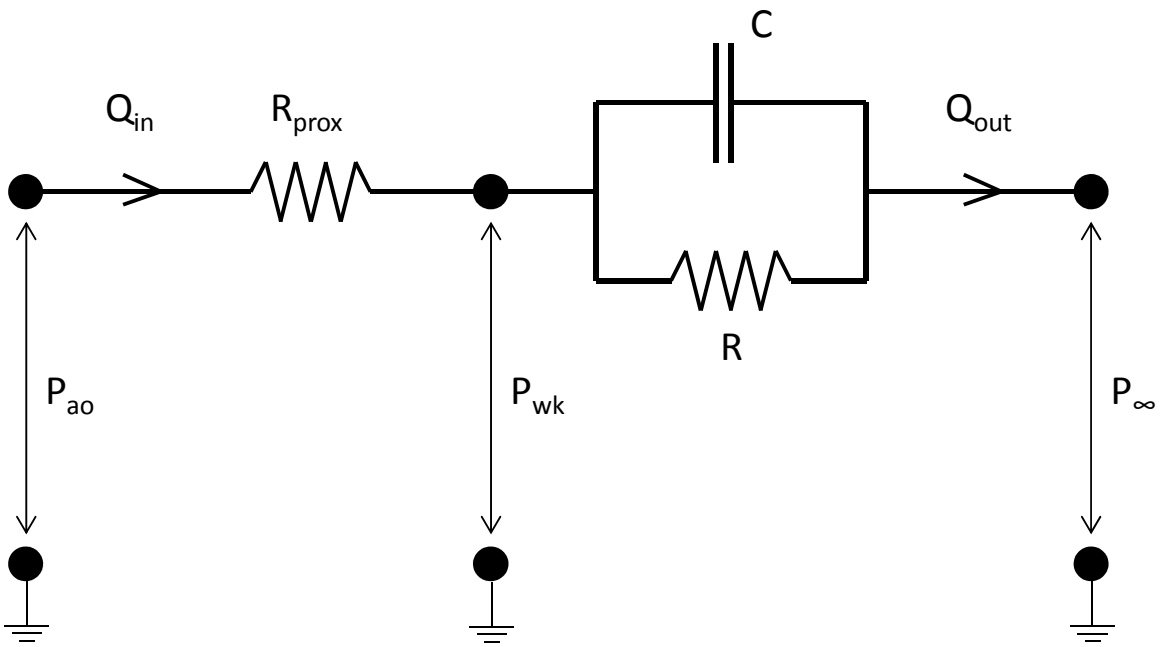

Figure 9.1: Schematic of the modified aortic model used in this research showing the flows in and out of the arterial system (Q_{in}, Q_{out}), the aortic pressure (P_{ao}), reservoir pressure (P_{wk}). The parameters of the system are: R_{prox}, proximal resistance of the aorta; C, compliance of the arterial system; R, peripheral systemic resistance; and P_∞ the downstream pressure of the arterial system.

In this model, the excess pressure component (P_{ao} - P_{wk}) describes pressure due to the dynamic viscous effects of the forward and backward travelling waves in the aorta. Whereas, the reservoir pressure simulates the ability of the arterial system to absorb flow ejected from the heart, store that flow as potential energy and volume, and release the volume later during the heartbeat as diastolic flow. Essentially, the arterial reservoir acts as means of spreading systolic flow ejected from the ventricle across the whole heartbeat before it reaches the capillaries. Thus, the reservoir helps smooth the flow of blood, oxygen, and nutrients to the organs of the body. An example of the aortic model splitting aortic pressure into its reservoir and excess pressure components is shown in Figure 9.2.

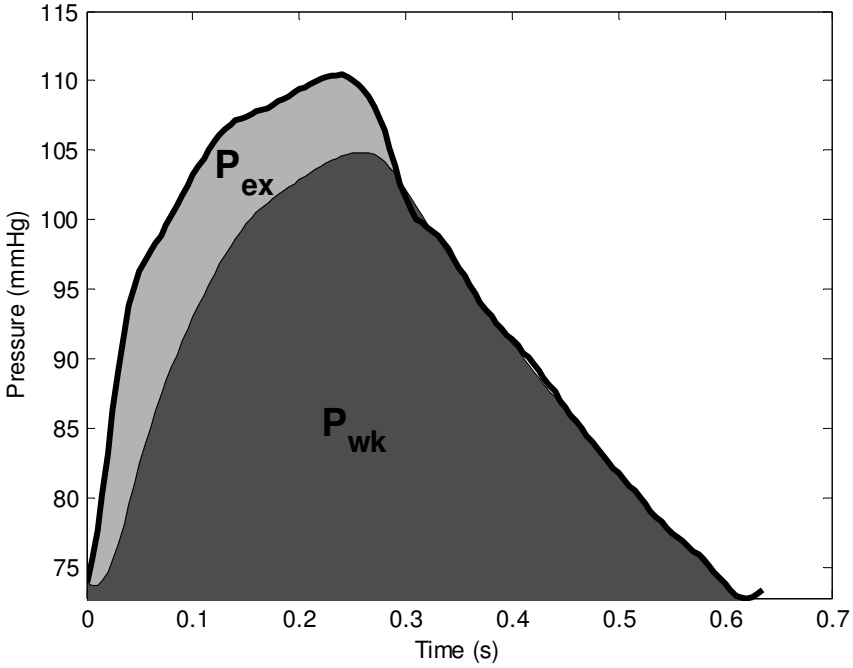

Figure 9.2: Aortic pressure separated into reservoir (P_{wk}) and excess pressure (P_{ex}) components.

The aorta model can be used to provide insight into how energy and blood is transferred from the ventricle, through the arterial system, and into the capillaries. The following sections develop the equations, discuss the validity of the assumptions, and outline the limitations of this model.

9.2 MODEL ASSUMPTIONS

The assumptions used to create the arterial flow model are:

- Conservation of mass
- Poiseuille flow
- Constant resistances, compliances, and downstream pressure
- Backwards wave reflections are minimal during systole in the central aorta
- The shape of the P_{ex} and Q_{in} are the same
- Reservoir pressure is independent of position in the arterial system

The validity of these assumptions is analysed in Section 9.5.

9.3 MODEL DEVELOPMENT

The arterial flow model is based on the work of (Wang et al., 2003). It is proposed that the arterial pressure waveform is made of two components representing: 1) the time-varying reservoir pressure (P_{wk}), which is independent of position along the arterial tree, and 2) the excess pressure (P_{ex}) which is dependent on time (t) and distance along the arterial tree (x):

$$P_{ao}(x,t) = P_{wk}(t) + P_{ex}(x,t) \tag{9.1}$$

Frank Otto's windkessel theory states that P_{wk} can be determined by assuming conservation of mass and a linear relation between pressure and volume:

$$\frac{dP_{wk}(t)}{dt} = \frac{dP_{wk}(t)}{dV_{wk}(t)} \frac{dV_{wk}(t)}{dt} = \frac{Q_{in}(t) - Q_{out}(t)}{C} \tag{9.2}$$

where,

$$C = \frac{dV_{wk}(t)}{dP_{wk}(t)} \tag{9.3}$$

In Equations (9.2) and (9.3), the linear relation between windkessel pressure and volume is represented by compliance (C). The flow out of the arterial system (Q_{out}) is defined assuming poiseuille resistance (R) and a constant pressure downstream sink (P_∞):

$$Q_{out}(t) = \frac{[P_{wk}(t) - P_\infty]}{R} \tag{9.4}$$

Hence, the driving force of the flow out of the arterial system is assumed to be pressure difference between P_{wk} and P_∞. P_∞ represents the asymptotic level to which diastolic pressure would decay if the heart stopped beating, and R symbolises the resistance of the peripheral circulation. Thus, substituting Equation (9.4) into Equation (9.2) gives:

$$\frac{dP_{wk}(t)}{dt} + \frac{P_{wk}(t) - P_\infty}{RC} = \frac{Q_{in}(t)}{C} \tag{9.5}$$

which has the general solution:

$$P_{wk}(t) - P_{\infty} = (P_0 - P_{\infty})e^{\left(\frac{-t_0}{\tau}\right)} + e^{\left(\frac{-t}{\tau}\right)} \int_{t_0}^{t} \frac{Q_{in}(t')}{C} e^{\left(\frac{t'}{\tau}\right)} dt' \quad \textbf{(9.6)}$$

where t_0 and P_0 are the time and pressure at the beginning of ejection and $\tau = RC$, the time decay constant. Equation (9.6) describes a hydraulic integrator where P_{wk} is related to the integral of Q_{in}. When $Q_{in} = 0$, as in diastole, Equation (9.6) simply describes a decaying pressure profile of decay rate τ.

In this research, the reflected or backward travelling waves are assumed to be negligible in the central aorta. Hence, Q_{in} is assumed to be linearly proportional to P_{ex}, as indicated by the work of (Wang et al., 2003), giving:

$$P_{ex}(t) = Q_{in}(t) R_{prox} \quad \textbf{(9.7)}$$

where R_{prox} symbolises the proximal viscous resistance of flow in the aorta. Please note that P_{ex} is now only a function of time. Substituting Equations (9.6) and (9.7) into Equation (9.1) gives:

$$P_{ao}(t) = P_{\infty} + (P_0 - P_{\infty})e^{\left(\frac{-t_0}{\tau}\right)} + e^{\left(\frac{-t}{\tau}\right)} \int_{t_0}^{t} \frac{Q_{in}(t')}{C} e^{\left(\frac{t'}{\tau}\right)} dt' + Q_{in}(t) R_{prox} \quad \textbf{(9.8)}$$

Equation (9.8) is now analogous to a 3-element windkessel model. The inputs, outputs and parameters of the aorta model are outlined in Table 9.1.

Table 9.1: Inputs, outputs, and parameters of the aorta model.

	Symbol	Description	Units
Inputs	Q_{in}	Flow into the aorta	ml/s
Outputs	P_{ao}	Aortic pressure	mmHg
	P_{wk}	Reservoir/windkessel pressure	mmHg
	P_{ex}	Excess pressure	mmHg
	Q_{out}	Flow out of the arterial system	ml/s
Parameters	R_{prox}	Proximal resistance of the aorta	mmHg.s/ml
	C	Compliance of the arterial system	ml/mmHg
	R	Peripheral systemic resistance	mmHg.s/ml
	P_{∞}	Downstream pressure of arterial system	mmHg

9.4 SIMULATION

The aorta model was simulated in Matlab. Q_{in}, as the only input, was used to drive the model. The Matlab function 'cumtrapz', which uses the trapezium rule to approximate an integral, was used to numerically integrate Q_{in}, as required by Equation (9.8). An example of inputs and simulated outputs of the aorta model for a healthy swine are shown in Figure 9.3. The parameter values used for this simulation are listed in Table 9.2.

Table 9.2: Parameters used to simulate healthy swine hemodynamics.

Parameter	Value
R_{prox}	0.1072 mmHg.s/ml
C	0.4734 ml/mmHg
R	1.3229 mmHg.s/ml
P_{∞}	30 mmHg

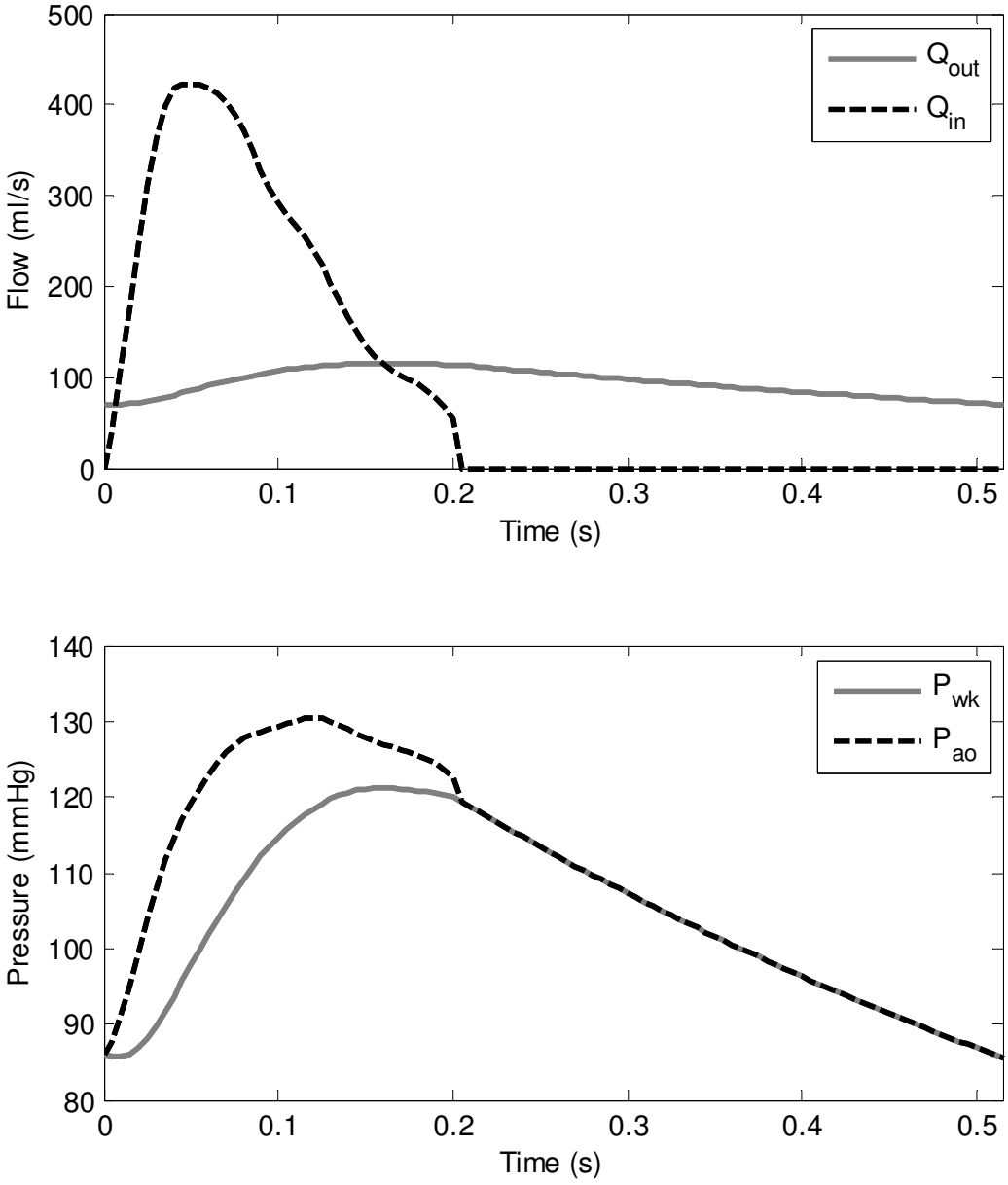

Figure 9.3: Example of the inputs and outputs of the model used to simulate healthy aortic hemodynamics in a pig. The flow into the aorta (Q_{in}) acts as the input for the model and flow out of the arterial system (Q_{out}), aortic pressure (P_{ao}), and reservoir pressures (P_{wk}) represent the outputs of the model.

9.5 DISCUSSION

9.5.1 VALIDITY OF ASSUMPTIONS AND MODELLING CONCEPTS

Many of the assumptions used in the aorta model have been previously discussed in Section 3.6.1, and thus will not be discussed further here. The new and most controversial assumptions used in this model are: 1) backward wave reflections are minimal during systole, and hence, the shape of P_{ex} is the same as Q_{in}; and 2) the reservoir pressure (P_{wk}) is independent of the position in the arterial system.

The first assumption is based on the findings of Davies et al. (Davies et al., 2010), who found that backward wave reflections only make a small contribution to the augmentation index in hypertensive patients. Moreover, the model is only intended to model central aorta dynamics, where backwards travelling waves are small during systole (Aguado-Sierra et al., 2008). Therefore, the author feels justified in making this assumption, and that it will have minimal impact in the situations expected in this work, validating this assumption, particularly for examining dynamics at the aorta.

The second assumption, that the reservoir pressure is independent on position in the arterial system, is based on the results of (Davies et al., 2007). In this study, it was shown that the shape of the reservoir pressure is relatively constant when calculated from measurements taken from different parts of the arterial system. Thus, reservoir pressure is essentially a constant of the arterial system.

9.5.2 MODEL SIMULATION

An example simulation of the aorta model is shown in Figure 9.3. In this simulation, the aortic pressure and reservoir pressure are the same during diastole. However, during systole P_{ao} is higher than P_{wk} due to the addition of the excess pressure generated from the viscous effects of Q_{in}. The difference in the shapes of Q_{in} and Q_{out} result from the storage capacity of the arterial reservoir, which absorbs some of the flow during systole and releases it during diastole. This ability helps the arterial system smooth the flow of blood before it hits the capillaries, ensuring that the organs of the body have a constant supply of oxygen and nutrients.

9.5.3 LIMITATIONS

The assumption that there are no backward travelling waves augmenting the pressure during systole limits the ability of the model to simulate more distal parts of the arterial system. Arteries that are further from the heart are more likely to encounter backward travelling waves during systole, as they are closer to the wave reflection sites. P_{ex} at these points will thus be a combination of pressure due to viscous effects of the forward flow, Q_{in}, and the backwards flow, meaning that the assumption that the shape of Q_{in} is equal to the shape of P_{ex} will no longer be valid.

9.6 SUMMARY

A model of arterial flow has been adapted to represent blood flow in the central aorta. This model separates aortic pressure into two components representing the compliant nature of the arterial system, called the reservoir pressure, and wave-phenomena, called the excess pressure. The model developed provides a foundation for subject-specific modelling of the aortic hemodynamics, specifically, how blood and energy is passed from the left ventricle to the aorta and onto the capillaries.

CHAPTER 10: AORTA MODEL ENERGETICS IN SEPTIC SHOCK

The aorta model of Chapter 9 is identified using aortic pressure and SV measurements from a porcine study of septic shock. The goals of this chapter are to: 1) help understand how the transfer of flow and energy, through the arterial system, is affected during septic shock; and 2) explain why the shape of aortic pressure waveform changes during septic shock.

10.1 INTRODUCTION

Arterial pressure and cardiac output (CO) are two of the main measures of cardiovascular health in the ICU. However, recently, the efficiency of hemodynamic monitoring to affect outcome has been questioned (Pinsky, 2003). The positive impact of CO and/or stroke volume (SV) monitoring has not been proven to affect outcome (Mutoh et al., 2007, Pinsky, 2007). Furthermore, although continuous blood pressure monitoring of the arterial waveform is commonplace, the most commonly used blood pressure indices ignore the shape of the arterial waveform and are calculated from discrete measurements of systolic and diastolic pressure. All the valuable morphological information stored in the form of the arterial pulse is ignored. These findings suggest that arterial pressure and SV are underutilised in guiding diagnosis and treatment in the intensive care environment.

This chapter looks at utilising SV and the shape of the aortic pressure waveform to better understand the dynamics of arterial flow and ventricular arterial coupling. The approach used in this chapter was based on the work of (Wang et al., 2003, Davies et al., 2010, Tyberg et al., 2009), where the aortic pressure is separated into two components representing the reservoir pressure and the excess pressure. These components were identified using measurements from a porcine study of septic shock (Lambermont et al., 2006) to create subject-specific models of aortic blood flow.

It is hypothesised that the work of the excess pressure represents the contractile state of the ventricle and that the reservoir pressure component is the energy that needs to be overcome for forward flow. Hence, the ratio of the excess pressure and reservoir work may represent a metric of ventricular arterial coupling. To test this hypothesis the modelled hydraulic energies of these components were compared to metrics obtained from left ventricular pressure-volume (P-V) loops, to understand their relationship to ventricular arterial (de)coupling during septic shock.

10.2 METHODS

10.2.1 PORCINE TRIALS AND MEASUREMENTS

All procedures and protocols used were approved by the Ethics Committee of the Medical Faculty at the University of Liege, Belgium. Experiments were performed on 4 healthy pure Pietrain pigs weighing between 20-30kg. The animals were premedicated, anesthetised, and ventilated as explained in (Lambermont et al., 2006). The animals received a 0.5-mg/kg endotoxin infusion over 30 minutes (from T0 to T30) to induce septic shock. Micro-tipped catheters were used to record continuous hemodynamic measurements during the study. Every 30 minutes (T0 to T120) 6-20 central aortic pressure waveforms (P_{ao}) were recorded. At the same time, descending left ventricular pressure-volume (P-V) loops (P_{lv}, V_{lv}) were stored during transient occlusion of the inferior vena cava. All measurements were recorded at a 200Hz sampling rate. In this study, 36 sets of measurements from the 4 pigs were used. Further details on these trials can be found in (Lambermont et al., 2006)

10.2.2 MODEL IDENTIFICATION

The measurements used in this study to identify the arterial model were the P_{ao} waveform and SV. Both measurements can be measured or inferred in the ICU. SV can be measured using a thermo-dilution technique (Ganz et al., 1971, Stetz et al., 1982), and P_{ao} can either be measured or estimated using one of the following methods (Chen et al., 1997, Cloud et al., 2003, Hope et al., 2004, O'Rourke, 2004, Pauca et al., 2001, Westerhof et al., 2008). To personalise Equation (9.8) from Chapter 9 to each subject the parameters τ, C, R_{prox}, and P_{∞} must be identified from these measurements, along with the Q_{in} waveform.

Initially, Q_{in} was estimated by drawing a line, across the aortic pressure pulse, from the start of ejection to the first diastolic point. The diastolic point was assumed to be the point of the maximum negative gradient between the aortic notch and maximum pressure in the measured P_{ao}. The difference between this line and the aortic pressure was used to approximate P_{ex}. To approximate Q_{in}, P_{ex} was scaled to have an area equal to SV, as Q_{in} is assumed to be linearly proportional to P_{ex}. The model was then fitted using this estimate of Q_{in} and initial approximations for τ, C, R_{prox}, and P_{∞}. The non-linear optimisation routine 'fminsearch' in Matlab, utilising a Nelder-Mead simplex method, was used to fit the model to one full period of the P_{ao} waveform.

During fitting a greater weighting was applied to the minimisation of error in the last 2/3 of diastole as it is believed that wave effects are minimal at this time (Wang et al., 2003). The P_{wk} and P_{ex} were

then separated from the modelled P_{ao}, and P_{ex} was scaled to calculate a new Q_{in}. This whole process was repeated with Equation (9.8) re-fitted to the measured P_{ao} to calculate new approximations for τ, C, R_{prox}, and P_{∞}. This process was repeated until the root-mean-square error over systole was less than 0.1%.

10.2.3 DATA AND STATISITICAL ANALYSIS

Hemodynamic measurements are presented as mean +/- standard deviation (SD). A paired sample t-test was used to check temporal variance over T0 - T60 to analyse the effect of the endotoxin intervention. P<0.05 was considered a statistically significant result. Windkessel models were fitted to 36 sets of measurements from the 4 pigs, over all time points.

Hydraulic work (W_{ao}) was calculated for each measurement by summing the work of the reservoir and excess pressure components of the aortic model ($W_{ao} = W_{wk} + W_{ex}$) at the end of systole, where W_{ex} is defined as the hydraulic work done at the end of systole. Left ventricular work (W_{lv}) was calculated from the area enclosed by the measured P-V loop. W_{ao} and W_{lv} were calculated using:

$$W_{ao} = W_{wk} + W_{ex} = \int_{t_0}^{t_{es}} P_{wk}(t)[Q_{in}(t) - Q_{out}(t)]dt' + \int_{t_0}^{t_{es}} P_{ex}(t)Q_{in}(t)dt' \quad \textbf{(10.1)}$$

$$W_{lv} = \int_{V_0}^{V} P_{lv}(t)dv' \quad \textbf{(10.2)}$$

where t_0 represents the start of ejection and t_{es} stands for the time of end systole. End of systole represents the time when the maximum amount of hydraulic energy is stored in the aortic reservoir.

The ratio of the W_{ex} to the W_{wk} was analysed and compared to the clinical gold standard ventricular arterial coupling metric, E_{es}/E_a, calculated from ventricular P-V loop analysis, as shown in Figure 10.1. End systolic elastance (E_{es}) is defined as the gradient of the linear least squares fit to the end systolic points in a series of descending P-V loops, representing the left ventricular contractility. Left ventricular afterload (E_a) is the gradient of the line from the origin in Figure 10.1 to the end systolic point of the first P-V loop, recorded before vena cava occlusion, a highly invasive manoeuvre.

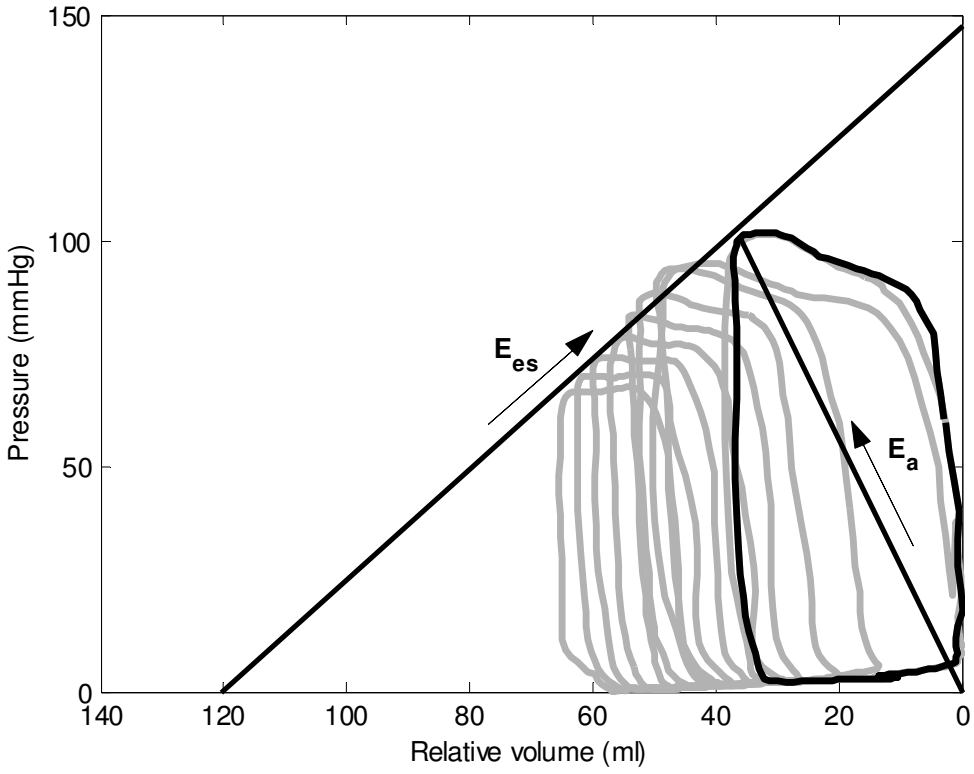

Figure 10.1: Left ventricular pressure volume loop analysis used to calculate end systolic elastance (E_{es}) and afterload (E_a) during a vena cava occlusion manoeuvre.

The volume stored in the aortic reservoir (V_{wk}), which is equal to the aortic volume (V_{ao}), was calculated by multiplying P_{wk} by the aortic compliance.

$$V_{ao} = V_{wk} = CP_{wk} \quad \textbf{(10.3)}$$

10.3 RESULTS

The windkessel model was fitted to the 36 sets of measurements from the 4 pigs. In this study, each animal acts as their own control with baseline (T0) measurements reflecting the undiseased state of the pig. The temporal variance in the measurements of the cohort were analysed between T0-T30, as well as T0-T60 and T30-T60. The reason temporal variance was analysed over T0-T60 and T30-T60 is because sometimes the symptoms of septic shock do not manifest immediately after the endotoxin infusion at T0 to T30. Statistically significant temporal changes ($P<0.005$) were noticed in the measured mean arterial pressure (MAP), left ventricular end diastolic volume (LVEDV), heart rate (HR), and maximum left ventricular pressure ($P_{lv,max}$) over the first hour, underlining the pathological

changes occurring in the animals due to the endotoxin infusion. A summary of the main hemodynamic measurements is seen in Figure 10.2.

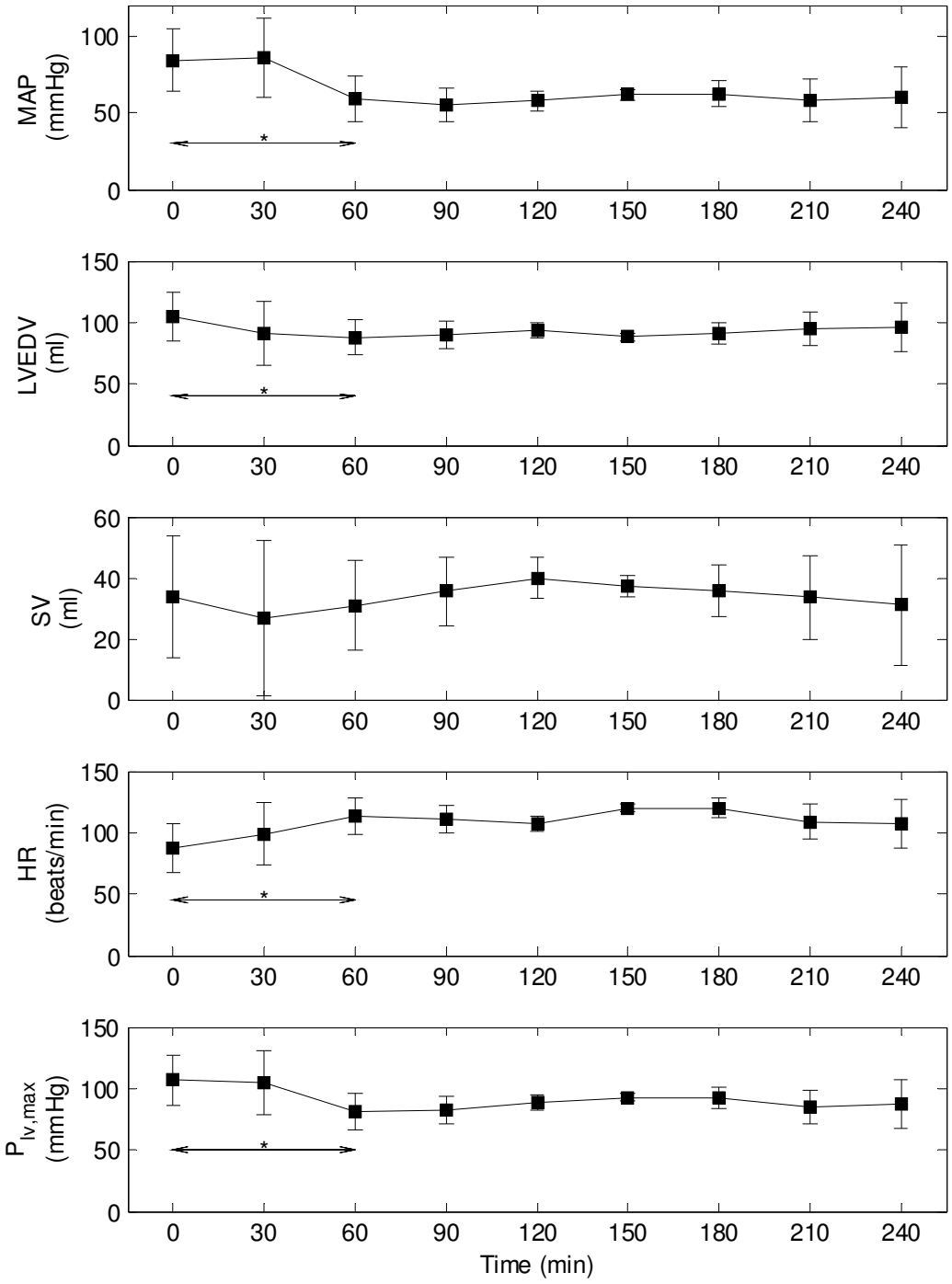

Figure 10.2: Evolution of mean arterial pressure (MAP), left ventricular end diastolic volume (LVEDV), stroke volume (SV), heart rate (HR), and maximum left ventricular pressure ($P_{lv,max}$) measurements during the trials. * indicates P<0.05 for expected temporal changes over T0-T30, T30-T60, or T0-T60 due to the induction of septic shock. Data presented as mean +/- SD.

10.3.1 COMPARISON OF VENTRICULAR AND ARTERIAL WORK

To verify the aortic model, the hydraulic energy of the aortic flow, calculated from model, was compared to the measured left ventricular work. The comparison between the hydraulic work and the area enclosed by measured P-V loops, is shown in Figure 10.3. W_{ao} matched W_{lv} to a bias and 2 standard deviations of -0.15 J +/- 0.13 J (as seen on Figure 10.3), and with a correlation coefficient of R^2 = 0.88. These results indicate that W_{ao} underestimates ventricular work, but, more importantly, closely follows the changes in W_{lv} that occur during the trials.

10.3.2 EFFECTS OF SEPTIC SHOCK ON AORTIC ENERGETICS AND VOLUME

The effects of septic shock on the aortic model were analysed by tracking the changes in W_{ao}, W_{ex}, and W_{wk}, throughout the duration of the experimental study. In this analysis, W_{ex} can be interpreted as the work required to overcome the resistance of the large arteries, whereas W_{wk} reflects the maximum potential energy stored in the arterial reservoir due to elastic distension of the arterial walls. The change in magnitudes of W_{ao}, W_{wk}, and W_{ex} (averaged across the four pigs) at 30 minute intervals during the experimental study are shown in Figure 10.4. Initially, at T0, W_{wk} makes up the majority of W_{ao}. However, after the endotoxin infusion, the magnitude of W_{wk} decreases, and W_{ex} increases to a point where they are approximately equal by the end of the experiment.

A decrease in W_{wk} indicates that a smaller proportion of the SV is being stored in the elastic arterial system for release during diastole. Figure 10.5 reinforces this point, showing the percentage of SV stored in the arterial reservoir, averaged across the four pigs. This ratio drops from a baseline level of 59.2% to 48.6% by the end of the study. This result is most likely due to a decrease in vascular tone due to the inflammatory effects of the endotoxins in the circulation.

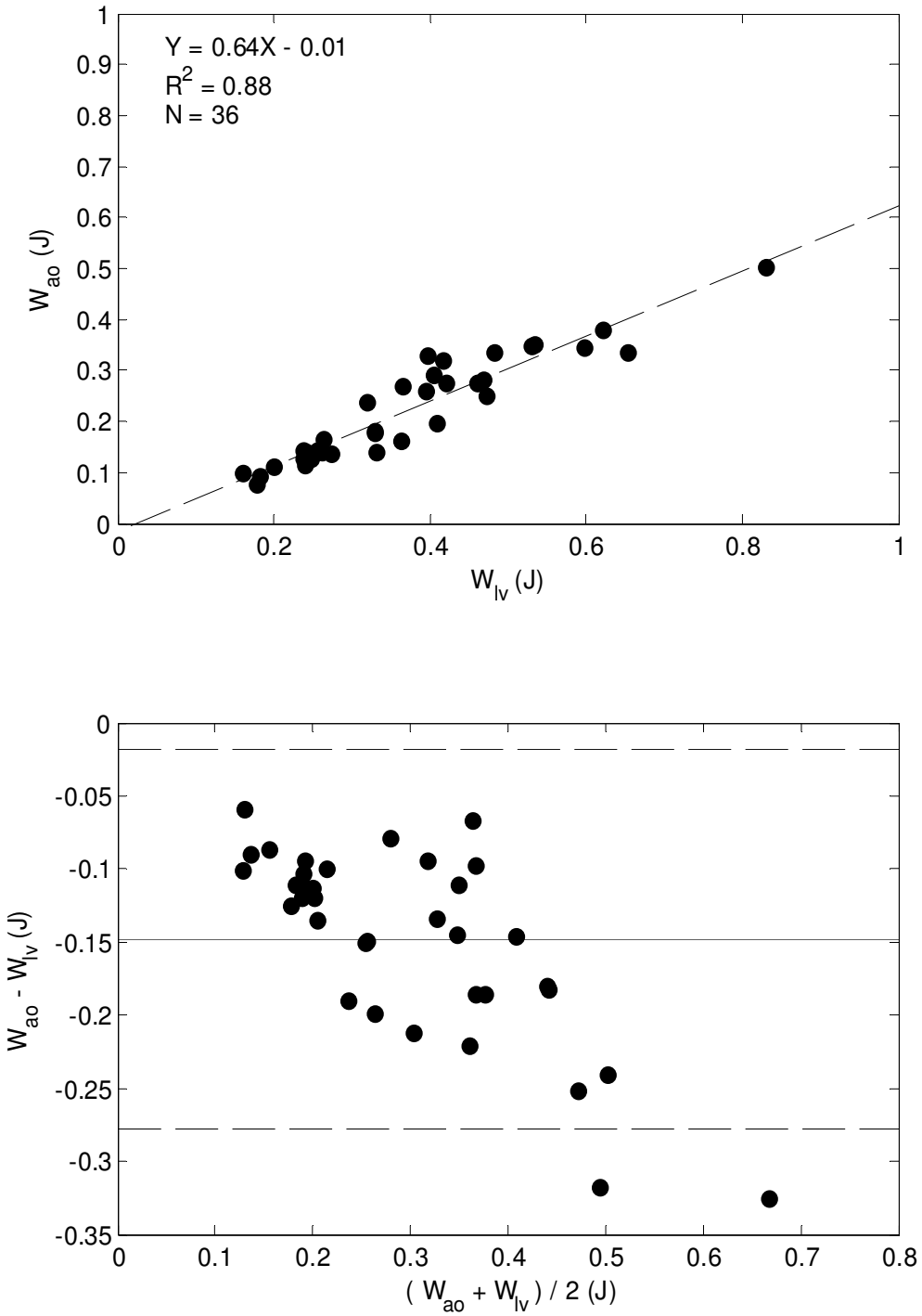

Figure 10.3: Regression (top) and Bland-Altman (bottom) analysis comparing work derived from the aorta model (W_{ao}) with work calculated from the area enclosed left ventricular pressure-volume loops (W_{lv}).

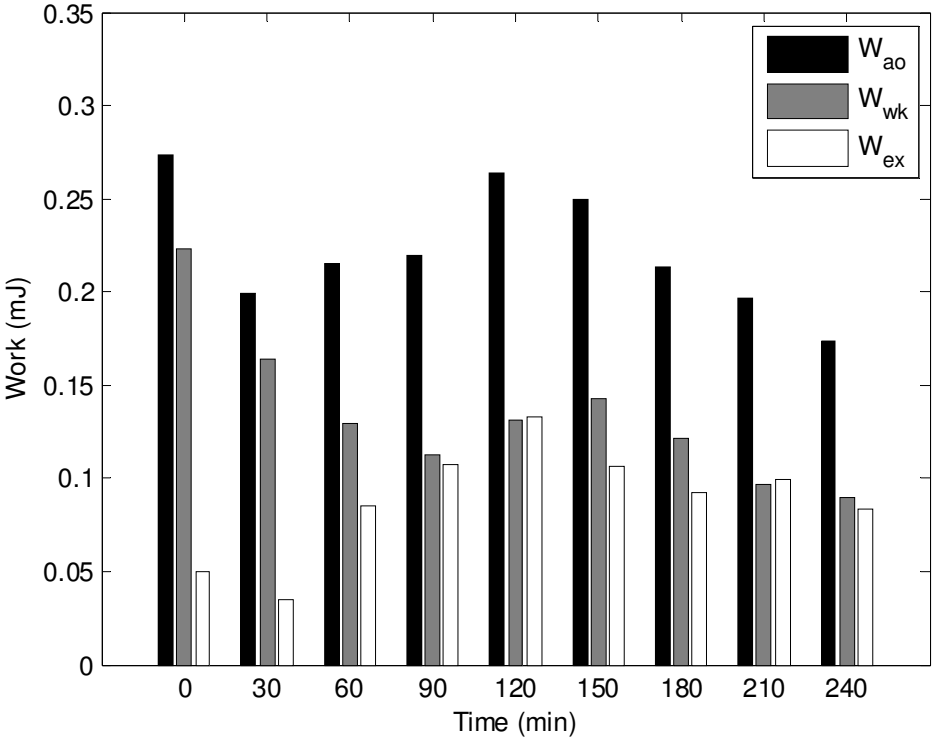

Figure 10.4: Temporal change in the total hydraulic work of aortic flow (W_{ao}) and its components, reservoir work (W_{wk}) and excess work (W_{ex}), across the duration of the pig study. Each bar represents the averaged value across the four pigs.

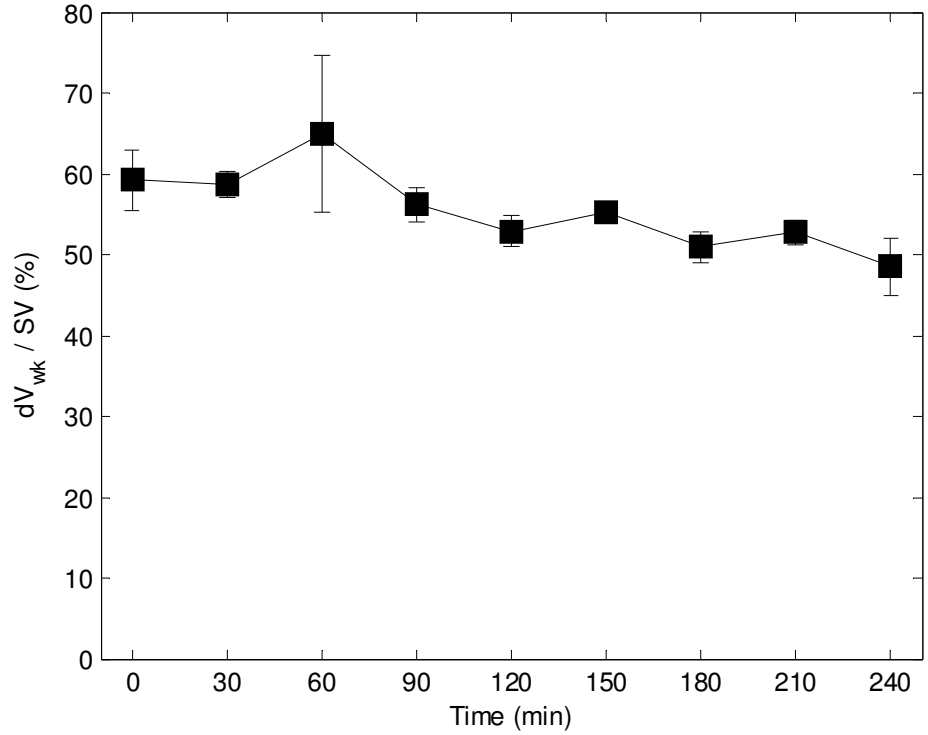

Figure 10.5: Change in volume stored in the arterial reservoir (dV_{wk}) as a percentage of stroke volume (SV). Data is presented as mean +/- SEM.

10.3.3 ESTIMATION OF VENTRICULAR ARTERIAL COUPLING

It was hypothesised that the ratio of W_{ex} to W_{wk} may be an indicator of ventricular arterial coupling, given that W_{ex} is a function of the flow energy ejected from the ventricle, and W_{wk} represents the work required to distend the arterial volume. Hence, W_{ex}/W_{wk} was compared to E_{es}/E_a to check this claim, as shown in Figure 10.6. Analysis of Figure 10.6 showed a very weak relationship between these indices, with low correlation of $R^2 = 0.24$, indicating they are not directly related, and proving this initial hypothesis wrong.

On further analysis, it was noticed that W_{ex} is strongly related to the inverse of E_a ($R^2 = 0.76$), as seen in Figure 10.7. However, changes W_{ex} or W_{wk}, or any combination of these two indices, were not reflective of changes in left ventricular contractility (E_{es}). Hence, demonstrating that the energetics of the aortic model are only capable of representing changes in the state of left ventricular afterload and not changes in left ventricular contractility.

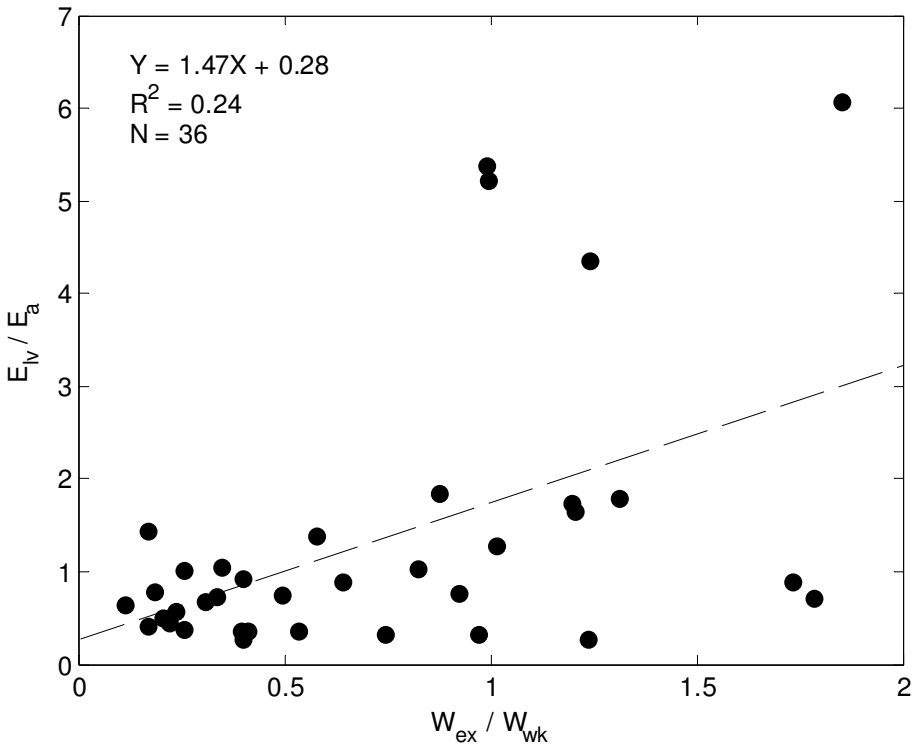

Figure 10.6: Comparison ventricular arterial coupling (E_{lv}/E_a), derived pressure volume loop analysis, with the ratio of excess to reservoir work (W_{ex}/W_{wk}), derived from the fitted aorta models.

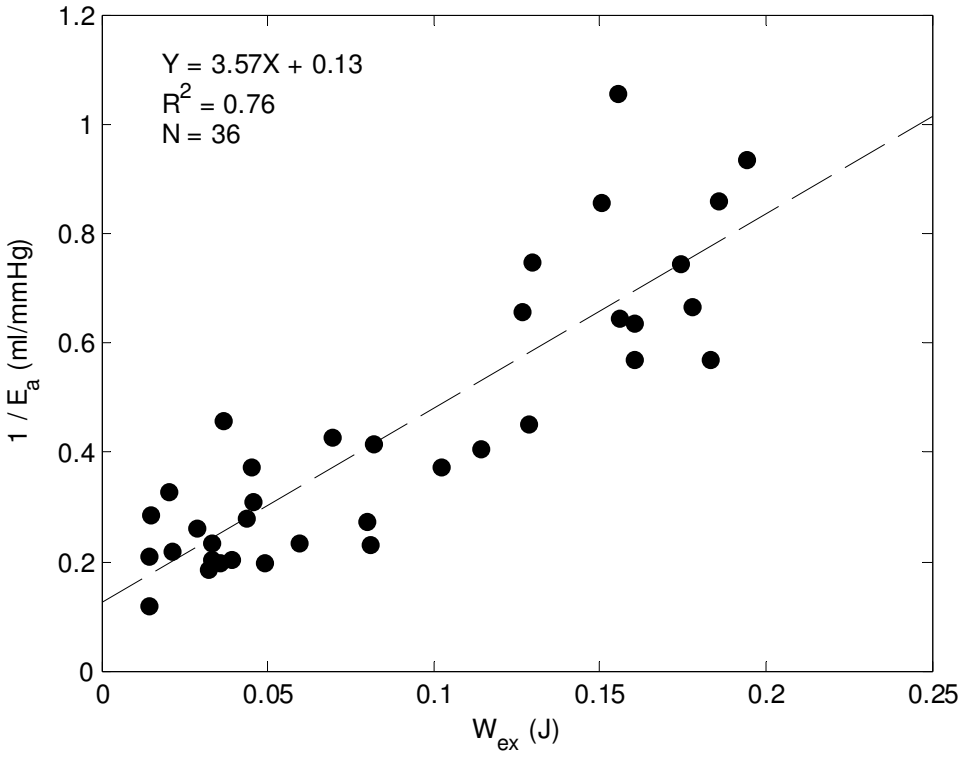

Figure 10.7: Comparison of the inverse of afterload (1/Ea) calculated from pressure-volume loop analysis with excess work (W_{ex}) derived from the aorta model.

10.4 DISCUSSION

A model of aortic blood flow, based on the works of (Davies et al., 2010, Tyberg et al., 2009, Wang et al., 2003), was identified using measurements from an experimental animal study on septic shock. Aortic models were fitted using only measurements of the aortic pressure waveform and SV, removing the reliance on knowing the flow Q_{in}, which can be highly invasive and difficult to measure clinically. In this study, the models were successfully fitted to 36 sets of these measurements and the energetics of these models were analysed.

10.4.1 MODEL ENERGETICS

The modelled derived W_{ao}, representing the total hydraulic work of flow in the aorta, tracked changes in the measured W_{lv} well with R^2 =0.88, although W_{ao} underestimated W_{lv} on average by -0.13J. The bias in W_{ao} was probably a result of the extra work required by the ventricle to push the flow through the aortic valve, which is not accounted for in the aortic model. Fisher and Wheatly et al. (Fisher and Wheatley, 1988) recorded an energy loss of around 0.16-0.33J for flow through bio-

prosthetic porcine aortic valves using SV between 60-80mls. Indicating that a bias of -0.13J, given that measured SVs in this study are around half those used in (Fisher and Wheatley, 1988), is a reasonable approximation for aortic valve energy loss. This result verifies the accuracy of the fitted models.

10.4.2 SEPTIC SHOCK TRENDS

The identified aortic models also appeared capable of capturing the effects of septic shock on the pig's hemodynamics. As the state of the pigs worsened, due to the inflammatory effects of the endotoxin, modelled systemic resistance decreased substantially and arterial compliance increased, as seen in Figure 10.8. The drop in resistance was generally larger than the increase in compliance causing the decay constant, τ, to decrease as $\tau = RC$. The combination of these factors caused the aortic reservoir to charge and discharge quicker than it would have done for a healthy subject.

The volume in the arterial reservoir could not accumulate faster than it was discharging, resulting in a flattening in the P_{wk} component of the aortic pressure. Hence, in the subjects with a low decay constant when normalised by heartbeat (τ / T), the shape of the aortic pressure begins to look similar to the shape of Q_{in}, as seen in Figure 10.9 with a noticeable flattening of the diastolic pressure observed when compared to the aortic pressure waveform measured before the endotoxin infusion. This effect is responsible for the relative decrease in the proportion of W_{wk} compared to W_{ao} and W_{ex} that occurs during the study, as shown in Figure 10.4.

These factors could explain why left ventricular afterload (E_a) decreases during septic shock as arterial pressure can never build up during the heartbeat because less energy and volume are stored in the arterial reservoir. Clinically, the inability of the arterial system to store volume in sepsis gradually leads to a decrease in mean arterial pressure resulting in hypotension. Hence, monitoring and understanding the reasons why the arterial reservoir loses its ability to store hydraulic energy and volume during sepsis could help develop and implement treatments for maintaining arterial pressure in ICU patients.

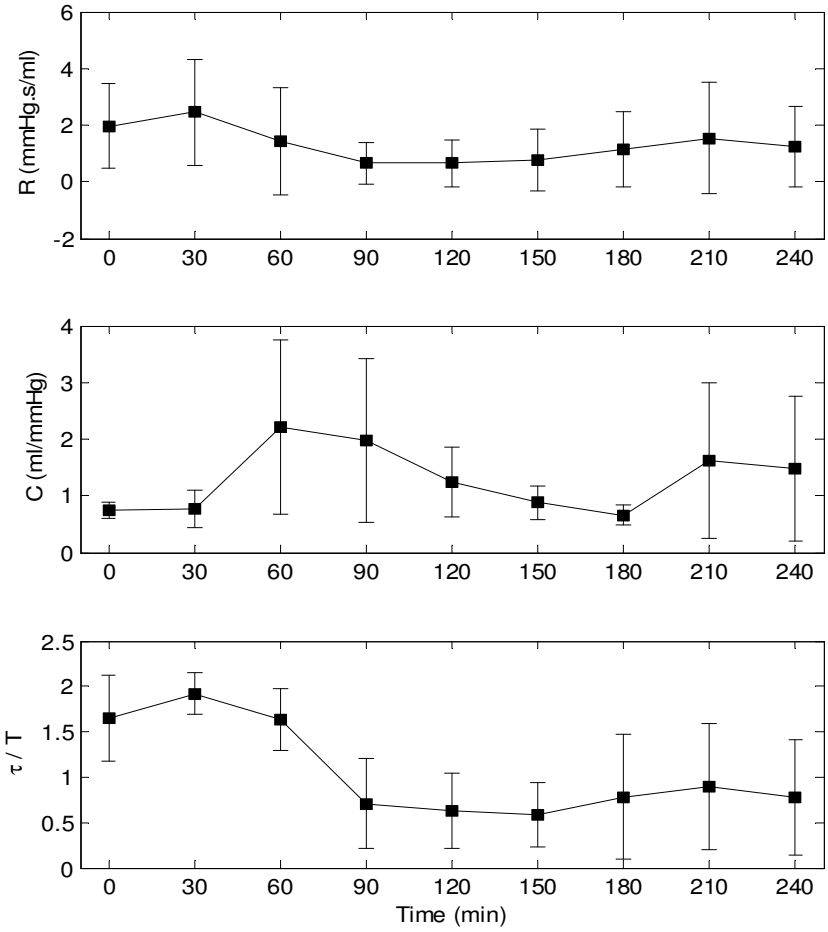

Figure 10.8: Temporal profile of systemic peripheral resistance, R (top), aortic compliance, C (middle), and ratio of the decay constant to heartbeat period, τ / T (bottom), during the pig study. Data is presented as mean +/- SD.

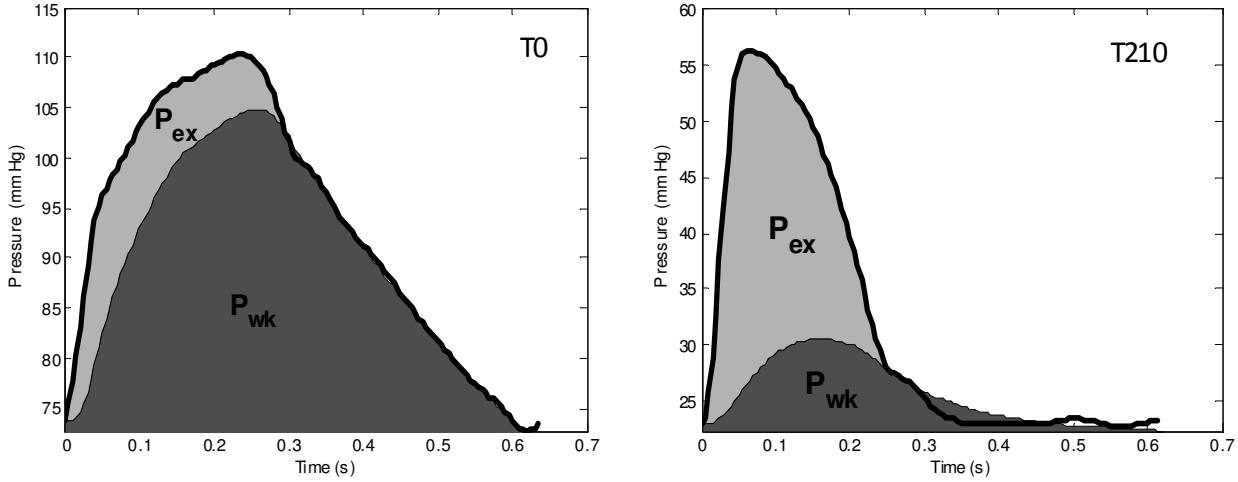

Figure 10.9: Example of the aortic pressure separated into reservoir and pressure (P_{wk}) and excess pressure (P_{ex}) components before the endotoxin infusion (T0) and 180 minutes (T210) after endotoxin infusion.

10.4.3 VENTRICULAR ARTERIAL COUPLING

The ratio of W_{ex}/W_{wk} did not relate well to E_{es}/E_a, a common clinical measure of ventricular arterial coupling, as seen in Figure 10.6. This result indicates that the initial hypothesis was incorrect. No relation was found between W_{ex} and E_{es}, which suggests that W_{ex} is not a function of the contractile state of the ventricle. However, W_{ex} did relate well to inverse of afterload (R^2 = 0.76), which was unexpected. Overall, these results show that W_{ex} could be a useful metric for describing acute changes in afterload (E_a) due to septic shock, which is important because septic shock is characterised by a sudden decrease in afterload due to a systemic inflammatory response to an infection.

10.4.4 LIMITATIONS

The main, and most controversial, assumption made during the fitting process is that P_{ex} is linearly proportional to Q_{in}, and thus, the two can be represented by a purely resistive relationship ($P_{ex} = R_{prox}Q_{in}$). This assumption is based on the work of (Wang et al., 2003), which shows that the magnitudes of backwards travelling waves in the aorta are minimal. In future work, this relationship needs to be tested and validated with accurate aortic flow data. However, the author feels justified in using this assumption in this study for two reasons: 1) the model was only fitted to central aortic pressure measurements, where backwards travelling waves are small during systole (Aguado-Sierra et al., 2008), due to the central aorta's distance from major reflection sites; and 2) in sepsis vascular tone decreases, reducing the production of reflective waves (O'Rourke and Yaginuma, 1984). However, the author realises the assumption may not be valid in subjects with high arterial stiffness, such as with hypertensive subjects.

10.5 SUMMARY

Measurements of SV and the aortic pressure waveform were used to identify subject-specific models of aortic flow and pressure in a porcine study. Analysis of the components that shape the aortic pressure waveform suggests that one of the main reasons left ventricular afterload decreases during septic shock is because the arterial reservoir loses its ability to store hydraulic energy in the form of stressed volume during systole. However, a larger more comprehensive study with accurate aortic flow measurements is required to validate the method and results of this work.

CHAPTER 11: CONCLUSIONS

This chapter presents the main conclusions of this research. Conclusions regarding the accuracy and validation of the model-based hemodynamic monitoring methods presented are outlined along with the clinical relevance and potential of these approaches. Suggestions for further possible improvements to this work and future avenues to expand into will be discussed in the subsequent chapter.

11.1 PATIENT-SPECIFIC CARDIOVASCULAR SYSTEM MODELS

The aim of this research was to identify subject-specific physiological models to assist with the hemodynamic monitoring of critically ill patients in the ICU. A parameter identification method was used to identify subject-specific six chamber lumped parameter models of the CVS from commonly available ICU measurements. Subject-specific models were retrospectively fitted to measurements obtained from two animal studies on pulmonary embolism and septic shock and one human study on cardiac recovery from mitral valve surgery. Static and dynamic variables of cardiac and circulatory function, derived from the subject-specific CVS models, were used to analyse the pathological effect and progression of disease along with the effectiveness of treatment in these studies.

The main accomplishment of this thesis was extending the parameter identification method of Starfinger et al (Starfinger, 2008) to uniquely identify patient-specific models of the CVS using typically available measurements in the ICU. This method utilises discrete measurements which are commonly recorded or inferable in the ICU including: mean aortic and pulmonary artery pressure, amplitude of the aortic and pulmonary artery pressure waveforms, maximum gradient of the aortic and pulmonary artery pressures, stroke volume, heart rate, and central venous pressure or measurements of the mitral and tricuspid valve closure times. These discrete measurements negate the need to use full waveforms, which are less robust and more difficult to use, simplifying and strengthening the reliance of the method.

More specifically, a proportional gain parameter identification method was developed on top of the scaling method of Starfinger et al (Starfinger, 2008), replacing the earlier integral-based method of Starfinger (Starfinger, 2008). The integral-based method required measurements of the ventricular volume waveforms that are infrequently measured in a critical care setting. The scaling method of

Starfinger (Starfinger, 2008) also required ventricular volume measurements (or estimates of them) and population-based assumptions to identify the valve resistances. These considerations all limited the patient-specificity and robustness of the method. Hence, the need for ventricular volume measurements and population-based assumptions reduce the real-time clinical applicability of the old approach. However, the proportional gain method described in this thesis relies only on the cardiac measurement of GEDV, which can be measured at the bedside, increasing the clinical applicability of the approach.

To develop a model-based approach one must find the optimal balance between model complexity and clinical applicability. A more complicated model than the six-chamber model could be used to better simulate the dynamics of the CVS. However, a more complex model requires a larger number of parameters, and is thus, more difficult to identify given the limited measurement set available in the ICU. Some of these additional parameters would need to be held constant or identified from estimates of pressure, volume, or flow. This approach limits the clinical usefulness of these parameters and potentially compromises the identifiability of the other model parameters. This research modified the minimal six chamber CVS model developed by Smith et al (Smith, 2004) to provide the optimal mix of model complexity and parameter identifiability. Hence, this balance enables the identification of patient-specific CVS model to realistically represent a patient's cardiovascular condition from available ICU measurements.

A proportional gain-based parameter identification method was developed and validated in two pig studies on septic shock and pulmonary embolism, as described in Chapter 5. The model outputs were shown to consistently converge to the observable hemodynamic measurements. The identified subject-specific models also matched independent measures of left ventricular pressures and volumes within an acceptable error range providing a true validation of the identification method. Moreover, model-based metrics and parameters were seen to track the experimentally derived metrics of right ventricle contractility and afterload in these studies. These results indicate the six-chamber CVS model and parameter identification method are able to extrapolate cardiac dynamics, such left and right ventricle preload and contractility, from known circulatory measurements. These findings indicate that the identified CVS models is a relatively accurate description of global cardiovascular dynamics, justifying the use of the six-chamber CVS model, and validating the parameter identification method.

Chapters 6 and 7 demonstrate that the subject-specific models are able to track clinically-relevant disease and treatment dependent changes in pulmonary embolism and septic shock which are common CVS diseases in the ICU. In the pulmonary embolism study, a decrease in pulmonary

vascular resistance was identified in all the swine after the insertion of autologous blood clots into the blood system. In the pigs near death, acute right ventricle dilation was noticed in the subject-specific models, resulting in left ward shift in the inter-ventricular septum, indicating cardiac decompensation. In the septic shock study, a decrease in the modelled systemic vascular resistance was seen in all the pigs after an endotoxin infusion. However, after hemofiltration therapy was initiated an improvement in systemic vascular resistance was noticed in two of the pigs, whereas, no improvement was noticed in the other two pigs. These studies indicate that the subject-specific CVS models can help track important diagnostic markers of two common disease states in the ICU. Analysis of the personalised models also made it easy to explain why some pigs were compensating well to the induced disease while others were not, a critical distinction highlighting the clinical value of the model.

The parameter identification was further tested with human measurements in the ICU on post mitral valve surgery patients. The retrospectively identified patient-specific CVS models observed two different responses to mitral valve correction. Three of the patients showed good recovery post operation with improved left ventricle function and decreased pulmonary vascular resistances, indicating decreased pulmonary congestion. The identified models of the other patient in the study observed left ventricle impairment and increasing hypertension due to elevated systemic vascular resistance and decreased left ventricle contractility. This finding indicated that the weakened left ventricle in this patient, due to the chronic effects of prolonged mitral regurgitation, was not compensating well to the affect of the mitral valve correction. These results illustrate how the model can be used to distinguish between patients who are responding well to surgery from those who are not initially recovering in the desired manner. Again, it shows the model's ability to clearly discriminate clinically relevant dynamics. This study, as shown in Chapter 8, provides the first clinical test of the model-based approach and proves it is possible to identify relevant diagnostic information from real clinical data.

More specifically, Chapters 5-8 demonstrate that the identified subject-specific six-chamber CVS models are capable of monitoring clinically useful metrics of left and right ventricle preload, afterload, and contractility. These determinants of cardiovascular function are of significant importance clinically as they can be controlled using common therapies. Preload can be increased using fluid resuscitation; afterload can be altered using vasodilators (noradrenaline, nitric oxide, milrinone) and vasoconstrictors (vasopressin, adrenaline, noradrenaline, dopamine); and contractility can be changed using inotropic agents (dopamine, dobutamine, adrenaline, noradrenaline, milrinone). However, in a clinical setting it can be difficult to directly and

continuously measure indices of preload, afterload, and contractility. The identified subject-specific CVS models solve this problem by aggregating known ICU measurements in a mathematical framework of cardiovascular physiology. The outputs and parameters of these identified models provide a direct and clear means of monitoring the effect of different hemodynamic therapies on cardiac and circulatory function (preload, afterload, and contractility). Hence, the approach shows the potential to be able to improve the medical decision support pathway for hemodynamic management in the ICU.

Overall, the model-based approach has been able to aggregate common ICU measurements into a clear physiological picture of a patient's cardiac and circulatory function. The method is capable of monitoring the progression of a disease and can be used to discriminate between hemodynamic recovery and deterioration as shown by tests in pig and human studies. Thus, this research suggests the approach has significant clinical diagnostic and therapy guidance potential.

11.2 PULSE WAVE ANALYSIS OF AORTIC FLOW AND ENERGETICS

A model of arterial flow has been adapted to represent blood flow in the central aorta. This model separates aortic pressure into two components representing the compliant nature of the arterial system, called the reservoir pressure, and wave-phenomena, called the excess pressure. The model developed provides a foundation for subject-specific modelling of the aortic hemodynamics, specifically, how blood and energy is passed from the left ventricle to the aorta and onto the capillaries.

Subject-specific models of aortic flow were identified using measurements of SV and the aortic pressure waveform in a porcine study of septic shock. Analysis of these models show the arterial system loses its ability to store blood as a hydraulic reservoir in septic shock. This phenomena was shown to be responsible for significant change in shape in the aortic pressure waveform. Furthermore, analysis of aortic flow energetics showed that the model could be used to estimate the left ventricular work and that the excess pressure hydraulic work was inversely related to changes in afterload. These findings suggest the aortic model could be used provide important additional information on ventricular arterial coupling in septic shock patients.

CHAPTER 12: FUTURE WORK

This chapter summarises further validations and tests to increase the clinical utility of the patient-specific CVS models. Potential further changes and improvements to the model identification methods are suggested and a further extension to the CVS model in the model in the form of gas exchange modelling is proposed.

12.1 INTEGRATE MODEL WITH CLINICAL THERAPIES AND TREATMENT PROTOCOLS

A main use for the patient-specific CVS models is to quantify response to therapy. For the approach to be clinically useful it must influence treatment decisions to manifest a physical change in the patient. Therefore, the method needs to be incorporated with a treatment protocol to provide a real world benefit as part of a functional hemodynamic management approach. A basic example of such a treatment protocol could be: if left ventricle contractility drops below a certain level in the model then titrate inotropes at a certain dosage in an attempt to increase contractility. However, in this thesis, the influence of common clinical therapies such as the use of inotropes, vaso-active drugs, and fluid resuscitation on the model metrics of preload, afterload, and contractility were not tested. Hence, the approach must be further validated for these treatment modalities before it can be used to influence therapy in the ICU. This could be done through retrospective analysis of the recently installed database in the Christchurch Hospital ICU.

12.2 TESTING ON OTHER DISEASES STATES

At the moment the patient-specific models have only be tested on humans recovering from mitral valve surgery. These patients, although common, only reflect a small portion of the patients in the ICU. Hence, the clinical applicability of the model-based approach in humans needs to be further tested using measurements of other disorders, including but not limited to: sepsis, acute respiratory distress syndrome (ARDS), pneumonia, and cardiogenic shock. These tests would help quantify the response of the parameters in the CVS model to these common ICU disorders.

The post mitral valve surgery patients are normally monitored using regular hemodynamic measurements, as well as a Swanz-Ganz catheter that measures CO and pulmonary artery pressure.

However, other patients are monitored using a different array of measurements. For example, in the Christchurch Hopstial ICU, the PiCCO monitoring system (PULSION Medical Systems AG, Munich, Germany) is normally used for CO and GEDV monitoring in septic shock patients. In these patients the pulmonary artery pressure is not normally measured. In this case, the parameter identification method would need to be adapted to use GEDV instead of pulmonary artery pressure. Hence, in summary, the approach needs to customisable to the variety of different measurement combinations that are commonly used for the typical ICU patient.

12.3 RELATIONSHIP OF LEFT AND RIGHT VENTRICLE END SYSTOLIC ELASTANCE

Few measurements of the heart are available in the ICU. As a consequence, an empirical relationship was required in the identification process to fit the left and right ventricular end systolic elastances based on the ratios of the aortic and pulmonary artery pressures. This relationship was based on earlier results where the subject-specific CVS models were fitted to a complete set of pig measurements, including the left and right ventricular volumes. However, it was difficult to find any empirical data in the literature to reinforce the use of this relationship in humans. Although the relationship is conceptually based on known physiological phenomena (the Anrep Effect), it still needs further validation in humans.

12.4 COMPUTATIONAL SPEED

Currently, the parameter identification method is run in Matlab. In Matlab, it takes around six minutes on average to identify one patient-specific CVS model from a set of measurements. For these models to be a hemodynamic monitoring utility, this run time must be significantly decreased to provide real-time information. Computational speed of the approach could be improved in a number of ways, by:

- providing better/smart parameter estimates at the beginning of the identification process,
- increasing the numerical efficiency of the ODE solvers and identification method,
- and/or running the models in a faster program language such as C or java.

Initial tests have shown that a compiled C-version of the 6 chamber model can run up to 100 faster than the Matlab code. Hence, these preliminary results indicate that patients-specific CVS models could be identified in as little as three to four seconds, which is an acceptable delay in the ICU.

12.5 PULSE CONTOUR CALCULATION OF CO

The parameter identification method is limited by the number of measurements available in an ICU setting. The approach cannot be used when CO is not measured. Hence, the measurement of CO limits the use of this model-based monitoring method.

To rectify this problem, CO could be calculated using the contour of the arterial pressure waveform. This is already done in a number of commercial medical devices (Cottis et al., 2003, Linton et al., 1993, Opdam et al., 2007). However, the published algorithms used in these proprietary devices are not fully reproducible. Therefore, a new method must be developed to identify CO from radial artery pressure.

To accomplish this goal, the model of aortic flow, in Chapter 9, could be used to infer SV or CO from the arterial pressure waveform. Morphological features of the arterial pressure contour can be used to identify the parameters in this model. Thus, arterial flow can be backwards calculated using the model. The accurate calculation of CO would significantly improve the clinical applicability of the model-based approach as it would greatly increase the number of patients it can be applied to.

12.6 CARDIOPULMONARY GAS EXCHANGE MODEL

One of the main jobs of the CVS is to deliver oxygen from the lungs to the tissues of the body. However, many pulmonary and cardiovascular disease states can disrupt the balance of oxygen supply and metabolic demand. For example, septic shock is known to impair oxygen saturation in the microcirculation. Hence, it is important to monitor oxygen perfusion in critical care.

In recent research there has been significant development in measuring blood oxygen concentration and tissue perfusion. These techniques include:

- sublingual carbon dioxide (PCO_2) monitoring,
- near infrared spectroscopy for tissue oxygenation and haemoglobin monitoring,

- fluorescence spectroscopy for monitoring mitochondrial energy state,
- as well as, the traditionally measured oxygen saturation via pulse oximetry (SpO_2).

In addition, information about inspired and expired O_2 and CO_2 are available in mechanically ventilated patients. Blood gas analysis can also be used to evaluate the concentrations of O_2 and CO_2 in the blood, and thus, evaluate how effectively the lungs are delivering O_2 and removing CO_2 from the blood. Hence, with these monitoring techniques, it may be possible to identify a cardiovascular gas exchange model. This could be done by integrating a gas exchange model with blood transport equations of the six-chamber CVS model. Such a model would provide parameters of arterial and venous oxygen 0_2 saturation, which would provide important information on the amount of shunting in the lungs and end organ oxygen uptake. Details of models which already incorporate O_2 and CO_2 components can be found in (Batzel et al., 2005, Harada et al., 2005, Hardman et al., 1998, Kappel et al., 2007, Lu et al., 2003).

APPENDIX A: STRUCTURAL IDENTIFIABILITY TEST

The following sections show the input file used to test global identifiability of the simplified six-chamber and the corresponding output file produced by DAISY.

12.7 INPUT FILE OF SIX-CHAMBER CVS MODEL

```
 WRITE "SIMPLIFIED CVS6 MODEL"$

% B_ is the variable vector
 B_ := {e_lv,e_rv,GEDV,CO,Pao,Ppa,Pvc,Vlv,Vrv,Vao,Vvc,Vpa,Vpu}$

 FOR EACH EL_ IN B_ DO DEPEND EL_,T$

% B1_ is the unknown parameter vector
 B1_ := {Rmt,Elv,Rav,Eao,Rsys,Evc,Rtc,Erv,Rpv,Epa,Rpul,Epu}$

% Constraints
 LET Tp = 1$                % period of one heartbeat

% NUMBER OF STATES
 NX_ := 6$

% NUMBER OF OUTPUTS
 NY_ := 5$

% MODEL EQUATIONS
 C_:={  df(Vlv,t) = (Epu*Vpu-Elv*e_lv*Vlv)/Rmt - (Elv*e_lv*Vlv-Eao*Vao)/Rav,
        df(Vao,t) = (Elv*e_lv*Vlv-Eao*Vao)/Rav - (Eao*Vao-Evc*Vvc)/Rsys,
        df(Vvc,t) = (Eao*Vao-Evc*Vvc)/Rsys    - (Evc*Vvc-Erv*e_rv*Vrv)/Rtc,
        df(Vrv,t) = (Evc*Vvc-Erv*e_rv*Vrv)/Rtc - (Erv*e_rv*Vrv-Epa*Vpa)/Rpv,
        df(Vpa,t) = (Erv*e_rv*Vrv-Epa*Vpa)/Rpv - (Epa*Vpa-Epu*Vpu)/Rpul,
        df(Vpu,t) = (Epa*Vpa-Epu*Vpu)/Rpul    - (Epu*Vpu-Elv*e_lv*Vlv)/Rmt,
        GEDV      = max(Vlv)+max(Vrv),
        Pao       = Eao*Vao,
        Ppa       = Epa*Vpa,
        Pvc       = Evc*Vvc,
        CO        = int((Pao-Pvc)/Rsys,t)}$

% Limit randon number generator to a range of 1:SEED_ for parameter estimates
 SEED_ := 100$

% Run daisy
 DAISY()$
```

12.8 OUTPUT FILE OF SIX-CHAMBER CVS MODEL

```
 WRITE "SIMPLIFIED CVS6 MODEL"$

SIMPLIFIED CVS6 MODEL

% B_ is the variable vector
 B_ := {e_lv,e_rv,GEDV,CO,Pao,Ppa,Pvc,Vlv,Vrv,Vao,Vvc,Vpa,Vpu}$

 FOR EACH EL_ IN B_ DO DEPEND EL_,T$

% B1_ is the unknown parameter vector
 B1_ := {Rmt,Elv,Rav,Eao,Rsys,Evc,Rtc,Erv,Rpv,Epa,Rpul,Epu}$

% Constraints
 LET Tp = 1$      % period of one heartbeat

% NUMBER OF STATES
 NX_ := 6$

% NUMBER OF OUTPUTS
 NY_ := 5$

%MODEL EQUATIONS
 C_:={   df(Vlv,t) = (Epu*Vpu-Elv*e_lv*Vlv)/Rmt - (Elv*e_lv*Vlv-Eao*Vao)/Rav,
         df(Vao,t) = (Elv*e_lv*Vlv-Eao*Vao)/Rav - (Eao*Vao-Evc*Vvc)/Rsys,
         df(Vvc,t) = (Eao*Vao-Evc*Vvc)/Rsys     - (Evc*Vvc-Erv*e_rv*Vrv)/Rtc,
         df(Vrv,t) = (Evc*Vvc-Erv*e_rv*Vrv)/Rtc - (Erv*e_rv*Vrv-Epa*Vpa)/Rpv,
         df(Vpa,t) = (Erv*e_rv*Vrv-Epa*Vpa)/Rpv - (Epa*Vpa-Epu*Vpu)/Rpul,
         df(Vpu,t) = (Epa*Vpa-Epu*Vpu)/Rpul     - (Epu*Vpu-Elv*e_lv*Vlv)/Rmt,
         GEDV      = max(Vlv)+max(Vrv),
         Pao       = Eao*Vao,
         Ppa       = Epa*Vpa,
         Pvc       = Evc*Vvc,
         CO        = int((Pao-Pvc)/Rsys,t)}$

% Limit randon number generator to a range of 1:SEED_ for parameter estimates
 SEED_ := 100$

% Run daisy
 DAISY()$

seed_ := 100$

NUMBER OF EQUATIONS$

n_ := 11$

VARIBLE VECTOR$

b_ := {e_lv,
```

```
e_rv,
gedv,
co,
pao,
ppa,
pvc,
vlv,
vrv,
vao,
vvc,
vpa,
vpu}$

UNKNOWN PARAMETER VECTOR$

b1_ := {rmt,
elv,
rav,
eao,
rsys,
evc,
rtc,
erv,
rpv,
epa,
rpul,
epu}$

RANKING AMONG THE VARIABLES$

bb_ := {e_lv,
e_rv,
gedv,
co,
pao,
ppa,
pvc,
df(e_lv,t),
df(e_rv,t),
df(gedv,t),
df(co,t),
df(pao,t),
df(ppa,t),
df(pvc,t),
df(e_lv,t,2),
df(e_rv,t,2),
df(gedv,t,2),
df(co,t,2),
df(pao,t,2),
df(ppa,t,2),
df(pvc,t,2),
```

```
df(e_lv,t,3),
df(e_rv,t,3),
df(gedv,t,3),
df(co,t,3),
df(pao,t,3),
df(ppa,t,3),
df(pvc,t,3),
df(e_lv,t,4),
df(e_rv,t,4),
df(gedv,t,4),
df(co,t,4),
df(pao,t,4),
df(ppa,t,4),
df(pvc,t,4),
df(e_lv,t,5),
df(e_rv,t,5),
df(gedv,t,5),
df(co,t,5),
df(pao,t,5),
df(ppa,t,5),
df(pvc,t,5),
df(e_lv,t,6),
df(e_rv,t,6),
df(gedv,t,6),
df(co,t,6),
df(pao,t,6),
df(ppa,t,6),
df(pvc,t,6),
vlv,
vrv,
vao,
vvc,
vpa,
vpu,
df(vlv,t),
df(vrv,t),
df(vao,t),
df(vvc,t),
df(vpa,t),
df(vpu,t)}$

NUMBER OF INPUT(S)$

nu_ := 2$

NUMBER OF OUTPUT(S)$

ny_ := 5$

MODEL EQUATION(S)$
```

```
c_ := {df(vlv,t)=(eao*rmt*vao + epu*rav*vpu - (rav + rmt)*e_lv*elv*vlv)/(rav*rmt),
df(vao,t)=( - ((rav + rsys)*eao*vao - evc*rav*vvc) + e_lv*elv*rsys*vlv)/(rav*rsys),
df(vvc,t)=( - ((rsys + rtc)*evc*vvc - eao*rtc*vao) + e_rv*erv*rsys*vrv)/(rsys*rtc),
df(vrv,t)=(epa*rtc*vpa + evc*rpv*vvc - (rpv + rtc)*e_rv*erv*vrv)/(rpv*rtc),
df(vpa,t)=( - ((rpul + rpv)*epa*vpa - epu*rpv*vpu) + e_rv*erv*rpul*vrv)/(rpul*rpv),
df(vpu,t)=( - ((rmt + rpul)*epu*vpu - epa*rmt*vpa) + e_lv*elv*rpul*vlv)/(rmt*rpul),
gedv=vlv + vrv,
pao=eao*vao,
ppa=epa*vpa,
pvc=evc*vvc,
co=(int(pao,t) - int(pvc,t))/rsys}$

CHARACTERISTIC SET$

aa_(1) := co*rsys - int(pao,t) + int(pvc,t)$

aa_(2) := df(gedv,t)*e_lv*eao*elv*epa*rmt*rpv*rsys*rtc + df(pao,t)*e_lv*elv*
epa*rpv*rsys*rtc*(rav + rmt) - df(pao,t)*e_rv*epa*erv*rav*rsys*(rmt*rpv +
rmt*rtc + rpul*rtc) - df(ppa,t)*e_lv*eao*elv*rpul*rpv*rsys*rtc + e_lv*e_rv*
gedv*eao*elv*epa*erv*rsys*(rmt*rpv + rmt*rtc + rpul*rtc) + e_lv*pao*eao*elv*
epa*rpv*rtc*(rav + rmt + rsys) - e_lv*ppa*eao*elv*epa*rsys*rtc*(rmt + rpul +
rpv) - e_lv*pvc*eao*elv*epa*rpv*(rav*rtc + rmt*rsys + rmt*rtc) - e_rv*pao*
eao*epa*erv*(rav*rmt*rpv + rav*rmt*rtc + rav*rpul*rtc + rmt*rpv*rsys + rmt*
rsys*rtc + rpul*rsys*rtc) + e_rv*pvc*eao*epa*erv*rav*(rmt*rpv + rmt*rtc +
rpul*rtc)$

aa_(3) := df(pao,t)*e_rv*erv*evc*rav*rsys + df(pvc,t)*e_lv*eao*elv*rsys*rtc -
e_lv*e_rv*gedv*eao*elv*erv*evc*rsys - e_lv*pao*eao*elv*evc*rtc + e_lv*pvc*
eao*elv*evc*(rsys + rtc) + e_rv*pao*eao*erv*evc*(rav + rsys) - e_rv*pvc*eao*
erv*evc*rav$

aa_(4) := df(e_lv,t)*df(pao,t)*elv*rav*rpul*rpv**2*rsys*rtc**2*(rav + rmt) +
df(e_lv,t)*pao*eao*elv*rpul*rpv**2*rtc**2*(rav**2 + rav*rmt + rav*rsys + rmt*
rsys) - df(e_lv,t)*pvc*eao*elv*rav*rpul*rpv**2*rtc**2*(rav + rmt) - df(e_rv,
t)*df(pao,t)*erv*rav**2*rmt*rpul*rpv*rsys*rtc*(rpv + rtc) + df(e_rv,t)*e_lv*
gedv*eao*elv*erv*rav*rmt*rpul*rpv*rsys*rtc*(rpv + rtc) - df(e_rv,t)*pao*eao*
erv*rav*rmt*rpul*rpv*rtc*(rav*rpv + rav*rtc + rpv*rsys + rsys*rtc) + df(e_rv,
t)*pvc*eao*erv*rav**2*rmt*rpul*rpv*rtc*(rpv + rtc) + df(gedv,t,2)*e_lv*eao*
elv*rav*rmt*rpul*rpv**2*rsys*rtc**2 + df(gedv,t)*e_lv**2*eao*elv**2*rpul*rpv**2*
rsys*rtc**2*(rav + rmt) + df(gedv,t)*e_lv*eao*elv*rav*rpv*rsys*rtc**2*( -
epa*rmt**2 + epu*rmt*rpv + epu*rpul*rpv) - df(pao,t)*e_lv*e_rv*elv*erv*rav*
rpul*rpv*rsys*rtc*(rav*rpv + rav*rtc + rmt*rpv + rmt*rtc) + df(pao,t)*e_lv*
elv*rpv*rsys*rtc**2*( - eao*rmt*rpul*rpv - epa*rav**2*rmt - epa*rav*rmt**2 +
epu*rav**2*rpv + epu*rav*rmt*rpv + epu*rav*rpul*rpv) + df(pao,t)*e_rv**2*erv**2*
rav**2*rmt*rpul*rsys*(rpv**2 + 2*rpv*rtc + rtc**2) + df(pao,t)*e_rv*erv*rav**2*
rsys*(epa*rmt**2*rpv*rtc + epa*rmt**2*rtc**2 + epa*rmt*rpul*rtc**2 - epu*rmt*
rpv**2*rtc - epu*rmt*rpv*rtc**2 - epu*rpul*rpv**2*rtc - epu*rpul*rpv*rtc**2 +
evc*rmt*rpul*rpv**2) + e_lv**2*e_rv*gedv*eao*elv**2*erv*rpul*rpv*rsys*rtc*(
rav*rpv + rav*rtc + rmt*rpv + rmt*rtc) - e_lv**2*ppa*eao*elv**2*rpul*rpv*
rsys*rtc**2*(rav + rmt) - e_lv**2*pvc*eao*elv**2*rpul*rpv**2*rsys*rtc*(rav +
rmt) + e_lv*e_rv**2*gedv*eao*elv*erv**2*rav*rmt*rpul*rsys*( - rpv**2 - 2*rpv*
```

```
rtc - rtc**2) + e_lv*e_rv*gedv*eao*elv*erv*rav*rsys*( - epa*rmt**2*rpv*rtc -
epa*rmt**2*rtc**2 - epa*rmt*rpul*rtc**2 + epu*rmt*rpv**2*rtc + epu*rmt*rpv*
rtc**2 + epu*rpul*rpv**2*rtc + epu*rpul*rpv*rtc**2 - evc*rmt*rpul*rpv**2) -
e_lv*e_rv*pao*eao*elv*erv*rpul*rpv*rtc*(rav**2*rpv + rav**2*rtc + rav*rmt*
rpv + rav*rmt*rtc + rav*rpv*rsys + rav*rsys*rtc + rmt*rpv*rsys + rmt*rsys*
rtc) + e_lv*e_rv*ppa*eao*elv*erv*rav*rmt*rpul*rsys*rtc*(rpv + rtc) + e_lv*
e_rv*pvc*eao*elv*erv*rav*rpul*rpv*(rav*rpv*rtc + rav*rtc**2 + rmt*rpv*rsys +
rmt*rpv*rtc + rmt*rsys*rtc + rmt*rtc**2) + e_lv*pao*eao*elv*rav*rpv*rtc*( -
epa*rav*rmt*rtc - epa*rmt**2*rtc - epa*rmt*rsys*rtc + epu*rav*rpv*rtc + epu*
rmt*rpv*rtc + epu*rpul*rpv*rtc + epu*rpv*rsys*rtc - evc*rmt*rpul*rpv) + e_lv*
ppa*eao*elv*rav*rsys*rtc**2*(epa*rmt**2 + epa*rmt*rpul + epa*rmt*rpv - epu*
rmt*rpv - epu*rpul*rpv - epu*rpv**2) + e_lv*pvc*eao*elv*rav*rpv*(epa*rav*rmt*
rtc**2 + epa*rmt**2*rsys*rtc + epa*rmt**2*rtc**2 - epu*rav*rpv*rtc**2 - epu*
rmt*rpv*rsys*rtc - epu*rmt*rpv*rtc**2 - epu*rpul*rpv*rsys*rtc - epu*rpul*rpv*
rtc**2 + evc*rmt*rpul*rpv*rsys + evc*rmt*rpul*rpv*rtc) + e_rv**2*pao*eao*erv**2*
rav*rmt*rpul*(rav*rpv**2 + 2*rav*rpv*rtc + rav*rtc**2 + rpv**2*rsys + 2*rpv*
rsys*rtc + rsys*rtc**2) + e_rv**2*pvc*eao*erv**2*rav**2*rmt*rpul*( - rpv**2 - 2*
rpv*rtc - rtc**2) + e_rv*pao*eao*erv*rav*(epa*rav*rmt**2*rpv*rtc + epa*rav*
rmt**2*rtc**2 + epa*rav*rmt*rpul*rtc**2 + epa*rmt**2*rpv*rsys*rtc + epa*rmt**2*
rsys*rtc**2 + epa*rmt*rpul*rsys*rtc**2 - epu*rav*rmt*rpv**2*rtc - epu*rav*
rmt*rpv*rtc**2 - epu*rav*rpul*rpv**2*rtc - epu*rav*rpul*rpv*rtc**2 - epu*rmt*
rpv**2*rsys*rtc - epu*rmt*rpv*rsys*rtc**2 - epu*rpul*rpv**2*rsys*rtc - epu*
rpul*rpv*rsys*rtc**2 + evc*rav*rmt*rpul*rpv**2 + evc*rmt*rpul*rpv**2*rsys) +
e_rv*pvc*eao*erv*rav**2*( - epa*rmt**2*rpv*rtc - epa*rmt**2*rtc**2 - epa*rmt*
rpul*rtc**2 + epu*rmt*rpv**2*rtc + epu*rmt*rpv*rtc**2 + epu*rpul*rpv**2*rtc +
epu*rpul*rpv*rtc**2 - evc*rmt*rpul*rpv**2)$

aa_(5) := df(e_lv,t)*df(pao,t)*elv*rav*rpv*rsys**2*rtc + df(e_lv,t)*pao*eao*
elv*rpv*rsys*rtc*(rav + rsys) - df(e_lv,t)*pvc*eao*elv*rav*rpv*rsys*rtc + df(
gedv,t)*e_lv**2*eao*elv**2*rpv*rsys**2*rtc - df(pao,t,2)*e_lv*elv*rav*rpv*
rsys**2*rtc - df(pao,t)*e_lv*e_rv*elv*erv*rav*rsys**2*(rpv + rtc) - df(pao,t)*
e_lv*eao*elv*rpv*rsys*rtc*(rav + rsys) - df(pao,t)*e_rv*erv*evc*rav**2*rpv*
rsys + e_lv**2*e_rv*gedv*eao*elv**2*erv*rsys**2*(rpv + rtc) - e_lv**2*ppa*
eao*elv**2*rsys**2*rtc - e_lv**2*pvc*eao*elv**2*rpv*rsys**2 + e_lv*e_rv*gedv*
eao*elv*erv*evc*rav*rpv*rsys - e_lv*e_rv*pao*eao*elv*erv*rsys*(rav*rpv + rav*
rtc + rpv*rsys + rsys*rtc) + e_lv*e_rv*pvc*eao*elv*erv*rav*rsys*(rpv + rtc) +
e_lv*pao*eao*elv*evc*rav*rpv*rtc - e_lv*pvc*eao*elv*evc*rav*rpv*(rsys + rtc) -
e_rv*pao*eao*erv*evc*rav*rpv*(rav + rsys) + e_rv*pvc*eao*erv*evc*rav**2*rpv$

aa_(6) := df(pao,t)*rav*rsys - e_lv*vlv*eao*elv*rsys + pao*eao*(rav + rsys) -
pvc*eao*rav$

aa_(7) :=  - df(pao,t)*rav*rsys + e_lv*gedv*eao*elv*rsys - e_lv*vrv*eao*elv*
rsys - pao*eao*(rav + rsys) + pvc*eao*rav$

aa_(8) := pao - vao*eao$

aa_(9) := pvc - vvc*evc$

aa_(10) := ppa - vpa*epa$
```

```
aa_(11) := df(gedv,t)*e_lv*eao*elv*rmt*rpv*rsys*rtc + df(pao,t)*e_lv*elv*rpv*
rsys*rtc*(rav + rmt) - df(pao,t)*e_rv*erv*rav*rmt*rsys*(rpv + rtc) + e_lv*
e_rv*gedv*eao*elv*erv*rmt*rsys*(rpv + rtc) + e_lv*pao*eao*elv*rpv*rtc*(rav +
rmt + rsys) - e_lv*ppa*eao*elv*rmt*rsys*rtc - e_lv*pvc*eao*elv*rpv*(rav*rtc +
rmt*rsys + rmt*rtc) - e_lv*vpu*eao*elv*epu*rpv*rsys*rtc - e_rv*pao*eao*erv*
rmt*(rav*rpv + rav*rtc + rpv*rsys + rsys*rtc) + e_rv*pvc*eao*erv*rav*rmt*(
rpv + rtc)$

THE SYSTEM IS ALGEBRAICALLY OBSERVABLE$

RANDOMLY CHOSEN NUMERICAL PARAMETER VECTOR$

b2_ := {rmt=8,
elv=91,
rav=28,
eao=20,
rsys=75,
evc=67,
rtc=83,
erv=88,
rpv=30,
epa=5,
rpul=35,
epu=49}$

EXHAUSTIVE SUMMARY$

flist_ := {rsys - 75,
(7*epa*rmt - 8*rpul)/(8*epa*rmt),
(5896*eao*elv*rtc - 5395*erv*evc*rav)/(5896*erv*evc*rav),
( - eao*elv + 65*rav)/rav,
( - 1320*eao*elv*rtc + 1079*erv*rav*rsys)/(1320*erv*rav*rsys),
( - 15*eao + 4*rsys)/(15*rsys),
( - 15*eao + 4*rsys)/(15*rsys),
(eao*elv - 65*rav)/rav,
(23584*elv*rsys*rtc - 80925*erv*evc*rav)/(80925*elv*rsys*rtc),
( - 6*eao*elv + 13*rav*rpv)/(6*rav*rpv),
( - 83*eao*elv + 65*rav*rtc)/(83*rav*rtc),
(1245*eao*erv*evc - 23584*rsys*rtc)/(1245*rsys*rtc),
(1125*eao*evc - 268*rsys**2)/(1125*rsys**2),
(1213875*eao*erv*evc*rav - 94336*elv*rsys**2*rtc)/(1213875*elv*rsys**2*rtc),
(105*eao*rav + 105*eao*rsys - 103*rav*rsys)/(105*rav*rsys),
( - 9*eao*rmt + 40*rav + 40*rmt)/(40*eao*rmt),
( - 50*rav + 3*rmt*rsys - 50*rmt)/(50*rmt*rsys),
(4972*eao*elv*rpv*rtc - 80925*erv*rav*rpv - 80925*erv*rav*rtc)/(80925*eao*elv*rpv*rtc),
(1245*erv*rpv + 1245*erv*rtc - 4972*rpv*rtc)/(1245*rpv*rtc),
( - 19888*elv*rpv*rsys*rtc + 1213875*erv*rav*rpv +
1213875*erv*rav*rtc)/(1213875*elv*rpv*rsys*rtc),
(8*elv*rav + 8*elv*rmt - 117*rav*rmt)/(8*rav*rmt),
( - 80*elv*rav - 80*elv*rmt + 39*rav*rmt*rpv)/(80*rav*rmt*rpv),
( - 664*elv*rav - 664*elv*rmt + 117*rav*rmt*rtc)/(664*rav*rmt*rtc),
```

(18675*erv*rpv + 18675*erv*rtc - 2486*rpv**2*rtc)/(18675*rpv**2*rtc),
(105*eao*rav + 105*eao*rsys - 103*rav*rsys)/(105*rav*rsys),
(- 1245*erv*rpv - 1245*erv*rtc + 4972*rpv*rtc)/(1245*rpv*rtc),
(- 105*eao*rav - 105*eao*rsys + 103*rav*rsys)/(105*rav*rsys),
(249*eao*elv*erv*rpv + 249*eao*elv*erv*rtc - 64636*rav*rpv*rtc)/(249*rav*rpv*rtc),
(- 9*eao*rmt + 40*rav + 40*rmt)/(40*eao*rmt),
(18675*eao*erv*rpv + 18675*eao*erv*rtc - 19888*rpv*rsys*rtc)/(18675*rpv*rsys*rtc),
(- 93375*eao*evc*rsys - 93375*eao*evc*rtc + 42344*rsys**2*rtc)/(93375*rsys**2*rtc),
(- 8497125*eao*erv*evc*rav - 8497125*eao*erv*evc*rsys +
2429152*elv*rsys**2*rtc)/(8497125*elv*rsys**2*rtc),
(660*eao*elv*rsys + 660*eao*elv*rtc - 1027*erv*rav*rsys)/(660*erv*rav*rsys),
(200*rav - 37*rmt*rsys + 200*rmt + 200*rsys)/(200*rmt*rsys),
(98883136*elv*rpv**2*rsys*rtc**2 - 1511274375*erv**2*rav*rpv**2 -
3022548750*erv**2*rav*rpv*rtc -
1511274375*erv**2*rav*rtc**2)/(1511274375*elv*rpv**2*rsys*rtc**2),
(- 840*epa*rmt**2 + 840*epu*rmt*rpv + 840*epu*rpul*rpv -
6289*rmt*rpul*rpv)/(840*rmt*rpul*rpv),
(73*rmt*rpv - 240*rmt - 240*rpul - 240*rpv)/(240*rmt*rpv),
(- 4150*rav*rtc + 299*rmt*rsys*rtc - 4150*rmt*rsys - 4150*rmt*rtc)/(4150*rmt*rsys*rtc),
(- 24720784*eao*elv*rpv**2*rtc**2 + 100751625*erv**2*rav*rpv**2 + 201503250*
erv**2*rav*rpv*rtc + 100751625*erv**2*rav*rtc**2)/(100751625*eao*elv*rpv**2*rtc**2),
(- 6446*elv*rmt*rpv*rsys*rtc + 93375*erv*rav*rmt*rpv + 93375*erv*rav*rmt*rtc +
93375*erv*rav*rpul*rtc)/(93375*elv*rmt*rpv*rsys*rtc),
(3223*eao*elv*rmt*rpv*rtc - 12450*erv*rav*rmt*rpv - 12450*erv*rav*rmt*rtc -
12450*erv*rav*rpul*rtc)/(12450*eao*elv*rmt*rpv*rtc),
(2490*erv*rmt*rpv + 2490*erv*rmt*rtc + 2490*erv*rpul*rtc -
41899*rmt*rpv*rtc)/(2490*rmt*rpv*rtc),
(- 1550025*erv**2*rpv**2 - 3100050*erv**2*rpv*rtc - 1550025*erv**2*rtc**2 +
24720784*rpv**2*rtc**2)/(1550025*rpv**2*rtc**2),
(3729*eao*rmt*rpv*rtc - 4150*erv*rav*rpv - 4150*erv*rav*rtc - 4150*erv*rmt*rpv -
4150*erv*rmt*rtc)/(4150*eao*rmt*rpv*rtc),
(- 130725*eao*erv*rav*rpv - 130725*eao*erv*rav*rtc - 130725*eao*erv*rpv*rsys -
130725*eao*erv*rsys*rtc + 512116*rav*rpv*rsys*rtc)/(130725*rav*rpv*rsys*rtc),
(830*elv*erv*rav*rpv + 830*elv*erv*rav*rtc + 830*elv*erv*rmt*rpv + 830*elv*
erv*rmt*rtc - 48477*rav*rmt*rpv*rtc)/(830*rav*rmt*rpv*rtc),
(512116*elv*rpv*rsys*rtc - 8497125*erv*rav*rpv - 8497125*erv*rav*rtc - 8497125*
erv*rpv*rsys - 8497125*erv*rsys*rtc)/(8497125*elv*rpv*rsys*rtc),
(1400*rav**2 - 309*rav*rmt*rsys + 1400*rav*rmt + 1400*rav*rsys + 1400*rmt*
rsys)/(1400*rav*rmt*rsys),
(- 3231*eao*rav*rmt*rpul*rpv - 5600*eao*rmt*rpul*rpv - 5600*epa*rav**2*rmt -
5600*epa*rav*rmt**2 + 5600*epu*rav**2*rpv + 5600*epu*rav*rmt*rpv + 5600*epu*
rav*rpul*rpv)/(5600*eao*rav*rmt*rpul*rpv),
(331969*elv*rmt*rpv*rsys*rtc - 1307250*erv*rav*rmt*rpv - 1307250*erv*rav*rmt*
rtc - 1307250*erv*rav*rpul*rtc - 1307250*erv*rmt*rpv*rsys - 1307250*erv*rmt*
rsys*rtc - 1307250*erv*rpul*rsys*rtc)/(1307250*elv*rmt*rpv*rsys*rtc),
(25200*epa*rmt**2 + 25200*epa*rmt*rpul + 25200*epa*rmt*rpv - 25200*epu*rmt*
rpv - 25200*epu*rpul*rpv - 25200*epu*rpv**2 +
10439*rmt*rpul*rpv**2)/(25200*rmt*rpul*rpv**2),
(- 2546240752*elv*rpv**2*rsys*rtc**2 + 10578920625*erv**2*rav*rpv**2 + 21157841250
*erv**2*rav*rpv*rtc + 10578920625*erv**2*rav*rtc**2 + 10578920625*erv**2*rpv**2*
rsys + 21157841250*erv**2*rpv*rsys*rtc + 10578920625*erv**2*rsys*rtc**2)/(10578920625

*elv*rpv**2*rsys*rtc**2),
(2583375*erv*rav*rpv*rtc + 2583375*erv*rav*rtc**2 + 2583375*erv*rmt*rpv*rsys +
2583375*erv*rmt*rpv*rtc + 2583375*erv*rmt*rsys*rtc + 2583375*erv*rmt*rtc**2 -
743314*rmt*rpv*rsys*rtc**2)/(2583375*rmt*rpv*rsys*rtc**2),
(619648381*eao*elv*rmt*rpul*rpv**2*rtc**2 + 1410522750*epa*erv*rav*rmt**2*
rpv*rtc + 1410522750*epa*erv*rav*rmt**2*rtc**2 + 1410522750*epa*erv*rav*rmt*
rpul*rtc**2 - 1410522750*epu*erv*rav*rmt*rpv**2*rtc - 1410522750*epu*erv*rav*
rmt*rpv*rtc**2 - 1410522750*epu*erv*rav*rpul*rpv**2*rtc - 1410522750*epu*erv*
rav*rpul*rpv*rtc**2 + 1410522750*erv*evc*rav*rmt*rpul*rpv**2)/(1410522750*
eao*elv*rmt*rpul*rpv**2*rtc**2),
(- 21700350*epa*erv*rmt**2*rpv*rtc - 21700350*epa*erv*rmt**2*rtc**2 - 21700350*
epa*erv*rmt*rpul*rtc**2 + 21700350*epu*erv*rmt*rpv**2*rtc + 21700350*epu*erv*
rmt*rpv*rtc**2 + 21700350*epu*erv*rpul*rpv**2*rtc + 21700350*epu*erv*rpul*
rpv*rtc**2 - 21700350*erv*evc*rmt*rpul*rpv**2 - 619648381*rmt*rpul*rpv**2*
rtc**2)/(21700350*rmt*rpul*rpv**2*rtc**2),
(- 145250*erv*rav**2*rpv - 145250*erv*rav**2*rtc - 145250*erv*rav*rmt*rpv -
145250*erv*rav*rmt*rtc - 145250*erv*rav*rpv*rsys - 145250*erv*rav*rsys*rtc -
145250*erv*rmt*rpv*rsys - 145250*erv*rmt*rsys*rtc + 128029*rav*rmt*rpv*rsys*
rtc)/(145250*rav*rmt*rpv*rsys*rtc),
(- 871500*epa*rav*rmt*rtc - 871500*epa*rmt**2*rtc - 871500*epa*rmt*rsys*rtc +
871500*epu*rav*rpv*rtc + 871500*epu*rmt*rpv*rtc + 871500*epu*rpul*rpv*rtc +
871500*epu*rpv*rsys*rtc - 871500*evc*rmt*rpul*rpv - 281369*rmt*rpul*rpv*rsys*
rtc)/(871500*rmt*rpul*rpv*rsys*rtc),
(- 1239296762*elv*rmt*rpul*rpv**2*rsys*rtc**2 - 10578920625*epa*erv*rav*rmt**2*
rpv*rtc - 10578920625*epa*erv*rav*rmt**2*rtc**2 - 10578920625*epa*erv*rav*
rmt*rpul*rtc**2 + 10578920625*epu*erv*rav*rmt*rpv**2*rtc + 10578920625*epu*
erv*rav*rmt*rpv*rtc**2 + 10578920625*epu*erv*rav*rpul*rpv**2*rtc + 10578920625*
epu*erv*rav*rpul*rpv*rtc**2 - 10578920625*erv*evc*rav*rmt*rpul*rpv**2)/(10578920625
*elv*rmt*rpul*rpv**2*rsys*rtc**2),
(72334500*epa*rav*rmt*rtc**2 + 72334500*epa*rmt**2*rsys*rtc + 72334500*epa*
rmt**2*rtc**2 - 72334500*epu*rav*rpv*rtc**2 - 72334500*epu*rmt*rpv*rsys*rtc -
72334500*epu*rmt*rpv*rtc**2 - 72334500*epu*rpul*rpv*rsys*rtc - 72334500*epu*
rpul*rpv*rtc**2 + 72334500*evc*rmt*rpul*rpv*rsys + 72334500*evc*rmt*rpul*rpv*
rtc + 16860877*rmt*rpul*rpv*rsys*rtc**2)/(72334500*rmt*rpul*rpv*rsys*rtc**2),
(63823783243*elv*rmt*rpul*rpv**2*rsys*rtc**2 + 148104888750*epa*erv*rav*rmt**2*
rpv*rtc + 148104888750*epa*erv*rav*rmt**2*rtc**2 + 148104888750*epa*erv*rav*
rmt*rpul*rtc**2 + 148104888750*epa*erv*rmt**2*rpv*rsys*rtc + 148104888750*
epa*erv*rmt**2*rsys*rtc**2 + 148104888750*epa*erv*rmt*rpul*rsys*rtc**2 - 148104888750
*epu*erv*rav*rmt*rpv**2*rtc - 148104888750*epu*erv*rav*rmt*rpv*rtc**2 - 148104888750
*epu*erv*rav*rpul*rpv**2*rtc - 148104888750*epu*erv*rav*rpul*rpv*rtc**2 - 148104888750
*epu*erv*rmt*rpv**2*rsys*rtc - 148104888750*epu*erv*rmt*rpv*rsys*rtc**2 - 148104888750
*epu*erv*rpul*rpv**2*rsys*rtc - 148104888750*epu*erv*rpul*rpv*rsys*rtc**2 + 148104888750
*erv*evc*rav*rmt*rpul*rpv**2 + 148104888750*erv*evc*rmt*rpul*rpv**2*rsys)/(148104888750
*elv*rmt*rpul*rpv**2*rsys*rtc**2)}$

MODEL PARAMETER SOLUTION(S)$

g_ := {{eao=20,
elv=91,
epa=5,
epu=49,

erv=88,
evc=67,
rav=28,
rmt=8,
rpul=35,
rpv=30,
rsys=75,
rtc=83}}$

SYSTEM GLOBALLY IDENTIFIABLE$

APPENDIX B: MITRAL VALVE REPLACEMENT PATIENT TREATMENT DATA

The following tables list the cardiovascular therapies used to treat the 4 patients post mitral valve surgery.

Table B.1: Treatment received by patient 1 (Weight = 96Kg) in the first 12 hours post mitral valve surgery

Therapy	Therapy type	T0	T1	T2	T3	T4	T5	T6	T7	T8	T9	T10	T11	T12
Ventilation	PEEP (cmH_20)	5	5	5	5	5	5							
	PIP (cmH_20)	16	17	15	14	11	11							
Inotropes	Noradrenaline (µg/kg/ml)	0.04	0.03	0.03	0.02	0.01	0.03	0.03	0.03	0.03	0.03			
	Milrinone (µg/kg/ml)													
	Dobutamine (µg/kg/ml)													
	Adrenaline (µg/kg/ml)													
Fluids	Fluid in (ml/hr)	41	539	539	23	22	124	24	22	72	171	120	122	24
	Fluid out (ml/hr)	40	135	205	115	170	145	170	20	25	35	200	140	100
	Fluid balance (ml/hr)	1	405	739	647	499	478	332	334	381	317	437	469	393

Table B.2: Treatment received by patient 2 (Weight = 56.5Kg) in the first 12 hours post mitral valve surgery

Therapy	Therapy type	T0	T1	T2	T3	T4	T5	T6	T7	T8	T9	T10	T11	T12
Ventilation	PEEP (cm H_20)	5	5	5	5	5	5	5						
	PIP (cm H_20)	10	19	19	11	11	11	11						
Inotropes	Noradrenaline (µg /kg/min)	0.02	0.05	4	0.07	0.02	0.02	0.01	0.01	0.01				
	Milrinone (µg /kg/min)	0.09	0.09	0.09	0.09	0.09	0.09	0.09	0.09	0.09	0.09	0.09	0.09	0.04
	Dobutamine (µg /kg/min)													
	Adrenaline (µg /kg/min)													
Fluids	Fluids in (ml/hr)	134	937	639	351	27	27	246	26	26	65	25	25	72
	Fluids out (ml/hr)	140	90	170	70	220	120	90	140	90	120	100	110	100
	Fluid balance (ml)	-6	841	1310	1591	1398	1305	1461	1346	1282	1227	1152	1067	1039

Table B.3: Treatment received by patient 3 (Weight = 65Kg) in the first 12 hours post mitral valve surgery

Therapy	Therapy type	T0	T1	T2	T3	T4	T5	T6	T7	T8	T9	T10	T11	T12
Ventilation	PEEP (cm H_20)	5	5	5	5	5	5	5	5	5	5	5	5	5
	PIP (cm H_20)	19	19	19	19	11	11	11	11	11	11	11	11	11
Inotropes	Noradrenaline (µg /kg/min)	0.07	0.06	0.06	0.03	0.02	0.04	0.04	0.03	0.03	0.03	0.03	0.03	0.03
	Milrinone (µg /kg/min)													
	Dobutamine (µg /kg/min)	3.2	3.2	6.4	6.4	3.9	2.6	2.6	5.8	5.8	5.8	4.5	4.5	4.5
	Adrenaline (µg /kg/min)	0.03												
Fluids	Fluids in (ml/hr)	533	639	534	28	528	30	181	32	63	32	32	532	261
	Fluids out (ml/hr)	230	320	420	340	220	180	130	60	124	105	35	65	35
	Fluid balance (ml)	303	622	736	424	732	582	633	605	544	471	468	935	1161

Table B.4: Treatment received by patient 4 (Weight = 69Kg) in the first 12 hours post mitral valve surgery

Therapy	Therapy type	T0	T1	T2	T3	T4	T5	T6	T7	T8	T9	T10	T11	T12
Ventilation	**PEEP (cm H_20)**	5	5	5	5	5	5							
	PIP (cm H_20)	17	19	18	18	10	11							
Inotropes	**Noradrenaline (µg/kg/min)**	0.16	0.11	0.07	0.08	0.08	0.06	0.03						
	Milrinone (µg /kg/min)	0.09	0.09	0.04	0.04	0.04								
	Dobutamine (µg /kg/min)													
	Adrenaline (µg /kg/min)													
Fluids	**Fluids in (ml/hr)**	52	547	40	41	531	26	123	220	220	120	120	170	120
	Fluids out (ml/hr)	155	195	115	115	60	175	40	70	75	110	60	40	70
	Fluid balance (ml)	-103	249	174	100	571	422	505	655	800	810	870	1000	1050

REFERENCES

AGUADO-SIERRA, J., DAVIES, J. E., HADJILOIZOU, N., FRANCIS, D., MAYET, J., HUGHES, A. D. & PARKER, K. H. 2008. Reservoir-wave separation and wave intensity analysis applied to carotid arteries: a hybrid 1D model to understand haemodynamics. *Conference proceedings,* 2008**,** 1381-4.

ALLENDER, S., SCHARBOROUGH, P., PETO, V. & RAYNER, M. 2008. European Cardiovascular Disease Statisitics: 2008 edition. London: British Heart Foundation.

AMOORE, J. N., SANTAMORE, W. P., CORIN, W. J. & GEORGE, D. T. 1992. Computer simulation of the effects of ventricular interdependence on indices of left ventricular systolic function. *J Biomed Eng,* 14**,** 257-62.

ANDERSON, F. A., JR. & SPENCER, F. A. 2003. Risk factors for venous thromboembolism. *Circulation,* 107**,** I9-16.

ANGUS, D. C., LINDE-ZWIRBLE, W. T., LIDICKER, J., CLERMONT, G., CARCILLO, J. & PINSKY, M. R. 2001. Epidemiology of severe sepsis in the United States: Analysis of incidence, outcome, and associated costs of care. *Critical care medicine,* 29**,** 1303-1310.

ANREP, G. V. 1912. On the part played by the suprarenals in the normal reactions of the body. *The Journal of Physiology,* 45**,** 307-317.

ANTONELLI, M., LEVY, M., ANDREWS, P. J., CHASTRE, J., HUDSON, L. D., MANTHOUS, C., MEDURI, G. U., MORENO, R. P., PUTENSEN, C., STEWART, T. & TORRES, A. 2007. Hemodynamic monitoring in shock and implications for management. International Consensus Conference, Paris, France, 27-28 April 2006. *Intensive care medicine,* 33**,** 575-90.

ANTONINI-CANTERIN, F., FAGGIANO, P., ZANUTTINI, D. & RIBICHINI, F. 1999. Is aortic valve resistance more clinically meaningful than valve area in aortic stenosis? *Heart (British Cardiac Society),* 82**,** 9-10.

ASANOI, H., SASAYAMA, S. & KAMEYAMA, T. 1989. Ventriculoarterial Coupling in Normal and Failing Heart in Humans. *Circulation research,* 65**,** 483-493.

ATHERTON, J. J., MOORE, T. D., LELE, S. S., THOMSON, H. L., GALBRAITH, A. J., BELENKIE, I., TYBERG, J. V. & FRENNEAUX, M. P. 1997. Diastolic ventricular interaction in chronic heart failure. *Lancet,* 349**,** 1720-4.

ATHERTON, J. J., MOORE, T. D., THOMSON, H. L. & FRENNEAUX, M. P. 1998. Restrictive left ventricular filling patterns are predictive of diastolic ventricular interaction in chronic heart failure. *Journal of the American College of Cardiology,* 31**,** 413-8.

BAHLOUL, M., CHAARI, A., KALLEL, H., ABID, L., BEN HAMIDA, C., DAMMAK, H., REKIK, N., MNIF, J., CHELLY, H. & BOUAZIZ, M. 2010. Pulmonary embolism in intensive care unit: Predictive factors, clinical manifestations and outcome. *Annals of Thoracic Medicine,* 5**,** 97-103.

BARRITT, D. W. & JORDAN, S. C. 1960. Anticoagulant drugs in the treatment of pulmonary embolism. A controlled trial. *Lancet,* 1**,** 1309-12.

BATZEL, J. J. & BACHAR, M. 2010. Modeling the Cardiovascular-Respiratory Control System: Data, Model Analysis, and Parameter Estimation. *Acta biotheoretica,* 58**,** 369-380.

BATZEL, J. J., KAPPEL, F. & TIMISCHL-TESCHL, S. 2005. A cardiovascular-respiratory control system model including state delay with application to congestive heart failure in humans. *Journal of mathematical biology,* 50**,** 293-335.

BELLU, G., SACCOMANI, M. P., AUDOLY, S. & D'ANGIO, L. 2007. DAISY: a new software tool to test global identifiability of biological and physiological systems. *Computer methods and programs in biomedicine,* 88**,** 52-61.

BERENHOLTZ, S. M., PRONOVOST, P. J., LIPSETT, P. A., HOBSON, D., EARSING, K., FARLEY, J. E., MILANOVICH, S., GARRETT-MAYER, E., WINTERS, B. D., RUBIN, H. R., DORMAN, T. & PERL, T.

M. 2004. Eliminating catheter-related bloodstream infections in the intensive care unit. *Critical care medicine,* 32**,** 2014-2020.

BERMEJO, J., GARCIA-FERNANDEZ, M. A., TORRECILLA, E. G., BUENO, H., MORENO, M. M., SAN ROMAN, D. & DELCAN, J. L. 1996. Effects of dobutamine on Doppler echocardiographic indexes of aortic stenosis. *Journal of the American College of Cardiology,* 28**,** 1206-13.

BEYAR, R., HAUSKNECHT, M. J., HALPERIN, H. R., YIN, F. C. & WEISFELDT, M. L. 1987. Interaction between cardiac chambers and thoracic pressure in intact circulation. *The American journal of physiology,* 253**,** H1240-52.

BINANAY, C., CALIFF, R. M., HASSELBLAD, V., O'CONNOR, C. M., SHAH, M. R., SOPKO, G., STEVENSON, L. W., FRANCIS, G. S., LEIER, C. V. & MILLER, L. W. 2005. Evaluation study of congestive heart failure and pulmonary artery catheterization effectiveness: the ESCAPE trial. *JAMA : the journal of the American Medical Association,* 294**,** 1625-33.

BLAIS, C., PIBAROT, P., DUMESNIL, J. G., GARCIA, D., CHEN, D. M. & DURAND, L. G. 2001. Comparison of valve resistance with effective orifice area regarding flow dependence. *American Journal of Cardiology,* 88**,** 45-52.

BLAND, J. M. & ALTMAN, D. G. 1986. Statistical methods for assessing agreement between two methods of clinical measurement. *Lancet,* 1**,** 307-10.

BLITZ, L. R. & HERRMANN, H. C. 1996. Hemodynamic assessment of patients with low-flow, low-gradient valvular aortic stenosis. *The American journal of cardiology,* 78**,** 657-61.

BOLDT, J. 2002. Clinical review: hemodynamic monitoring in the intensive care unit. *Critical care (London, England),* 6**,** 52-9.

BOLLING, S. F., PAGANI, F. D., DEEB, G. M. & BACH, D. S. 1998. Intermediate-term outcome of mitral reconstruction in cardiomyopathy. *The Journal of thoracic and cardiovascular surgery,* 115**,** 381-6; discussion 387-8.

BONOW, R. O., CARABELLO, B. A., KANU, C., DE LEON, A. C., JR., FAXON, D. P., FREED, M. D., GAASCH, W. H., LYTLE, B. W., NISHIMURA, R. A., O'GARA, P. T., O'ROURKE, R. A., OTTO, C. M., SHAH, P. M., SHANEWISE, J. S., SMITH, S. C., JR., JACOBS, A. K., ADAMS, C. D., ANDERSON, J. L., ANTMAN, E. M., FUSTER, V., HALPERIN, J. L., HIRATZKA, L. F., HUNT, S. A., NISHIMURA, R., PAGE, R. L. & RIEGEL, B. 2006. ACC/AHA 2006 guidelines for the management of patients with valvular heart disease: a report of the American College of Cardiology/American Heart Association Task Force on Practice Guidelines (writing committee to revise the 1998 Guidelines for the Management of Patients With Valvular Heart Disease): developed in collaboration with the Society of Cardiovascular Anesthesiologists: endorsed by the Society for Cardiovascular Angiography and Interventions and the Society of Thoracic Surgeons. *Circulation,* 114**,** e84-231.

BOWDITCH, H. P. 1871. Über die eigenthümlichkeiten der reizbarkeit, welche die muskelfasern des herzens zeigen. Berichte über die verhandlungen der königlich sächsischen gesellschaft zu Leipzig. *Mathematisch-Physische Classe,* 23**,** 652-689.

BRAUNWALD, E., BRAUNWALD, N. S., ROSS, J., JR. & MORROW, A. G. 1965. Effects of Mitral-Valve Replacement on the Pulmonary Vascular Dynamics of Patients with Pulmonary Hypertension. *The New England journal of medicine,* 273**,** 509-14.

BRUN-BUISSON, C. 2000. The epidemiology of the systemic inflammatory response. *Intensive care medicine,* 26**,** S64-S74.

BURKHOFF, D. & TYBERG, J. V. 1993. Why does pulmonary venous pressure rise after onset of LV dysfunction: a theoretical analysis. *The American journal of physiology,* 265**,** H1819-28.

CAMPBELL, K. B., KIRKPATRICK, R. D., KNOWLEN, G. G. & RINGO, J. A. 1990. Late-systolic pumping properties of the left ventricle. Deviation from elastance-resistance behavior. *Circulation research,* 66**,** 218-33.

CARABELLO, B. A. 2008. The current therapy for mitral regurgitation. *Journal of the American College of Cardiology,* 52**,** 319-26.

CARSON, J. L., KELLEY, M. A., DUFF, A., WEG, J. G., FULKERSON, W. J., PALEVSKY, H. I., SCHWARTZ, J. S., THOMPSON, B. T., POPOVICH, J., JR., HOBBINS, T. E. & ET AL. 1992. The clinical course of pulmonary embolism. *The New England journal of medicine,* 326**,** 1240-5.

CASALE, P. N., PALACIOS, I. F., ABASCAL, V. M., HARRELL, L., DAVIDOFF, R., WEYMAN, A. E. & FIFER, M. A. 1992. Effects of dobutamine on Gorlin and continuity equation valve areas and valve resistance in valvular aortic stenosis. *American Journal of Cardiology,* 70**,** 1175-1179.

CHAN, C. M. & KLINGER, J. R. 2008. The right ventricle in sepsis. *Clin Chest Med,* 29**,** 661-76, ix.

CHARLTON, B. G. 1997. Restoring the balance: evidence-based medicine put in its place. *Journal of evaluation in clinical practice,* 3**,** 87-98.

CHASE, J. G., LE COMPTE, A., PREISER, J. C., SHAW, G. M., PENNING, S. & DESAIVE, T. 2011. Physiological Modelling, Tight Glycemic Control and the ICU Clinician: What are models and how can they affect practice? *Annals of Intensive Care,* 1**,** 11.

CHASE, J. G., SHAW, G., LE COMPTE, A., LONERGAN, T., WILLACY, M., WONG, X. W., LIN, J., LOTZ, T., LEE, D. & HANN, C. 2008. Implementation and evaluation of the SPRINT protocol for tight glycaemic control in critically ill patients: a clinical practice change. *Critical care (London, England),* 12**,** R49.

CHEN, C. H., NEVO, E., FETICS, B., PAK, P. H., YIN, F. C., MAUGHAN, W. L. & KASS, D. A. 1997. Estimation of central aortic pressure waveform by mathematical transformation of radial tonometry pressure. Validation of generalized transfer function. *Circulation,* 95**,** 1827-36.

CHIARI, L., CAPPELLO, A., TARTARINI, R., PAOLINI, F. & CALZAVARA, P. 1998. Model-based dialysis adequacy prediction by continuous dialysate urea monitoring. *The International journal of artificial organs,* 21**,** 526-34.

CHUNG, D. C., NIRANJAN, S. C., CLARK, J. W., JR., BIDANI, A., JOHNSTON, W. E., ZWISCHENBERGER, J. B. & TRABER, D. L. 1997. A dynamic model of ventricular interaction and pericardial influence. *The American journal of physiology,* 272**,** H2942-62.

CLANCY, T. V., NORMAN, K., REYNOLDS, R., COVINGTON, D. & MAXWELL, J. G. 1991. Cardiac output measurement in critical care patients: Thoracic Electrical Bioimpedance versus thermodilution. *The Journal of trauma,* 31**,** 1116-20; discussion 1120-1.

CLOUD, G. C., RAJKUMAR, C., KOONER, J., COOKE, J. & BULPITT, C. J. 2003. Estimation of central aortic pressure by SphygmoCor requires intra-arterial peripheral pressures. *Clin Sci (Lond),* 105**,** 219-25.

CONNORS, A. F., JR., SPEROFF, T., DAWSON, N. V., THOMAS, C., HARRELL, F. E., JR., WAGNER, D., DESBIENS, N., GOLDMAN, L., WU, A. W., CALIFF, R. M., FULKERSON, W. J., JR., VIDAILLET, H., BROSTE, S., BELLAMY, P., LYNN, J. & KNAUS, W. A. 1996. The effectiveness of right heart catheterization in the initial care of critically ill patients. SUPPORT Investigators. *Jama,* 276**,** 889-97.

COOK, D., CROWTHER, M., MEADE, M., RABBAT, C., GRIFFITH, L., SCHIFF, D., GEERTS, W. & GUYATT, G. 2005. Deep venous thrombosis in medical-surgical critically ill patients: prevalence, incidence, and risk factors. *Critical care medicine,* 33**,** 1565-71.

COTTIS, R., MAGEE, N. & HIGGINS, D. J. 2003. Haemodynamic monitoring with pulse-induced contour cardiac output (PiCCO) in critical care. *Intensive Crit Care Nurs,* 19**,** 301-7.

CRITCHLEY, L. A. & CRITCHLEY, J. A. 1999. A meta-analysis of studies using bias and precision statistics to compare cardiac output measurement techniques. *Journal of clinical monitoring and computing,* 15**,** 85-91.

DALEN, J. E. & ALPERT, J. S. 1975. Natural history of pulmonary embolism. *Progress in cardiovascular diseases,* 17**,** 259-70.

DAVIES, J. E., BAKSI, J., FRANCIS, D. P., HADJILOIZOU, N., WHINNETT, Z. I., MANISTY, C. H., AGUADO-SIERRA, J., FOALE, R. A., MALIK, I. S., TYBERG, J. V., PARKER, K. H., MAYET, J. & HUGHES, A. D. 2010. The arterial reservoir pressure increases with aging and is the major determinant of the aortic augmentation index. *Am J Physiol Heart Circ Physiol,* 298**,** H580-6.

DAVIES, J. E., HADJILOIZOU, N., LEIBOVICH, D., MALAWEERA, A., ALASTUEY-ARIMON, J., WHINNETT, Z. I., MANISTY, C. H., FRANCIS, D. P., AGUADO-SIERRA, J., FOALE, R. A., MALIK, I. S., PARKER, K. H., MAYET, J. & HUGHES, A. D. 2007. Importance of the aortic reservoir in determining the shape of the arterial pressure waveform - The forgotten lessons of Frank. *Artery Research,* 1**,** 40-45.

DELLINGER, R. P. 2003. Cardiovascular management of septic shock. *Critical care medicine,* 31**,** 946-55.

DELLINGER, R. P., CARLET, J. M., MASUR, H., GERLACH, H., CALANDRA, T., COHEN, J., GEA-BANACLOCHE, J., KEH, D., MARSHALL, J. C., PARKER, M. M., RAMSAY, G., ZIMMERMAN, J. L., VINCENT, J. L. & LEVY, M. M. 2004. Surviving Sepsis Campaign guidelines for management of severe sepsis and septic shock. *Critical care medicine,* 32**,** 858-73.

DESAIVE, T., GHUYSEN, A., LAMBERMONT, B., KOLH, P., DAUBY, P. C., STARFINGER, C., HANN, C. E., CHASE, J. G. & SHAW, G. M. 2008. Cardiovascular Modelling and Identification in Septic Shock - Experimental validation. *Proceedings of the 17th IFAC World Congress.* Seoul, Korea.

DETAINT, D., SUNDT, T. M., NKOMO, V. T., SCOTT, C. G., TAJIK, A. J., SCHAFF, H. V. & ENRIQUEZ-SARANO, M. 2006. Surgical correction of mitral regurgitation in the elderly: outcomes and recent improvements. *Circulation,* 114**,** 265-72.

DEVEREUX, R. B., PERLOFF, J. K., REICHEK, N. & JOSEPHSON, M. E. 1976. Mitral valve prolapse. *Circulation,* 54**,** 3-14.

EDWARDS, F. H., PETERSON, E. D., COOMBS, L. P., DELONG, E. R., JAMIESON, W. R., SHROYER, A. L. W. & GROVER, F. L. 2001. Prediction of operative mortality after valve replacement surgery. *Journal of the American College of Cardiology,* 37**,** 885-92.

ELLIOTT, C. G. 1992. Pulmonary physiology during pulmonary embolism. *Chest,* 101**,** 163S-171S.

ELZINGA, G., VAN GRONDELLE, R., WESTERHOF, N. & VAN DEN BOS, G. C. 1974. Ventricular interference. *The American journal of physiology,* 226**,** 941-7.

ENRIQUEZ-SARANO, M., SCHAFF, H. V., ORSZULAK, T. A., TAJIK, A. J., BAILEY, K. R. & FRYE, R. L. 1995. Valve repair improves the outcome of surgery for mitral regurgitation. A multivariate analysis. *Circulation,* 91**,** 1022-8.

EVANS, A., SHAW, G. M., LE COMPTE, A., TAN, C. S., WARD, L., STEEL, J., PRETTY, C. G., PFEIFER, L., PENNING, S., SUHAIMI, F., SIGNAL, M., DESAIVE, T. & CHASE, J. G. 2011. Pilot proof of concept clinical trials of Stochastic Targeted (STAR) glycemic control. *Ann Intensive Care,* 1**,** 38.

FEINSTEIN, A. R. & HORWITZ, R. I. 1997. Problems in the "evidence" of "evidence-based medicine". *The American journal of medicine,* 103**,** 529-35.

FISHER, J. & WHEATLEY, D. J. 1988. Hydrodynamic function of ten prosthetic heart valves in the aortic position. *Clin Phys Physiol Meas,* 9**,** 307-17.

FLAMENG, W., HERIJGERS, P. & BOGAERTS, K. 2003. Recurrence of mitral valve regurgitation after mitral valve repair in degenerative valve disease. *Circulation,* 107**,** 1609-13.

FOGLIARDI, R., DIDONFRANCESCO, M. & BURATTINI, R. 1996. Comparison of linear and nonlinear formulations of the three-element windkessel model. *American Journal of Physiology-Heart and Circulatory Physiology,* 271**,** H2661-H2668.

FOLTZ, B. D., HESSEL, E. A., 2ND & IVEY, T. D. 1984. The early course of pulmonary artery hypertension in patients undergoing mitral valve replacement with cardioplegic arrest. *The Journal of thoracic and cardiovascular surgery,* 88**,** 238-47.

FORD, L. E., FELDMAN, T. & CARROLL, J. D. 1994. Valve Resistance. *Circulation,* 89**,** 893-895.

FORD, L. E., FELDMAN, T., CHIU, Y. C. & CARROLL, J. D. 1990. Hemodynamic Resistance as a Measure of Functional Impairment in Aortic Valvular Stenosis. *Circulation research,* 66**,** 1-7.

FOSTER, E., WASSERMAN, H. S., GRAY, W., HOMMA, S., DI TULLIO, M. R., RODRIGUEZ, L., STEWART, W. J., WHITLOW, P., BLOCK, P., MARTIN, R., MERLINO, J., HERRMANN, H. C., WIEGERS, S. E., SILVESTRY, F. E., HAMILTON, A., ZUNAMON, A., KRAYBILL, K., GERBER, I. L., WEEKS, S. G., ZHANG, Y. & FELDMAN, T. 2007. Quantitative assessment of severity of mitral regurgitation

by serial echocardiography in a multicenter clinical trial of percutaneous mitral valve repair. *The American journal of cardiology,* 100**,** 1577-83.

FOURRIER, F., CHOPIN, C., GOUDEMAND, J., HENDRYCX, S., CARON, C., RIME, A., MAREY, A. & LESTAVEL, P. 1992. Septic shock, multiple organ failure, and disseminated intravascular coagulation. Compared patterns of antithrombin III, protein C, and protein S deficiencies. *Chest,* 101**,** 816-23.

FRANK 1898. Die Grundform des arteriellen Pulses. Erste Abhandlung. Mathematische Analyse. *Z Biol,* 37**,** 483-526.

FRANK, O. 1895. Zur Dynamik des Herzmuskels. *Z Biol,* 32**,** 370-437.

FRANKLIN, C. & MATHEW, J. 1994. Developing Strategies to Prevent Inhospital Cardiac-Arrest - Analyzing Responses of Physicians and Nurses in the Hours before the Event. *Critical care medicine,* 22**,** 244-247.

FUNG, Y. C. 1993. *Biomechanics : mechanical properties of living tissues,* New York, Springer-Verlag.

GAMMIE, J. S., SHENG, S., GRIFFITH, B. P., PETERSON, E. D., RANKIN, J. S., O'BRIEN, S. M. & BROWN, J. M. 2009. Trends in mitral valve surgery in the United States: results from the Society of Thoracic Surgeons Adult Cardiac Surgery Database. *The Annals of thoracic surgery,* 87**,** 1431-7; discussion 1437-9.

GAN, C. T. J., LANKHAAR, J. W., MARCUS, J. T., WESTERHOF, N., MARQUES, K. M., BRONZWAER, J. G. F., BOONSTRA, A., POSTMUS, P. E. & VONK-NOORDEGRAAF, A. 2006. Impaired left ventricular filling due to right-to-left ventricular interaction in patients with pulmonary arterial hypertension. *American Journal of Physiology-Heart and Circulatory Physiology,* 290**,** H1528-H1533.

GANZ, W., DONOSO, R., MARCUS, H. S., FORRESTER, J. S. & SWAN, H. J. 1971. A new technique for measurement of cardiac output by thermodilution in man. *The American journal of cardiology,* 27**,** 392-6.

GHUYSEN, A., LAMBERMONT, B., KOLH, P., TCHANA-SATO, V., MAGIS, D., GERARD, P., MOMMENS, V., JANSSEN, N., DESAIVE, T. & D'ORIO, V. 2008. Alteration of right ventricular-pulmonary vascular coupling in a porcine model of progressive pressure overloading. *Shock (Augusta, Ga.),* 29**,** 197-204.

GIRARD, T. D., OPAL, S. M. & ELY, E. W. 2005. Insights into severe sepsis in older patients: From epidemiology to evidence-based management. *Clinical Infectious Diseases,* 40**,** 719-727.

GOLDFINE, H., AURIGEMMA, G. P., ZILE, M. R. & GAASCH, W. H. 1998. Left ventricular length-force-shortening relations before and after surgical correction of chronic mitral regurgitation. *Journal of the American College of Cardiology,* 31**,** 180-185.

GOLDHABER, S. Z. 1998. Pulmonary embolism. *The New England journal of medicine,* 339**,** 93-104.

GOLDHABER, S. Z. 2002. Echocardiography in the management of pulmonary embolism. *Annals of internal medicine,* 136**,** 691-700.

GOLDHABER, S. Z. & ELLIOTT, C. G. 2003a. Acute pulmonary embolism: part I: epidemiology, pathophysiology, and diagnosis. *Circulation,* 108**,** 2726-9.

GOLDHABER, S. Z. & ELLIOTT, C. G. 2003b. Acute pulmonary embolism: part II: risk stratification, treatment, and prevention. *Circulation,* 108**,** 2834-8.

GOLDHABER, S. Z., HENNEKENS, C. H., EVANS, D. A., NEWTON, E. C. & GODLESKI, J. J. 1982. Factors associated with correct antemortem diagnosis of major pulmonary embolism. *The American journal of medicine,* 73**,** 822-6.

GOLDHABER, S. Z. & MORRISON, R. B. 2002. Cardiology patient pages. Pulmonary embolism and deep vein thrombosis. *Circulation,* 106**,** 1436-8.

GRAPSA, J., DAWSON, D., PANDIS, D., NTALARIZOU, E., CHEUNG, W. S., EFTHIMIADIS, I., ZIMBARRA CABRITA, I., PUNJABI, P. & NIHOYANNOPOULOS, P. 2012. Mitral valve repair results in better right ventricular remodelling than valve replacement for degenerative mitral regurgitation: a three-dimensional echocardiographic study. *Hellenic journal of cardiology : HJC = Hellenike kardiologike epitheorese,* 53**,** 279-86.

GROENEVELD, A. B., NAUTA, J. J. & THIJS, L. G. 1988. Peripheral vascular resistance in septic shock: its relation to outcome. *Intensive care medicine,* 14**,** 141-7.

GROSSMAN, W., BRAUNWALD, E., MANN, T., MCLAURIN, L. P. & GREEN, L. H. 1977. Contractile state of the left ventricle in man as evaluated from end-systolic pressure-volume relations. *Circulation,* 56**,** 845-52.

GUYTON, A. C. & HALL, J. E. 2000. *Textbook of medical physiology,* Philadelphia, Saunders.

HANN, C. E., CHASE, J. G., DESAIVE, T., FROISSART, C. B., REVIE, J., STEVENSON, D., LAMBERMONT, B., GHUYSEN, A., KOLH, P. & SHAW, G. M. 2010. Unique parameter identification for cardiac diagnosis in critical care using minimal data sets. *Computer methods and programs in biomedicine,* 99**,** 75-87.

HANN, C. E., CHASE, J. G. & SHAW, G. M. 2005. Efficient implementation of non-linear valve law and ventricular interaction dynamics in the minimal cardiac model. *Computer methods and programs in biomedicine,* 80**,** 65-74.

HANN, C. E., CHASE, J. G. & SHAW, G. M. 2006. Integral-based identification of patient specific parameters for a minimal cardiac model. *Computer methods and programs in biomedicine,* 81**,** 181-92.

HARADA, T., KUBO, H., MORI, T. & SATO, T. 2005. Pulmonary and cardiovascular integrated model controlled with oxygen consumption. *Conference proceedings,* 1**,** 304-7.

HARDMAN, J. G., BEDFORTH, N. M., AHMED, A. B., MAHAJAN, R. P. & AITKENHEAD, A. R. 1998. A physiology simulator: validation of its respiratory components and its ability to predict the patient's response to changes in mechanical ventilation. *British journal of anaesthesia,* 81**,** 327-32.

HAYEK, E., GRING, C. N. & GRIFFIN, B. P. 2005. Mitral valve prolapse. *Lancet,* 365**,** 507-18.

HEIDENREICH, P. A., TROGDON, J. G., KHAVJOU, O. A., BUTLER, J., DRACUP, K., EZEKOWITZ, M. D., FINKELSTEIN, E. A., HONG, Y. L., JOHNSTON, S. C., KHERA, A., LLOYD-JONES, D. M., NELSON, S. A., NICHOL, G., ORENSTEIN, D., WILSON, P. W. F., WOO, Y. J., COORDINA, A. H. A. A., COUNCIL, S., INTER, C. C. R., CARDIOLOGY, C. C., PREVENTION, C. E., THROMBOSI, C. A., C, C. C. C., NURSING, C. C., DIS, C. K. C., ANESTHE, C. C. S. & QUALITY, I. C. 2011. Forecasting the Future of Cardiovascular Disease in the United States A Policy Statement From the American Heart Association. *Circulation,* 123**,** 933-944.

HEIT, J. A., SILVERSTEIN, M. D., MOHR, D. N., PETTERSON, T. M., O'FALLON, W. M. & MELTON, L. J., 3RD 2000. Risk factors for deep vein thrombosis and pulmonary embolism: a population-based case-control study. *Archives of internal medicine,* 160**,** 809-15.

HOCHMAN, J. S. & OHMAN, E. M. 2009. *Cardiogenic Shock,* Dallas, USA, Wiley-Blackwell.

HOLLENBERG, S. M., KAVINSKY, C. J. & PARRILLO, J. E. 1999. Cardiogenic shock. *Annals of internal medicine,* 131**,** 47-59.

HOPE, S. A., TAY, D. B., MEREDITH, I. T. & CAMERON, J. D. 2004. Use of arterial transfer functions for the derivation of central aortic waveform characteristics in subjects with type 2 diabetes and cardiovascular disease. *Diabetes care,* 27**,** 746-751.

HOPE, S. A., TAY, D. B., MEREDITH, I. T. & CAMERON, J. D. 2005. Waveform dispersion, not reflection, may be the major determinant of aortic pressure wave morphology. *Am J Physiol Heart Circ Physiol,* 289**,** H2497-502.

HOSENPUD, J. D. & GREENBERG, B. H. 2007. *Congestive Heart Failure,* Philadelphia, Lippincott Williams & Wilkins.

HUNTER, K. S., LEE, P. F., LANNING, C. J., IVY, D. D., KIRBY, K. S., CLAUSSEN, L. R., CHAN, K. C. & SHANDAS, R. 2008. Pulmonary vascular input impedance is a combined measure of pulmonary vascular resistance and stiffness and predicts clinical outcomes better than pulmonary vascular resistance alone in pediatric patients with pulmonary hypertension. *American heart journal,* 155**,** 166-74.

JOHNSTON, I. G., FRASER, J. E., SABAPATHY, S. & KRUGER, P. S. 2008a. The pulmonary artery catheter in Australasia: a survey investigating intensive care physicians' knowledge and perception of future trends in use. *Anaesthesia and intensive care,* 36**,** 84-89.

JOHNSTON, I. G., FRASER, J. F., SABAPATHY, S. & KRUGER, P. S. 2008b. The pulmonary artery catheter in Australasia: a survey investigating intensive care physicians' knowledge and perception of future trends in use. *Anaesthesia and intensive care,* 36**,** 84-9.

KAPPEL, F., FINK, M. & BATZEL, J. J. 2007. Aspects of control of the cardiovascular-respiratory system during orthostatic stress induced by lower body negative pressure. *Mathematical biosciences,* 206**,** 273-308.

KASPER, D. L. & HARRISON, T. R. 2005. *Harrison's principles of internal medicine,* New York, McGraw-Hill, Medical Pub. Division.

KASS, D. A. & MAUGHAN, W. L. 1988. From 'Emax' to pressure-volume relations: a broader view. *Circulation,* 77**,** 1203-12.

KASS, D. A., MAUGHAN, W. L., GUO, Z. M., KONO, A., SUNAGAWA, K. & SAGAWA, K. 1987. Comparative influence of load versus inotropic states on indexes of ventricular contractility: experimental and theoretical analysis based on pressure-volume relationships. *Circulation,* 76**,** 1422-36.

KASS, D. A., MIDEI, M., GRAVES, W., BRINKER, J. A. & MAUGHAN, W. L. 1988. Use of a conductance (volume) catheter and transient inferior vena caval occlusion for rapid determination of pressure-volume relationships in man. *Catheterization and Cardiovascular Diagnosis,* 15**,** 192-202.

KELLY, R. P., TING, C. T., YANG, T. M., LIU, C. P., MAUGHAN, W. L., CHANG, M. S. & KASS, D. A. 1992. Effective arterial elastance as index of arterial vascular load in humans. *Circulation,* 86**,** 513-21.

KENNEDY, P. J., LEATHLEY, C. M. & HUGHES, C. F. 2010. Clinical practice variation. *The Medical journal of Australia,* 193**,** S97-9.

KLABUNDE, R. E. 2004. *Cardiovascular Physiology Concepts*, Lippincott Williams and Wilkins.

KNOWLTON, F. P. & STARLING, E. H. 1912. The influence of variations in temperature and blood-pressure on the performance of the isolated mammalian heart. *Journal of Physiology-London,* 44**,** 206-220.

KONSTAM, M. A., COHEN, S. R., SALEM, D. N., CONLON, T. P., ISNER, J. M., DAS, D., ZILE, M. R., LEVINE, H. J. & KAHN, P. C. 1985. Comparison of Left and Right Ventricular End-Systolic Pressure-Volume Relations in Congestive Heart-Failure. *Journal of the American College of Cardiology,* 5**,** 1326-1334.

KREIMEIER, U. 2000. Pathophysiology of fluid imbalance. *Critical care (London, England),* 4 Suppl 2**,** S3-7.

KROEKER, C. A., SHRIVE, N. G., BELENKIE, I. & TYBERG, J. V. 2003. Pericardium modulates left and right ventricular stroke volumes to compensate for sudden changes in atrial volume. *Am J Physiol Heart Circ Physiol,* 284**,** H2247-54.

KUSIAK, V. & BREST, A. N. 1986. Acute mitral regurgitation: pathophysiology and management. *Cardiovasc Clin,* 16**,** 257-80.

LAMBERMONT, B., DELANAYE, P., DOGNE, J. M., GHUYSEN, A., JANSSEN, N., DUBOIS, B., DESAIVE, T., KOLH, P., D'ORIO, V. & KRZESINSKI, J. M. 2006. Large-pore membrane hemofiltration increases cytokine clearance and improves right ventricular-vascular coupling during endotoxic shock in pigs. *Artificial organs,* 30**,** 560-564.

LAMBERMONT, B., GHUYSEN, A., KOLH, P., TCHANA-SATO, V., SEGERS, P., GERARD, P., MORIMONT, P., MAGIS, D., DOGNE, J. M., MASEREEL, B. & D'ORIO, V. 2003. Effects of endotoxic shock on right ventricular systolic function and mechanical efficiency. *Cardiovascular research,* 59**,** 412-418.

LAMBERMONT, B., KOLH, P., GHUYSEN, A., SEGERS, P., DOGNE, J. M., TCHANA-SATO, V., MORIMONT, P., BENOIT, P., GERARD, P., MASEREEL, B. & D'ORIO, V. 2004. Effect of a novel

thromboxane A2 inhibitor on right ventricular-arterial coupling in endotoxic shock. *Shock (Augusta, Ga.),* 21**,** 45-51.

LANG, R. M., BOROW, K. M., NEUMANN, A. & JANZEN, D. 1986. Systemic vascular resistance: an unreliable index of left ventricular afterload. *Circulation,* 74**,** 1114-23.

LE COMPTE, A., CHASE, J. G., LYNN, A., HANN, C., SHAW, G., WONG, X. W. & LIN, J. 2009. Blood glucose controller for neonatal intensive care: virtual trials development and first clinical trials. *Journal of diabetes science and technology,* 3**,** 1066-81.

LEUNG, D. Y., GRIFFIN, B. P., STEWART, W. J., COSGROVE, D. M., 3RD, THOMAS, J. D. & MARWICK, T. H. 1996. Left ventricular function after valve repair for chronic mitral regurgitation: predictive value of preoperative assessment of contractile reserve by exercise echocardiography. *Journal of the American College of Cardiology,* 28**,** 1198-205.

LEVITZKY, M. G. 2007. Pulmonary physiology. *Lange physiology series.* 7th ed. New York: McGraw-Hill Medical.

LI, J. K. J., CUI, T. & DRZEWIECKI, G. M. 1990. A Nonlinear Model of the Arterial System Incorporating a Pressure-Dependent Compliance. *Ieee Transactions on Biomedical Engineering,* 37**,** 673-678.

LIGHTHILL, M. J. 1978. *Waves in fluids,* Cambridge [Eng.] ; New York, Cambridge University Press.

LINTON, R. A., BAND, D. M. & HAIRE, K. M. 1993. A new method of measuring cardiac output in man using lithium dilution. *British journal of anaesthesia,* 71**,** 262-6.

LITTLE, W. C. & FREEMAN, G. L. 2006. Pericardial disease. *Circulation,* 113**,** 1622-32.

LONERGAN, T., COMPTE, A. L., WILLACY, M., CHASE, J. G., SHAW, G. M., HANN, C. E., LOTZ, T., LIN, J. & WONG, X. W. 2006. A pilot study of the SPRINT protocol for tight glycemic control in critically Ill patients. *Diabetes technology & therapeutics,* 8**,** 449-62.

LU, K., CLARK, J. W., GHORBEL, F. H., WARE, D. L., ZWISCHENBERGER, J. B. & BIDANI, A. 2003. Whole-Body Gas Exchange in Human Predicted by a Cardiopulmonary Model. *Cardiovascular Engineering,* 3**,** 1-19.

LUALDI, J. C. & GOLDHABER, S. Z. 1995. Right-Ventricular Dysfunction after Acute Pulmonary-Embolism - Pathophysiologic Factors, Detection, and Therapeutic Implications. *American heart journal,* 130**,** 1276-1282.

LYNCH, P. J. & JAFFE, C. C. 2006. Electrical conduction system of the heart.

MACLEAN, L. D., MULLIGAN, W. G., MCLEAN, A. P. & DUFF, J. H. 1967. Patterns of septic shock in man--a detailed study of 56 patients. *Annals of surgery,* 166**,** 543-62.

MANGANO, D. T. 1994. Perioperative cardiac morbidity--epidemiology, costs, problems, and solutions. *West J Med,* 161**,** 87-9.

MARTIN, G. S., MANNINO, D. M., EATON, S. & MOSS, M. 2003. The epidemiology of sepsis in the United States from 1979 through 2000. *The New England journal of medicine,* 348**,** 1546-54.

MARTINEZ-SELLES, M., GARCIA-FERNANDEZ, M. A., LARIOS, E., MORENO, M., PINTO, A., GARCIA-ROBLES, J. A., PEREZ-DAVID, E. & FERNANDEZ-AVILES, F. 2009. Etiology and short-term prognosis of severe mitral regurgitation. *The international journal of cardiovascular imaging,* 25**,** 121-6.

MASCHERBAUER, J., SCHIMA, H., ROSENHEK, R., CZERNY, M., MAURER, G. & BAUMGARTNER, H. 2004. Value and limitations of aortic valve resistance with particular consideration of low flow - low gradient aortic stenosis: an in vitro study. *European heart journal,* 25**,** 787-793.

MCKINLAY, M. & O'LOUGHLIN, V. 2007. *Human Anatomy*, McGraw-Hill.

MELCHIOR, F. M., SRINIVASAN, R. S. & CHARLES, J. B. 1992. Mathematical modeling of human cardiovascular system for simulation of orthostatic response. *The American journal of physiology,* 262**,** H1920-33.

MERMEL, L. A., MCCORMICK, R. D., SPRINGMAN, S. R. & MAKI, D. G. 1991. The Pathogenesis and Epidemiology of Catheter-Related Infection with Pulmonary-Artery Swan-Ganz Catheters - a Prospective-Study Utilizing Molecular Subtyping. *American Journal of Medicine,* 91**,** S197-S205.

MERX, M. W. & WEBER, C. 2007. Sepsis and the heart. *Circulation,* 116**,** 793-802.

MICHARD, F., ALAYA, S., ZARKA, W., BAHLOUL, M., RICHARD, C. & TEBOUL, J. L. 2003. Global end-diastolic volume as an indicator of cardiac preload in patients with septic shock. *Chest,* 124**,** 1900-1908.

MITCHELL, G. F., PARISE, H., BENJAMIN, E. J., LARSON, M. G., KEYES, M. J., VITA, J. A., VASAN, R. S. & LEVY, D. 2004. Changes in arterial stiffness and wave reflection with advancing age in healthy men and women: the Framingham Heart Study. *Hypertension,* 43**,** 1239-45.

MOKADAM, N. A., STOUT, K. K. & VERRIER, E. D. 2011. Management of acute regurgitation in left-sided cardiac valves. *Texas Heart Institute journal / from the Texas Heart Institute of St Luke's Episcopal Hospital, Texas Children's Hospital,* 38**,** 9-19.

MORRELL, M. T. & DUNNILL, M. S. 1968. The post-mortem incidence of pulmonary embolism in a hospital population. *The British journal of surgery,* 55**,** 347-52.

MUTOH, T., KAZUMATA, K., AJIKI, M., USHIKOSHI, S. & TERASAKA, S. 2007. Goal-directed fluid management by bedside transpulmonary hemodynamic monitoring after subarachnoid hemorrhage. *Stroke; a journal of cerebral circulation,* 38**,** 3218-24.

MUTUNGA, M., FULTON, B., BULLOCK, R., BATCHELOR, A., GASCOIGNE, A., GILLESPIE, J. I. & BAUDOUIN, S. V. 2001. Circulating endothelial cells in patients with septic shock. *Am J Respir Crit Care Med,* 163**,** 195-200.

NADLER, S. B., HIDALGO, J. H. & BLOCH, T. 1962. Prediction of blood volume in normal human adults. *Surgery,* 51**,** 224-32.

NAEIJE, R. 2003. Pulmonary vascular resistance. A meaningless variable? *Intensive care medicine,* 29**,** 526-9.

NKOMO, V. T., GARDIN, J. M., SKELTON, T. N., GOTTDIENER, J. S., SCOTT, C. G. & ENRIQUEZ-SARANO, M. 2006. Burden of valvular heart diseases: a population-based study. *Lancet,* 368**,** 1005-11.

O'NEILL, D. & PERRIN, D. 2002. Fluid resuscitation in critical care. *Nurs Times,* 98**,** 39-40.

O'ROURKE, M. F. 2004. Estimation of central aortic pressure by SphygmoCor requires accurate peripheral pressure measurement. *Clin Sci (Lond),* 106**,** 434-5; author reply 436-7.

O'ROURKE, M. F. & YAGINUMA, T. 1984. Wave reflections and the arterial pulse. *Archives of internal medicine,* 144**,** 366-71.

OLANSEN, J. B., CLARK, J. W., KHOURY, D., GHORBEL, F. & BIDANI, A. 2000. A closed-loop model of the canine cardiovascular system that includes ventricular interaction. *Computers and Biomedical Research,* 33**,** 260-95.

OPDAM, H. I., WAN, L. & BELLOMO, R. 2007. A pilot assessment of the FloTrac cardiac output monitoring system. *Intensive care medicine,* 33**,** 344-9.

OSPINA-TASCON, G. A., BUCHELE, G. L. & VINCENT, J. L. 2008. Multicenter, randomized, controlled trials evaluating mortality in intensive care: doomed to fail? *Critical care medicine,* 36**,** 1311-22.

OSRANEK, M., EISENACH, J. H., KHANDHERIA, B. K., CHANDRASEKARAN, K., SEWARD, J. B. & BELOHLAVEK, M. 2008. Arterioventricular coupling and ventricular efficiency after antihypertensive therapy: a noninvasive prospective study. *Hypertension,* 51**,** 275-81.

OTTO, C. M. 2001. Clinical practice. Evaluation and management of chronic mitral regurgitation. *The New England journal of medicine,* 345**,** 740-6.

PAEME, S., MOORHEAD, K. T., CHASE, J. G., LAMBERMONT, B., KOLH, P., D'ORIO, V., PIERARD, L., MOONEN, M., LANCELLOTTI, P., DAUBY, P. C. & DESAIVE, T. 2011. Mathematical multi-scale model of the cardiovascular system including mitral valve dynamics. Application to ischemic mitral insufficiency. *Biomed Eng Online,* 10**,** 86.

PAOLOCCI, N., KATORI, T., CHAMPION, H. C., ST JOHN, M. E., MIRANDA, K. M., FUKUTO, J. M., WINK, D. A. & KASS, D. A. 2003. Positive inotropic and lusitropic effects of HNO/NO- in failing hearts: independence from beta-adrenergic signaling. *Proceedings of the National Academy of Sciences of the United States of America,* 100**,** 5537-42.

PARKER, K. H. & JONES, C. J. 1990. Forward and backward running waves in the arteries: analysis using the method of characteristics. *Journal of biomechanical engineering,* 112**,** 322-6.

PARKER, M. M., SHELHAMER, J. H., BACHARACH, S. L., GREEN, M. V., NATANSON, C., FREDERICK, T. M., DAMSKE, B. A. & PARRILLO, J. E. 1984. Profound but reversible myocardial depression in patients with septic shock. *Annals of internal medicine,* 100**,** 483-90.

PARRILLO, J. E., PARKER, M. M., NATANSON, C., SUFFREDINI, A. F., DANNER, R. L., CUNNION, R. E. & OGNIBENE, F. P. 1990. Septic shock in humans. Advances in the understanding of pathogenesis, cardiovascular dysfunction, and therapy. *Annals of internal medicine,* 113**,** 227-42.

PASTERKAMP, E., KRUITHOF, C. J., VAN DER MEER, F. J., ROSENDAAL, F. R. & VANDERSCHOOT, J. P. 2005. A model-based algorithm for the monitoring of long-term anticoagulation therapy. *Journal of thrombosis and haemostasis,* 3**,** 915-21.

PAUCA, A. L., O'ROURKE, M. F. & KON, N. D. 2001. Prospective evaluation of a method for estimating ascending aortic pressure from the radial artery pressure waveform. *Hypertension,* 38**,** 932-7.

PERKINS, G. D., MCAULEY, D. F., DAVIES, S. & GAO, F. 2003. Discrepancies between clinical and postmortem diagnoses in critically ill patients: an observational study. *Critical Care,* 7**,** R129-R132.

PINSKY, M. R. 2003. Rationale for cardiovascular monitoring. *Current opinion in critical care,* 9**,** 222-4.

PINSKY, M. R. 2005. Cardiovascular issues in respiratory care. *Chest,* 128**,** 592S-597S.

PINSKY, M. R. 2007. Hemodynamic evaluation and monitoring in the ICU. *Chest,* 132**,** 2020-9.

PIRONET, A., REVIE, J., PAEME, S., DAUBY, P. C., CHASE, J. G. & DESAIVE, T. 2012. Development and Identification of a Closed-Loop Moded of the Cardiovascular System Incuding the Atria. *Proc 8th IFAC Symposium on Biological and Medical Systems (BMS2012).* Budapest, Hungary.

RAMRITU, P., HALTON, K., COOK, D., WHITBY, M. & GRAVES, N. 2008. Catheter-related bloodstream infections in intensive care units: a systematic review with meta-analysis. *Journal of Advanced Nursing,* 62**,** 3-21.

RAMSAY, J. G. 1999. Cardiac management in the ICU. *Chest,* 115**,** 138S-144S.

REVIE, J. A., STEVENSON, D., CHASE, J. G., LAMBERMONT, B., GHUYSEN, A., KOLH, P., SHAW, G. M. & DESAIVE, T. 2012. Model-Based Monitoring of Septic Shock Treated with Large-Pore Hemofiltration Therapy. *Proc 8th IFAC Symposium on Biological and Medical Systems (BMS2012).* Budapest, Hungary.

REVIE, J. A., STEVENSON, D. J., CHASE, J. G., HANN, C. E., LAMBERMONT, B. C., GHUYSEN, A., KOLH, P., MORIMONT, P., SHAW, G. M. & DESAIVE, T. 2011a. Clinical detection and monitoring of acute pulmonary embolism: proof of concept of a computer-based method. *Ann Intensive Care,* 1**,** 33.

REVIE, J. A., STEVENSON, D. J., CHASE, J. G., HANN, C. E., LAMBERMONT, B. C., GHUYSEN, A., KOLH, P., SHAW, G. M., HELDMANN, S. & DESAIVE, T. 2011b. Validation of subject-specific cardiovascular system models from porcine measurements. *Computer methods and programs in biomedicine,* 109**,** 197-210.

RIVERS, E., NGUYEN, B., HAVSTAD, S., RESSLER, J., MUZZIN, A., KNOBLICH, B., PETERSON, E. & TOMLANOVICH, M. 2001. Early goal-directed therapy in the treatment of severe sepsis and septic shock. *The New England journal of medicine,* 345**,** 1368-77.

SAFDAR, N., KLUGER, D. M. & MAKI, D. G. 2002. A review of risk factors for catheter-related bloodstream infection caused by percutaneously inserted, noncuffed central venous catheters - Implications for preventive strategies. *Medicine,* 81**,** 466-479.

SAGAWA, K. 1981. The end-systolic pressure-volume relation of the ventricle: definition, modifications and clinical use. *Circulation,* 63**,** 1223-7.

SAGAWA, K., SUGA, H., SHOUKAS, A. A. & BAKALAR, K. M. 1977. End-systolic pressure/volume ratio: a new index of ventricular contractility. *The American journal of cardiology,* 40**,** 748-53.

SAKKA, S. G., RUHL, C. C., PFEIFFER, U. J., BEALE, R., MCLUCKIE, A., REINHART, K. & MEIER-HELLMANN, A. 2000. Assessment of cardiac preload and extravascular lung water by single transpulmonary thermodilution. *Intensive care medicine,* 26**,** 180-7.

SALANDIN, V., ZUSSA, C., RISICA, G., MICHIELON, P., PACCAGNELLA, A., CIPOLOTTI, G. & SIMINI, G. 1988. Comparison of cardiac output estimation by thoracic electrical bioimpedance, thermodilution, and Fick methods. *Critical care medicine,* 16**,** 1157-8.

SANDHAM, J. D., HULL, R. D., BRANT, R. F., KNOX, L., PINEO, G. F., DOIG, C. J., LAPORTA, D. P., VINER, S., PASSERINI, L., DEVITT, H., KIRBY, A. & JACKA, M. 2003. A randomized, controlled trial of the use of pulmonary-artery catheters in high-risk surgical patients. *The New England journal of medicine,* 348**,** 5-14.

SANTAMORE, W. P. & BURKHOFF, D. 1991. Hemodynamic consequences of ventricular interaction as assessed by model analysis. *The American journal of physiology,* 260**,** H146-57.

SARNOFF, S. J. & MITCHELL, J. H. 1961. The regulation of the performance of the heart. *The American journal of medicine,* 30**,** 747-71.

SCHNEIDER, A. J., TEULE, G. J., GROENEVELD, A. B., NAUTA, J., HEIDENDAL, G. A. & THIJS, L. G. 1988. Biventricular performance during volume loading in patients with early septic shock, with emphasis on the right ventricle: a combined hemodynamic and radionuclide study. *American heart journal,* 116**,** 103-12.

SEFERIAN, E. G. & AFESSA, B. 2006. Demographic and clinical variation of adult intensive care unit utilization from a geographically defined population. *Critical care medicine,* 34**,** 2113-9.

SEGERS, P., STERGIOPULOS, N., SCHREUDER, J. J., WESTERHOF, B. E. & WESTERHOF, N. 2000a. Left ventricular wall stress normalization in chronic pressure-overloaded heart: a mathematical model study. *Am J Physiol Heart Circ Physiol,* 279**,** H1120-7.

SEGERS, P., STERGIOPULOS, N. & WESTERHOF, N. 2000b. Quantification of the contribution of cardiac and arterial remodeling to hypertension. *Hypertension,* 36**,** 760-5.

SHAH, M. R., HASSELBLAD, V., STEVENSON, L. W., BINANAY, C., O'CONNOR, C. M., SOPKO, G. & CALIFF, R. M. 2005. Impact of the pulmonary artery catheter in critically ill patients: meta-analysis of randomized clinical trials. *JAMA : the journal of the American Medical Association,* 294**,** 1664-70.

SHEKERDEMIAN, L. & BOHN, D. 1999. Cardiovascular effects of mechanical ventilation. *Archives of disease in childhood,* 80**,** 475-80.

SLEIGH, J. W. 1997. Logical limits of randomized controlled trials. *Journal of evaluation in clinical practice,* 3**,** 145-8.

SMISETH, O. A., THOMPSON, C. R., LING, H., ROBINSON, M. & MIYAGISHIMA, R. T. 1996. A potential clinical method for calculating transmural left ventricular filling pressure during positive end-expiratory pressure ventilation: an intraoperative study in humans. *Journal of the American College of Cardiology,* 27**,** 155-60.

SMITH, B. W. 2004. *Minimal Haemodynamic Modelling of the Heart and Circulation for Clinical Application.* Doctor of Philosophy, University of Canterbury.

SMITH, B. W., ANDREASSEN, S., SHAW, G. M., JENSEN, P. L., REES, S. E. & CHASE, J. G. 2007. Simulation of cardiovascular system diseases by including the autonomic nervous system into a minimal model. *Computer methods and programs in biomedicine,* 86**,** 153-60.

SMITH, B. W., CHASE, J. G., NOKES, R. I., SHAW, G. M. & WAKE, G. 2004. Minimal haemodynamic system model including ventricular interaction and valve dynamics. *Medical engineering & physics,* 26**,** 131-9.

SMITH, B. W., CHASE, J. G., SHAW, G. M. & NOKES, R. I. 2005. Experimentally verified minimal cardiovascular system model for rapid diagnostic assistance. *Control Engineering Practice,* 13**,** 1183-1193.

SMITH, B. W., CHASE, J. G., SHAW, G. M. & NOKES, R. I. 2006. Simulating transient ventricular interaction using a minimal cardiovascular system model. *Physiological measurement,* 27**,** 165-79.

SMITH, W. R., POSES, R. M., MCCLISH, D. K., HUBER, E. C., CLEMO, F. L. W., ALEXANDER, D. & SCHMITT, B. P. 2002. Prognostic judgments and triage decisions for patients with acute congestive heart failure. *Chest,* 121**,** 1610-1617.

SMULDERS, Y. M. 2000. Pathophysiology and treatment of haemodynamic instability in acute pulmonary embolism: the pivotal role of pulmonary vasoconstriction. *Cardiovascular research,* 48**,** 23-33.

SONI, N. & WILLIAMS, P. 2008. Positive pressure ventilation: what is the real cost? *British journal of anaesthesia,* 101**,** 446-57.

STARFINGER, C. 2008. *Patient-Specific Modelling of the Cardiovascular System for Diagnosis and Therapy Assistance in Critical Care.* Doctor of Philosophy Doctorate, University of Canterbury.

STARFINGER, C., CHASE, J. G., HANN, C. E., SHAW, G. M., LAMBERMONT, B., GHUYSEN, A., KOLH, P., DAUBY, P. C. & DESAIVE, T. 2008a. Model-based identification and diagnosis of a porcine model of induced endotoxic shock with hemofiltration. *Mathematical biosciences,* 216**,** 132-9.

STARFINGER, C., CHASE, J. G., HANN, C. E., SHAW, G. M., LAMBERT, P., SMITH, B. W., SLOTH, E., LARSSON, A., ANDREASSEN, S. & REES, S. 2008b. Model-based identification of PEEP titrations during different volemic levels. *Computer methods and programs in biomedicine,* 91**,** 135-44.

STARFINGER, C., HANN, C. E., CHASE, J. G., DESAIVE, T., GHUYSEN, A. & SHAW, G. M. 2007. Model-based cardiac diagnosis of pulmonary embolism. *Computer methods and programs in biomedicine,* 87**,** 46-60.

STARLING, E. H. & VISSCHER, M. B. 1927. The regulation of the energy output of the heart. *The Journal of physiology,* 62**,** 243-61.

STARLING, M. R. 1993. Left ventricular-arterial coupling relations in the normal human heart. *American heart journal,* 125**,** 1659-66.

STARLING, M. R. 1995. Effects of valve surgery on left ventricular contractile function in patients with long-term mitral regurgitation. *Circulation,* 92**,** 811-8.

STEIN, P. D. & HENRY, J. W. 1995. Prevalence of acute pulmonary embolism among patients in a general hospital and at autopsy. *Chest,* 108**,** 978-81.

STETZ, C. W., MILLER, R. G., KELLY, G. E. & RAFFIN, T. A. 1982. Reliability of the thermodilution method in the determination of cardiac output in clinical practice. *The American review of respiratory disease,* 126**,** 1001-4.

STEVENSON, D., REVIE, J., CHASE, J. G., HANN, C. E., SHAW, G. M., LAMBERMONT, B., GHUYSEN, A., KOLH, P. & DESAIVE, T. 2012a. Algorithmic processing of pressure waveforms to facilitate estimation of cardiac elastance. *Biomed Eng Online,* 11**,** 28.

STEVENSON, D., REVIE, J., CHASE, J. G., HANN, C. E., SHAW, G. M., LAMBERMONT, B., GHUYSEN, A., KOLH, P. & DESAIVE, T. 2012b. Beat-to-beat estimation of the continuous left and right cardiac elastance from metrics commonly available in clinical settings *BioMed Eng Online*.

STOUFFER, G. A. 2008. Cardiovascular hemodynamics for the clinician. Malden, MA: Blackwell Futura.

SUGA, H., HISANO, R., GOTO, Y., YAMADA, O. & IGARASHI, Y. 1983. Effect of positive inotropic agents on the relation between oxygen consumption and systolic pressure volume area in canine left ventricle. *Circulation research,* 53**,** 306-18.

SUGA, H., SAGAWA, K. & SHOUKAS, A. A. 1973. Load independence of the instantaneous pressure-volume ratio of the canine left ventricle and effects of epinephrine and heart rate on the ratio. *Circulation research,* 32**,** 314-22.

SUNAGAWA, K., MAUGHAN, W. L., BURKHOFF, D. & SAGAWA, K. 1983. Left ventricular interaction with arterial load studied in isolated canine ventricle. *The American journal of physiology,* 245**,** H773-80.

SURI, R. M., SCHAFF, H. V., DEARANI, J. A., SUNDT, T. M., 3RD, DALY, R. C., MULLANY, C. J., SARANO, M. E. & ORSZULAK, T. A. 2008. Determinants of early decline in ejection fraction after surgical correction of mitral regurgitation. *The Journal of thoracic and cardiovascular surgery,* 136**,** 442-7.

THIELE, R. H. & DURIEUX, M. E. 2011. Arterial waveform analysis for the anesthesiologist: past, present, and future concepts. *Anesthesia and analgesia,* 113**,** 766-76.

TIBBY, S. M. & MURDOCH, I. A. 2003. Monitoring cardiac function in intensive care. *Archives of disease in childhood,* 88**,** 46-52.

TONELLI, M. R. 1998. The philosophical limits of evidence-based medicine. *Acad Med,* 73**,** 1234-40.

TSITLIK, J. E., HALPERIN, H. R., POPEL, A. S., SHOUKAS, A. A., YIN, F. C. & WESTERHOF, N. 1992. Modeling the circulation with three-terminal electrical networks containing special nonlinear capacitors. *Annals of biomedical engineering,* 20**,** 595-616.

TUMAN, K. J., MCCARTHY, R. J., MARCH, R. J., NAJAFI, H. & IVANKOVICH, A. D. 1992. Morbidity and duration of ICU stay after cardiac surgery. A model for preoperative risk assessment. *Chest,* 102**,** 36-44.

TYBERG, J. V., DAVIES, J. E., WANG, Z., WHITELAW, W. A., FLEWITT, J. A., SHRIVE, N. G., FRANCIS, D. P., HUGHES, A. D., PARKER, K. H. & WANG, J. J. 2009. Wave intensity analysis and the development of the reservoir-wave approach. *Medical & biological engineering & computing,* 47**,** 221-32.

UCKUN, S., DAWANT, B. M. & LINDSTROM, D. P. 1993. Model-based diagnosis in intensive care monitoring: the YAQ approach. *Artif Intell Med,* 5**,** 31-48.

UHLAND, H. & GOLDBERG, L. M. 1964. Pulmonary Embolism: A Commonly Missed Clinical Entity. *Diseases of the chest,* 45**,** 533-6.

URSINO, M. 1999. A mathematical model of the carotid baroregulation in pulsating conditions. *IEEE transactions on bio-medical engineering,* 46**,** 382-92.

VINCENT, J. L. 2004. Evidence-based medicine in the ICU: important advances and limitations. *Chest,* 126**,** 592-600.

VINCENT, J. L., GRIS, P., COFFERNILS, M., LEON, M., PINSKY, M., REUSE, C. & KAHN, R. J. 1992. Myocardial depression characterizes the fatal course of septic shock. *Surgery,* 111**,** 660-7.

WALSH, T. S., MCCLELLAND, D. B., LEE, R. J., GARRIOCH, M., MACIVER, C. R., MCARDLE, F., CROFTS, S. L., MELLOR, I. & GRP, A. S. 2005. Prevalence of ischaemic heart disease at admission to intensive care and its influence on red cell transfusion thresholds: multicentre Scottish Study. *British journal of anaesthesia,* 94**,** 445-452.

WANG, J. J., O'BRIEN, A. B., SHRIVE, N. G., PARKER, K. H. & TYBERG, J. V. 2003. Time-domain representation of ventricular-arterial coupling as a windkessel and wave system. *Am J Physiol Heart Circ Physiol,* 284**,** H1358-68.

WAUTHY, P., PAGNAMENTA, A., VASSALLI, F., NAEIJE, R. & BRIMIOULLE, S. 2004. Right ventricular adaptation to pulmonary hypertension: an interspecies comparison. *Am J Physiol Heart Circ Physiol,* 286**,** H1441-7.

WEBER, K. T., JANICKI, J. S., HUNTER, W. C., SHROFF, S., PEARLMAN, E. S. & FISHMAN, A. P. 1982. The contractile behavior of the heart and its functional coupling to the circulation. *Progress in cardiovascular diseases,* 24**,** 375-400.

WEIL, M. H. 1998. The assault on the Swan-Ganz catheter - A case history of constrained technology, constrained bedside clinicians, and constrained monetary expenditures. *Chest,* 113**,** 1379-1386.

WENNBERG, J. E. 2002. Unwarranted variations in healthcare delivery: implications for academic medical centres. *BMJ (Clinical research ed.),* 325**,** 961-4.

WERDAN, K. 2001. Pathophysiology of septic shock and multiple organ dysfunction syndrome and various therapeutic approaches with special emphasis on immunoglobulins. *Ther Apher,* 5**,** 115-22.

WESTERHOF, B. E., GUELEN, I., STOK, W. J., LASANCE, H. A., ASCOOP, C. A., WESSELING, K. H., WESTERHOF, N., BOS, W. J., STERGIOPULOS, N. & SPAAN, J. A. 2008. Individualization of transfer function in estimation of central aortic pressure from the peripheral pulse is not required in patients at rest. *Journal of applied physiology,* 105**,** 1858-63.

WESTERHOF, N., LANKHAAR, J. W. & WESTERHOF, B. E. 2009. The arterial Windkessel. *Medical & biological engineering & computing,* 47**,** 131-141.

WHITE, F. M. 1991. *Viscous Fluid Flow,* USA, McGraw-Hill Inc.

WIENER, R. S. & WELCH, H. G. 2007. Trends in the use of the pulmonary artery catheter in the United States, 1993-2004. *JAMA : the journal of the American Medical Association,* 298**,** 423-9.

WILLIAMS, L. & FRENNEAUX, M. 2006. Diastolic ventricular interaction: from physiology to clinical practice. *Nature clinical practice Cardiovascular medicine,* 3**,** 368-76.

WONG, X. W., CHASE, J. G., HANN, C. E., LOTZ, T. F., LIN, J., LE, A. J. & SHAW, G. M. 2008. Development of a clinical type 1 diabetes metabolic system model and in silico simulation tool. *Journal of diabetes science and technology,* 2**,** 424-35.

YALEMEDICALGROUP.ORG. 2012. *Prolapsed Mitral Valve* [Online]. Available: http://www.yalemedicalgroup.org/stw/Page.asp?PageID=STW022880.

YIU, S. F., ENRIQUEZ-SARANO, M., TRIBOUILLOY, C., SEWARD, J. B. & TAJIK, A. J. 2000. Determinants of the degree of functional mitral regurgitation in patients with systolic left ventricular dysfunction: A quantitative clinical study. *Circulation,* 102**,** 1400-6.

YU, D. T., PLATT, R., LANKEN, P. N., BLACK, E., SANDS, K. E., SCHWARTZ, J. S., HIBBERD, P. L., GRAMAN, P. S., KAHN, K. L., SNYDMAN, D. R., PARSONNET, J., MOORE, R. & BATES, D. W. 2003. Relationship of pulmonary artery catheter use to mortality and resource utilization in patients with severe sepsis. *Critical care medicine,* 31**,** 2734-41.

ZILE, M. R., GAASCH, W. H. & LEVINE, H. J. 1985. Left-Ventricular Stress-Dimension-Shortening Relations before and after Correction of Chronic Aortic and Mitral Regurgitation. *American Journal of Cardiology,* 56**,** 99-105.